

Retinal degeneration and remodelling in experimental glaucoma

James Rhys Tribble

A thesis submitted to Cardiff University in accordance with the requirements for
the degree of Doctor of Philosophy in disciplines of Visual Neuroscience and
Molecular Biology

School of Optometry and Vision Science

Cardiff University

Submitted December 2015

Acknowledgements

I would like to express my sincerest gratitude to my supervisors Professors James Morgan and Frank Sengpiel for their continued support, encouragement and enthusiasm throughout my PhD.

I am grateful to all the staff and fellow PhD students that I have had the pleasure of working with over the years, who have made this such an enjoyable experience. In particular Dr's Irina Erchova, Pete Williams and Stephen Cross who taught me many techniques that have been instrumental in this thesis.

I had the pleasure to conduct a number of experiments in The Jackson Laboratory in Maine for which I am extremely grateful to Professor Gareth Howell and Dr Pete Williams and all those in the Howell lab who contributed in both my results and in making the trip so enjoyable.

I am grateful to Professor Paul Morgan who kindly provided the C1 esterase inhibitor and Professor Bruce Caterson for antibodies 1B5, 2B6, and 3B3 as well as much positive discussion. The donor eyes and visual fields were provided through welcome collaboration with Professor Michael Fautsch (Mayo Clinic, Minnesota) and processed with the much appreciated help of Asta Vasalauskaite.

Lastly I am eternally grateful for the love and tireless support provided by my friends and family, in particular my parents, "in laws" and my wife Louise.

All work presented in this thesis is my own except for the following contributions.

Chapter 3

- 16 of the RGCs analysed were labelled and imaged by Dr. Paulina Samsel and 8 by Dr. Stephen Cross (both James Morgan Group, Cardiff). All analysis was performed by myself.

Chapter 4

- Retinal dissection and Diolistic labelling of mouse RGC was divided between myself and Dr. Peter Williams (Simon John Group, The Jackson Laboratory, Maine).
- IHC and imaging of mouse retinas was performed by Mr. Keating Pepper (Gareth Howell Group, The Jackson Laboratory).
- Optic nerves for both mouse and rat were graded by technicians in the John Lab
- Half of the RGCs used in the Rat NT, OHT.PBS and OHT.C1inh groups were labelled by Dr. Stephen Cross.

Chapter 6

- Human retinas were dissected and cryo-protected in collaboration with Ms Asta Vasalauskaite.

Summary

Glaucoma is an optic neuropathy characterised by the loss of retinal ganglion cells (RGC). Dendritic atrophy occurs early in the disease, prior to soma and axonal degeneration. RGCs exhibit reduced branching density and dendritic field size. This thesis seeks to further characterise dendritic atrophy in glaucoma in the context of two external factors that may contribute to the disease pathology – immune system effects mediated via complement and the influence of the perineuronal net (PNN), a specialised extracellular matrix that surrounds RGCs. RGC morphology was investigated in a rat bead model of experimental glaucoma using ballistic labelling techniques; morphological changes were related to synaptic loss and PNN composition using immunohistochemistry. A model was derived for the classification of diseased RGCs in order to prevent labelling bias in subsequent investigations. The immune system was modulated using a complement inhibitor (using a transgenic mouse and pharmacological agent in rats) and PNNs disrupted using the bacterial enzyme Chondroitinase ABC. Experimental glaucoma caused significant dendritic loss, with partial protection conferred by both complement inhibition and PNN digestion. Analysis of retinal sections also revealed partial protection of synapses. PNNs did not show any changes in their composition in the rat in experimental glaucoma but human glaucoma eyes showed increased glycosaminoglycan sulphation in the RGC layer which was correlated with visual deficit. Manipulation of the RGC external environment therefore proved successful in protecting from dendritic atrophy.

Abbreviations

AUC	area under the curve
BAX	Bcl-2-associated X protein
BDNF	brain derived neurotrophic factor
BN	Brown Norway
BSS	balanced salt solution
C-0-S	no sulphation of N-acetylgalactosamine
C-4-S	sulphation of 4-hydroxyl group of N-acetylgalactosamine
C-6-S	sulphation of 6-hydroxyl group of N-acetylgalactosamine
C1-C9	complement protein 1-9
C1q	complement component 1, q subcomponent
C1qa	complement component 1, q subcomponent, alpha polypeptide
C1qKO	C1q knock out mouse
CART	cocaine- and amphetamine-regulated transcript
CGO	centre of gravity offset
Cl ⁻	chloride ion
CNS	central nervous system
CO ₂	carbon dioxide
CR1	complement receptor 1
CR3	complement receptor 3
CS	chondroitin sulphate
CSase ABC	chondroitinase ABC
D2	DBA/2J
D2.C1qa	DBA/2J-C1qa ^{+/-}
D2- <i>Gpnmb</i> ⁺	DBA/2J- <i>Gpnmb</i> ⁺
Dil	1,1'-Diocadecyl-3,3,3',3'-Tetramethylindocarbocyanine Perchlorate
DiO	3,3'-Diocadecyloxacarbocyanine Perchlorate
dLGN	Lateral geniculate nucleus
DS	dermatan sulphate
DSGC	directionally selective ganglion cells
ECM	extracellular matrix
EM	electron microscopy
ETFE	ethylene tetrafluoroethylene
GABA	gamma-aminobutyric acid

GAG	glycosaminoglycan
Gal	galactose
GCL	ganglion cell layer
GFAP	glial fibrillary acidic protein
GlcA	glucuronic acid
HBSS	Hank's balanced salt solution
HS	heparan sulphate
IHC	immunohistochemistry
INL	inner nuclear layer
iNOS	inducible nitric oxide synthase
IOP	intraocular pressure
IPL	inner plexiform layer
IS	inner photoreceptor segments
JAM-B	junctional adhesion molecule B
KS	keratan Sulphate
LED	local edge detector
LRP	low-density lipoprotein receptor-related protein
LTD	long-term depression
LTP	long-term potentiation
MAC	membrane attack complex
MBL	mannan-binding lectin
MOD	moderate
NFL	nerve fibre layer
NOE	no or early
NT	normal tension
NTG	normal tension glaucoma
OCT	optimal cutting temperature compound
OHT	ocular hypertensive
ONH	optic nerve head
ONL	outer nuclear layer
OPL	outer plexiform layer
OS	outer photoreceptor segments
PB	phosphate buffer
PBPF	primary branch point field

PBS	phosphate buffered saline
PCA	principal component analysis
PD	primary dendrites
PDL	primary dendrite length
PFA	paraformaldehyde
PG	proteoglycans
PNN	perineuronal net
PPD	paraphenylenediamine
PS	phosphatidylserine
PSD95	post-synaptic density protein-95
RFC	receptive field centre
RGC	retinal ganglion cell
ROI	regions of interest
SBPF	secondary branch point field
SEV	severe
SIM-32	anti-non phosphorylated neurofillament-H antibody
SPIG1	SPARC-related protein-containing immunoglobulin domains 1
TM	trabecular meshwork
TNF	tumour necrosis factor
TrkB	tyrosine receptor kinase B
WFA	<i>Wisteria floribunda</i>

Contents

Declaration	II
Acknowledgements	III
Summary	V
Abbreviations	VI
Contents	IX
List of Figures	XIII
List of Tables	XV
Chapter 1: Introduction	2
1.1 The Neural Retina.....	2
1.1.1 Retinal connectivity.....	2
1.1.2 Retinal laminae.....	3
1.2 The Non-Neural Retina.....	6
1.2.1 Glial cells.....	6
1.2.1 Perineuronal nets	6
1.3 Mammalian vision, RGC homologues and classification	13
1.3.1 Structure function relationship	16
1.3.2 Mammalian RGC homologues and classification	18
1.4 Glaucoma.....	22
1.4.1 Clinical etiology and morbidity.....	22
1.4.2 Animal models of Glaucoma	23
1.4.3 Pathophysiology	26
1.4.4 The Complement system in glaucoma	30
1.4.5 RGC atrophy and apoptosis.....	35
1.4.6 RGC functional changes in glaucoma	38
1.5 Aims and Hypothesis.....	39
Chapter 2: General Methods	41
2.1 Animal Husbandry	41
2.2 Glaucoma induction and treatment.....	42
2.2.1 IOP measurement.....	42
2.2.2 Intracameral injection of paramagnetic beads	42
2.2.3 Intravitreal injection of neuroprotective substances.....	43
2.3 Diolistic labelling.....	45

2.3.1 DiOlistic bullet preparation	45
2.3.2 Retinal dissection	45
2.3.3 DiOlistic labelling	46
2.4 Histology.....	48
2.4.1 Perfusion fixation	48
2.4.2 Tissue preparation and sectioning	48
2.4.3 Immunohistochemistry	49
2.5 Imaging and Image Analysis	52
2.5.1 Imaging and quantification of fluorescent intensity	52
2.5.2 Imaging flat mounted retina	54
2.5.3 RGC Image Analysis	56
Chapter 3: RGC classification in disease	60
3.1 Introduction.....	60
3.1.1 Hypothesis	64
3.1.2 Aims.....	64
3.2 Methods	65
3.2.1 DiOlistics labelling and imaging.....	65
3.2.2 New measurements	65
3.2.3 Sun classification	67
3.2.4 Principal component analysis.....	68
3.2.5 Discriminant analysis.....	69
3.3 Results	70
3.3.1 Classification according to Sun.....	70
3.3.2 Retinal eccentricity does not affect classification	72
3.3.3 RGCs differ in size and asymmetry of the proximal dendritic tree	74
3.3.3 Discriminant analysis.....	78
3.3.4 RGC types are discriminated by proximal dendritic morphology	81
3.3.5 Population variance in new parameters does not adequately define groups	81
3.3.6 RGC subgroups cannot be differentiated.....	81
3.4 Discussion.....	83
Chapter 4: Synaptic loss in experimental glaucoma.....	86
4.1 Introduction.....	86
4.1.1 Hypothesis.....	89
4.1.2 Aims.....	89

4.2 Methods	90
4.2.1 Animal husbandry and Mouse strain and breeding	90
4.2.2 Induction of glaucoma, IOP monitoring and C1 inhibitor injection.....	90
4.2.3 Diolistic labelling and confocal imaging of RGCs	91
4.2.4 Optic nerve grading	91
4.2.4 IHC for synaptic loss	92
4.3 Results	93
4.3.1 C1 inhibition protects against dendritic atrophy in the mouse in early glaucom	93
4.3.2 Protection by C1 inhibition is repeated in the rat.....	97
4.3.3 Synapse protection differs in the mouse and rat.....	102
4.4 Discussion.....	105
Chapter 5: The role of PNNs in RGC degeneration and remodelling	108
5.1 Introduction.....	108
5.1.1 Hypothesis	111
5.1.2 Aims.....	111
5.2 Methods	112
5.2.1 Assessment of CSase ABC toxicity	112
5.2.2 Induction of Glaucoma and treatment with CSase ABC.....	113
5.2.3 Effect of Glaucoma and CSase ABC treatment on RGC morphology	113
5.3 Results	115
5.3.1 Chondroitinase ABC is not toxic to RGCs and other retinal neurons.	115
5.3.3 IOP changes in experimental glaucoma	120
5.3.4 RGC atrophy and apoptosis following experimental glaucoma	122
5.3.5 CSase ABC treatment protects RGC dendrites from glaucomatous damage	126
5.3.6 No class bias detected in analysis	129
5.4 Discussion.....	130
Chapter 6: GAG pattern changes in glaucoma	133
6.1 Introduction.....	133
6.1.1 Hypothesis	135
6.1.2 Aims.....	135
6.2 Methods	136
6.2.1 Glaucoma induction and intravitreal injection of CSase ABC in BN rats.....	136
6.3 Results	140
6.3.1 The GAG profile in the rat retina is unaltered in experimental glaucoma.....	140

6.3.3 The retinal GAG sulphation pattern changes in human glaucoma	142
6.3.5 The GAG pattern differs in areas of high visual deficit	145
6.3.6 The magnitude of GAG pattern change in the IPL shows relationship to visual deficit.....	146
6.4 Discussion	149
Chapter 7: General Discussion.....	152
7.1 RGC dendritic and synaptic atrophy.....	152
7.2 The influence of the RGC external environment on dendritic atrophy	155
7.2.1 The immune system	155
7.2.2 The retinal ECM	156
7.2.2 Association of the Immune system with the ECM	157
7.3 Functional consequences of RGC structure change.....	159
7.4 Conclusions and future direction	161
References	164
Appendix.....	207
Appendix A	207
Appendix B	208

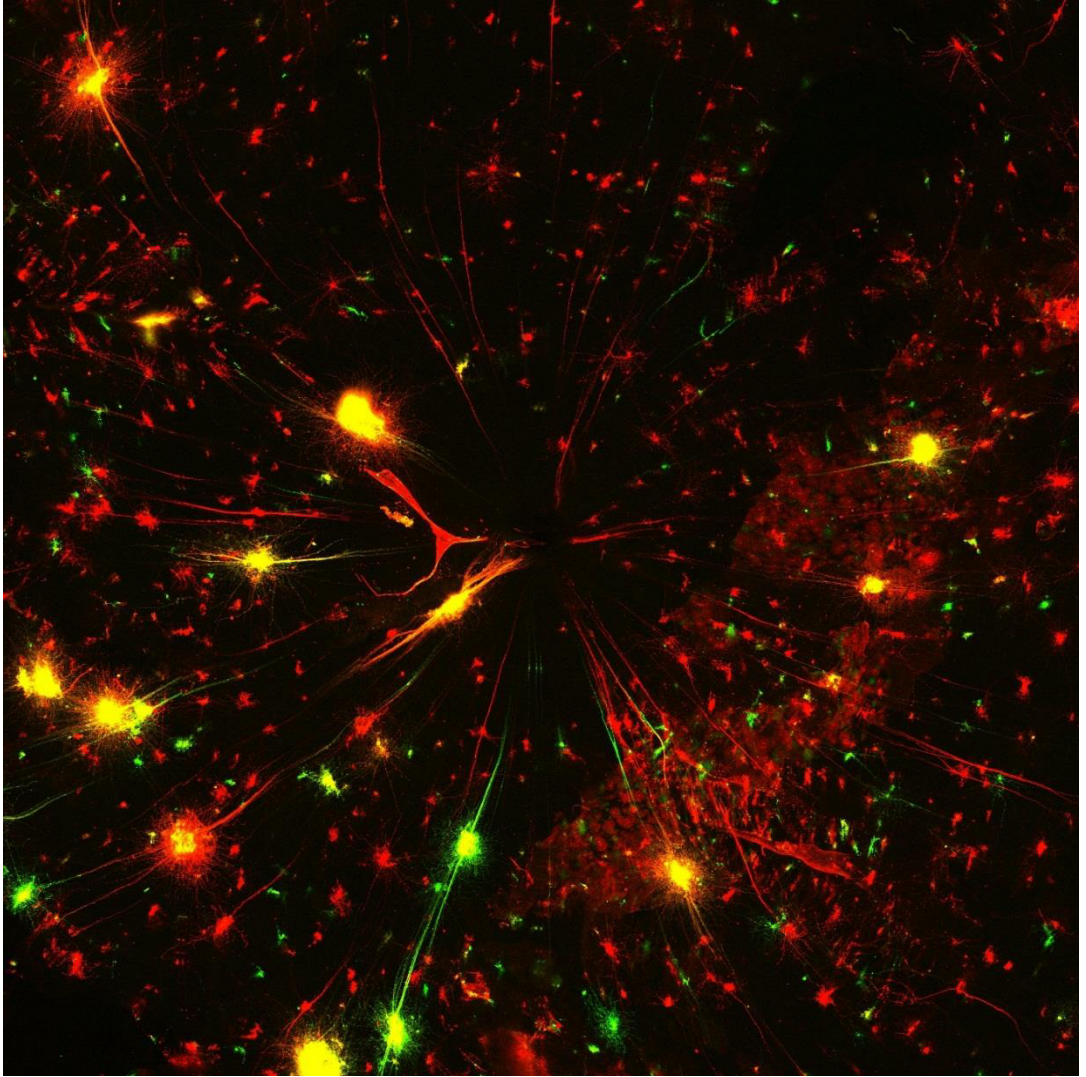
List of Figures

Figure 1.1 Retinal laminae.....	5
Figure 1.2 PNN structure.....	9
Figure 1.3 The Complement System.....	33
Figure 2.1 Magnetic bead model.....	44
Figure 2.2 Diolistic labelling.....	47
Figure 2.3 Epitopes of “stub” antibodies.....	51
Figure 2.4 Fluorescence quantification.....	53
Figure 2.5 Imaging nuclear layers for cell counts.....	57
Figure 2.6 RGC image analysis.....	58
Figure 3.1 Sholl plot model: normal and diseased cells.....	62
Figure 3.2 RGC types.....	71
Figure 3.3 Variation of Sholl plots between RGC types.....	72
Figure 3.4 Distribution of recorded RGCs.....	72
Figure 3.5 Principle component analysis of RGCs.....	76
Figure 3.6 Discriminant analysis of RGCs.....	79
Figure 4.1 RGC morphological changes in the D2.C1 mouse.....	95
Figure 4.2 Typical morphology of mouse RGCs belonging to different genotypes.....	96
Figure 4.3 Comparison of IOPs between treatment groups.....	98
Figure 4.4 Typical morphology of rat RGCs belonging to the experimental groups.....	100
Figure 4.5 RGC morphological changes following C1inh treatment.....	101
Figure 4.6 Typical PSD95 staining amongst different genotypes.....	103
Figure 4.7 Typical PSD95 staining amongst different rat experimental groups.....	103
Figure 4.8 C1 inhibition protects from synaptic loss in the rat but not the mouse.....	104
Figure 5.1 Experimental plan for the role of PNNs in RGC degeneration and remodelling...	110
Figure 5.2 CSase ABC action <i>in vivo</i> following intravitreal injection.....	116
Figure 5.3 CSase ABC non-toxic to retinal neurons.....	117
Figure 5.4 CSase ABC effects on RGC morphological analysis in normal eyes.....	119
Figure 5.5 IOP changes induced by microbead injection.....	121
Figure 5.6 Representative RGC morphology.....	124
Figure 5.7 Cell counts reveal RGC loss.....	125
Figure 5.8 CSase ABC protects from RGC dendritic atrophy.....	128
Figure 6.1 Visual field tests corresponding to donor eyes.....	139
Figure 6.2 GAG labelling in the rat retina.....	141

Figure 6.3 Alcian Blue staining of human retina.....	143
Figure 6.4 Sulphation pattern changes in the human retina in glaucoma.....	144
Figure 6.5 The degree of sulphation pattern change varies according to visual deficit.....	148

List of Tables

Table 1.1 Aspects of mammalian vision.....	15
Table 1.2 RGC homologues among mammalian species.....	19
Table 2.1 Cryo-sectioning details.....	49
Table 2.2 Antibody details.....	50
Table 2.3 Parameters for imaging retina.....	54
Table 3.1 Sun <i>et al.</i> (2002a) classification parameters.....	63
Table 3.2 Percentage of RGC types in sample.....	70
Table 3.3 PCA rotated pattern matrix.....	75
Table 3.4 Correlations between variables and discriminant functions.....	80
Table 3.5 RGC group Centroid.....	80
Table 3.6 Summary of classification.....	82
Table 5.1 RGC class distribution among experimental groups.....	129
Table 6.1 Donor eye details.....	137



Chapter 1: Introduction

1.1 The Neural Retina

1.1.1 Retinal connectivity

The vertebrate retina is organised into three cellular layers, intersected by two synaptic layers. Six distinct neural cell types occupy and form synapses in these separate layers (Kolb *et al.* 2001). The outermost layer, known as the outer nuclear layer (ONL), contains the light sensitive photoreceptors (Dowling 2012). Photoreceptors have well defined nuclear and outer segment portions, the latter where phototransduction is initiated. Vertebrate retinas contain two different types of photoreceptors (rods and cones) in varying ratios and spatial organisations (Curcio *et al.* 1987; Ahnelt 1998). The inner nuclear layer (INL) sits at the middle of the retina and contains the cell bodies of bipolar cells, horizontal cells, amacrine cells and interplexiform cells (Dowling 2012). Bipolar cells extend dendrites through the INL making synaptic contacts with invaginations of the photoreceptors in the outermost synaptic layer, the outer plexiform layer (OPL) (Kolb 1970), and in the inner plexiform layer (IPL) their axons synapse with retinal ganglion cells (RGC) dendrites (Famiglietti and Kolb 1976). The RGC cell bodies occupy the most inner nuclear layer, known as the ganglion cell layer (GCL), the axons of which extend into a discrete nerve fibre layer (NFL) which then traverse and exit the retina at the optic nerve head (ONH), bundling to form the optic nerve (Dowling 2012). Visual information transfers vertically through the retinal layers in a centrifugal manner through photoreceptors, bipolar cells and RGCs as well as horizontally and in reverse, as feedback and modulation. Horizontal cells lie at the border of the INL and extend processes horizontally to synapse with photoreceptors (Stell 1967; Ahnelt and Kolb 1994) and bipolar cells creating feedback interaction (Werblin 2010; Dowling 2012). Interplexiform cells, as suggested by their name, ramify in both plexiform layers, their function is not well understood but they appear to receive input from amacrine cells and feed back to bipolar and horizontal cells (Kolb and West 1977). Amacrine cells represent a

very diverse class of neurone; they do not possess an axon, however their processes can both receive and make synapses, characteristics of both dendrites and axons respectively (Dowling and Boycott 1966). They ramify either diffusely or in discrete layers of the IPL (Kolb *et al.* 1981). Amacrine cells make synaptic contact with RGCs (Taylor 1999; Lin *et al.* 2000; Flores-Herr *et al.* 2001) and bipolar cells (McGilllem *et al.* 2000); their contribution to the horizontal transfer of information can be seen in a type that extend processes laterally to over 3mm in distance (Dowling 2012).

The displacement of cells from the layer in which they are normally found is common. Bipolar and horizontal cells are sometimes found in the ONL (Dowling 2012), while ganglion cells have also been observed in the INL (Buhl and Dann 1988; Jeon *et al.* 1998; Dowling 2012). The occurrence of displaced amacrine cells is far greater; a substantial population can be found in the GCL in almost all vertebrate retinas with the degree of displacement greater in sub-primate species (Perry and Walker 1980; Mueller *et al.* 2007).

1.1.2 Retinal laminae

Synapses in the OPL occur on the invaginations of the photoreceptors and are thus planar in nature (Sjostrand 1958). Conversely, synaptic organisation in the IPL is widely varied due to numerous functionally different subtypes of bipolar cells, amacrine cells and RGCs (Kolb *et al.* 1981; Kolb *et al.* 1992). At its most basic, the centrifugal transfer of visual information in the retina can be divided into two pathways responding to the presence (ON) or absence (OFF) of light (Hartline 1938). The ON and OFF pathways are represented in separate laminae of the IPL based on the depth of synaptic contacts (Famiglietti and Kolb 1976). The axon terminals of ON-bipolar cells terminate proximally in IPL, forming the ON-sublamina (sublamina b) while OFF-bipolar cells terminate in the distal IPL forming the OFF-sublamina (sublamina a) (Famiglietti and Kolb 1976). RGCs also follow this pattern, their dendrites

ramifying in a planar nature in either the ON or OFF sublaminae (or both in bistratified types), and thus confer an ON or OFF nature to the RGC (Famiglietti and Kolb 1976; Miller and Dacheux 1976; Kolb and Nelson 1993). Planar amacrine cells also ramify in the ON or OFF sublaminae, while diffuse types spread through both (Kolb et al. 1981). This organisation is displayed in figure 1.1.

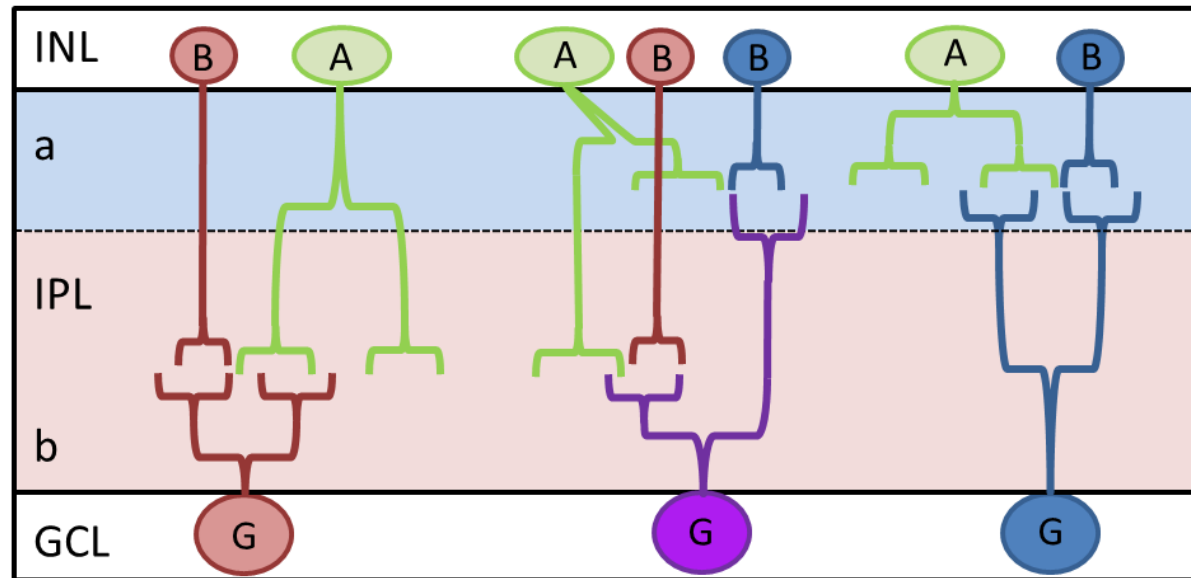


Figure 1.1 Retinal laminae. The ON (red) and OFF (blue) parallel pathways are divided into distinct layers in the IPL. Here bipolar cell axons terminate in the according layer where they synapse with the dendritic arbours of RGCs and confer ON or OFF response characteristics to that RGC. Bi-stratified RGCs (purple) receive input from both pathways. Amacrine cells will ramify in either starter or diffusely between the two.

1.2 The Non-Neural Retina

1.2.1 Glial cells

The retina contains three glial cell types that provide the neuronal cells with mechanical support, metabolic support and removal of cell/debris (Dowling 2012). Müller cells span the width of the retina, extending from the inner limiting membrane at the ONL/inner segment border to the inner limiting membrane/NFL border. They have numerous roles including providing metabolic support, maintaining potassium homeostasis, protecting from glutamate toxicity through reuptake and facilitating connections in the IPL (Reichenbach and Bringmann 2013). Microglia, which are found throughout the retina, monitor neuronal integrity (Nimmerjahn *et al.* 2005) providing phagocytosis of damaged neural cells. Astrocytes, the support cells of the brain, are found to a small extent in the retina. They are far more extensive in the ONH, migrating from the brain in development (Norton *et al.* 1992). Here, they wrap around RGC axons providing metabolic and structural support, potassium homeostasis and form the basis of a blood-brain barrier in the optic nerve (Stone *et al.* 1995). The response and resolution of insult is also a role of glial cells, however their activation, pro-inflammatory cytokine release and cell recruitment can lead to aberrant damage, a feature of retinal disease that is now coming to the fore (Johnson *et al.* 2007; Tezel and Wax 2007).

1.2.1 Perineuronal nets

In 1898 Camillo Golgi presented his findings following investigation of neurons using his 'black reaction'. Here he described the organelle which now bears his name; however, his communication gave equal attention to the external surface of the neurons where he described *"a delicate covering, mainly reticular in structure, but also in the form of tiny tiled scales or an interrupted envelope, which surrounds the cell body of all nerve cells and continues along their protoplasmic extensions"* (Golgi 1898; Golgi 1989). Golgi had described

the perineuronal net (PNN), a specialised form of extracellular matrix (ECM) found in the CNS which surround the surface of neurons and extend out into the neuropil. PNNs surrounding RGCs in the retina are now evident (Aquino *et al.* 1984; Pastrana *et al.* 2006). Long believed to be a static structure, the PNN is now understood to be dynamic, displaying roles in synaptic formation, functioning and plasticity in the adult central nervous system (CNS) (Wang and Fawcett 2012; Berretta *et al.* 2015).

1.2.1.1 PNN structure and chemistry

PNNs are composed of proteoglycans (PG), glycosaminoglycans (GAG) and link proteins (summarised in figure 1.2). The GAG Hyaluronan forms the backbone of the PNN, to which PGs of the lectican family attach via link proteins (Caterson 2012); tenascin-R binds up to three lecticans together at their terminal domain (Galtrey and Fawcett 2007). There are four lecticans found in PNNs – aggrecan, brevican, neurocan and versican, which vary in their overall length and the length of their GAG attachments (Yamaguchi 2000). Aggrecan is found on all PNN-positive neurons, while the presence of the other lecticans varies among neuronal types (Berretta *et al.* 2015). In the retina the presence of the CNS-only lecticans neurocan (Inatani *et al.* 1999) and brevican (Inatani and Tanihara 2002) as well as the more ubiquitous aggrecan and versican (Milev *et al.* 1998b) have also been detected. A dense surround of Chondroitin Sulphate (CS) PGs can be seen around RGCs when labelled immunohistochemically (Aquino *et al.* 1984) while *Wisteria floribunda* (WFA) which is immunoreactive to PNNs also labels RGCs (Pastrana *et al.* 2006). Serine residues on the core lectican allow for the attachment of GAG side chains via a 'linkage region' which comprises a 4 sugar sequence (xylose, galactose (Gal), Gal, glucuronic acid (GlcA) respectively). The GAG chains elongate from this linkage region as repeating disaccharide units consisting of a hexosamine (glucosamine or galactosamine) and either galactose or an uronic acid (glucuronic acid or iduronic acid). The disaccharide unit is native to one of 4 subgroups:

Chondroitin Sulphate (CS)/Dermatan Sulphate (DS), Hyaluronan, Heparan Sulphate (HS) and Keratan Sulphate (KS) (Caterson 2012). These are summarised in figure 1.2. There are numerous sulphotransferases involved in GAG synthesis which add sulphate residues to the 2-, 4- and 6-hydroxyl groups of various sugars; for CS/DS, sulphate residues can be added to the 4-/and or 6-hydroxyl group of N-acetylgalactosamine producing C-4-S and C-6-S groups. Sugar modification by the addition of carboxyl groups and sulphation further increases the potential combinations within a GAG chain such that a CS/DS glycan of 10 units can produce 1008 combinations (Cummings 2009). These units create varying spatial orientations of negatively charged groups which produce diverse binding sites for chemokines, growth factors and cell surface molecules.

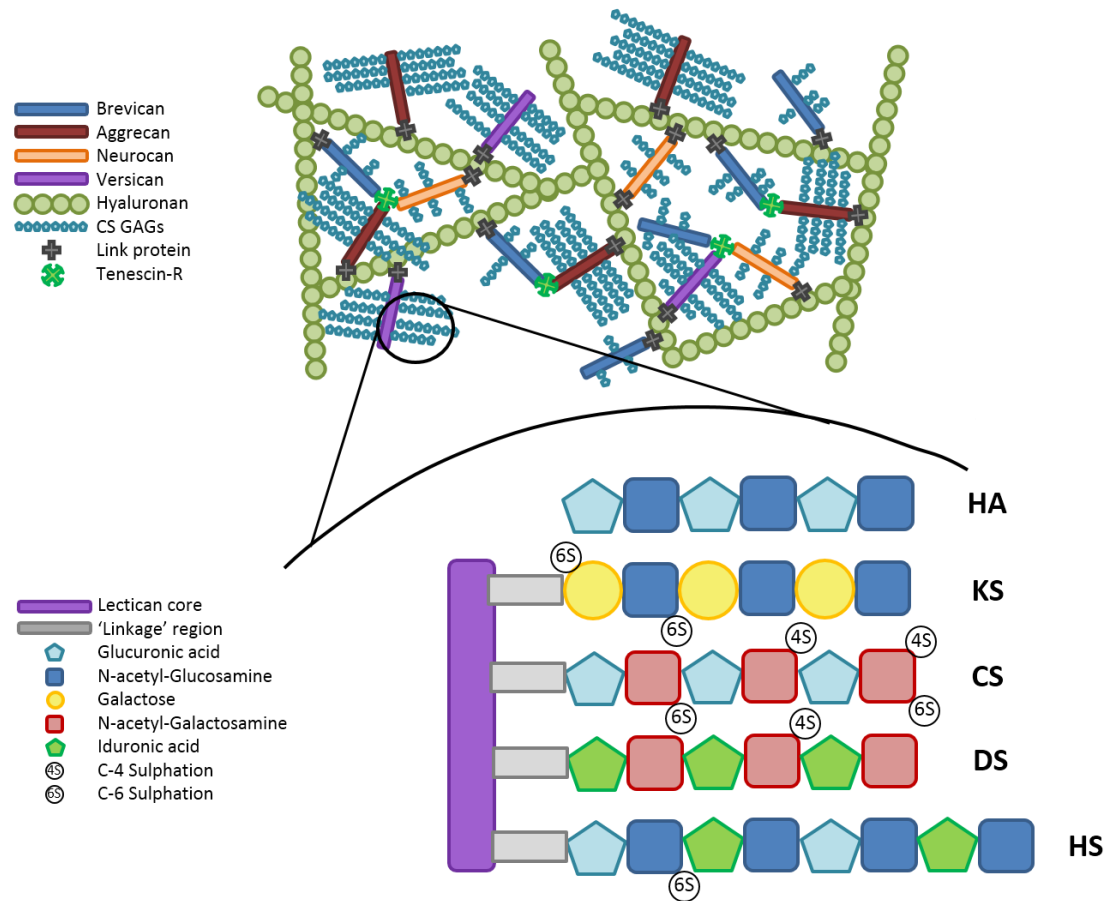


Figure 1.2 PNN structure. PNNs are comprised of a hyaluronan backbone to which lecticans attach via link proteins. The lecticans exhibit different properties due to their varying number and length of GAG chain attachments. These chains are either Keratan Sulphate (KS), Chondroitin Sulphate (CS), Dermatan Sulphate (DS) or Heparan Sulphate (HS) which comprise distinct disaccharide units. The potential sulphation modifications (of 4- and/or 6-hydroxyl groups) are represented by the presence of 6S or 4S. Hyaluronan (HA) is the only GAG that is never sulphated and is also not attached to a lectican core, but rather forms the backbone of the PNN. Adapted from Caterson (2012).

1.2.1.2 The developing CNS

The components of the PNN play important roles in neuronal maturation, axon guidance and synaptogenesis in the developing CNS. The diversity and spatio-temporal expression of these molecules means that CSPGs have been shown to increase axon elongation (Lander *et al.* 1985) as well as inhibit neurite outgrowth (Cole and McCabe 1991; Grumet *et al.* 1993) while C-4-S has been demonstrated as a negative guidance cue in axonal outgrowth (Wang *et al.* 2008). In the retina CS expression recedes from the centre, coinciding with RGC differentiation, axon growth and fasciculation towards the optic fissure. This CS gradient may act as a guidance cue (Brittis *et al.* 1992). The importance of PNNs in synaptogenesis is demonstrated by dark rearing (which prolongs the critical period in the visual cortex); in rodents (Pizzorusso *et al.* 2002; Carulli *et al.* 2010) dark rearing has been shown to prevent PNN formation as well as downregulate expression of various synthases of PNN components. Sensory deprivation through whisker removal also reduces PNN formation (McRae *et al.* 2007; Nakamura *et al.* 2009). These findings demonstrate the importance of PNN formation in activity driven synaptogenesis.

1.2.1.3 PPN role in the adult CNS

The end of the critical period coincides with changes to the composition of PNNs. In the rat retina this maturation has been observed by the decrease of neurocan immunoreactivity to barely detectable levels in the inner retinal layers by postnatal day 42 (Inatani *et al.* 1999). The formation of PNNs in the brain coincides with the ending of synaptic refinement (Blue and Parnavelas 1983) and myelination (Ishiguro *et al.* 1991; Brauer *et al.* 2000) in a number of CNS regions (Dityatev *et al.* 2007; McRae *et al.* 2007) and is thought to stabilise the favourable synaptic connections made during the critical period. CSPGs and tenascin have been shown to repel neuronal processes and are therefore thought to act as a barrier to further synaptogenesis in the adult CNS (Faissner *et al.* 1988; Morganti *et al.* 1990). Removal

of PNNs by enzymatic digestion (Pizzorusso *et al.* 2002) or genetic deletion (Carulli *et al.* 2010) extends the critical period and allows for increased synaptogenesis and enhanced developmental plasticity. In the former study, this plasticity was achieved in adult animals. The PNN components form perisynaptic condensations with the pre- and post-synaptic terminals of neurons. Here the PNN can regulate synapses through controlling synaptic trafficking of receptors and restrict the mobility of neurotransmitters (Frischknecht *et al.* 2009). This is exemplified by the role of PNNs in memory plasticity. Enzymatic digestion (Bukalo *et al.* 2001), genetically induced deficiency (Saghatelian *et al.* 2001) and antibody targeted inhibition (Brakebusch *et al.* 2002) of PNNs have been shown to reduce long-term potentiation (LTP) and long-term depression (LTD) in hippocampal neurons. Components of the PNN also influence voltage gated calcium channel activity; their disruption has been shown to impair LTP (Evers *et al.* 2002). As such enzymatic digestion of PNNs can enhance object recognition in rodents through LTD (Romberg *et al.* 2013) and improve water maze performance (Lee *et al.* 2012). Conditioned fear memories, which are governed by LTP and LDP (Nabavi *et al.* 2014), are protected from extinction-induced erasure by PNNs; when PNNs are removed enzymatically the fear memories can be erased (Gogolla *et al.* 2009). These studies show that PNNs therefore influence both synaptic and structural plasticity. PNNs bind and aid in the sequestration of neurotrophins (e.g. Fibroblast growth factor and transforming growth factor- β (Milev *et al.* 1998c)) and transcription factors and so prevent further neuronal growth (Wang and Fawcett 2012). The highly negative charge generated by the numerous sulphated GAG chains also maintains ionic balances in the neurons local environment (Karetko and Skangiel-Kramska 2009) and so contributes to homeostatic support.

1.2.1.4 PPN and CNS disease

Abnormalities in the CNS extracellular matrix and PNNs are associated with a number of CNS pathologies. Following traumatic brain or spinal cord injury there is an upregulation of CSPGs associated with the formation of glial scars (Soleman *et al.* 2013). Glial scars represent an attempt to contain the degenerative inflammatory response (Faulkner *et al.* 2004) but also form a barrier to axonal re-innervation (Bradbury and Carter 2011). They are rich in CSPGs (Soleman *et al.* 2013) and other PGs such as the neurite repellent semaphorins (Pasterkamp and Kolodkin 2003). After ischemic stroke injury, the resultant peri-infarct region shows an upregulation of CSPGs, neurocan, phosphocan, brevican and versican (Fawcett and Asher 1999; Asher *et al.* 2002; Katsman *et al.* 2003; Carmichael *et al.* 2005) and thus prevents re-innervation. However, outside of the infarct, a downregulation of CSPGs and loss of PNNs has been observed (Katsman *et al.* 2003; Hobohm *et al.* 2005; Karetko-Sysa *et al.* 2011) and may represent an effort to circumvent the infarct and increase compensatory synaptogenesis. Mutations in genes controlling expression of CNS ECM components are associated with epilepsy (Dityatev 2010). This may be due to the role of PNNs in regulating appropriate synaptogenesis; in epilepsy, seizures are the result of hyper-excitability and abnormal neuronal connectivity (Dityatev 2010). Following seizure, a reduction of PNN components hyaluronan, aggrecan, neurocan, phosphocan and Tenascin-R has been observed (Dityatev and Fellin 2008; McRae *et al.* 2012). This may increase aberrant synaptogenesis which contributes to the cyclical progression of epileptogenesis (McRae *et al.* 2012). These CNS pathologies demonstrate the inhibitory properties of PNNs and their PG components towards neuronal outgrowth and synaptogenesis and provide further evidence that PNN removal increases plasticity.

1.3 Mammalian vision, RGC homologues and classification

The human visual system is often divided into two pathways – Parvocellular and Magnocellular, each with a distinct class of RGC (Polyak 1941). The former represents the output of midget RGCs. These cells have small soma and dendritic fields and make up 90% of RGCs in the fovea (Perry *et al.* 1984) where they can connect to a single photoreceptor (Boycott *et al.* 1969). These features afford high spatial sensitivity to the Parvocellular pathway. The Magnocellular pathway comprises the output of parasol RGCs whose dendritic fields span much larger areas (Perry *et al.* 1984). This gives the cells a greater number of photoreceptor connections and so a higher temporal and contrast sensitivity. Parasol RGCs represent only 10% of total RGCs and are found mostly in the periphery (Perry *et al.* 1984).

In the study of the rabbit retina in particular, where high acuity is less of a concern than the detection of movement to this prey species, an interesting RGC type was discovered. These bi-stratified cells respond to the direction of movement (Barlow and Hill 1963) in low acuity peripheral vision. The rabbit's high acuity vision, predominating in its visual streak, is theorised to come from a different RGC type than its morphological and functional homologue in the primate. Here the local edge detector RGCs signal fine spatial information, but through a different mechanism to that of midget type cells (van Wyk *et al.* 2006). Morphological homologues to these RGC types have been uncovered in the primate retina which now boasts 22 described types (Petrusca *et al.* 2007), one of which, the melanopsin RGC, is intrinsically photoreceptive and is involved in the circadian rhythm and pupillary light reflex rather than image forming vision (Berson 2003). Together, Parasol, Midget and small bi-stratified cells make up 75% of RGCs in the primate peripheral retina (Yamada *et al.* 2005). The remaining RGC types therefore represent a small proportion of total cells; locating them in the first instance has therefore proved to be the greatest boundary to their electrophysiological study. The primary role of vision in various mammalian species and its

relationship to aspects of visual information and neuronal connectivity is portrayed in Table 1.1 below.

Table 1.1 Aspects of mammalian vision

Species	Binocular field/Visual field	Number of RGCs/ peak density	Spatial frequency cut off* (cycles/degree)	Ipsilateral projections (% of total projections)	Displaced amacrine cells (% of total cells in CGL)
Human	140°/200°	700,000-1,500,000/ 150,000 mm ²	64	50%	3% fovea/ 80%/periphery
Non-human primate (NHP)	140°/200°	900,000-1,500,000/ 140,000 mm ²	46	50%	5-7% fovea/60-84% periphery
Cat	120°/200°	190,000/ 10,000 mm ²	6	17%	80%
Rabbit	24°/360°	250,000 ^A -400,000 ^P / 5,000 mm ²	3.4	5%	35%
Rat	80°/320°	90,000 ^A -120,000 ^P / 4,000 mm ²	1.2	3% ^A 10% ^P	50%
Mouse	60°/	30,000 ^A -90,000 ^P / 4,000 mm ²	0.5	3% ^A 10% ^P	60%

A=albino, P=pigmented, *as determined by behavioural acuity. References: Visual field (Pettigrew and Sanderson 1986). RGC number (Pettigrew and Sanderson 1986; Pettigrew *et al.* 1988; Wilks *et al.* 2013). RGC density: Human and NHP (Pereira Carneiro Muniz *et al.* 2014), other (Pettigrew and Sanderson 1986; Pettigrew *et al.* 1988). Spatial frequency cut off (Pettigrew and Sanderson 1986; Pettigrew *et al.* 1988). Ipsilateral projections (Wilks *et al.* 2013). Displacement of amacrine cells: Human and NHP (Pereira Carneiro Muniz *et al.* 2014), cat (Wassle *et al.* 1987), rabbit (Hughes and Vaney 1980), rat (Perry 1981), mouse (Jeon *et al.* 1998).

1.3.1 Structure function relationship

The functioning of RGCs has partly been elucidated by the study of RGC receptive fields which has uncovered the relationship between dendritic structure and the functioning of the cell. The area in which a response is elicited from an RGC is termed its receptive field (Hartline 1938). The RGC receptive field is an elegant description of how retinal connectivity culminates in single RGC responses through the relationship of RGC function to retinal structure, cell morphology and synaptic organisation.

1.3.1.1 Receptive field centre

The receptive field centre (RFC) is derived from direct synaptic contact of bipolar cell axons onto RGC dendrites. As these synapses are always excitatory, the RFC response reflects that of the underlying bipolar cells and is therefore ON and/or OFF in nature. Stratification of the RGC dendrites into either sublamina a or b governs the connection to either OFF or ON bipolar cells respectively (Famiglietti and Kolb 1976). The RGCs dendritic field size is also close to the spatial extent of the RFC (Brown and Major 1966; Dowling and Boycott 1966; Amthor *et al.* 1989b; Yang and Masland 1992) and reflects the area covered by the bipolar cell receptive fields. The sensitivity of the RFC is also a function of the dendritic field architecture. Labelling of post-synaptic density protein-95 (PSD95) in rabbit RGC showed that synaptic density peaked towards the centre of the dendritic field (Jakobs *et al.* 2008). This partially reflects the RFC Gaussian sensitivity profile, although sensitivity drops off at the centre. This is caused by the absence of synapses onto soma and primary dendrites as shown by serial reconstructions (Stevens *et al.* 1980; Kolb and Nelson 1993). This drop has been observed electrophysiologically over the soma centre (Brown *et al.* 2000). Since the density of synapses per length of dendrite does not vary (Jakobs *et al.* 2008) and bipolar cell coverage is uniform across the rabbit retina (MacNeil *et al.* 2004), sensitivity should change

with the density of the dendritic field and peak where the number of synapses per area is highest. This was shown computationally for cat α RGCs (Freed *et al.* 1992) and experimentally in rabbit RGCs; although some large cells showed that sensitivity was not predicted by dendritic architecture (Brown *et al.* 2000).

1.3.1.2 Receptive field surround

The mechanisms resulting in the receptive field surround response have proved more difficult to resolve. Three inhibitory effects are now evident, direct inhibitory input by amacrine cells onto RGC dendrites and lateral inhibition pre-synaptic to the RGC both at the level of the IPL and OPL. Direct inhibitory input reflects RGC dendritic structure to the greatest extent. Evidence for direct inhibition of RGCs comes from voltage-clamping studies which allow isolation of direct chloride ion (Cl^-) mediated input. Here, increasing spot stimuli diameter elicited a greater reduction in the RGC response in the rabbit retina while blockade of gamma-aminobutyric acid (GABA_A) receptors by bicuculline is suggestive of GABAergic amacrine mediated inhibition (Flores-Herr *et al.* 2001). Application of tetrodotoxin, which blocks action potentials by binding to voltage-gated sodium channels, to rabbit retina blocked the surround inhibition in some classes of RGC, implicating the action of spiking amacrine cells in the surround response (Taylor 1999). Amacrine cell inhibition of RGCs is dependent on the release rate of GABA or glycine, producing either sustained or transient inhibition through altering Cl^- permeability. In primate RGCs glycine receptors are distributed such that their density is greater on distal dendrites compared to proximal dendrites indicating their role in the inhibitory surround (Lin *et al.* 2000).

1.3.2 Mammalian RGC homologues and classification

Many mammalian species appear to share functional homologues of RGC types (summarised in Table 1.2). These RGCs respond to the same 'trigger feature' and with similar response properties. In the rodent and primate most of the functional RGC types have therefore been inferred to exist based on morphological similarities to cat and rabbit cells (Sanes and Masland 2015). Within the same species, some morphologically similar types which respond to the same 'trigger feature' will differ in their response latencies, producing either brisk or sluggish responses (DeVries 2000; Jackman *et al.* 2009). Midget and parasol cells are easily differentiated, as are their equivalents of other species. But in the rodent species the overlap among morphological types is extensive, such that the dendritic field diameter range of a given type encompasses sizes belonging to all other RGC types (Sun *et al.* 2002b, a). In the mouse, morphological discrimination has yielded 22 RGC types – more than are currently functionally described (Voelgyi *et al.* 2009); in combination genetic, molecular, morphological and electrophysiological profiling suggests at least 25 types (Sanes and Masland 2015). This highlights a key dilemma in the identification of RGC types in that no one method can adequately describe the diversity and capture every cell type. Electrophysiological characterisation and classification does not present a practical solution for most studies as the intricate nature of single cell recording does not yield sufficient cells to study in a time effective manner while multi-array electrodes do not fully capture the range of physiological responses available to RGC types, nor is it conducive to cell filling for subsequent morphological analysis (Sanes and Masland 2015).

Table 1.2 RGC homologues among mammalian species

Physiological response	Cat	Rabbit	Mouse	Rat	Macaque	Human
On brisk-transient	On α /Y cell	α /G ₁₁ On	Y/G ₂	Y/A2 _i	Parasol	P1 _b , P2 _b
Off brisk-transient	Off α /Y cell	α /G ₁₁ Off	Y/G ₃	Y/A2 _o	u/Large radiate cell	P1 _a , P2 _a
On brisk-sustained	On β /X cell	β /G ₄ On	X/?	X/?	Midget	M _b
Off brisk-sustained	Off β /X cell	β /G ₄ Off	X/G ₃	X/B2	Midget	M _a
On-direction selective	On- δ	On- δ /G ₁₀	On-DS/G ₉	?/C1	?/Large moderate	G ₂₁
Off-sluggish sustained	Off- δ	?/G ₉				G ₁₉
On sluggish-transient	ϵ	On sluggish-transient /?	/G ₁₂	?/C3	?/Large very sparse	G ₂₀
Off sluggish-transient	η	?/G ₅ ?	/G ₁₃	?/C4	?/Narrow thorny	G ₈ G ₁₆
On-Off phasic/ local edge detector	ζ	LED/G ₂	/G ₃	?/C4	On-Off phasic/maze cell	G ₈ G ₁₆
On-Off transient (Sivyer 2002)	θ	On-Off transient/ G ₁	/G ₁₆		?/Broad thorny?	G ₅
On-off direction selective	ι	ON-Off DS/G ₇	ON-Off DS /G ₁₇	ON-Off DS /D2	?/Multi-tufted	
On-off nondirection selective			/G ₁₆	?/D1	?/Type VI wide field	
Melanopsin expressing RGC ¹			/G ₁₂	?/Miss-classified C3	Giant sparse	
Blue-On Yellow-Off		?/G ₃			/Large bi-stratified	G ₁₇
Uniformity detector		?/G ₆			/G ₆	

RGCs are depicted as 'Physiologically described'/'Morphologically described' where '?' denotes detection by only one method and blank no detection. ¹ Although not a physiological response, Melanopsin expressing RGCs best describes this RGC type. References: Cat (Berson *et al.* 1999a; Berson *et al.* 1999b; Isayama *et al.* 1999; O'Brien *et al.* 1999; Troy and Shou 2002), Rabbit (Amthor *et al.* 1989b, a; He and Masland 1997; Rockhill *et al.* 2002), Mouse (Sun *et al.* 2002b; Sun *et al.* 2006; Voelgyi *et al.* 2009; Sanes and Masland 2015), Rat (Sun *et al.* 2002a; Heine and Passaglia 2011), Macaque and Human (Demonasterio 1978; Dacey 1993; Yamada *et al.* 2005; Petrusca *et al.* 2007).

1.3.2.1 Morphological classification

Morphological classification is reliant on the measurement of the soma and dendritic field size, as well as the depth of stratification (Huxlin and Goodchild 1997; Sun et al. 2002b, a; Coombs *et al.* 2006; Voelgyi et al. 2009). However, as discussed, in the rodent there is considerable overlap among types such that classification becomes semi-quantitative as measurements are matched to the closest type and often include identification of qualitative features i.e. “Curvy, recursive dendrites” (Sun *et al.* 2002a), “branches twist and turn” (Huxlin and Goodchild 1997). These criteria do however afford practical advantages over other techniques in that certain RGC types can be easily identified. ON-OFF directionally selective ganglion cells (DSGC) for example are clearly identified by their bi-stratified dendritic trees. These parameters are compromised in disease where the dendritic tree is subject to atrophy and so morphological classification may not be suitable.

1.3.2.2 Immunohistochemical classification

Antibodies directed against Thymocyte antigen 1 (Thy1) and Brn3 label all RGC types indiscriminately (Barnstable and Drager 1984; Nadal-Nicolas *et al.* 2009). However, more recently a number of biomarkers and subtype specific gene expressions have been identified that can usefully classify RGCs. SIM-32, which labels neurofilament H in RGC somas, axons and dendrites stains group RGC_A more intensely and has been used to differentiate this class (Sanes and Masland 2015). These cells are specifically labelled in a *Kcng4-cre;Thy1-stop-YFP* transgenic mouse where *Kcng4* encodes a voltage-gated potassium channel subunit (Duan *et al.* 2015). A number of other transgenic mouse lines have now been created which identify unique RGC types. Junctional adhesion molecule B (JAM-B) selectively identifies local edge detector RGCs in *TYW3* transgene mice (*JAM-B-CreER;Thy1-STOP-YFP*). Green fluorescent protein (GFP) insertion into the SPARC-related protein-containing immunoglobulin domains 1 (*SPIG1*) gene (also referred to as *Fstl-4*) identifies ON DSGC

which respond preferentially to upwards motion (Yonehara *et al.* 2009) whereas in Homeobox d10-GFP transgenic mice all ON DSGCs are labelled - those responding to upwards, downward and forward motion (Dhande *et al.* 2013). Other RGC types can also be discriminated by immunohistochemistry. Anti-melanopsin labels the intrinsically photosensitive melanopsin RGC in addition to 4 other RGC types which contain trace amounts of melanopsin (Sanes and Masland 2015). ON-OFF DSGCs can be differentiated by antibodies directed against cocaine- and amphetamine-regulated transcript (CART) (Kay *et al.* 2011). Immuno-labelling of CART in Thy1-YFP-H mice showed that only bistratified cells are labelled, while the number of CART positive cells (~15%) is roughly equal to the total number of bistratified cells as identified by morphological classification (Sun *et al.* 2002a, Voelgyi *et al.* 2009). The use of immunohistochemical and gene expression based classification in disease is also complicated by the expressional changes of Thy1 which occur as an early event in pathologies such as glaucoma (Schlamp *et al.* 2001; Huang *et al.* 2006), while the function of many of these novel genes and proteins are yet unknown, not least changes to their expression in disease states.

1.4 Glaucoma

1.4.1 Clinical etiology and morbidity

Glaucoma is a disease where retinal ganglion cell death results in a progressive loss of vision. Understanding of the pathophysiology is incomplete, but the disease is associated with a number of risk factors including ethnicity (Leske *et al.* 1995; Gordon *et al.* 2002), myopia (Suzuki *et al.* 2006; Chen *et al.* 2012), family history (Tielsch *et al.* 1994; Leske *et al.* 1995), age (Dielemans *et al.* 1994; Le *et al.* 2003; Peters *et al.* 2014) and intraocular pressure (IOP) (Dielemans *et al.* 1994; Stewart *et al.* 2000; Le *et al.* 2003). Clinical diagnosis is primarily achieved by fundus imaging and visual field testing (King *et al.* 2013). IOP is currently the only modifiable risk factor. High IOP can result from aqueous humour outflow restriction in the trabecular meshwork (TM) (as in open angle glaucoma) or structural obstruction (as in closed angle glaucoma), however, glaucoma often (in 30-40% of cases) presents without high IOP (Klein *et al.* 1992; Dielemans *et al.* 1994) in what is termed normal tension glaucoma (NTG). Disease onset is insidious with structural changes to the NFL (Alasil *et al.* 2014) and optic nerve head (Pederson and Anderson 1980) preceding perceptible visual deficits in some cases, but not in others (Malik *et al.* 2012). Visual loss is progressive and irreversible (Bengtsson *et al.* 2009), resulting in scotomas with central visual loss typically occurring later in the disease (Sihota *et al.* 2007). Treatment, commonly topical application of prostaglandin analogues, aims to lower IOP and so manage and slow disease progression (Agis 2000; Higginbotham *et al.* 2004; Kass *et al.* 2010). Glaucoma is the second leading cause of irreversible blindness worldwide and is set to become an increasing health burden due to an ageing population (Resnikoff *et al.* 2004) with 80 million sufferers estimated by 2020 (Quigley and Broman 2006); more than 1 million glaucoma related visits are made to the UK NHS each year (King *et al.* 2013).

1.4.2 Animal models of Glaucoma

1.4.2.1 Genetic models

Animal models of glaucoma attempt to replicate RGC damage through the elevation of IOP. Spontaneous development of glaucoma has been noted in a number of species (Kolker *et al.* 1963; Gelatt *et al.* 1977), the best characterised and defined being the DBA/2J mouse strain. Mutations in *Gpnmb* and *tyrp1* genes cause the dispersion of iris pigment (Chang *et al.* 1999; Anderson *et al.* 2002) which blocks TM outflow resulting in a sustained IOP elevation at roughly 9 months of age (John *et al.* 1998). The model shares characteristics with human glaucoma, namely its age related and variable onset, chronic IOP elevation and chronic RGC death (Libby *et al.* 2005a). In combination with the ease of manipulation of mouse genetics, the model offers extensive flexibility and exploration of genetic interactions (Howell *et al.* 2011). However, the model lacks control over IOP and incurs the expense of ageing animals, some of which will not develop the disease.

1.4.2.2 Inducible models

Finer control of IOP elevation onset and duration is afforded by inducible models of experimental glaucoma. These models are open to the criticism that they lack they lack associations with human glaucoma and therefore may involve distinct pathways (Libby *et al.* 2005a) (although not to the extent of optic nerve crush models (Kalesnykas *et al.* 2012)). Inducible models involve the disruption of aqueous humour outflow mostly by the occlusion of the TM. Laser induced photocoagulation, the first of such models, produces robust IOP increases and offers the fine control of IOP lacking in the spontaneous models (Gaasterl.D and Kupfer 1974). However, the cost of necessary equipment has been largely uncondusive to its widespread use. The injection of hypertonic saline into the episcleral vessels has proved the most robust model (Morrison *et al.* 1997), but again its use has been limited by its highly intricate nature. These issues have been overcome through the intracameral

injection of substances which directly block the TM; the techniques being quick and simple to perform. The first of these was devised by Quigley and Addicks (Quigley and Addicks 1980) who injected fixed autologous red blood cells into the anterior chamber in primates. The peak IOP was considerable and difficult to control, often resulting in corneal ectasia. Moreover the anterior chamber was nearly completely filled and so the retina was obscured from monitoring. The use of microbeads proved more effective (Weber and Zelenak 2001); partial filling of the anterior chamber allowed for fundus imaging and peak IOP was not so extreme. However, repeat injections (sometimes weekly) were required to sustain IOP as the beads tended to escape from the TM. A number of variants of the microbead occlusion model have since been reported in rodents (Urcola *et al.* 2006; Sappington *et al.* 2010; Cone *et al.* 2012; Dai *et al.* 2012b; Foxton *et al.* 2013; Frankfort *et al.* 2013; Smedowski *et al.* 2014). These differ in microbead size and material, injected volume, injection technique and the inclusion of viscoelastic substances. All models show fairly robust IOP increases accompanied by axonal loss and RGC death (to varying degrees) however there appears to be little correlation between the volume of beads injected, the resultant IOP increase and RGC death (Morgan and Tribble 2015) making inference of glaucomatous processes difficult. The use of ferromagnetic microparticles by Samsel *et al.* (2011) allowed for control of bead dispersion within the anterior chamber by use of a magnet. Beads could be manipulated into the iridocorneal angle leaving the visual axis clear and allowing for a reduced injection volume. This is particularly salient for *in vivo* imaging and electrophysiological assessment.

1.4.2.3 Effect of species and strain

The size of the mouse globe can be prohibitive to both the injection of large volumes and the ease of surgical manipulation. The mouse can also be intractable, particularly where IOP measurement is concerned, with the necessary anaesthesia a known confounder to measurement accuracy (Jia *et al.* 2000). Cone *et al.* (2012) showed that even the route of

anaesthesia can significantly affect the IOP reading with gas (Isoflurane) and intraperitoneal (ketamine/xylazine/acepromazine) anaesthesia producing a difference of 2.2mmHg on average. The rat offers the possibility of awake IOP measurement which prevent these effects. The same study investigated the effect of strain on IOP and found significantly greater peak IOP, but a lessor susceptibility to RGC death, in C57BL/6 than CD1 mice. In the rat, magnetic microbead injections following the same protocol produced 30% cell death in the Brown Norway (Samsel *et al.* 2011) and 80% in the Swiss Albino (Dai *et al.* 2012).

1.4.3 Pathophysiology

RGCs are an extremely vulnerable cell type. The cells have a high energy demand due to their highly active spiking (Zador 1998; Laughlin 2001) and unmyelinated region of axon (Barron *et al.* 2004). Any insult that restricts energy can therefore jeopardise the cell. Glaucoma is idiopathic with respect to current understanding, but appears to result from numerous homeostatic disruptions leading to RGC atrophy and apoptosis.

1.4.3.1 ONH disruption

The lamina cribrosa (a mesh like connective tissue structure in the ONH) is believed by many to be the region where initial insult to RGC axons occurs (Burgoyne *et al.* 2005; Downs *et al.* 2011). Disk changes are manifest as an excavation of connective tissue and a compression of lamina sheets (Quigley *et al.* 1983) that may be induced by high IOP. This results in connective tissue remodelling (Hernandez *et al.* 1990; Fukuchi *et al.* 1992; Fukuchi *et al.* 1994), astrocyte dysfunction (Hernandez *et al.* 1995; Varela and Hernandez 1997; Neufeld 1999a) and altered blood flow and nutrient supply (Minckler *et al.* 1977). This is theorised to disrupt RGC structural and homeostatic support. RGC axonal transport has been shown to be impaired with high IOP (Anderson and Hendrick.A 1974; Quigley and Anderson 1976), cited as evidence of direct axonal insult through connective tissue compression. These lamina changes have been replicated in non-human primates (Yang *et al.* 2007a; Yang *et al.* 2007b; Roberts *et al.* 2009), however human work require on post-mortem tissue, of which eyes in the early disease stages are rare (Downs *et al.* 2011). However, disk cupping is also a feature of NTG and so can occur in the absence of elevated IOP. In these instances, the dysregulation of blood flow in the ONH could lead to a similar pathophysiology that is triggered at a lower level of IOP (Anderson 2011). Alternatively, ischemia and re-perfusion injury could occur independently of IOP and produce the similar clinical presentation of NTG and primary open angle glaucoma (Anderson 2011).

Rodent and rabbit models have demonstrated similar ONH disruption despite the absence of a comparable lamina cribrosa in these species (Morrison *et al.* 1995; Morcos and Chan-Ling 2000). ONH astrocyte proliferation, extracellular matrix remodelling (Johnson *et al.* 2000) and axonal transport disruption (Martin *et al.* 2006; Salinas-Navarro *et al.* 2010; Chidlow *et al.* 2011) have been observed. However in other studies axonal transport disruption is minimal or absent (Bunt-Milam *et al.* 1987; Dai *et al.* 2012b; Abbott *et al.* 2014). In these animals direct mechanical injury to axons is unlikely, and so the removal of axon homeostatic support appears more culpable. This is supported by the partial protection to RGCs conferred by the transplantation of olfactory ensheathing cells into the ONH to provided glial-like support to RGCs where ONH astrocytic processes have retracted (Dai *et al.* 2012a).

1.4.3.2 Lack of Neurotrophic support

High IOP has been shown to disrupt axoplasmic transport (Anderson and Hendrick.A 1974; Quigley and Anderson 1976; Martin *et al.* 2006; Salinas-Navarro *et al.* 2010; Chidlow *et al.* 2011), in particular that of brain derived neurotrophic factor (BDNF) (Pease *et al.* 2000; Quigley *et al.* 2000). BDNF is a neurotrophic factor which has been shown to promote RGC survival when exogenously applied in vitro (Johnson *et al.* 1986; Thanos *et al.* 1989) and in vivo (Mansourrobaey *et al.* 1992; Mey and Thanos 1993; Peinado-Ramon *et al.* 1996; Chen and Weber 2001). Axonal compression is thought to prevent retrograde transport of BDNF complexed with its receptor (Tyrosine receptor kinase B (TrkB)) from RGC innervation targets in the CNS. High IOP results in the accumulation of TrkB posterior to the ONH (Pease *et al.* 2000). Activation of TrkB leads to RGC survival through downstream signalling pathways involving PI3K/Akt and Erk1/2 (Chen and Weber 2004). Blockade of transport would therefore lead to RGC death through the attenuation of survival signalling.

However this is complicated by the findings of retinal and RGC TrkB expression (Jelsma *et al.* 1993; Ugolini *et al.* 1995; Vecino *et al.* 1998), even following glaucomatous injury (Cui *et al.* 2002), and evidence of endogenous BDNF produced locally in the retina (Herzog and von Bartheld 1998; Cui *et al.* 2002; Spalding *et al.* 2004; Harada *et al.* 2011) and by RGCs themselves (Vecino *et al.* 2002). This suggests a more complex role of neurotrophic support in glaucoma. Neurotrophic signalling also appears to have numerous and often opposing effects. TrkB mRNA variants have been found in the rat retina (Jelsma *et al.* 1993); short variants (which lack an intracellular tyrosine kinase domain) are involved in other signalling pathways (Baxter *et al.* 1997; Haapasalo *et al.* 2002) and can competitively inhibit long variants (Eide *et al.* 1996). In some instances TrkB signalling can initiate cell death (Hu and Kalb 2003) as can precursor forms of BDNF (Lee *et al.* 2001; Teng *et al.* 2005).

1.4.3.3 Immune activation

Microglia are recruited in response to CNS injury and have roles in neuronal protection and regeneration (Streit 2000). Aberrant microglial responses, in particular the release of cytotoxic substances (Colton and Gilbert 1987; Liu *et al.* 2002), are implicated in a number of neurodegenerative diseases such as Alzheimer's disease (Meyer-Luehmann *et al.* 2008) and Parkinson's disease (Teismann *et al.* 2003). Glial activation in chronic glaucoma has been detected in the ONH (as above 1.4.3.2) and retina in the human (Wang *et al.* 2002), non-human primates (Tanihara *et al.* 1997), rat (Wang *et al.* 2000; Naskar *et al.* 2002; Lam *et al.* 2003) and mouse (Inman and Horner 2007; Bosco *et al.* 2011; Rojas *et al.* 2014) mostly through glial fibrillary acidic protein (GFAP) immuno-labelling. The findings of autoantibodies in glaucoma patients (Bell *et al.* 2013), microglia associated loss of RGCs in un-operated contralateral eyes in experimental animal models (Kanamori *et al.* 2005; Ramirez *et al.* 2010; Gallego *et al.* 2012) and progressive RGC loss in animal models

immunised with heat shock proteins and other retinal antigens (Wax *et al.* 2008; Joachim *et al.* 2012) is suggestive of a systemic immune response in glaucoma. Further to this, T-lymphocytes taken from glaucomatous mice and transferred into tail veins of wildtype control animals cause the loss of RGCs. In these animals, retinas showed no signs of uveitis or other gross inflammatory change, and only a low frequency of activated microglia which were observed in contact with transferred lymphocytes that had migrated into the retina (Gramlich *et al.* 2015).

Microarray analysis (Ahmed *et al.* 2004; Howell *et al.* 2011) and quantitative PCR (Agudo *et al.* 2008; Johnson *et al.* 2011) have implicated immune activation as an early pathogenic event in glaucoma. In the rat ONH, IL-6 family cytokines undergo a massive upregulation (>1500%) accompanied by increased microglia activation-associated genes and a downregulation of ciliary neurotrophic factor (a glial-proliferation repressor, (Fischer *et al.* 2004)). Astrocyte specific genes, including GFAP are not upregulated (Johnson *et al.* 2011). Together these data and others (Son *et al.* 2010), suggest that immune cell recruitment, rather than astrocyte reactivity contribute to early RGC damage. In the DBA2J upregulation of genes involved in the leukocyte transendothelial migration pathway was found to precede detectable RGC damage. Radiation treatment protected RGCs from damage in the targeted eye compared to control. L-selectin ligands were not activated in the treated eyes, preventing immune cell binding and translocation into the ONH (Howell *et al.* 2012). However, this was not replicated in an inducible model of glaucoma where radiation treatment did not significantly reduce axon loss nor alter the infiltration of immune cells into the ONH. This may reflect the differing nature of immune activation in acute and chronic models (Johnson *et al.* 2015).

1.4.4 The Complement system in glaucoma

1.4.4.1 Complement activation

The complement system is a series of circulating proteins that act to enhance immune system responses. The proteins act in a triggered enzyme cascade to produce 3 effects: chemotactic recruitment of immune cells, cell opsonisation and cell lysis (Janeway *et al.* 2001). These effects can target both invading pathogens and native cells for clearance by the immune system. There are 3 branches of activation in the complement system, which all converge on the creation of a common convertase (Ricklin and Lambris 2007). These are the classical pathway, the mannan-binding lectin (MBL) pathway and the alternative pathway (Janeway *et al.* 2001). The complement system is depicted in figure 1.3. Complement proteins are numbered (C1, C2, C3 etc), however this is in order of their discovery not activation. The classical pathway is initiated by the binding of complement component 1 (C1) to antigen:antibody complexes or directly to cell surfaces. C1 is comprised of C1q (a lectin of 6 globular heads linked together by a collagen-like tail) and a (C1r:C1s)₂ complex. Binding of more than one of the tails to a cell surface induces a conformational change in the (C1r:C1s)₂ complex which results in C1r activation and autocatalytic cleavage of C1s (Ricklin and Lambris 2007; Bally *et al.* 2009). Activated C1s is a serine protease that cleaves C4 and C2 into 2 fragments. The larger fragments C4b and C2b bind to the cell surface before combining to generate C4b.C2b, also known as C3 convertase (Janeway *et al.* 2001). The MBL pathway uses the MBL protein which is similar in structure to C1q and contains 2 proteases, MASP-1 and MASP-2, which are homologous to C1r and C1s (Gal *et al.* 2007). It binds specifically to mannose residues which are accessible on pathogen surfaces but hidden by other sugar groups on vertebrate cells. Binding activates MASP-1 and MASP-2 to cleave C4 and C2, forming C3 convertase as in the classical pathway (Janeway *et al.* 2001). C3 convertase cleaves C3 into fragments C3a and C3b, these are the most common effector proteins of the complement pathway, and their roles will be discussed later. C3b can also be

spontaneously generated as in the alternative pathway. Spontaneous hydrolysis of the thioester bond in C3 allows binding of factor B, which is in turn cleaved to fragments Ba and Bb. Bb remains bound to C3 forming the C3(H₂O)Bb complex, a C3 convertase, which can in turn generate C3b and C3a (Janeway et al. 2001; Dunkelberger and Song 2010). This amplification process is controlled by complement regulatory proteins decay-accelerating factor (DAF), factor I and factor H which prevent factor B binding to C3b (Dunkelberger and Song 2010).

1.4.4.2 Complement effector proteins

All 3 pathways converge on the formation of a C3 convertase and the subsequent formation of fragments C3a and C3b. As C3 convertases formation requires its components to be bound to cell surfaces, C3b is subsequently deposited onto the cell surface where it can bind covalently at up to 1000 molecules per convertase. C3 is the most abundant complement protein at a concentration of 1.2mg ml⁻¹ (Janeway *et al.* 2001). Complement activation therefore deposits large amounts of C3b onto cell surfaces where it acts as an effector molecule for the initiation of phagocytosis. Complement receptor 1 (CR1) expressed on macrophages, monocytes and leukocytes can trigger phagocytosis when bound by C3b on cellular surfaces (Woodruff *et al.* 2010). C3b also binds to C4b.C2b and C3(H₂O)Bb respectively to form C5 convertase. This cleaves C5 into C5a and C5b fragments. This is limited by the availability of free C3b to complex with C3 convertases and so C5 fragment formation is more restricted than that of C3 fragments (Janeway *et al.* 2001). C3a, C4a and C5a act as chemokines to enhance immune cell recruitment. These fragments increase vascular permeability and induce adhesion molecules in the vascular endothelium and can act directly on immune cells to enhance adherence to blood vessels, induce TNF- α release and increase expression of complement receptors to amplify phagocytosis (Janeway et al. 2001; DiScipio and Schraufstatter 2007; Woodruff et al. 2010). C5b bound to cell surfaces

can initiate the formation of the membrane attack complex (MAC). C6, C7, C8 and 10-16 molecules of C9 bind in turn to form a pore, 100Å in diameter, in the lipid bilayer (Podack *et al.* 1982). This causes the loss of cellular homeostasis as water, ions and other solutes pass freely by diffusion across the pore resulting in cell lysis. This terminal effect is only initiated in very few instances, again due to the limited formation of C5 fragments, and its importance is demonstrated by susceptibility to only a few bacterial infections in cases of C5-C9 deficiencies (Janeway *et al.* 2001).

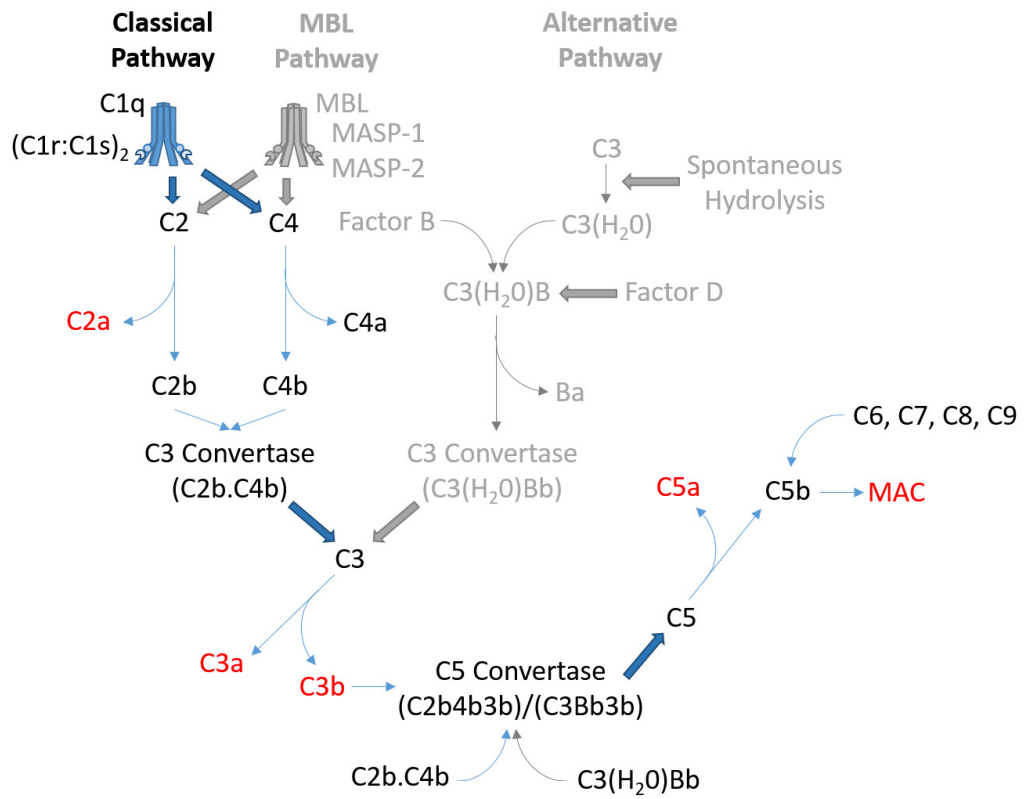


Figure 1.3 The Complement System. Complement proteins are cleaved (filled arrows) into protein fragments either enzymatically as in the classical and MBL pathways, or spontaneously in the alternative pathway. These fragments either form convertases with subsequent complement proteins, producing the complement cascade, or act as effector molecules of the immune system (red). Ca fragments have chemotactic properties, while C3b is an opsonin which tags pathogens and cellular debris for clearance. The classical pathway is implicated in a number of neurodegenerative diseases.

1.4.4.3 Complement in glaucoma

While the majority of complement proteins are produced in the liver (Li *et al.* 2007) the blood-brain barrier does not render the CNS complement free as there is increasing evidence of complement production by epithelial and endothelial cells, monocytes, astrocytes, microglia and neurons (Woodruff *et al.* 2009). RGCs have been shown to produce C1q, C3, and a number of complement receptors (Stevens *et al.* 2007; Orsini *et al.* 2014). The synthesis of complement proteins increases in the CNS in injury (Woodruff *et al.* 2009) and early complement activation is a feature of a number of neurodegenerative diseases (Wang *et al.* 2011; Daborg *et al.* 2012). Early activation of the complement system in glaucoma has been identified in mice (Howell *et al.* 2011) and rats (Ahmed *et al.* 2004; Kim *et al.* 2005) by microarray analysis. C1q and C3 have been detected at significantly increased levels in the NFL, GCL and IPL but not in the ONH following experimental glaucoma in the rat and is associated with increased GFAP labelling (Kuehn *et al.* 2006) while C1q has also been shown to co-localised with synapses in the IPL in early DBA2J glaucoma (Stevens *et al.* 2007) suggesting a role in dendritic and synaptic pruning. In human glaucomatous samples complement proteins are detected at higher levels in the retina than in control eyes, including downregulation of complement factor H (Tezel *et al.* 2010), a complement regulator. In human retina, C1q and C3 staining is co-localised with GFAP in the NFL, GCL and IPL (Kuehn *et al.* 2006). C1qa (the gene encoding the alpha polypeptide of C1q) deficient DBA2J mice are protected from progression to the later stages of glaucoma compared to wild-type animals (Howell *et al.* 2011), while C5 sufficient DBA2Js (wild-type DBA2Js are naturally C5 deficient) suffer earlier onset of severe glaucoma, characterised by increased RGC loss and axonal damage (Howell *et al.* 2013).

1.4.5 RGC atrophy and apoptosis

RGCs apoptosis has been demonstrated in both human (Kerrigan *et al.* 1997; Cordeiro *et al.* 2011) and experimental (Chaudhary *et al.* 1999; Kermer *et al.* 2000; Huang *et al.* 2005; Libby *et al.* 2005a; Calandrella *et al.* 2007) glaucoma. It is increasingly clear that apoptosis in other CNS neuropathies is compartmentalised with axon, soma and dendrites degenerating differentially through local pathways (Mattson and Duan 1999; Coleman and Perry 2002; Williams *et al.* 2006). This is true in glaucoma (Whitmore *et al.* 2005) with axonal, somatic and dendritic degeneration occurring at distinct times points in disease progression.

1.4.5.1 Axonal degeneration

Axon loss in human glaucoma is evident from axon counts in the optic nerve (Quigley *et al.* 1982) and RNFL thinning (Bowd *et al.* 2000). Both features are reproduced in experimental glaucoma models in non-human primates (Cull *et al.* 2012), rat (Chauhan *et al.* 2002; Abbott *et al.* 2014) and mouse (Schlamp *et al.* 2006; Buckingham *et al.* 2008; Liu *et al.* 2014) while axon loss is also reported in other species (Brooks *et al.* 1995). Damage and loss of axons has been shown to precede soma loss (Buckingham *et al.* 2008; Soto *et al.* 2011) with the initial site of insult thought to be to the axon, as demonstrated in Bcl-2-associated X protein (BAX) deficient DBA2J mice (Howell *et al.* 2007a). In these animals RGCs are not lost through glaucoma induced apoptosis (Libby *et al.* 2005b). RGCs showed axonal degeneration only posterior to the glial-lamina, with the anterior axon segment left intact. These axons showed compartmentalised atrophy typical of Wallerian degeneration (Stoll *et al.* 2002); indeed DBA2Js with the *Wld^s* gene were protected from axonal damage (Howell *et al.* 2007a) while in rats the gene has delayed ON degeneration following transection (Beirowski *et al.* 2008). Abnormal mitochondria, phagocytic vacuoles and neurofilament accumulation (characteristics of axonal degeneration) have been observed in EM sections in experimental glaucoma (Kitaoka *et al.* 2013).

1.4.5.2 Soma loss

The loss of RGCs in animal glaucoma models is routinely demonstrated by cell counts in the GCL, a hallmark which is also identified in the human disease (Quigley *et al.* 1989; Lei *et al.* 2009). RGC atrophy can be divided into pre- and post-BAX activation; the pre-BAX phase exhibiting soma and dendritic atrophy and the down-regulation of RGC specific gene expression (Nickells 2012). Following BAX activation the cell is consigned to a terminal fate through mitochondrial membrane instability, cytochrome c release and caspase activation (McKinnon *et al.*, 2002). Soma atrophy, manifest as a reduction in size is observed in numerous species (Weber *et al.* 1998; Morgan *et al.* 2000; Shou *et al.* 2003; Urcola *et al.* 2006). This soma shrinkage offers an explanation for the smaller RGC size observed in glaucoma as opposed to selective/type specific RGC loss (Morgan 2002).

1.4.5.3 Dendritic atrophy

The maintenance of the dendritic tree is also a high energy demand for RGCs. Dendrites represent up to 97% of the surface area of some neurons (Ulfhake and Kellerth 1981) and require the trafficking of sufficient mitochondria and synaptic proteins (Schwarz 2013). The paradigm for energy demand and homeostatic disruption in RGC axons therefore likely extends to dendrites as well (Crish and Calkins 2011). The atrophy of dendrites is a feature of glaucoma common to experimental models in the primate (Weber *et al.* 1998), cat (Shou *et al.* 2003), rat (Morgan *et al.* 2006; Urcola *et al.* 2006) and mouse (Leung *et al.* 2011; Feng *et al.* 2013; Williams *et al.* 2013). The overall dendritic field area is reduced, as is branching density. The reduction of dendrites has been shown to precede soma and axon loss. Dendritic atrophy has also been observed in human post-mortem retina with advanced glaucoma (Pavlidis *et al.* 2003) although here, early changes to dendritic and synaptic architecture have yet to be explored. Type specific susceptibility to dendritic atrophy has been reported by some authors (Weber *et al.* 1998; Shou *et al.* 2003; Leung *et al.* 2011; El-

Danaf and Huberman 2015) but not others (Ahmed *et al.* 2001; Kalesnykas *et al.* 2012). The reduction of dendrites should result in decreased synaptic contact with bipolar cell axons. In a rat model of experimental glaucoma, synaptic loss was reported through reduction of c-fos activation, a functional marker for synaptic activity (Fu *et al.* 2009). However, c-fos also appears to have roles in the activation of apoptosis (Oshitari *et al.* 2002) and so the results should be treated with caution. A reduction in RGC synaptic density, labelled through biolistic transfection with PSD95-CSP was reported following IOP elevation in a mouse bead model (Della Santina *et al.* 2013). Some RGCs with apparently unchanged dendritic architecture showed reduced synaptic density, indicating that synaptic loss precedes the loss of dendrites, rather than presenting as a consequence of dendritic loss. Interestingly, Park *et al.* (2014) have demonstrated increased expression of synaptophysin and PSD95 following IOP elevation that persists for 4 weeks. This was accompanied by a decrease in synaptic ribbons between RGCs and bipolar cells; those synapses that persisted showed an enlarged morphology with increased vesicle accumulation. This may represent a corrective measure to the loss of synapses where immature synapses are formed in response (Park *et al.* 2014). El-Danaf and Huberman (2015) have also shown that dendritic remodeling in M1 photosensitive RGCs in the mouse occurs within the first week IOP elevation where dendrites are formed that extend to the OFF sublamina to compensate for preferential OFF RGC loss. The loss of dendrites and accompanying synapses has major implications for the functioning of RGC in light of the relationship between the dendritic and receptive fields.

1.4.6 RGC functional changes in glaucoma

The first receptive field recordings made in experimental glaucoma were performed by (Weber and Harman 2005). Primate retina were maintained in vitro and RGC properties recorded intracellularly before filling the cells with acridine orange. RGCs showed reduced dendritic field size and branching in the glaucomatous eyes and also demonstrated reduced spatial and temporal frequency sensitivity. The biophysical properties remained similar between groups suggesting that the functional deficits were the result of synaptic loss rather than the result of membrane disruption. Subsequent electrophysiological study in a rat experimental model demonstrated conflicting results. Here receptive field expansion was shown in the glaucomatous eye (King *et al.* 2006), attributed to increased dendritic field size observed by the authors in previous work (Ahmed *et al.* 2001). The increase in receptive field size was likely artefactual, based on their grouping for analysis; dendritic field size and subsequently RF size increase with retinal eccentricity which would confound the average RF size. It is also possible that the IOP increase resulted in corneal ectasia which would alter the optics of the eye, increasing the point spread function of light and the resultant stimulus size on the retina of the glaucomatous eye. More recent work in the mouse has shown type specific changes to RFs in experimental glaucoma. Off-transient RGCs suffered reduced RF size at an earlier time point compared to other cell types, occurring before detectable dendritic change (Della Santina *et al.* 2013). On-sustained, Off-sustained and Off-transient types showed reduced spike rates in glaucomatous eyes accompanied by reduced PSD-95 labelling.

1.5 Aims and Hypothesis

This thesis attempts to investigate the changes to dendritic structure that occur in experimental glaucoma. This will primarily be conducted in a rat magnetic bead model of glaucoma (Samsel et al. 2011) using ballistic labelling techniques, supplemented with immunohistochemistry (IHC), to identify RGC dendritic and synaptic loss. Various morphological analyses of the dendritic tree should provide a sensitive marker for the degree of glaucomatous damage. Dendritic loss in glaucoma appears to be the result of many extrinsic stressors affecting RGCs. Manipulations of the RGC extracellular environment, namely inhibition of the complement system and digestion of PNNs, will therefore be explored as potential therapies for the protection and/or re-growth of RGC dendrites following glaucomatous atrophy.

This thesis will therefore address 4 key aims presented as separate experimental chapters.

1. Given that morphological analysis of the dendritic tree will serve as the main marker for glaucomatous damage, these measurements must be free from confounding effects. The first aim is therefore to derive an RGC morphological classification system that is robust even following RGC dendritic atrophy in order to control for type specific bias in morphological analysis.
2. Complement system activation is an early feature of glaucoma (Howell et al. 2011) and immune activated clearance of dendrites and synapses has been shown in other neurodegenerative diseases (Brown and Neher 2014). The second aim is to investigate whether the loss of RGC dendrites and accompanying synapses can be prevented through inhibition of the complement pathway.

3. PNNs are noted for their restriction of neuronal plasticity. The digestion of PNNs following experimental glaucoma induced damage may free surviving RGCs and allow for the recovery of dendritic field morphology. This chapter will explore the potential of PNN digestion as a therapy for glaucoma.

4. The immediate extracellular environment of the RGC is influenced by PNNs. Changes to this environment as the result of glaucomatous disease processes could affect the functioning of the RGC. The final aim of this thesis is therefore to explore the extent to which the retinal GAG profile changes in both experimental and human glaucoma.

The hypothesis of this thesis is that RGC dendritic atrophy can be lessened or prevented by manipulation of the RGC external environment, in particular the immune system and extracellular matrix.

Chapter 2: General Methods

2.1 Animal Husbandry

Experiments conducted in this thesis were in accordance with Home Office regulations and performed under licenses PPL 30/3084 and PIL IB6A7ED75. Male retired breeder Brown Norway (BN) rats (inbred BN/RijHsd, Harlan) and male Wistar rats (outbred Hsd:WI, Harlan) were used. Rats were housed in 24 hour light, maintained at 40-60lux, in order to minimise diurnal variations in IOP (Moore *et al.* 1996). Food and water were available *ad libitum*. Animals were acclimatised for 2 weeks prior to any experiments. Animals were killed via raising concentration of CO₂ (confirmed with cervical dislocation) or perfusion fixation.

2.2 Glaucoma induction and treatment

Glaucoma was induced in the left eye following a modified method of Samsel *et al.* (2011) described below; the right eye served as an un-operated control.

2.2.1 IOP measurement

IOP was measured using a Tonolab rebound tonometer (Tiolat) calibrated for the Rat eye. Rats were awake and unrestrained, requiring only topical anaesthetic drops (0.4% Oxybuprocaine hydrochloride (Midoptic)) to inhibit the blink reflex. IOP was taken as the mean of 5 repeat readings where 6 readings were taken and the first discarded (Prashar *et al.* 2007). Prior to the induction of Glaucoma, baseline IOP for each eye was established, taken as the mean IOP from 3 separate days. Following induction of glaucoma, the IOP was measured every 3rd day until the animal was killed.

2.2.2 Intracameral injection of paramagnetic beads

Paramagnetic polystyrene beads of 5µm diameter (Kisker Biotech.) were suspended in balanced salt solution (BSS) to give a 30mg/ml paramagnetic bead solution. The preservative (Sodium Azide) in the solution was first removed by 4 successive washes (BSS) and centrifugations (1600g). The bead solution was then sterilised by γ-irradiation using a Gammacell 1000 Elite (Nordon International Inc. 22TBq Caesium Source) with a dose of ~2000cGy. Animals were anaesthetised under Isoflurane and topical 0.4% Oxybuprocaine hydrochloride applied to the eye. Using a Hamilton syringe and tribevelled 33G needle (WPI Europe) 10µl of bead solution was injected into the anterior chamber of the left eye using a self-sealing incision (Fine 1991). A 0.45 Tesla magnet (Geomag) was then used to distribute the beads around the entirety of the iridocorneal angle in order to block aqueous humour outflow. This is demonstrated in figure 2.1. Topical 0.5% Chloramphenicol (Midoptic) was administered post injection. The right eye remained an un-operated control.

IOP was measured in both eyes (as in section 2.2.1) the following day and thereafter in 3 day intervals. The pressure increase was adjudged to be adequate provided an IOP increase of 5mmHg over the contralateral eye sustained for 2 weeks; subsequent injections were undertaken if necessary. A total of 3 injections was permitted. If the IOP did not naturally fall to baseline following the 2 week period then Brinzolamide/Timolol maleate eye drops (Azarga®, Alcon) were administered daily until a return to baseline was achieved.

2.2.3 Intravitreal injection of neuroprotective substances

Intravitreal injection of neuroprotective substances were performed as a treatment for RGCs following experimental glaucoma. The animal was anaesthetised with isoflurane and topical 0.4% Oxybuprocaine hydrochloride applied to left eye. In order to visualise the needle in the vitreous chamber the pupil was dilated by administration of topical 1% Tropicamide (Midoptic) and a glass cover slip (which neutralised the refraction of the lens) mounted on the cornea with a carbomer gel (Clinitas hydrate, Altacor). This ensured that the needle did not damage the retina (other than at the entry site) and allowed the checking of the return of retinal blood supply following the injection of fluid. A Hamilton syringe and tribevelled 33G needle were used. The contents were injected slowly over 5 seconds and the needle left in place for 30 seconds prior to removal to allow diffusion of the contents and improve the chance of retention. 0.5% Chloramphenicol drops were applied pre and post injection.

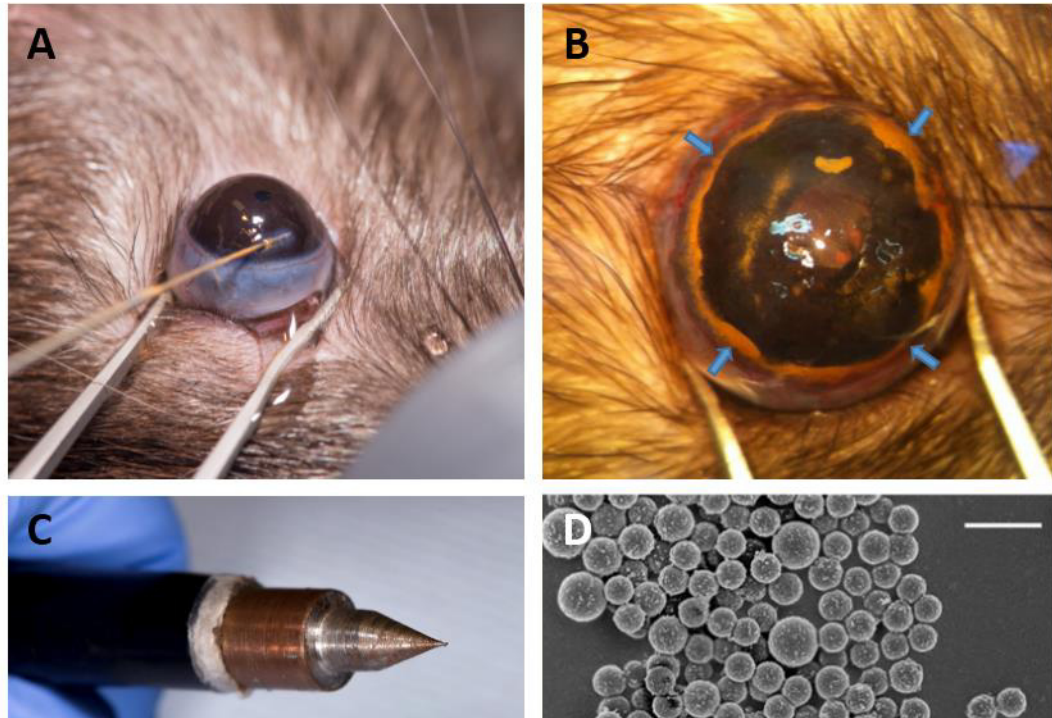


Figure 2.1 Magnetic bead model. Paramagnetic microspheres are injected into the anterior chamber of the rat eye using an intrastromal self-sealing incision (A). The microspheres are then drawn into the iridocorneal angle, as shown by the blue arrows (B), using a magnet with a machined head attached (C) which allows more precise distribution for a 360° occlusion of the trabecular meshwork (TM). The microspheres are 4-5 μ m in diameter, as shown by a scanning electron micrograph (D) and so block the pores of the TM. Scale bar=10 μ m.

2.3 Diolistic labelling

In order to visualise RGCs retina were labelled 'DiOlistically' following a modified protocol of (Gan *et al.* 2000) using a Helios[®] gene gun system (Bio-rad). The labelling process is depicted in figure 2.2.

2.3.1 DiOlistic bullet preparation

The Helios[®] gene gun uses 1cm bullets cut from Ethylene tetrafluoroethylene (ETFE) tubing. 2mg of 1,1'-Dioctadecyl-3,3,3',3'-Tetramethylindocarbocyanine Perchlorate (DiI) (Life Technologies) was dissolved in 200µl of Methylene chloride (Sigma). The solution was pipetted onto 100mg of 0.7µm diameter tungsten particles (Biorad) on a glass slide. This was repeated with 4mg of 3,3'-Dioctadecyloxycarbocyanine Perchlorate (DiO) (Life Technologies). After drying the DiO and DiI coated tungsten was mixed and funnelled into a 30cm length of ETFE tubing placed on a tubing prep station (Biorad). The tubing was rotated overnight in darkness giving an even coating of tungsten particles throughout. Excess tungsten was removed before cutting the tubing into 1mm length bullets which were stored in foil at room temperature.

2.3.2 Retinal dissection

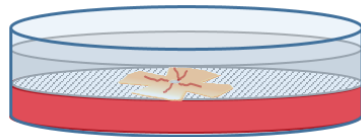
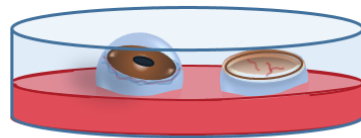
Animals were killed by CO₂, confirmed by cervical dislocation. A cauteriser (low-temp adjustable fine tip, Bovie Medical Corporation) was used to mark the cornea nasally and thus maintain orientation. The eyes were enucleated and placed in Hank's balanced salt solution (HBSS, Life Technologies) on ice. For dissection, a puncture was made at the limbus from which a cut through the sclera and retina was used to maintain orientation. The anterior chamber and lens were removed. The retina was gently manipulated from the sclera and removed through cutting the optic nerve. Retinae were transferred onto Millipore cell culture inserts (0.4µm pore, Fisher Scientific) and 3 smaller cuts were made in order to

flatten the retina into a 4 leafed flat mount, ganglion cell layer up. The vitreous was removed from the retinal surface to prevent obstruction to ballistic labelling.

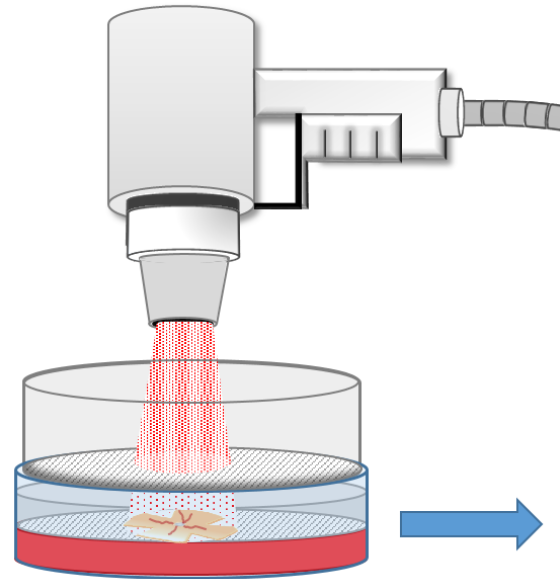
2.3.3 DiOlistic labelling

DiO/Dil bullets were fired, one per retina, at a pressure of 828 kPa (120 psi) and a gun nozzle to retinal surface distance of 4cm. To prevent aggregated particles reaching the retina a cell culture insert (BD Falcon 3.0µm, BD Biosciences) was placed between the retina and gun. Retinas were then cultured on the Millipore cell culture inserts in Neurobasal-A medium (Life Technologies) supplemented with 1% N2, 1% 0.8mM Glutamine, 2% B-27 and 1% 0.8mM penicillin/streptomycin for 30 minutes at 37°C with 4% CO₂ (Williams *et al.* 2010). Retinas were then flat mounted on Histobond coated slides (Fisher Scientific) by cutting out the insert mesh; this prevented folding of the retina when transferring to a slide. The retina was then fixed with 4% paraformaldehyde (PFA) in 0.5M phosphate buffer (PB, pH 7.4) for 30 minutes and washed with phosphate buffered saline (PBS, pH 7.4). Nuclear stain (TO-PRO-3 iodide, Life Technologies) was applied for visualisation of ganglion cell and inner nuclear layers. After 10 minutes retinas were washed with PBS before application of anti-fade mounting media (ProLong Gold, Invitrogen), cover slipping and sealing. Retinas were imaged as described under confocal imaging in section 2.5.2.

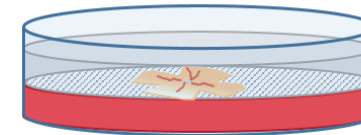
1. Anterior chamber removed at the limbus to leave eye cup.
Dissection in ice cold HBSS



2. Retina dissected free and flat mounted onto cell culture insert



Helios gene gun. Particles propelled by helium blast from attached cylinder



3. Retina DiOlistically labelled.
Cell culture insert used as filter to prevent over-labelling

4. Retina cultured in Neurobasal-A for 30mins (37°C, 4% CO₂) before fixation

Figure 2.2 Diolistic Labelling. Summary of Diolistic labelling process from retinal dissection to labelling and culture.

2.4 Histology

2.4.1 Perfusion fixation

Animals where tissue was needed for histology were killed via perfusion fixation. For perfusion, either a perfusion pump or hydrostatic pressure (reservoir ~1 meter above animal) was used. A barbiturate (Euthatal, Merial) overdose was administered via intraperitoneal injection. Anaesthesia was assessed via toe, tail and blink reflexes; when adequate the animal was positioned on its back and an incision made from the sternum to the diaphragm along the animals midline. The ribs were cut at the midline and the thoracic cavity held open with haemostatic clamps. The heart was freed from the surrounding connective tissue and the pericardium opened. PB (0.5M) with 10U/ml heparin sulphate (Wockhardt UK Ltd) was run through plastic tubing connected to a needle from a reservoir. The needle was inserted into the left ventricle of the heart and clamped in place. The right atrium was immediately cut to allow circulatory drainage. Following complete exsanguination the PB was replaced with ice cold 4% PFA and the animal was perfused until pallor of the liver was observed. The relevant tissue was then removed and immersed in 4% PFA overnight at 4°C.

2.4.2 Tissue preparation and sectioning

The preparation and sectioning of whole eyes and retina is detailed in Table 2.1. Tissue was fixed in 4% PFA by immersion or perfusion fixation and cryo-protected in 30% sucrose. Tissue was embedded in optimal cutting temperature compound (OCT, Sigma), frozen in dry ice or liquid nitrogen cooled isopentane and kept at -80°C until sectioning. Sectioning was performed on a Leica CM3050S Cryostat. Sections were collected on superfrost plus slides (Fisher Scientific), air dried and kept at -20°C until needed.

Table 2.1 Cryo-sectioning details

Tissue	Fixation method	Cryo-protection	Sectioning plane	Section thickness (μm)
Whole eye	Perfusion fixation, 4% PFA in 0.5M PB	30% Sucrose	Sagittal	10
Retina	Immersion fixation, 4% PFA in 1M PBS	30% Sucrose	Transverse	10

2.4.3 Immunohistochemistry

Cryo-sections were air dried for 30 minutes following removal from -20°C storage. Sections were rehydrated with PBS for 5 minutes before segregating with a hydrophobic marker pen (Vector laboratories). The primary antibodies including the corresponding blocks and secondary antibodies used are reported in the relevant chapter method sections. Details of the Primary antibodies used are summarised in Table 2.2. The function of primary antibodies 1B5, 2B6 and 3B3 which detect CS/DS GAG chains following CSase ABC digestion is summarised in Figure 2.3. Sections were blocked for 1 hour before application of the primary antibody (substituted for PBS for secondary only controls). Primary antibody incubation was conducted at 4°C overnight. Sections were then washed 3 times in PBS and the relevant secondary antibody applied. The secondary antibody incubation was 2 hours at room temperature before 3 PBS washes. Nuclear stain (either Hoescht-33342 (10mg/ml at 1:1000, Life technologies) 1:1000 or TO-PRO-3 1:1000) was applied and washed with PBS 3 times after 10 minutes. Anti-fade mountant was applied and the slides cover slipped; once dry the slides were sealed. Slides were stored at 4°C before imaging once the mountant had cured.

Table 2.2 Antibody details

Primary Antibody	Target	Dilution	Species/Isoform	Secondary Antibody	Dilution
Polyclonal Anti-PSD95 (abcam)	Cytoplasmic tail of NMDA receptor	0.9mg/ml at 1:250	Rabbit/IgG	Goat anti- rabbit IgG AF 555 (abcam)	2 mg/ml at 1:500
1B5(+)* (gift from Prof. Caterson)	Unsaturated C-0-S 'stub'	2µg/ml at 1:5	Mouse/IgG	Goat anti- mouse IgG AF 488 (abcam)	2 mg/ml at 1:200
2B6(+)* (gift from Prof. Caterson)	Unsaturated C-4-S 'stub'	2µg/ml at 1:5	Mouse/IgG	Goat anti- mouse IgG AF 488 (abcam)	2 mg/ml at 1:200
3B3(+)* (gift from Prof. Caterson)	Unsaturated C-6-S 'stub'	2µg/ml at 1:5	Mouse/IgM	Goat anti- mouse IgM AF 488 (abcam)	2 mg/ml at 1:200

*(+) refers to the presence of a digestion step using CSaseABC prior to antibody block.

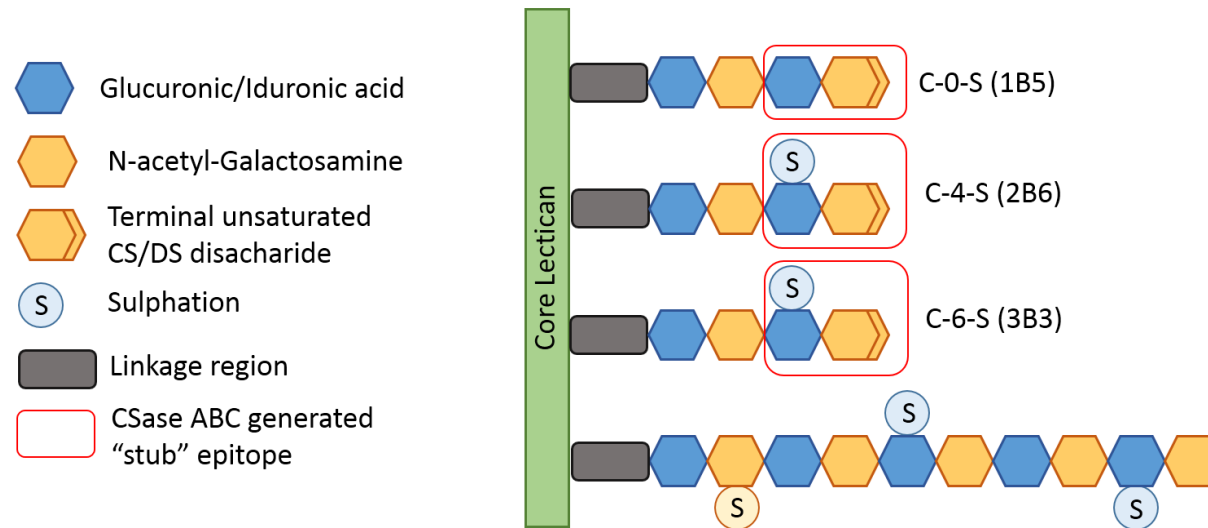


Figure 2.3 Epitopes of “stub” antibodies. Chondroitin sulphate (CS) and dermatan sulphate (DS) GAG chains are attached to a lectican core protein via a linkage region. These chains consist of repeating Glucuronic/Iduronic acid and N-acetyl-Galactosamine disaccharides. These sugars can be non-sulphated (C-0-S), 4-sulphated (C-4-S) or 6-sulphated (C-6-S). The enzyme CSase ABC remove CS/DS disaccharides leaving a terminal unsaturated residue “stub” that is either C-0-S, C-4-S or C-6-S. These epitopes can be recognised by antibodies 1B5, 2B6 and 3B3 respectively. The epitopes generated therefore reflect the sulphation pattern of the GAG chain. Adapted from Caterson (2012).

2.5 Imaging and Image Analysis

All image analysis was conducted on masked images. Following image capture, a custom macro (developed by our group (Cross 2012)) in Image J was used to mask raw image files for processing and analysis. The macro replaced the image file name with a random 6 digit number, saving the file in a new masked folder.

2.5.1 Imaging and quantification of fluorescent intensity

Following IHC cryo-sections were imaged using a Leica DM6000B (with Leica DFC350FX camera) with an x20 air objective (NA 0.7). Multi-channel images were captured using the appropriate filter cubes for the secondary antibody fluorophores and nuclear stains (see Table 2.3). For fluorescent intensity measurements, firstly the background fluorescence level was set using 2° only control sections. Positive control sections were then used to set suitable imaging parameters in order to avoid saturation in subsequent imaging. These parameters were kept constant between sections of the various experimental groups. Quantification of the fluorescence intensity in regions of interest (ROI) was performed in FIJI on 8-bit images in the relevant colour channels. The nuclear layers were used to delineate the boundaries of the GCL/NFL complex, IPL and INL. In these ROIs the average pixel intensity was measured (Figure 2.4) Data was analysed using microsoft excel and statistical analysis performed using SPSS (version 18.0-23.0 IBM).

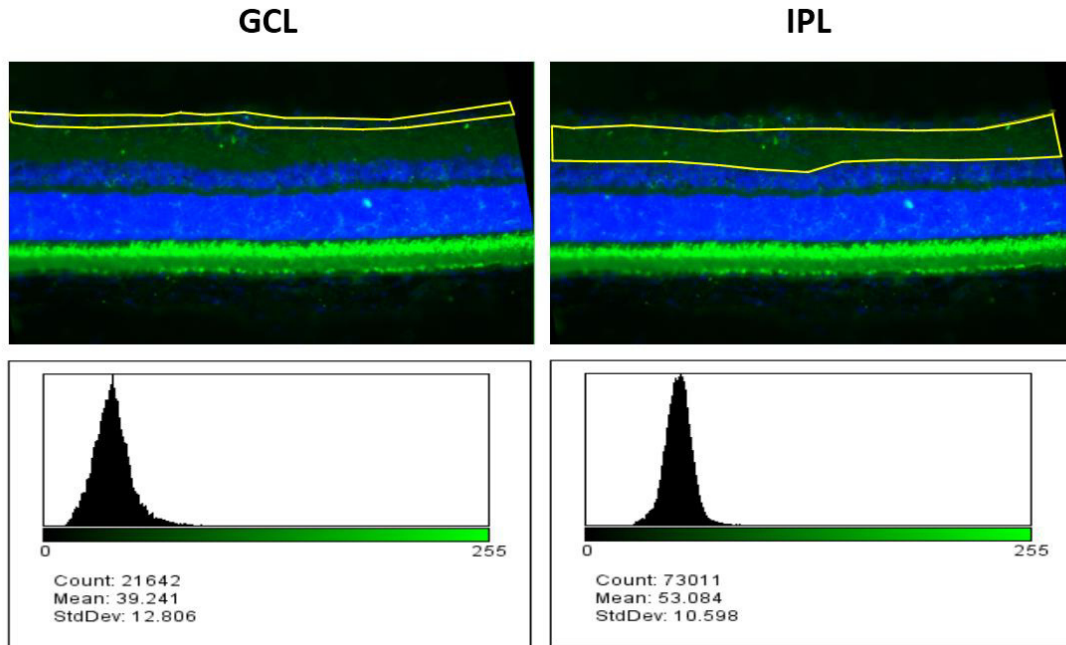


Figure 2.4 Fluorescence quantification. The retinal layers (GCL/NFL complex, IPL, INL, OPL, INL, Photoreceptor segments) were isolated as discrete ROIs for the quantification of fluorescent intensity as seen in the example images of NFL/GCL and IPL isolation. The mean pixel intensity (fluorescent intensity) could then be related to antibody binding and the relative amount of antibody target present in the tissue. The ROIs excluded blood vessels from analysis.

2.5.2 Imaging flat mounted retina

A Zeiss LSM 510 confocal microscope (Carl Zeiss AG) with an x20 air objective (NA 0.8) was used to image both RGCs labelled through Diolistics and nuclear layers for cell counts in flat mounted retinas.

Table 2.3 Parameters for imaging retina

Probe	Target	Microscope	Peak excitation (nm)	Peak emission (nm)	Channel colour
Dil	Cell membrane	Zeiss LSM 510, HeNe543 laser	550	570	Red
DiO	Cell membrane	Zeiss LSM 510, Argon/2 488 laser	490	505	Green
TO-PRO-3	Nucleus	Zeiss LSM 510, HeNe633 laser	642	655	Blue
Alexa Fluor 488	Relevant primary Ab	Leica DM6000B, GFP filter cube	500	520	Green
Alexa Fluor 555	Relevant primary Ab	Leica DM6000B, N2.1 filter cube	555	568	Red
Hoechst-33342	Nucleus	Leica DM6000B, A4 filter cube	350	454	Blue

2.5.2.1 RGC imaging in flat mounted retina

Z-stack 1024x1024 pixel images, at a scaling of 0.54 μ m/pixel on the x and y axes with a slice thickness of 0.5-1 μ m/pixel on the z axis were captured. This gave a 556 μ m² surface area that was more than adequate to capture the entire dendritic arbour of any RGC imaged, while the depth could be varied according to sample thickness in order to include full dendritic

stratification. Multichannel images were captured of single RGCs where RGC labelling was captured in channel 1 and/or 2 (the excitation and emission wavelengths of the various RGC labels are displayed in Table 2.3) with TO-PRO-3 stained ganglion cell and inner nuclear layers captured in a third channel. The retinal layers allowed for the measurement of RGC stratification within the IPL. RGCs were identified based on the presence of an axon and residence within the GCL. The eccentricity of each imaged RGC, measured as the distance in μm from the optic nerve head in the x and y plane was recorded using a custom scanning stage with a stepper motor attached to the microscope.

2.5.2.2 Cell counts

TOPRO-3 stained cell nuclei in the GCL were imaged in flat mounted retina. A $556\mu\text{m}^2$ area (1024×1024 pixel) was captured using the at x20 objective. Images were taken superior-nasally, superior-temporally, inferior-nasally and inferior-temporally at $1000\mu\text{m}$ and $3000\mu\text{m}$ from the ONH giving 8 images per retina. Figure 2.5 shows the imaged areas in relation to their position in the retina. Images were cut to $500\mu\text{m}^2$ using Image J, this gave an overall area of 2% that of the total retina for central and peripheral retina from which to estimate cell loss. Images were masked using a custom macro and cell counts of the GCL were performed using the counter plugin for Image J. Data was analysed using microsoft excel and statistical analysis performed using SPSS.

2.5.3 RGC Image Analysis

Changes to the morphology of the dendritic arbour are a sensitive marker for early degeneration and potential recovery. This morphology was quantified through a number of methods. Data was analysed using microsoft excel and statistical analysis performed using SPSS.

2.5.3.1 Sholl analysis

Sholl analysis is a measure of branching density and complexity performed through measuring the frequency of dendrite intersections of circles of increasing diameter, concentric with the cell soma. The concept is demonstrated in Figure 2.6 (Panel B). Sholl analysis was performed automatically using the simple neurite tracer plugin (Longair *et al.* 2011) for Fiji (Schindelin *et al.* 2012). RGCs were first traced in 3D before running Sholl analysis where distance between circles was set to 10 μ m and the number of rings set to 40 giving a total measurable distance of 400 μ m from the soma centre. This was adequate to accommodate even the largest RGC.

2.5.3.2 Mean and total dendritic length

The simple neurite tracer plugin allowed for the collection of tracings as data of individual dendrite length (Figure 2.6 Panel A) organised in a hierarchial manner (i.e. dendrite ordering, branching lineage). This data was used to calculate total number of dendrites, total dendrite length and average dendrite length of the dendritic tree. Dendrites were then grouped according to the centrifugal method and the number, total length and mean length calculated for each dendrite order (i.e. primary dendrites, secondary dendrites and so forth).

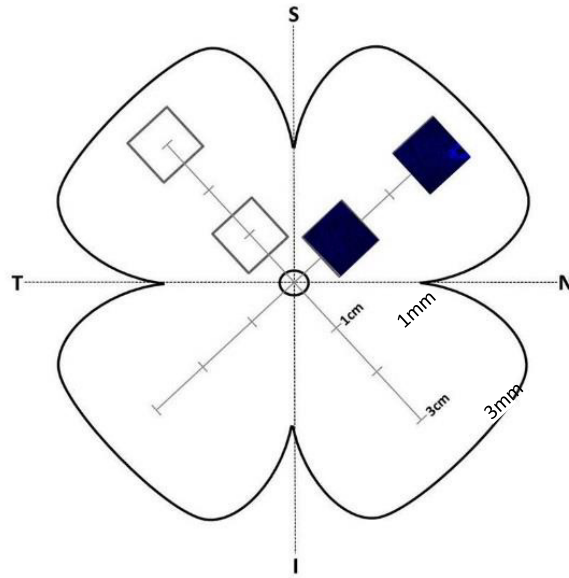


Figure 2.5 Imaging nuclear layers for cell counts. A) Images were taken at eccentricities of $1000\mu\text{m}$ and $3000\mu\text{m}$ from the ONH in all 4 retinal quadrants. The sampled area of each image was cut to $500\mu\text{m}^2$. This gave a total sampled area of 1000mm^2 each for central and peripheral retina representing 2% of the total retinal area of $50,265\text{mm}^2$ (assuming $4000\mu\text{m}$ radius)

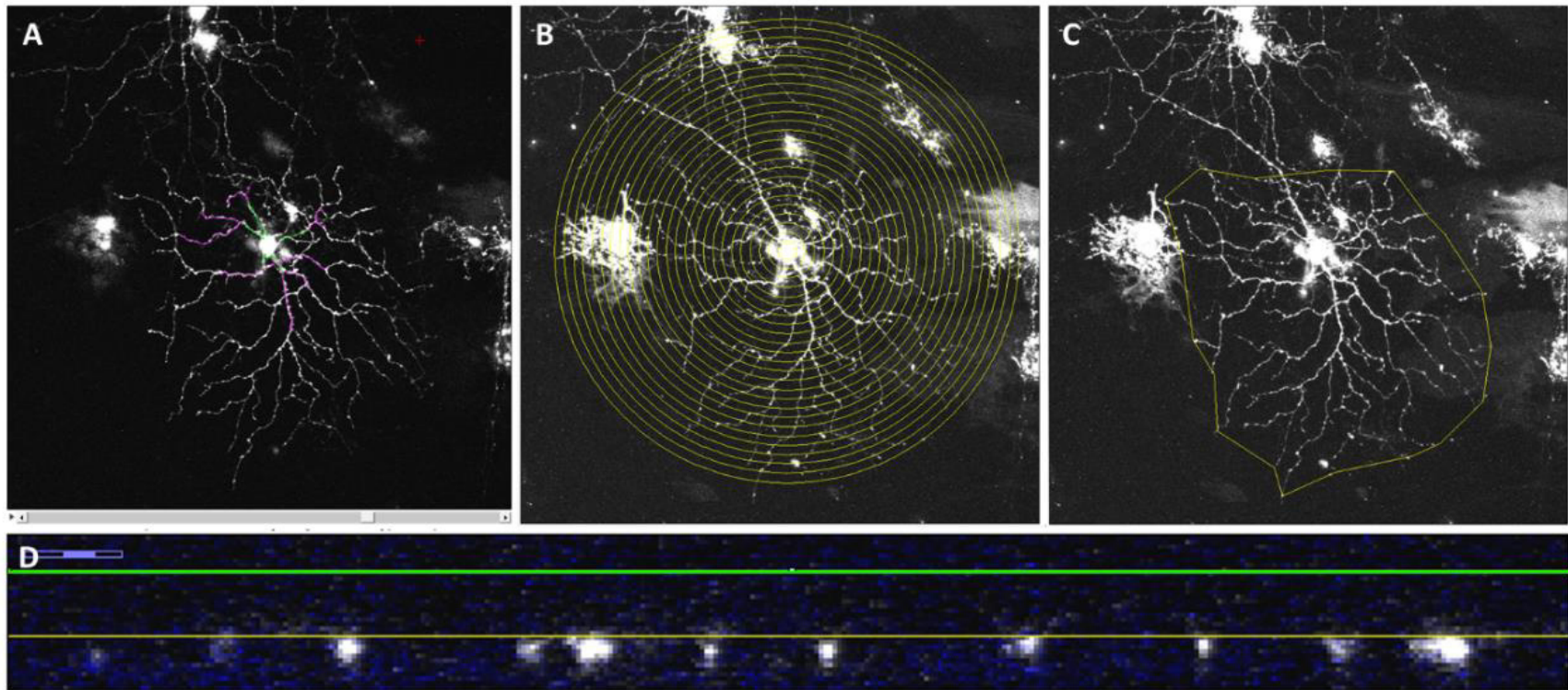


Figure 2.6 RGC image analysis. **A)** Dendritic length measured using the simple neurite tracer plugin is stored in a hierarchical manner, allowing separation of data into, for example, primary (green) and secondary (purple) dendrites. **B)** Sholl analysis measures the number of dendrite intersections of concentric circles of increasing diameter. This is performed automatically by the simple neurite tracer plugin. **C)** Connecting the dendritic tips gives the dendritic field area. **D)** The depth of stratification is measured in re-sliced stacks where the depth of dendritic tips (yellow) is expressed as a percentage of IPL depth (green).

2.5.3.3 Dendritic field size

Dendritic field size was measured using the polygon tool in FIJI where the outer dendritic terminals were connected and the area of the shape in pixels measured (Figure 2.6 Panel C). Area in pixels was then converted to μm^2 . The dendritic field diameter was also measured through assuming a circle of equal area and finding diameter through $(\sqrt{x/\pi})^2$ where x is area. Data was analysed using microsoft excel and statistical analysis performed using SPSS.

2.5.3.4 Dendritic stratification depth

The stratification of dendrites in the IPL into one of the 5 layers identifies a cell as either ON or OFF in nature (Dowling 2012). This metric is also used in the classification of RGCs into morphological types (Sun et al. 2002a). Dendritic stratification depth was measured in by re-slicing the z-stack image to the x,z,y plane. The total thickness of the IPL was measured as the distance between GCL and INL nuclei (Figure 2.6 Panel D). The distance from the GCL to dendritic tips was then expressed as a percentage of the IPL thickness. RGCs whose dendrites stratified at >40% were classified as On RGCs.

Chapter 3: RGC classification in disease

3.1 Introduction

The study of RGC morphology is vital in the understanding of glaucoma and other inner retinal degenerative diseases. RGC morphology, concomitant with function, provides a correlate for the mechanism of visual decline. The morphological differences between functionally discrete RGC types are more subtle in the rodents than the well-defined primate RGCs. Therefore, classification has tended towards the grouping of cells based on the size, branching density and stratification of the dendritic tree in the mouse (Sun et al. 2002b; Coombs et al. 2006) and rat (Huxlin and Goodchild 1997; Sun et al. 2002a). RGC classification in retinal degenerative diseases, where the dendritic architecture (including dendritic field size and branching density) is altered (Weber et al. 1998; Shou et al. 2003; Leung et al. 2011; Kalesnykas et al. 2012; Feng et al. 2013), is thus problematic. Without classification, bias in the labelling of any given RGC type could show artifactual shrinkage or recovery of the dendritic tree in disease based on either the physiological difference in morphology or type susceptibility (Weber et al. 1998; Shou et al. 2003; Feng et al. 2013; El-Danaf and Huberman 2015).

RGCs can also be classified by immunohistochemical and genetic means. The former, is limited in that only a few type specific labels are available. Thy1 and Brn3 label all RGC indiscriminately (Barnstable and Drager 1984; Nadal-Nicolas et al. 2009), whereas SIM-32 labels a subset (RGC_A) more intensely than other RGCs (Sanes and Masland 2015). Antibodies directed against melanopsin and CART can discriminate the group of 5 melanopsin containing RGCs and the bistratified ON-OFF DSGCs respectively. A number of genetic models now selectively label certain RGC types including RGC_A in *Kcng4-cre;Thy1-stop-YFP* transgenic mice, local edge detector RGCs in *TYW3* transgene mice (*JAM-B-CreER;Thy1-STOP-YFP*) and ON DSGCs in *Homeobox d10-GFP* transgenic mice (Yonehara et al. 2009;

Dhande et al. 2013; Duan et al. 2015). However, these mostly rely on Thy1 promoters to selectively express fluorescent proteins in RGCs and Thy1 is known to be downregulated early in glaucoma (Schlamp et al. 2001; Huang et al. 2006). The discrepancy between the observed morphology of Thy1 driven fluorescent labelling and diolistic labelling in glaucoma was shown by Williams *et al.* (2013). RGCs showed significantly reduced branching densities when viewed by YFP compared to DiO demonstrating that Thy1.YFP expression was compromised and did not reveal the dendritic tree in its entirety. As the use of fluorescent dyes such as in diolistics is not contingent on cell health, morphological classification represents the best method to classify RGCs at present. The possibility that a robust RGC classification system can be derived from dendrite features that are relatively resistant to the effects of early disease was explored, based on the observation that early to moderate RGC damage consistently affects distal dendrites, leaving more proximal dendritic structures intact (Weber et al. 1998; Morgan et al. 2006; Williams et al. 2013). This concept is illustrated in Figure 3.1 based on modelling of typical Sholl profiles in normal and diseased retina. The new classification system was based on the RGC types defined by Sun *et al.* (2002a) which represent the most complete classification of rat RGCs. RGCs were classified into RGC_A, RGC_B, RGC_C and RGC_D groups. These types and subtypes are summarised in table 3.1. RGC_A are typically large cells with large somas and dendritic fields. Their dendrites branch radially and at regular distances and give a moderate branching density. RGC_B are typically small cells with small somas and small, densely branched dendritic fields which are often asymmetric. RGC_C soma and dendritic fields are typically sized between RGC_A and RGC_B, they branch radially but at a greater density and with a more irregular branching pattern and more curved dendrites than RGC_A. RGC_D are also of moderate size and are easily identified by their bistratified dendritic tree.

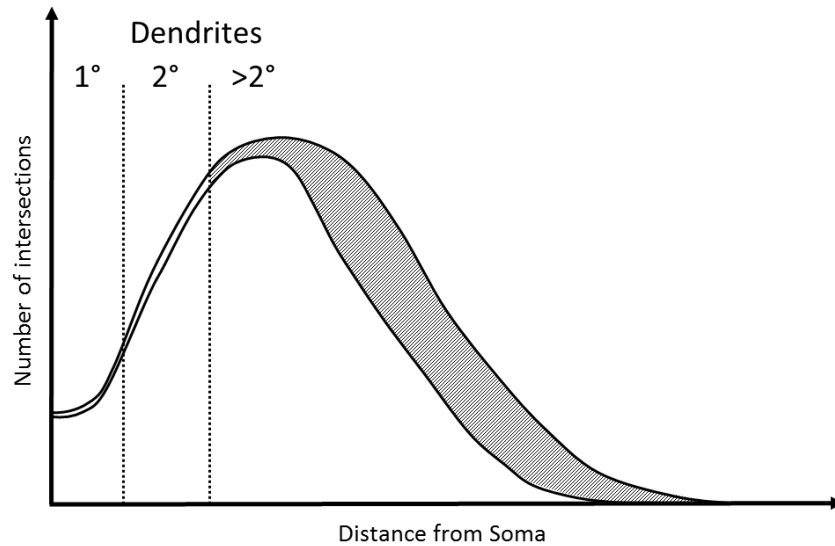


Fig 3.1 Sholl plot model: normal and diseased cells. Graphical representation of a Sholl plot from healthy and degenerate RGCs as observed in Weber *et al.*, (1998), Morgan *et al.*, (2006) and Williams *et al.*, (2013). Under moderate degeneration Sholl plots show significant deviation from healthy plots distal to the soma, with little deviation proximal to the soma. The difference between healthy and diseased sholl profiles is highlighted by the gray shaded area. Primary and secondary dendrites occur within this proximal region and are therefore more likely preserved. Measurements of primary and secondary dendrites may therefore provide robust and stable classification criteria.

Table 3.1 Sun *et al.* (2002a) classification parameters

Type	Subtype	Soma size (μm) Mean \pm SD <i>Range</i>	DF diam. (μm) Mean \pm SD <i>Range</i>	Stratification (% of IPL depth) Mean \pm SD
RGC _A	A1	24\pm3 <i>18-32</i>	310\pm71 <i>142-430</i>	79 \pm 7
	A2i	23\pm5	294\pm55	35 \pm 14
	A2o	<i>12-32</i>	<i>182-391</i>	78 \pm 7
RGC _B	B1	17\pm3 <i>11-23</i>	165\pm31 <i>120-224</i>	41 \pm 12
	B2	14\pm2 <i>11-18</i>	135\pm23 <i>66-178</i>	52 \pm 8
	B3i	16\pm3	181\pm41	41 \pm 14
	B3o	<i>10-25</i>	<i>110-284</i>	81 \pm 5
	B4	15\pm2 <i>10-20</i>	156\pm35 <i>72-219</i>	36 \pm 16
RGC _C	C1	17\pm2 <i>12-21</i>	306\pm81 <i>168-467</i>	74 \pm 10
	C2i	16\pm2	239\pm46	46 \pm 13
	C2o	<i>11-21</i>	<i>145-321</i>	78 \pm 9
	C3	15\pm3 <i>10-21</i>	239\pm78 <i>127-455</i>	77 \pm 10
	C4i	15\pm3	224\pm47	49 \pm 12
	C4o	<i>8-21</i>	<i>139-320</i>	80 \pm 7
RGC _D	D1	15\pm5 <i>8-25</i>	151\pm31 <i>93-203</i>	38 \pm 17/62 \pm 12*
	D2	15\pm3 <i>8-21</i>	224\pm47 <i>98-334</i>	38 \pm 12/64 \pm 9*

RGCs labelled with Inner (i) and outer (o) represent cells that are morphologically similar other than the retinal lamina in which they stratify (i= sublamina b/ON; o= sublamina a/OFF). *RGC_D are bistratified.

3.1.1 Hypothesis

A new set of parameters based on primary and secondary dendrite features can be used to indicate the class composition of a population of labelled RGCs.

3.1.2 Aims

1. To find new parameters of primary and secondary dendrite features that can describe RGC types that would be resistant to the effects of early dendritic degeneration.
2. To derive a classification model based on these variables that is validated against a current morphological classification (Sun et al. 2002a) based on the entire dendritic field.

3.2 Methods

3.2.1 DiOlistics labelling and imaging

DiOlistic labelling was conducted as described in section 2.3. Briefly, 15 BNs (5 months) were killed; their retinas dissected and labelled Diolistically with DiO and DiI. Following 30mins incubation at 37°C, 4% CO₂, retinas were fixed in 4% PFA, and TOPRO-3 nuclear stain applied. Single RGCs were imaged on a Zeiss LSM 510 confocal microscope as described in section 2.7.1. The eccentricity of each imaged RGC relative to the optic nerve head was recorded using the stepper stage on the confocal microscope which is accurate to 1µm. Only RGCs with a dendritic tree easily distinguishable from other cells and whose primary dendrite origins at the soma were not obscured were included for analysis.

3.2.2 New measurements

All measurements were conducted on z-collapsed images using Image J unless otherwise stated. The following dendrite parameters were determined:

3.2.2.1 Primary dendrite features

The following primary dendrite features were measured:

- The number of primary dendrites (PD) – dendrites originating directly from the soma.
- Mean primary dendrite length (PDL) - the distance from the soma to the primary branch point was measured for each primary dendrite using the simple neurite tracer plugin (Longair et al. 2011) in Fiji (Schindelin et al. 2012) and a mean distance given for each cell.
- Primary branch point field (PBPF) area - the primary branch points were connected and the area of the resultant field measured to give the PBPF area.

- PBPF centre of gravity offset (CGO) from the soma - as a measure of asymmetry in the dendritic tree the PBPF's centre of gravity offset from the soma was measured. The PBPF centroid was found and its distance from the soma centre measured. This was expressed as a percentage of the diameter of the PBPF to account for RGC size variation.
- PD distribution - as a further measure of asymmetry, the distribution of primary dendrites about 360° of the cell soma was measured using the oval profile plugin in Image J (NIH). A circle with a radius of 25µm from the soma centre was drawn, and the angle at which each primary dendrite intersected the circle measured. The angle formed between the primary dendrite immediately clockwise and counter clockwise of the axon was taken so that a larger angle would represent greater asymmetry in the PBPF.
- PD cross-sectional area – as a measure of primary dendrite thickness at the origin from the soma, primary dendrite traces derived from the simple neurite tracer plugin were re-sliced (to either ZX or ZY) to give a cross-sectional view and the area at the origin measured.
- PD Feret diameter – As a further measure of dendrite thickness, the minimum and maximum Feret diameters of the re-sliced dendrite were measured.

3.2.2.2 Secondary dendrite features

The following secondary dendrite features were measured:

- Secondary branch point field (SBPF) area – measured as with PBPF area
- SBPF centre of gravity offset (CGO) from the soma – measured as with PBPF CGO
- Proximal branching density – as a measure of branching density in the proximal dendritic tree the PBPF area was expressed as a percentage of the SBPF area.

3.2.2.3 Other features

To increase the likelihood of successful classification, other features that should remain resistant to early degeneration were measured. The following features were measured:

- Soma diameter – calculated assuming that the measured soma area was circular
- RGC eccentricity – the distance of the RGC soma (as recorded during imaging) from the ONH expressed as a vector length.

3.2.3 Sun classification

RGCs were classified according to (Sun et al. 2002a) on the basis of dendritic field diameter, dendrite stratification within the IPL, soma diameter and branching density as shown in table 3.1. Sholl analysis using FastSholl (Gutierrez and Davies 2007) plug-in for MATLAB (MathWorks) was conducted on all cells. For each of the resulting groups, the mean and SD of each new variable was calculated (see appendix A).

3.2.4 Principal component analysis

RGCs were first randomly assigned two one of either a training data sample or hold-out sample. Each RGC was assigned a random number from a chi-square distribution with 1 degree of freedom using the random number generator function in SPSS (version 18.0, IBM). The numbers were then sorted in ascending order with the first 30 RGCs assigned to a hold-out sample and the remaining 101 RGCs to the training sample. A principal component analysis (PCA) was performed in SPSS to reveal which variables were useful in discriminating RGC types. For PCA, no group variables are defined and variance between the whole population is analysed. In this way, variables that contribute highly to population variance are identified and those that do not can be discarded. PCA provides more meaningful results with correlation between variables. Therefore, Pearson's correlation and Spearman's rank tests (SPSS) were performed on normally and non-normally distributed variables respectively. New variables which showed a significant correlation ($P < 0.05$) to at least $\frac{3}{4}$ of total variables were included. A PCA with extraction of Eigenvalues greater than 1 through an oblique (promax) rotation with Kaiser normalisation was performed on the training sample including only the remaining variables.

3.2.5 Discriminant analysis

A discriminant analysis (SPSS) was performed in order to reveal if the new parameters could classify RGCs into the same groupings as Sun *et al.* (2002a). For the analysis, each RGC was assigned a group (according to (Sun et al. 2002a)). Prior probability for each of these groups was calculated based on group percentages of the training sample population to account for frequency of RGC types among a population. The analysis was run so that the RGC types were defined based on the new variables from the training sample (n=101) and then used to discern the RGC type of each cell in the hold-out sample (n=30). The ability of the new variables to discriminate RGC type was adjudged based on the percentage of correctly classified cells.

3.3 Results

3.3.1 Classification according to Sun

One-hundred and thirty one RGCs from 20 retinas imaged were included in the analysis based on the described exclusion criteria. Typical cells for each of the 4 classes are shown in Figure 3.2. The mean Sholl profile for each RGC type is plotted in Figure 3.3. Classification according to (Sun et al. 2002a) criteria gave comparable percentages of cell types in the overall population, summarised in Table 3.2. Our sample therefore provides a similar breakdown of the RGC population for the derivation of classification parameters.

Table 3.2 Percentage of RGC types in sample

	RGC type (% of total number of RGCs)			
	RGC _A	RGC _B	RGC _C	RGC _D
Present study	24	29	32	15
Sun <i>et al.</i> (2002a)	18	29	35	18

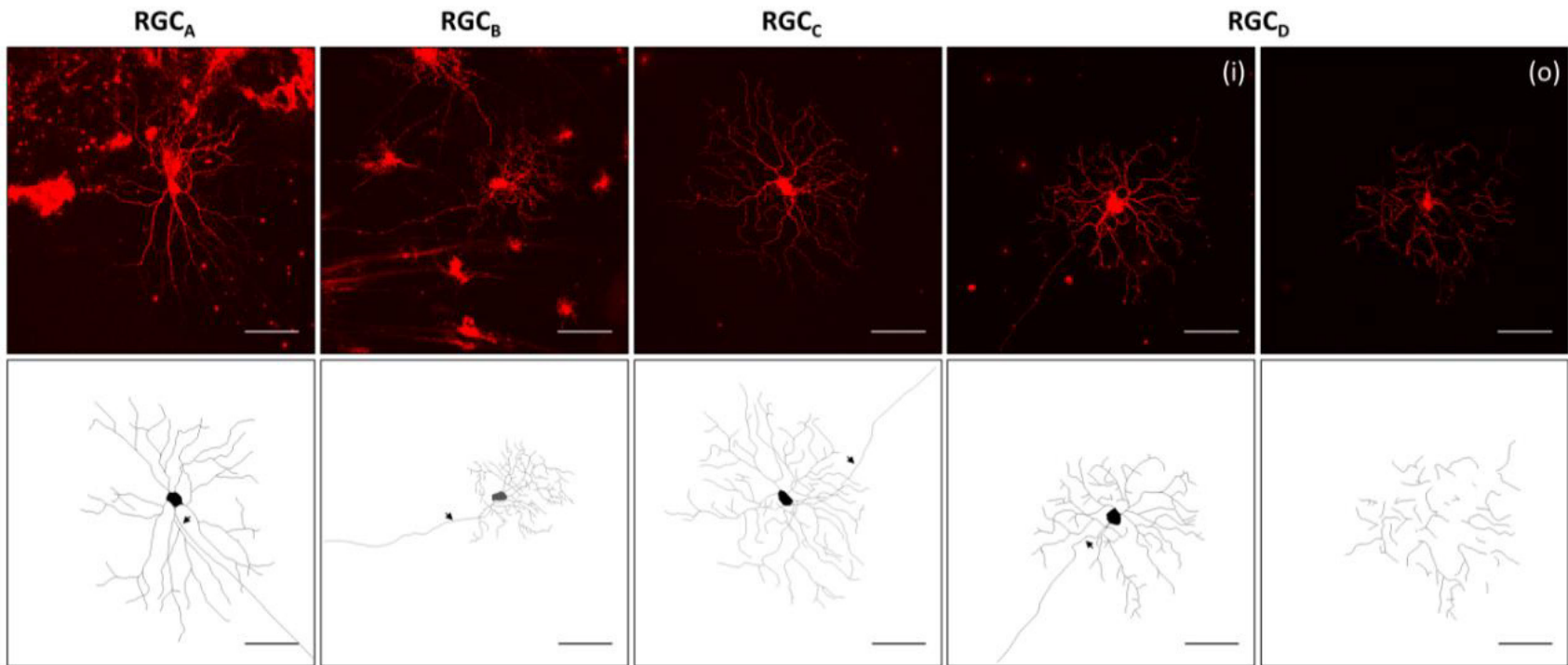


Fig 3.2 RGC types. Z-compressed confocal images and tracings of RGCs of each type demonstrating typical morphology. Bistratified RGC_D is depicted as inner (i) and outer (o) IPL stratifications. Arrows denote axon. Scale bar = 100 μ m

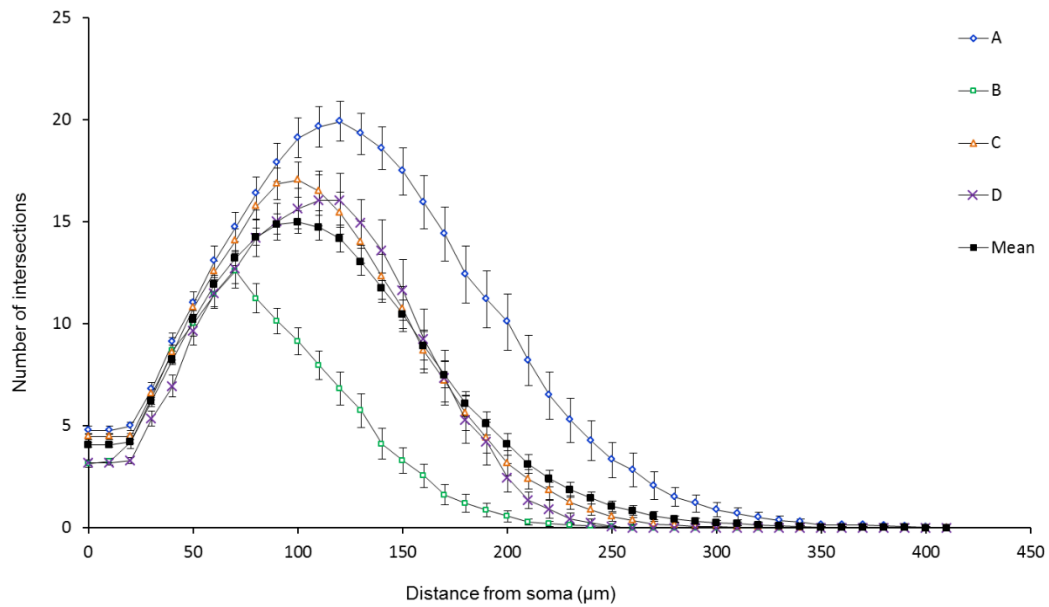


Figure 3.3 Variation of Sholl plots between RGC types. Sholl plots of RGCs grouped according to type reveals the variation within the pooled population when compared to the mean Sholl plot. These highlight how analysis of an unclassified population of RGCs could suffer from intrinsic bias through disproportionate numbers of cell types; the leftward shift observed in degeneration (see figure 3.1) is also seen here when comparing healthy types. Error bars show SEM.

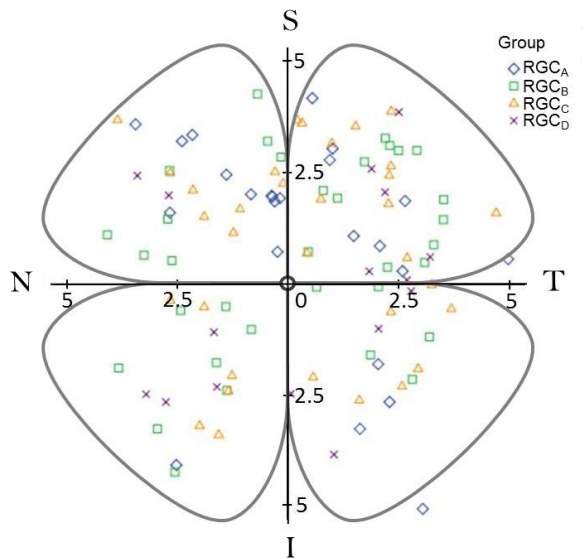


Figure 3.4 Distribution of recorded RGCs. Retinal eccentricity of 114 RGCs shown as distance (mm) from the ONH. No one RGC type appears localised to a particular retinal quadrant or eccentricity demonstrating minimal regional labelling biases in DiOlistic labelling.

3.3.2 Retinal eccentricity does not affect classification

The retinal locations of 114 RGCs are shown in Figure 3.4 (the locations of 26 cells were not measured). One-way ANOVA with post-hoc Bonferroni showed no significant difference between RGC types with respect to retinal eccentricity when expressed as vector length ($P > 0.05$). This confirmed that labelling was not regionally biased. RGC distance from the ONH centre expressed as distance in x, y plane and vector distance all showed no correlation ($P > 0.05$) to any new variables or to dendritic field diameter and soma diameter demonstrating that retinal eccentricity had no effect on variable measurements and no effect on classification according to (Sun et al. 2002a)

3.3.3 RGCs differ in size and asymmetry of the proximal dendritic tree

RGC distance from the ONH in the x and y plane and as vector length were all discarded as variables for PCA due to the lack of correlation (as discussed in section 3.2.4). Primary dendrite length and proximal branching density showed a significant correlation with fewer than half of the total variables ($P > 0.05$) and so were excluded from PCA. The remaining variables all showed a significant correlation ($P < 0.05$) to at least $\frac{1}{4}$ of total variables and so were included. A Kaiser Myer Olkin measure of sampling adequacy (0.844) indicated a sufficiently large sample size while Bartlett's test of sphericity ($P = 0.0001$) allowed rejection of the null hypothesis that the correlation matrix was an identity matrix. PCA produced a 3 component solution that accounted for 77.1% of the variance within the data. The rotated pattern matrix showing the variables contributions to the components is shown in Table 3.3. The first component comprised soma diameter, primary dendrite cross-sectional area and min and max Feret and accounted for 45.5% of the variance in the data. This component represents the size of the RGC soma and primary dendrite thickness. The second component comprised the number of primary dendrites and PBPF and SBPF areas representing proximal dendritic tree size (accounting for 21.2% of the variance). The third component comprised both PBPF and SBPF CGO and PD range (accounting for 10.4% of the variance) thus representing asymmetry in the proximal dendritic tree. The contribution of the individual variables to the 3 dimensional separation of the RGC population is shown in Figure 3.5.

Table 3.3 PCA rotated pattern matrix

Variable	Rotated pattern matrix		
	Component 1	Component 2	Component 3
Soma diameter	0.713	0.296	-0.31
PD max feret	0.991	-0.047	-0.009
PD min feret	0.974	-0.027	-0.045
PD cross-sectional area	0.989	-0.024	0.007
PBPF area	0.042	0.852	0.103
SBPF area	0.097	0.864	0.176
PDN	-0.118	0.715	-0.199
PD asymmetry	0.074	-0.495	0.520
PBPF CGO	-0.080	0.064	0.871
SBPF CGO	-0.013	0.110	0.928

Bold text denotes component to which each variable gives its greatest contribution

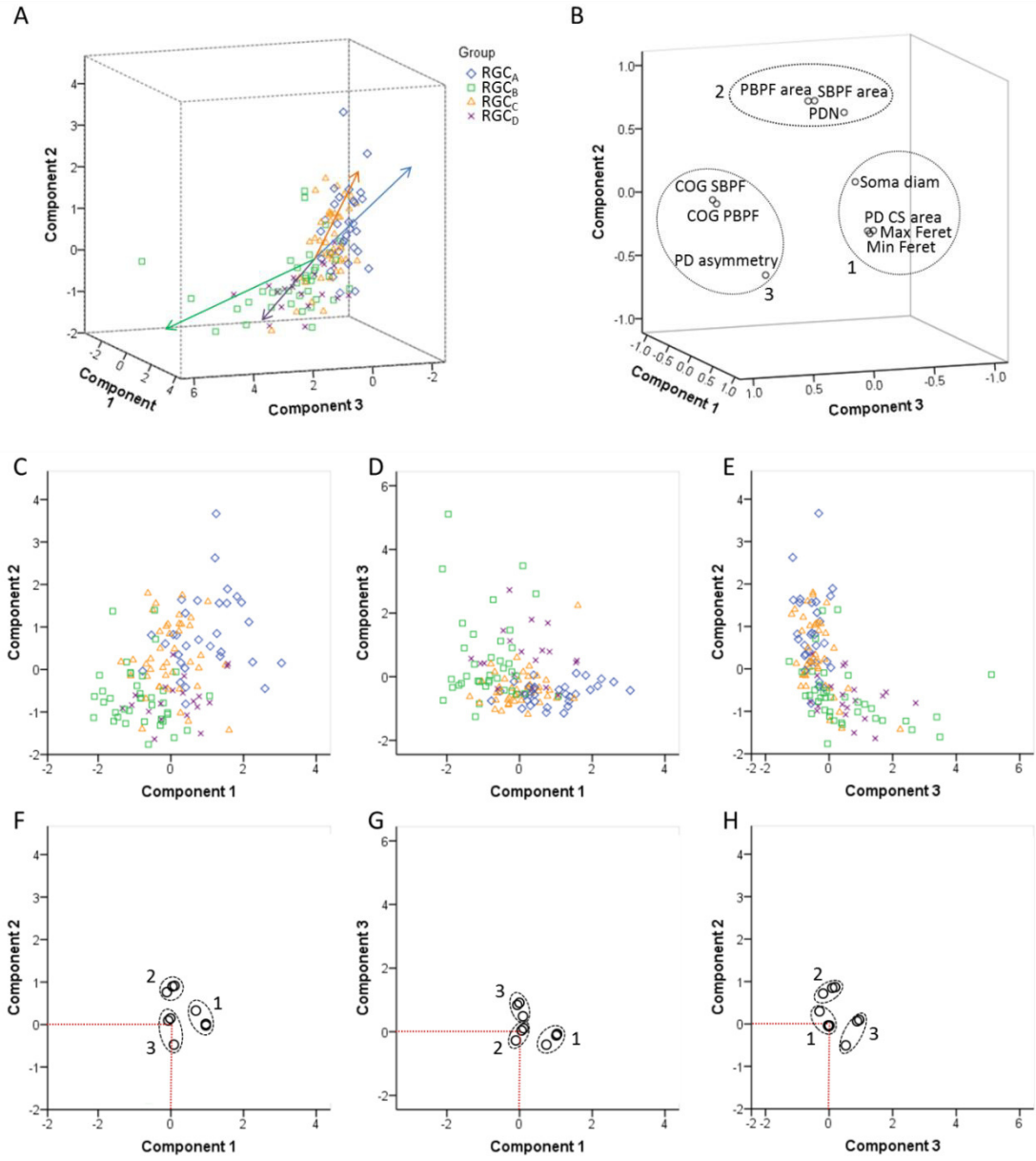


Figure 3.5 Principle component analysis of RGCs. Figure legend overlaid.

Figure 3.5 Principle component analysis of RGCs. The component scores of each RGC ($n=131$) for the 3 components are plotted in X, Y and Z dimensions (**A**, **C**, **D** and **E**). When labelled according to type (RGC_A =blue, RGC_B =green, RGC_C =orange, RGC_D =purple), separation of the population into RGC types along the components can be observed. The contribution of the individual variables to this separation can be seen when the variable's weightings towards each component are plotted in the same rotated space (**B**, **F**, **G** and **H**). The components represent condensed variables derived from correlated/co-varying variables (those encompassed by broken lines). Plots **C**, **D** and **E** are projected to only X and Y planes in order to demonstrate the distribution of the groups along individual components. The contribution of the variables to this distribution is shown by the weightings plotted underneath (**F**, **G** and **H**); the component that sits at 0,0 (as shown by the red broken lines) shows little contribution from its constituent variables to the separation. RGC soma and proximal dendritic field size, where $RGC_A > RGC_C > RGC_D > RGC_B$, can be seen in the population distribution across Components 1 and 2 (**C** and **F**). Here RGC groups are partially separated. Further separation of RGC_B and RGC_D from RGC_A and RGC_C is achieved along the 3rd component through higher asymmetry in the proximal dendritic field (**D** and **G**, **E** and **H**).

3.3.3 Discriminant analysis

RGC groups were separated by 3 discriminant functions. The loadings of the individual variables onto the discriminant functions are shown in table 3.4. The first discriminant function accounted for 71.7% of between group variance within the data and describes RGC proximal dendritic tree size and symmetry and, soma size and dendrite thickness. It correlated positively with soma diameter, primary dendrite cross-sectional area, min and max Feret, SBPF area and number of PDs. The first discriminant function also showed a negative correlation with PD range. The second discriminant function (which accounted for 22.2% of the remaining between group variance) correlated positively with PBPF CGO, describing asymmetry in the proximal dendritic field, with a contribution from soma and dendrite thickness. The third discriminant function accounting for the remaining 6.2% of between group variance; the function showed a negative correlation to SBPF CGO and a positive correlation to PBPF area. The largest determinant of RGC classification is therefore primary dendrite thickness and soma and proximal dendritic tree size, with a smaller contribution of asymmetry of the proximal dendritic tree. This is evident in the clear separation of the group centroids (table 3.5) where the first discriminant function separates all RGC types in order of size (where $RGC_A > RGC_C > RGC_D > RGC_B$). The separation was achieved due to the significant difference of the centroids between RGC groups ($P < 0.001$). A Chi-square statistical test of the discriminant functions showed that function 3 gave no additional discriminating ability ($P = 0.176$) and so does not contribute to the separation of RGC groups.

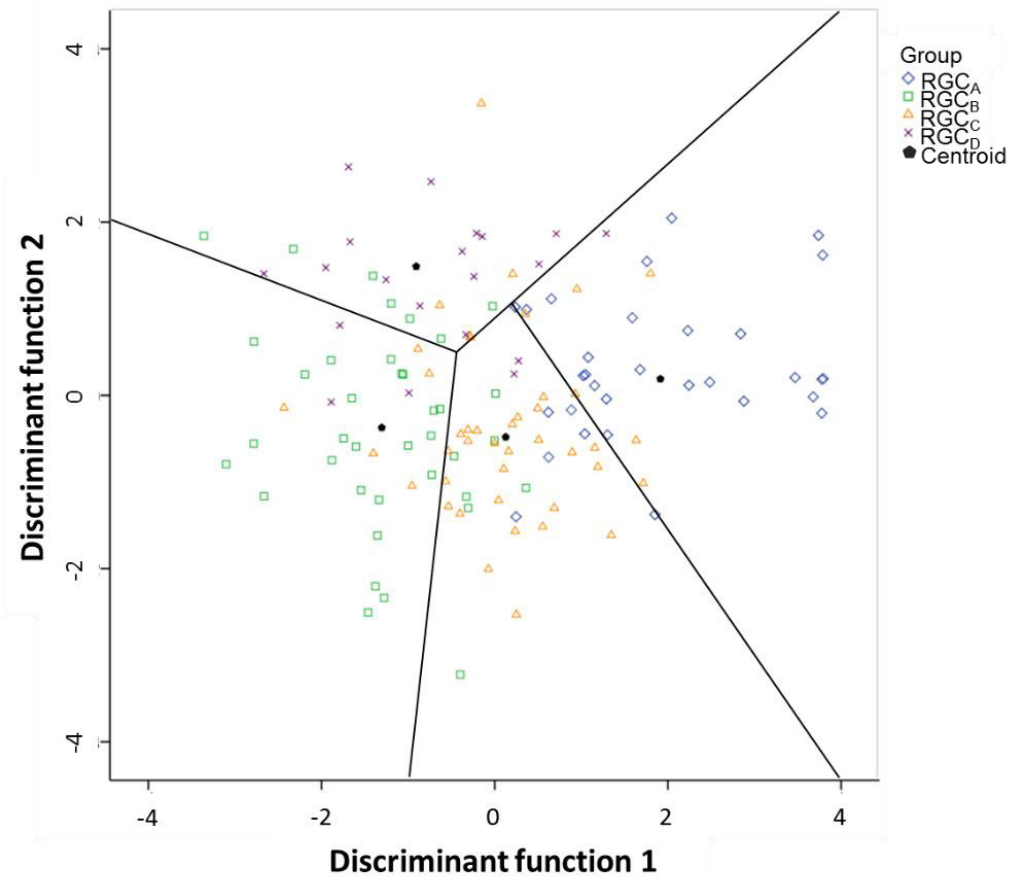


Figure 3.6 Discriminant analysis of RGCs. The discriminant scores of each RGC (n=131) are plotted in X, Y dimensions corresponding to the first two discriminant functions. Here variance between groups is maximised so that group centroids (black pentagons) are at maximal distance from each other. Individual RGCs are classified into the group whose centroid is closest (the black lines define the approximate boundaries for each group). When labelled according to type it can be seen that the majority of RGCs are correctly classified to their group by the discriminant functions.

Table 3.4 Correlations between variables and discriminant functions

Variable	Structure matrix		
	Function 1	Function 2	Function 3
Soma diameter	0.619	0.361	0.183
PD max feret	0.525	0.378	0.107
PD min feret	0.543	0.467	0.199
PD cross-sectional area	0.566	0.416	-0.028
PBPF area	0.300	-0.353	0.560
SBPF area	0.487	-0.131	0.088
PDN	0.481	-0.268	0.067
PD asymmetry	-0.552	0.483	-0.233
PBPF CGO	-0.326	0.450	-0.302
SBPF CGO	-0.328	0.119	-0.605

Bold text denotes function to which each variable gives its greatest contribution

Table 3.5 RGC group Centroid

Group	Group Centroids		
	Function 1	Function 2	Function 3
RGC _A	1.912	0.189	-0.284
RGC _B	-1.306	-0.373	-0.379
RGC _C	0.126	-0.048	0.427
RGC _D	-0.908	1.488	0.194

3.3.4 RGC types are discriminated by proximal dendritic morphology

The discriminant functions generated through discriminant analysis correctly classified 73.3% (n=74) of RGCs from the training sample and 63.3% (n=19) from the hold out sample. This was greater than the correct by-chance classification of 25%. The predicted group percentages for each RGC type are summarised in table 3.6. These data show that RGC groups can usefully be discriminated by primary and secondary dendrite variables. Misclassification followed a similar trend with roughly 25% misclassified to the RGC type closest in morphology to the correct group. All misclassified RGCs had at least 1 variable (average 3 variables) that was greater than 1 standard deviation from the mean of its correct type.

3.3.5 Population variance in new parameters does not adequately define groups

The relationship between population wide variance and between group variance was explored. The component scores generated through PCA were used as variables for discriminant analysis. The components alone achieved only a correct classification in 62.6% of the training sample and 60% of the hold out sample. This indicates that population variance in morphology does not adequately describe the difference between groups.

3.3.6 RGC subgroups cannot be differentiated

The difference in population variance and between group variance could be driven by the division of RGCs in subgroups. Discriminant analysis was performed as described initially but where RGCs were grouped according to the subgroups described by Sun *et al.* (2002a). The original hold-out sample did not contain two of the subgroups and so the sample size was increased to 40 RGCs following the same random assignment method (section 3.2.4). Again, prior probability was calculated based on subgroup frequency. Correctly classification was

achieved in 53.8% (n=49) of RGCs from the training sample and 35% (n=14) from the hold out sample. This was greater than the correct by chance classification (8.3%) but did not give an adequate classification indicating that the ability to resolve subgroups is beyond the new variables.

Table 3.6 Summary of classification

	<i>A priori</i> RGC type	Predicted RGC type (% correct)				Number of <i>A priori</i> RGC
		RGC _A	RGC _B	RGC _C	RGC _D	
Training sample (n=101)	RGC _A	75%	0%	25%	0%	24
	RGC _B	0%	64%	25%	11%	28
	RGC _C	6%	12%	77%	6%	34
	RGC _D	7%	13%	0%	80%	15
	Number of predicted RGC	21	24	39	17	
Hold-out sample (n=30)	RGC _A	71%	0%	29%	0%	7
	RGC _B	0%	70%	20%	10%	10
	RGC _C	25%	0%	63%	12.5%	8
	RGC _D	0%	0%	60%	40%	5
	Number of predicted RGC	7	7	12	4	

3.4 Discussion

These data show that RGCs can be discriminated on the basis of soma and proximal dendritic field size. This is in agreement with (Sun et al. 2002a) and other classifications based on RGC morphology (Sun et al. 2002b; Coombs et al. 2006) where larger RGC_A and RGC_C are separated from the smaller RGC_B and RGC_D based on soma and dendritic field size. Dendrite thickness is also an effective parameter for classifying RGC types due to its strong relationship with other features of dendritic tree morphology. Primary dendrite thickness has been found to correlate with soma size, dendritic field size, total dendritic length and branching density in rat triceps surae motoneurons (Chen and Wolpaw 1994) and cat spinal α - and γ -motoneurons (Ulfhake and Cullheim 1981; Ulfhake and Kellerth 1981), all parameters used in the classification of RGC types. Secondary dendrite thickness, at the origin of the primary branch point, was also shown to correlate to dendritic field size in mouse RGCs (Loopuijt *et al.* 2007). However, its subsequent use in a classification model including total number of branch points, stratification and eccentricity yielded only 9 different types of RGC, none of which the authors cared to compare to previously reported types (Loopuijt et al. 2007). Asymmetry in the proximal dendritic tree has a small discriminatory effect on RGC types; a parameter that is often overlooked in morphological analysis.

Given the large variability in RGC morphology and overlap between groups for any single morphological criterion, complete neuronal classification would prove challenging. Consistent with this, all misclassified RGCs exhibited one or more variable measurement greater than 1SD from the mean of its type. Interestingly, the same problem was reported by (Jelinek and Fernandez 1998) when classifying cat RGCs based on fractal dimension where discriminant analysis returned 62.3% correct classification. The inclusion of dendritic stratification depth within the IPL could enhance the correct classification of RGC types, in

particular the classification of RGC_D due to their bistratified dendritic tree. Population wide variance does not describe between group variance. This was attributed to the subdivision of the groups into further discrete RGC types. However, the new parameters only achieved a correct classification of 35% based on the subgroups described by (Sun et al. 2002a). This would likely increase given a larger population from which to construct a more representative model. It is also possible that the misclassified atypical cells represent previously unidentified cell types given that the number of RGC types currently defined in the closely related mouse is 22 (Voelgyi et al. 2009).

Robust discrimination between cell types is important in the study of degeneration, both in terms of reducing pseudo-degenerative effects owing to inter-type differences in dendritic morphology and also in investigating inter-type susceptibility to disease. Type specific degeneration has been noted in the primate (Weber et al. 1998), cat (Shou et al. 2003), mouse (Leung et al. 2011; Feng et al. 2013; El-Danaf and Huberman 2015) and rat (Thanos 1988) but not in DBA/2J (Jakobs *et al.* 2005) or thy1-YFP-H transgenic mice with experimental glaucoma (Kalesnykas et al. 2012). The Sholl plots in Figure 3.3 demonstrate the differences in branching pattern and density between RGC types and illustrate effectively how disparity in cell types between populations could be confused for atrophy in studies of degeneration. Given that significant reduction in branching occurs only in the distal region of the dendritic tree, as illustrated in Figure 3.1, and that the soma only undergoes substantial change with advanced/chronic glaucoma (Weber et al. 1998) the new parameters should remain relatively robust. However, the ability of the system to classify cell types will likely diminish under substantial degeneration.

The use of DiOlistic labelling resulted in a number of cells being excluded from analysis as the soma and proximal dendrites were obscured. However DiOlistic labelling is not contingent on cell health (Honig and Hume 1986). This is vital given that the classifications purpose is for use in degeneration where Biolistics is affected by the viability of transcriptional pathways necessary for the expression of fluorescent markers (Williams et al. 2013). Ballistic labelling techniques are open to the criticism that they bias for larger cell types since the likelihood of a hitting a cell increases with its size. This bias was not observed suggesting that the difference in cell soma size is insufficient to have a large effect on labelling probability. A higher proportion of RGC_A (at 24%) was found in comparisons to the 18% reported by (Sun et al. 2002a); however this was much smaller than the 60% previously reported (Huxlin and Goodchild 1997). If soma size were the largest determinant of a given cell being labelled one would expect a higher proportion of RGC_A than RGC_B; almost twice as many RGC_B to RGC_A were labelled in this study.

The reproducibility of this model and its applicability to disease requires testing on a range of degenerated RGC populations, the scope of which was beyond the current study. However, applying the model to a degenerated population of RGCs would not serve to validate the model given that the correct type of an RGC cannot be determined from its post-degenerative morphology. This would instead require following the degeneration of single RGCs over time while accounting for reporter expression changes in degeneration.

The main role of this classification procedure is therefore not the definitive classification of all RGC types but to provide a degree of confidence regarding RGC proportions in a sample population where traditional methods of classification are vulnerable to bias. The model provides a framework to check for labelling bias in the analysis of RGCs in retinal disease.

Chapter 4: Synaptic loss in experimental glaucoma

4.1 Introduction

Synaptic loss has been detected in a number of experimental glaucoma models (Fu et al. 2009; Della Santina et al. 2013). As dendrites are atrophied the RGC will lose synaptic contact with underlying bipolar cells. Whether synaptic loss precedes, and is a driver for, or is a consequence of dendritic loss is unknown (Lee *et al.* 2011). In other neurodegenerative diseases mitochondrial dysfunction leads to synaptic and dendritic loss (Williams et al. 2010; Reddy *et al.* 2012; Williams *et al.* 2012). C1q has been shown to be important in RGC synapse elimination during the period of synaptic refinement. C1q is localised to synapses in development and C1qKO mice show impaired synaptic refinement within the Lateral geniculate nucleus (dLGN). At P5, C1qKO mice showed normal dLGN projections but significantly higher numbers of contralateral projections at P10 and persisting to P30 when segregation is normally complete and the mouse dLGN is dominantly ipsilateral. There was no increase in the number of cells, while the normal phenotype at P5 suggested no disruption to axon-pathfinding, which are indicative of a failure in synaptic refinement. At P40, 80% of dLGN neurons remained multiply innervated (compared to 0% in WT) as detected by patch-clamping, again indicating a failure to eliminate synapses. (Stevens *et al.* 2007). These data show the relationship between the classical complement pathway and synapse elimination. C1q is also thought to tag synapses for clearance in disease in a similar way to development (Stevens et al. 2007).

C1q can directly bind to cell surfaces and initiate the classical pathway of the complement cascade, generating the effector molecule C3b that opsonises cells for immune clearance by phagocytosis. Early complement upregulation, in particular of C1q, has been shown in both genetic (Howell *et al.* 2011) and inducible models of experimental glaucoma (Ahmed et al. 2004; Kim et al. 2005). The increased expression of various complement proteins, in

particular C1q and C3 is also evident in human glaucoma (Kuehn et al. 2006; Tezel et al. 2010). Generation of C3a, C4a and C5a is known to enhance immune cell recruitment (Janeway et al. 2001), a feature of early glaucoma (Agudo et al. 2008; Johnson et al. 2011; Howell et al. 2012), and enhance secretion of inflammatory and neurotoxic compounds from infiltrating immune cells (Janeway et al. 2001; DiScipio and Schraufstatter 2007; Woodruff et al. 2010). Inhibition of components of the complement cascade has shown promise in reducing RGC death in glaucoma. C1q deficient DBA2J mice show reduced RGC death compared to age matched DBA2Js (Howell et al. 2011), while restoring normal C5 levels to the naturally C5 deficient DBA2J exacerbates glaucomatous cell loss (Howell et al. 2013). Given the role of C1q in synapse elimination in development, this chapter sought to investigate whether inhibition of C1q could protect against aberrant immune mediated synaptic clearance directed by the complement system.

Two experimental models of glaucoma were used to investigate whether C1q inhibition could preserve RGC dendrites and synapses. The first model used the DBA2J mouse model; in these mice mutations in the *gpnmb*⁺ and *tyrp1* genes cause iris dispersion at ~9months of age (John et al. 1998; Anderson et al. 2002). This results in a sustained IOP increase and RGC loss. The DBA/2J-*gpnmb*⁺ mouse, which has a functional *gpnmb* gene, does not develop iris dispersion, nor a raised IOP and so provides a control against which RGC damage can be assessed (Howell *et al.* 2007b). The DBA/2J-C1qa^{+/-} transgenic mouse is deficient in C1q and is generated by backcrossing C57BL6.C1qaKO mice with DBA2J mice. The DBA/2J-C1qa^{+/-} retains >99% of the DBA2J genetic background, and does not generate significantly different IOP profiles to the DBA2J (Howell et al. 2011) and so the effects of complement deficiency on RGC dendritic and synaptic loss could be investigated using this mouse. Given the role of C1q in synaptic refinement, it was important to preclude the possibility that any difference in dendritic and synaptic measurements were not the result

of an *a priori* greater number of dendrites/synapses in the DBA/2J-C1qa^{+/-}. For this, all 3 genotypes were compared prior to the age of increased IOP onset and associated dendritic and synaptic loss. The second experimental glaucoma model used was the magnetic bead model (Samsel et al. 2011). In this model BN rats with an IOP increase were treated with exogenous C1 esterase inhibitor (C1inh) or vehicle only and the effects of subsequent complement inhibition on RGCs investigated. C1inh is found naturally in the plasma and inhibits initiation of the classical complement pathway by binding C1r:C1s causing it to dissociate from C1q (Janeway et al. 2001).

4.1.1 Hypothesis

It is hypothesised that C1 targets synapses on RGCs for immune clearance in experimental glaucoma. Inhibition of C1 via genetic modification or pharmaceutical administration could therefore protect RGCs from synaptic and dendritic loss.

4.1.2 Aims

- To determine whether C1 inhibition confers a protective effect against synaptic loss in experimental glaucoma
- To determine whether this translates to a protection of dendrites where synaptic clearance may drive dendritic loss.

4.2 Methods

4.2.1 Animal husbandry and Mouse strain and breeding

Mice were bred and housed at the Jackson Laboratories, Maine in accordance with their Institutional Biosafety Committee (IBC) and the Animal Care and Use Committee (ACUC). Mice were housed in a 14hr light/10hr dark cycle and had access to food and water *ad libitum*. DBA/2J (D2; n=24), DBA/2J-*Gpnmb*⁺ (D2-*Gpnmb*⁺; n=22), and DBA/2J-C1qa^{+/-} (D2.C1qa; n=18) strains were used. The generation of these strains is described in detail elsewhere (Howell et al. 2007b; Howell et al. 2011). Two groups of mice at either 3-5months (n=34) or 9-11months (n=30) were used. BN rat husbandry is described in section 2.1 with the exception that animals were housed in 12hr light/dark cycle. Rats were aged 5-6 month (n=27).

4.2.2 Induction of glaucoma, IOP monitoring and C1 inhibitor injection

Glaucoma was induced in the left eye of 20 animals as described in section 2.2.2. The right eye was a normotensive, un-operated control. IOPs were measured by rebound tonometry (section 2.2.1) for 3 days prior to glaucoma induction and every 3 days thereafter. One day prior to glaucoma induction rats received an intravitreal injection of either 5 μ l (100 Units/ml in PBS) of C1 esterase inhibitor (human, CINRYZE, Shire) or vehicle only (PBS) to the left eye. The injection procedure was as described in section 2.2.3. Injections were repeated every 4 days for the duration of the experiment. Rat groups are hereafter referred to as OHT (ocular hypertensive; bead injection and vehicle only intravitreal injection; n=10), OHT.C1inh (bead injection and C1inhibitor intravitreal injection, n=10) and NT.C1inh (normotensive; C1inhibitor intravitreal injection, n=7).

4.2.3 Diolistic labelling and confocal imaging of RGCs

RGCs were labelled DiOlistically to visualise dendritic morphology 2 weeks after glaucoma induction in 11 rats. Mice (n=15 D2, n=8 D2.Gpnmb+, n=10 D2.C1qa) followed the same protocol (section 2.3) as rats with the exception that death was via cervical dislocation and the gene gun firing pressure was reduced to 100psi. For mice, the head was removed during the retina incubation period and placed in Smith Rudt's solution (SR; 0.8% PFA, 1.2% Glutaraldehyde in 0.1M Phosphate Buffer) for 48hrs before dissecting the ONs. For rats, only the brain and attached ONs were placed in Smith Rudt's solution. The nerves were cut distal to the optic chiasm with a 45° cut in order to maintain orientation and stored in 0.4% PFA (in 0.1M PB) until grading. The nerves were graded as described in section 5.2.4 below. RGCs in the rat were imaged as described in section 2.5.2. For the mouse, imaging followed the same protocol with the exception of the use of a Leica TCS SP8 with a white light laser. RGC morphology was measured as described in section 2.5.3 using Sholl analysis and dendritic length and field area measurements.

4.2.4 Optic nerve grading

ON were processed for grading as described by (Smith *et al.* 2001). The tissue was prepared by immersing sequentially in 2% osmium tetroxide (in 0.1M PB), 0.1M sodium acetate and 2% uranyl acetate (in 0.1M sodium acetate). The tissue was dehydrated in graded ethanol, before embedding in resin. Sections were cut (1µm thick), dried and stained in 1% paraphenylenediamine (PPD) in isopropanol:methanol (1:1) (Smith *et al.* 2001). The myelin stain PPD differentially stains the axoplasm of damaged axons, which appear darker, compared to healthy axons. The ratio of damaged to healthy axons was qualitatively judged to categorise ONs into 'no or early' (NOE), 'moderate' (MOD) and 'severe' (SEV) gradings (Anderson *et al.* 2005). NOE ONs are indistinguishable from ONs of strains that do not develop glaucoma. MOD ONs have significant numbers of damaged and degenerated axons,

but the remaining axons appear healthy. With comparison to ON counts these ONs have approximately 90-50% of axons remaining (typically 60%). In SEV ONs, the number of damaged axons is greater than the number of healthy axons (Anderson et al. 2005). ONs were scored by two masked investigators (John Lab), and in cases where their gradings did not agree, a third investigator adjudicated with the majority grade assigned to that ON.

4.2.4 IHC for synaptic loss

In 31 mice and 9 rats, whole eyes were fixed in 4% PFA in place of DiOlistic labelling. The eyes were fixed overnight before cryo-protecting in 30% sucrose as described in section 2.4.2. Sections were processed IHC conducted as described in section 2.4.3. Briefly, sections were blocked in 5% serum following rehydration, before applying rabbit anti-PSD95 for 8 hours at 4°C. Alexaflour 488 was applied followed by Hoescht, interjected by wash steps. Slides were mounted and imaged as described in section 2.5.1 with the exception that sections in the mouse eye were imaged on a Leica TCS SP8. The mouse sections were cut to cut to 14µm and so were imaged as z-stacks with a slice thickness of 1µm. Z-compressed images were created for fluorescent intensity analysis which was conducted for both species as described in section 2.5.1.

4.3 Results

4.3.1 C1 inhibition protects against dendritic atrophy in the mouse in early glaucoma

Early loss of dendrites in the D2 mice, as shown previously (Williams et al. 2013), was confirmed. All animals were categorised as NOE and thus represent the early stage of the disease. Dendritic field area was significantly reduced in 9-11month D2 animals (n=58 RGCs, 8 animals) compared to age matched D2.Gpmnb+ (n=37 RGCs, 5 animals) (P=0.01, One-way ANOVA with post-hoc Bonferroni correction following Log10 transform) but total dendritic length (P=0.802, statistical test as before) and Sholl area under the curve (AUC) remained unchanged (P=0.208, as before). D2.C1qa animals were protected from this dendritic atrophy. No significant difference in total dendritic length, dendritic field area or Sholl AUC was found between 9-11month D2.C1qa animals (n=52 RGCs, 6 animals) compared to D2.Gpmnb+ (total dendritic length P=1, dendritic field area P=1, Sholl AUC P=1; as before). D2.C1qa animals showed significantly higher total dendritic length, dendritic field area and Sholl AUC compared to age matched D2 animals (P=0.005, P=0.001, P=0.001; as before).

Next I sought to establish whether this was the result of a protective effect, or a greater number of synapses *a priori* in the D2.C1qa animals before the onset of glaucoma, given that the dendritic atrophy in the D2 animals was mild, resulting in only partial morphological change in RGCs compared to D2.Gpmnb+. C1 plays an important role in synaptic refinement during development (Stevens et al. 2007) and so a deficiency in C1 could leave more adult synapses in the IPL in D2.C1qa animals compared to wild type. This could also result in a denser dendritic tree following a failure to clear synapses. 3-5 month D2 animals (n=63 RGCs, 7 animals) showed no significant difference in dendrite morphology to 3-5 month D2.C1qa (n=30 RGCs, 4 animals). Total dendritic length, dendritic field area and Sholl AUC showed no significant difference (P=1,

P=1, P=1 respectively, as before). The dendritic morphology in 9-11month animals was compared to that of 3-5month animals which are pre-glaucomatous. D2.C1qa animals showed no significant difference in dendritic morphology between 3-5month (n=30 RGCs, 4 animals) and 9-11month animals D2s (n=52 RGCs, 6 animals). Total dendritic length, dendritic field area and Sholl AUC showed no significant difference (P=1, P=0.111, P=0.714 respectively, as before). C1 inhibition therefore offers a mild protective effect against dendritic atrophy in the mouse.

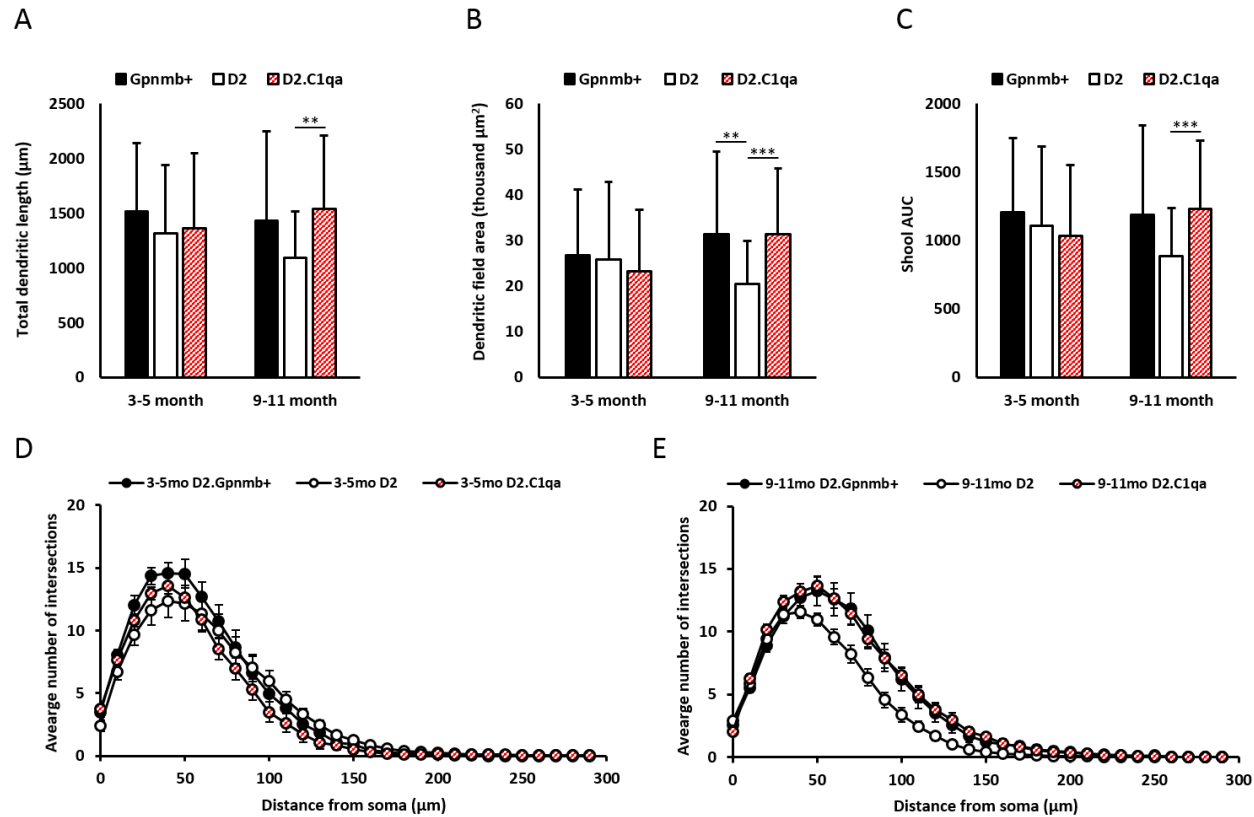


Figure 4.1 RGC morphological changes in the D2.C1 mouse. In early glaucomatous animals (9-11months) total dendritic length (A), dendritic field area (B) and Sholl AUC (C) were significantly higher in D2.C1qa than D2 animals. At 9-11 months D2.C1qa animals were not significantly different from other genotypes at 3-5 months in all dendritic morphology variables. These data suggest a moderate protective effect of C1q knockout to RGC dendrites in glaucoma. Sholl analysis shows similar profiles for pre-glaucomatous D2 animals (D) and a leftward shift for D2 animals in the early stages of glaucoma (E). For 3-5-month Gpnb+ n=27 RGCs (3 animals), D2 n=63 RGCs (7 animals), D2.C1qa n=30 RGCs (4 animals). For 9-11month Gpnb+ n=37 RGCs (5 animals), D2 n=58 RGCs (8 animals), D2.C1qa n=52 RGCs (6 animals). Error bars show SD for A, B and C and SEM for D and E. *P<0.05, **P<0.01, ***P<0.001

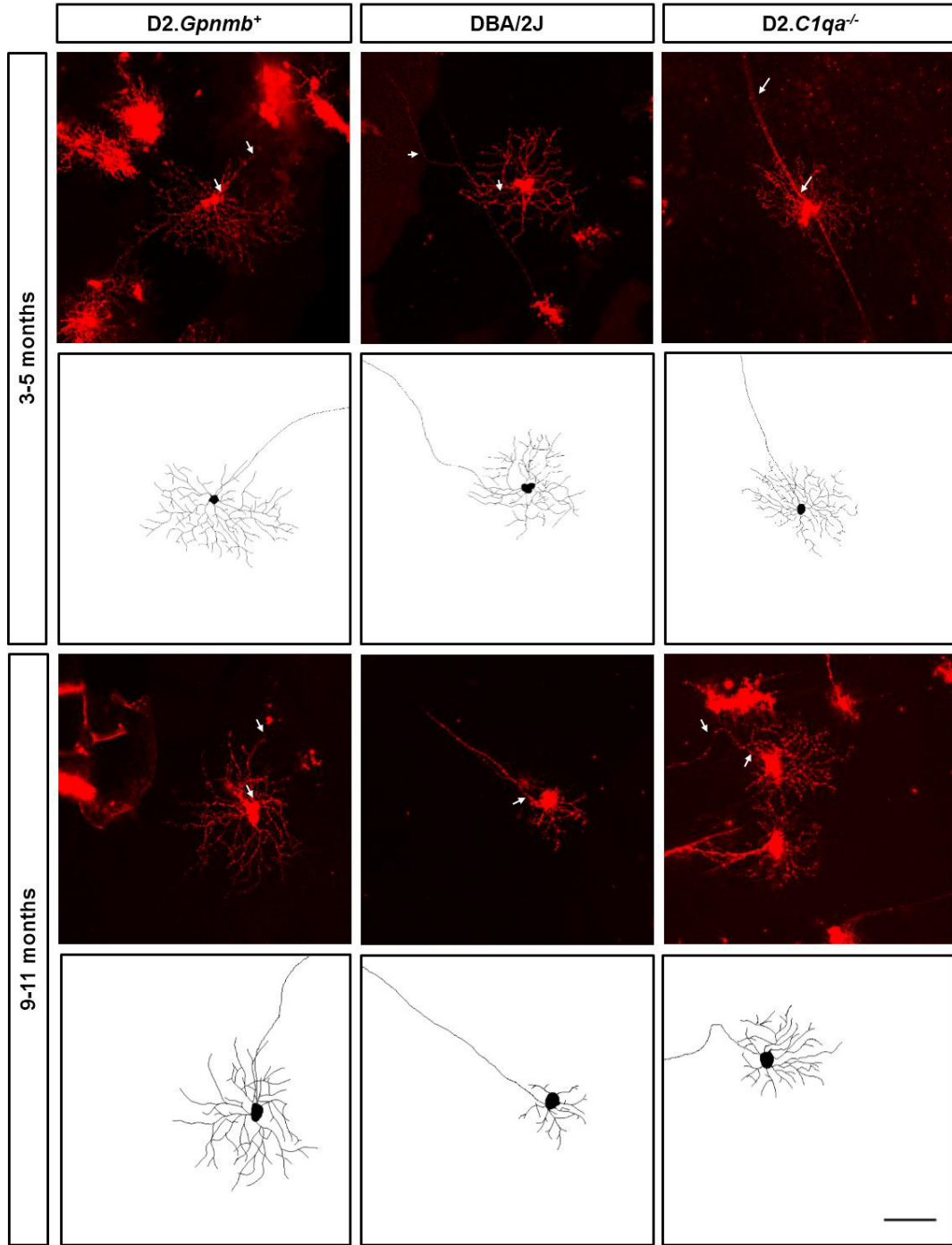


Figure 4.2 Typical morphology of mouse RGCs belonging to different genotypes. Dendritic field size was markedly reduced in DBA/2J eyes at 9-11months compared to D2.Gpnmb⁺; C1q deficiency was protective against this effect as RGCs showed larger and more complex dendritic fields. Images are shown as z-compressed, DiOlistically labelled RGCs (where the arrows denote the axon) and the trace the RGCs dendrites below. Scale bar shows 100µm.

4.3.2 Protection by C1 inhibition is repeated in the rat

Next I sought to establish whether the protective effect of C1 inhibition could be extended to a rat bead model of glaucoma where the increase in IOP and associated RGC loss was more acute. Ocular hypertension was induced in 20 animals of which 10 were given an intravitreal injection of C1inh and 10 vehicle only. The pressure increase achieved, and its duration, was comparable in both OHT groups (Figure 4.3). No significant difference was found between the mean IOP, AUC and peak IOP in the control (right) eyes between all groups, therefore, these were subsequently pooled to form the NT group. Comparable Mean IOP, AUC and peak IOP were achieved for the bead injected eye in OHT group and in the OHT.C1inh group; these showed no significant difference (Mean IOP $P=0.751$, AUC $P=0.718$ One-way ANOVA with post-hoc Bonferroni correction; Peak IOP $P=1.0$ (adjusted significance) Kruskal-Wallis test). The Mean IOP, AUC and peak IOP was significantly higher than in NT eyes for both OHT ($P=0.001$, $P=0.001$, $P=0.012$ respectively; statistical tests as before) and OHT.C1inh ($P=0.001$, $P=0.001$, $P=0.011$ respectively; statistical tests as before). Mean IOP, AUC and peak IOP in NT.C1inh eyes was also significantly different from both OHT ($P=0.001$, $P=0.001$, $P=0.009$ respectively; as before) and ONH.C1inh eyes ($P=0.001$, $P=0.001$, $P=0.008$ respectively; as before). OHT and OHT.C1inh groups showed increases of Mean IOP, peak IOP and IOP AUC of 50% and 70%, 66% and 87% and 117% and 116% respectively over NT control eyes. Additionally, the intravitreal injection of C1inh had no significant effect on IOP as shown by the similarity of NT.C1inh eyes compared to NT control eyes of all groups ($P=0.899$, $P=0.054$, $P=1$ respectively; as before).

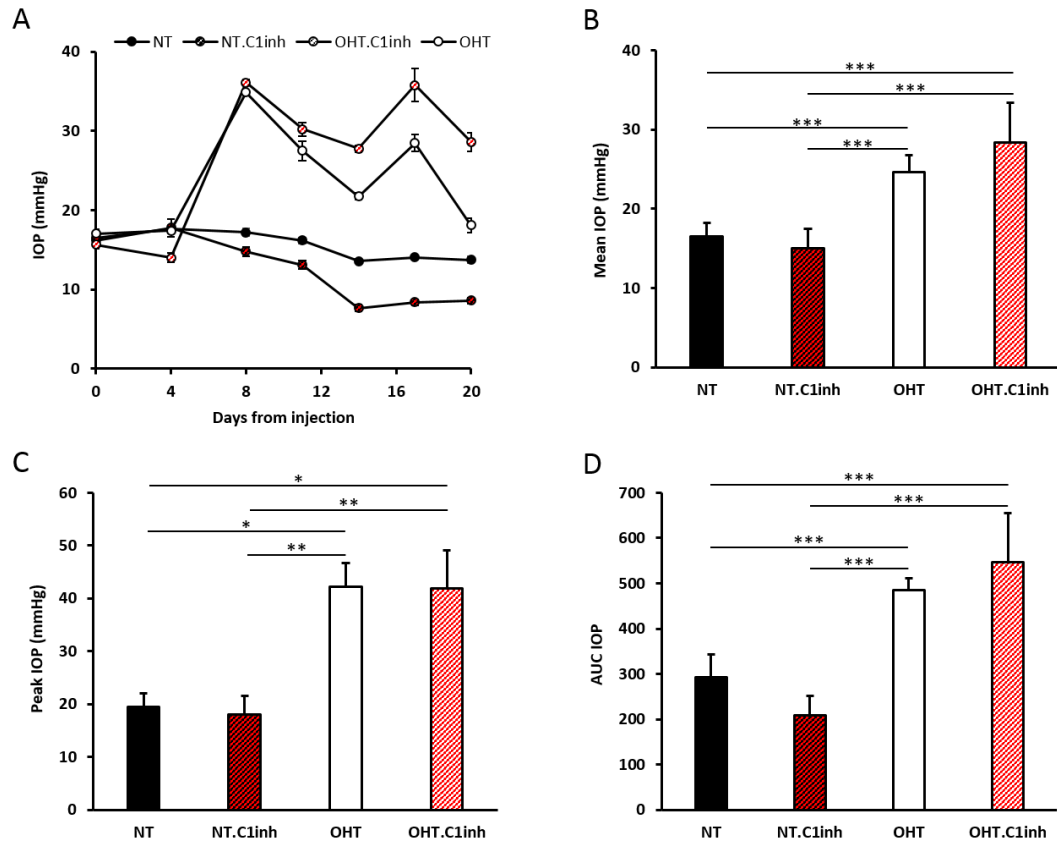


Figure 4.3 Comparison of IOPs between treatment groups. **A)** The average IOP profiles show an acute IOP increase lasting roughly 2 weeks in bead injected eyes of both OHT groups compared to NT controls. The mean IOP (**B**), peak IOP (**C**) and AUC (**D**) was significantly higher in OHT compared to NT groups over the duration of the experiment but was not significantly different among OHT and NT groups. Control right eyes are pooled from all 3 groups to form the NT group. Error bars show SD; *P<0.05, **P<0.01, ***P<0.001.

Typical RGC morphologies belonging to the different groups are displayed in Figure 4.4. ON grading demonstrated that both OHT and OHT.C1inh groups suffered axonal loss in bead injected eyes as the result of IOP increase with the ONs categorised on average to MOD in both groups (Figure 4.5 Panel A). C1inh alone had no observable adverse effect on RGC axons as indicated by the categorisation of NT.C1inh ONs as NOE. RGC morphological analysis revealed that C1 inhibition was again protective to dendrites. Sholl AUC, dendritic field area and total dendritic length were all reduced in RGCs from OHT.PBS eyes (n=38 RGCs, 7 animals) compared to NT eyes (n=43 RGCs, 18 animals) ($P=0.001$, $P=0.001$, $P=0.001$ respectively, (adjusted significance) Kruskal-Wallis test). C1inh injection into OHT eyes did not completely prevent dendropathy (n=36 RGCs, 7 animals) as Sholl AUC, dendritic field area and total dendritic length were all reduced compared to NT eyes ($P=0.021$, $P=0.005$, $P=0.012$ respectively, as before), although to a lesser extent than in OHT eyes treated with PBS only. RGCs from OHT.C1inh eyes were not significantly larger (dendritic field area, $P=0.383$, (adjusted significance) Kruskal-Wallis test) but were denser (Sholl AUC, $P=0.01$; total dendritic length, $P=0.006$, as before) than those from OHT eyes. They also showed no significant difference to NT.C1inh eyes (n=49 RGCs, 4 animals) for all 3 morphological analyses ($P=0.079$, $P=0.062$, $P=0.233$ respectively, as before). C1inh injection into NT eyes showed no detrimental changes to RGC morphology compared to NT controls ($P=1$, $P=1$, $P=1$ respectively, as before). Sholl analysis showed a reduced branching complexity in both groups of OHT eyes compared to NT control with reduced dendrite intersections at distances of 50-230 μm and 70-180 μm for OHT and OHT.C1inh respectively. Taken together these data indicate a partial protection of dendrites conferred by C1inh injection in OHT eyes. The protective effect of C1 inhibition to dendrites therefore extends to more acute damage induced by a bead model of glaucoma.

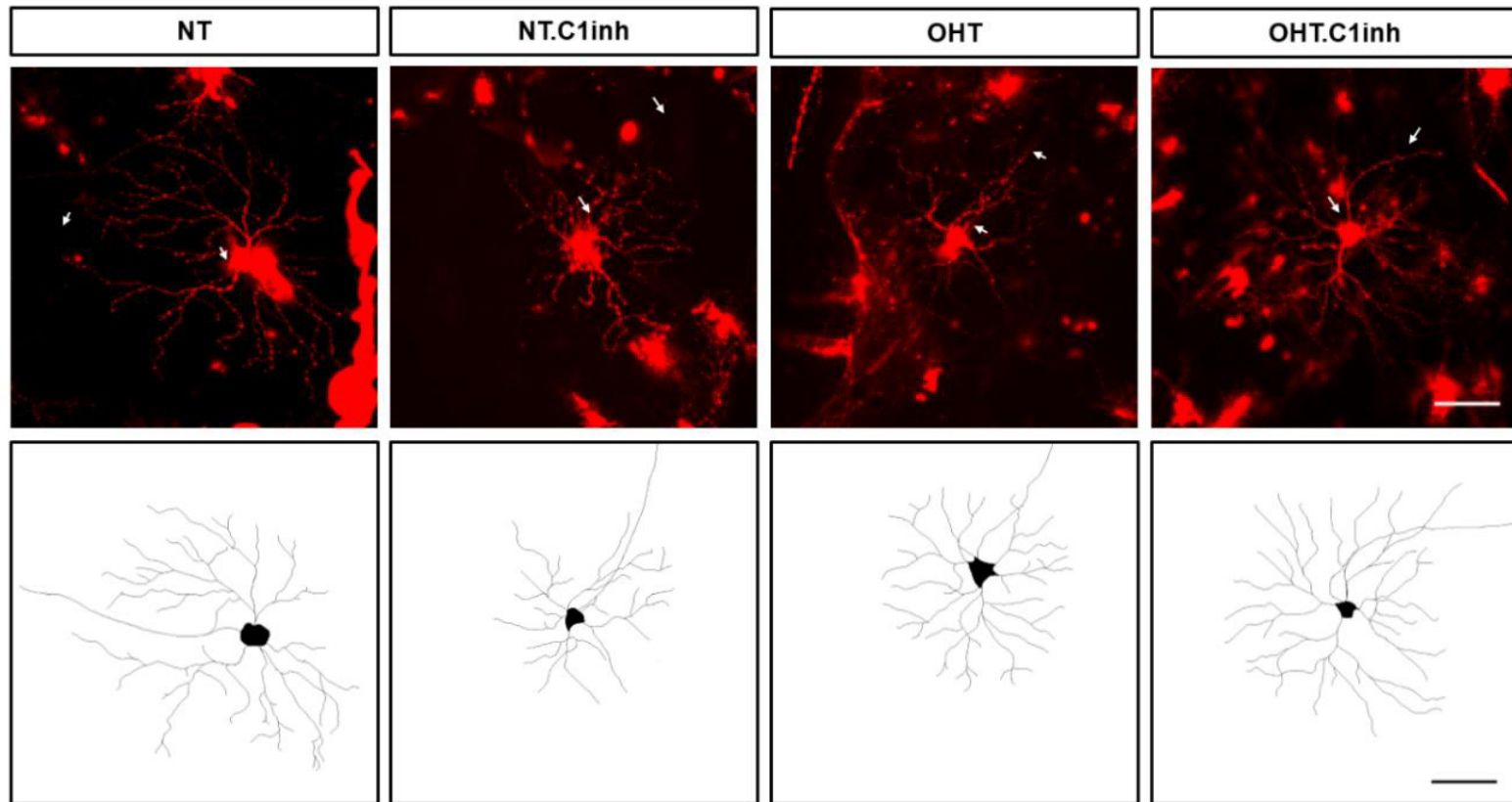


Figure 4.4 Typical morphology of rat RGCs belonging to the experimental groups. Branching density and dendritic field size was markedly reduced in OHT eyes compared to NT eyes, with C1inh treatment partially mitigating this effect. Images are shown as z-compressed DiOlistically labelled RGCs (where the arrows denote the axon) and the trace the RGCs dendrites below. Scale bar shows 100 μ m.

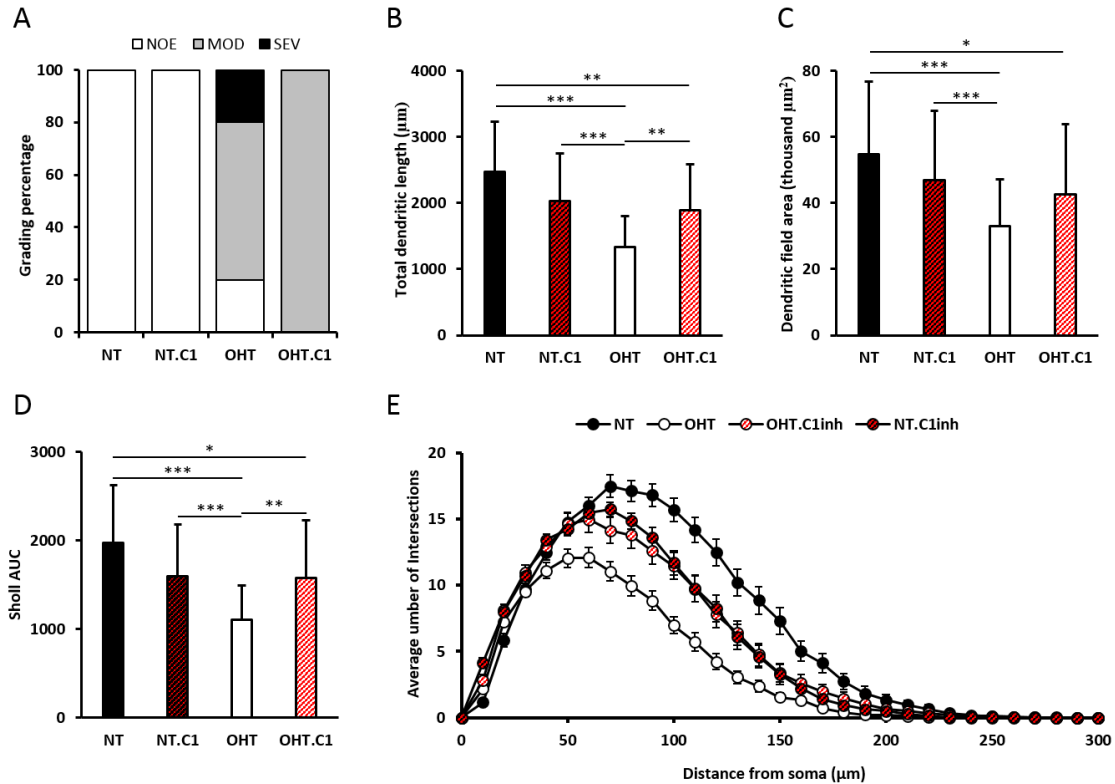


Figure 4.5 RGC morphological changes following C1inh treatment. ON grading (A) showed comparable moderate damage to the ONs of both OHT groups, indicating that ON death was comparable. C1inh injection had no negative effects on ONs. The total dendritic length (B), dendritic field area (C) and Sholl AUC (D) showed that RGC size and branching were reduced in both OHT groups from NT eyes. C1inh injection offered partial protection against dendropathy in OHT eyes as shown by the significantly greater total dendritic length (B), dendritic field area (C) and Sholl AUC (D). C1inh injection into NT eyes had no significant effects on dendritic morphology. Error bars show SD. Sholl analysis (E) showed the typical 'leftward shift' in OHT RGCs compared to NT controls. Again, C1inh injection into OHT eyes offered a degree of protection with significant decreases in dendrite intersections compared to NT controls reduced from a distance of 50-230μm in OHT eyes to 70-180 μm in OHT.C1inh eyes. NT n= 43 RGCs (18 animals), NT.C1 n= 49 RGCs (4 animals), OHT n=38 RGCs (7 animals), OHT.C1 n=36 RGCs (7 animals). Error bars show SEM. *P<0.05, **P<0.01, ***P<0.001.

4.3.3 Synapse protection differs in the mouse and rat

Given that C1 has roles in synaptic phagocytosis (Stevens et al. 2007), I sought to investigate whether the protection to dendrites was the result of the maintenance of synapses that would otherwise be lost. IHC of PSD95 labelling (see Figure 4.6 for typical images) in the IPL revealed a significant reduction in pixel intensity in 9-11 month D2s (n=25 sections, 3 animals) compared to aged matched D2-*Gpnmb*⁺ (n=28 sections, 5 animals) (P=0.001 (adjusted significance), Kruskal-Wallis test) and pre-glaucomatous (3-5 month) D2s (n=34 sections, 6 animals) (P=0.001, statistical test as before) as expected. However, C1q deficiency was not protective for synapses as 9 month D2.C1qa animals (n=30 sections, 3 animals) also showed significantly reduced IPL pixel intensity compared to aged matched D2-*Gpnmb*⁺ (P=0.001, as before) but showed no significant difference when compared to pre-glaucomatous (3-5 month) D2.C1q animals (n=29 sections, 5 animals) (P=1.0, as before). The loss of synapses was equivalent in both D2 and D2.C1qa animals aged 9-11 months (P=1.0, as before). These data suggest that synaptic loss occurred in RGCs in both D2 and D2.C1qa animals but that the relative loss was lower for D2.C1qa.

In the rat, experimentally induced glaucoma resulted in synaptic loss as expected with reduced PSD95 labelling in the IPL (Figure 4.7) in OHT.PBS retinal sections (n=16 sections, 3 animals) compared to NT (n=18 sections, 9 animals) (P=0.026, One-way ANOVA with post-hoc Bonferroni). Inhibition of C1 prevented this loss in OHT.C1inh animals (n=14 sections, 3 animals) where PSD95 labelling in the IPL was significantly higher than OHT.PBS animals (P=0.01, statistical test as before) but not different from NT (P=0.147, as before). These results are summarised in Figure 5.8. C1 inhibition is therefore protective to both dendrites and synapses in the rat bead model of glaucoma.

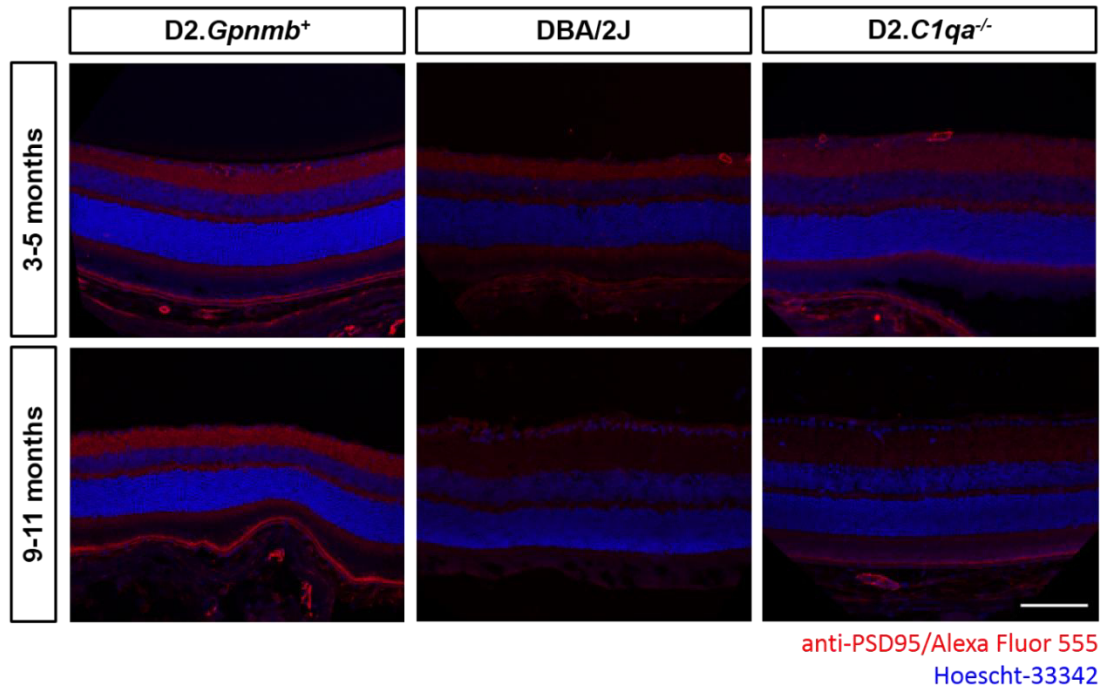


Figure 4.6 Typical PSD95 staining amongst different genotypes. PSD95 labelling (red) of synapses in the IPL was quantified as pixel intensity. Both D2 and D2.C1qa animals showed a reduction in synapses in the IPL as a result of glaucomatous damage at 9-11 months compared to age matched non-glaucomatous retina (D2.*Gpnmb*⁺) and pre-glaucomatous mice of the same genotype. Nuclei are labelled with Hoescht-33342 (blue). Scale bar shows 100µm. For 3-5month *Gpnmb*⁺ n=36 sections (9 animals), D2 n=34 sections (6 animals), D2.C1qa n=29 sections (5 animals). For 9-11month *Gpnmb*⁺ n=28 sections (5 animals), D2 n=25 sections (3 animals), D2.C1qa n=30 sections (3 animals).

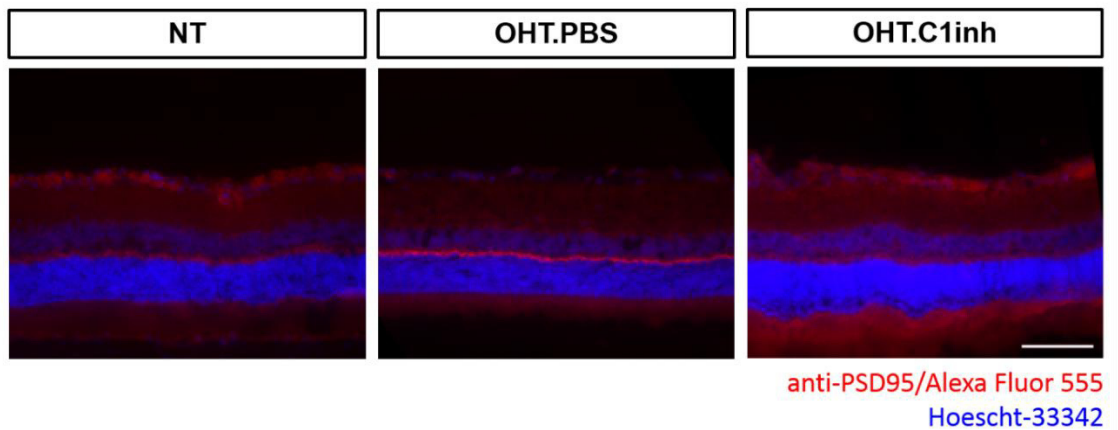


Figure 4.7 Typical PSD95 staining amongst different rat experimental groups. PSD95 labelling (red) of synapses in the IPL was quantified as pixel intensity. Glaucomatous damage resulted in synapses reduction in the IPL in OHT.PBS but not OHT.C1inh when compared to NT retina. Nuclei are labelled with Hoescht-33342 (blue). Scale bar shows 100µm. NT n= 18 sections (9 animals), OHT n=16 sections (3 animals), OHT.C1 n=14 sections (3 animals).

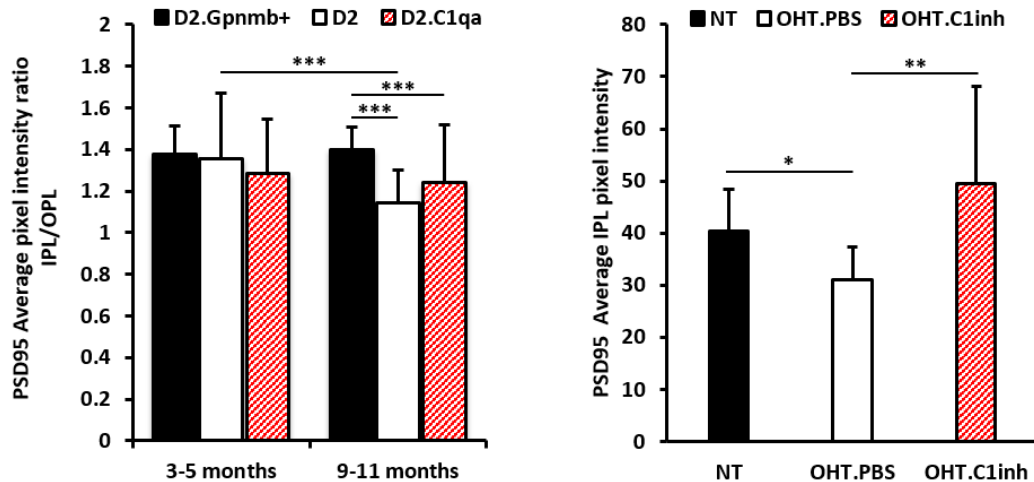


Figure 4.8 C1 inhibition protects from synaptic loss in the rat but not the mouse. The average pixel intensity was significantly reduced in the IPL in both D2 and D2.C1qa compared to D2. *Gpnmb*⁺. However, when compared to pre-glaucomatous animals of the same genotype D2 showed a significant reduction in pixel intensity while D2.C1qa did not. In the rat the loss of dendrites in glaucoma was repeated with OHT.PBS showing significantly reduced average pixel intensity in the IPL compared to NT. This loss was not observed in OHT.C1inh animals, which were statistically unchanged from NT. *P<0.05, **P<0.01, ***P<0.001. For 3-5-month *Gpnmb*⁺ n=36 sections (9 animals), D2 n=34 sections (6 animals), D2.C1qa n=29 sections (5 animals). For 9-11-month *Gpnmb*⁺ n=28 sections (5 animals), D2 n=25 sections (3 animals), D2.C1qa n=30 sections (3 animals). For rats, NT n= 18 sections (9 animals), OHT n=16 sections (3 animals), OHT.C1 n=14 sections (3 animals).

4.4 Discussion

These data show that C1q deficient mice and rats exhibit reduced RGC dendritic atrophy from experimental glaucoma. It is possible that this protective effect is the result of reduced phagocytosis of stressed RGCs. Phagocytosis is initiated following the detection of 'eat-me' signals such as phosphatidylserine (PS), calreticulin and DNA on cell surfaces (Paidassi *et al.* 2011). Blocking of PS reduced neuronal death via apoptosis by 90% in vitro (Neher *et al.* 2011), demonstrating that phagocytosis of stressed, pre-apoptotic cells is common (Brown and Neher 2012). C1q bound to glycoproteins on the stressed neuronal surfaces is recognised directly by microglia or can convert complement protein 3 (C3) to C3b for opsonisation. C1q in association with calreticulin is recognised by low-density lipoprotein receptor-related protein (LRP) on microglia (Fricker *et al.* 2012). LRP activates PI3k (Misra and Pizzo 1998) which has a well-established role in phagocytosis (Tamura *et al.* 2009); calreticulin activation of LPR has been shown as a mechanism for the initiation of phagocytosis of apoptotic cells (Gardai *et al.* 2005). The opsonin C3b can activate complement receptor 3 (CR3) on microglia (Linnartz *et al.* 2012). CR3 has been shown to act through the DAP12-ITAM-syk signalling cascade which results in cytoskeletal rearrangement and engulfment (Shi *et al.* 2006; Linnartz *et al.* 2012). C1q inhibition could reduce C1q binding to RGCs and the production of C3b and thus present fewer 'eat me' signals presented to microglia. C1q inhibitor is also known to directly bind LRP (Lillis *et al.* 2005) and so could also have prevented phagocytic signalling through competitive inhibition. Elimination of RGCs through the end stage MAC of the complement system is unlikely as neurons in the CNS express high levels of CD95 which inhibit the formation of this complex (Wang *et al.* 2007).

C1q inhibition could also have produced indirect effects on the immune system. C1q is known to alter the phenotype of glial cells, in particular through increasing chemokine production (mostly to recruit cells for debris clearance) (Fraser *et al.* 2006; Paidassi *et al.* 2011). Deficiency in C3 was shown to change the activation profile of macrophages/microglia in a mouse model of Alzheimer's disease where levels of CD68, F4/80, iNOS and tumour necrosis factor (TNF) were reduced (Maier *et al.* 2008). In glaucoma models iNOS (Neufeld 1999b; Neufeld *et al.* 2002) and TNF- α (Tezel and Wax 2000; Kitaoka *et al.* 2006) have shown toxic effects towards RGCs. It is possible that C1q deficiency, and subsequent downstream inactivation of the classical complement cascade, may therefore have altered the macrophage/microglia phenotype, creating a less neurotoxic environment and protecting RGC dendrites. CD68 (a phagocytic marker) and F4/80 appear to aid in macrophage/microglia binding to target cells, the latter through CSPGs (Stacey *et al.* 2003), and so their reduction may also limit direct phagocytosis by macrophage/microglia.

Interestingly, this protection did not extend to synapses as shown by reduced PSD95 labelling in the IPL in both D2 and D2.C1qa mice. However, in the rat C1 inhibition proved effective in preventing the synaptic loss suffered by OHT.PBS animals. C1q is known to tag RGC synapses for clearance by immune cells in development (Stevens *et al.* 2007) and so could have functioned in a similar manner here. The differences in synaptic protection between rats and mice may reflect different mechanisms of damage among the two models, in particular the chronic versus acute nature of IOP increase. Alternatively, IHC detection may have been too crude a method to detect subtle differences in the loss of synapses between D2 and D2.C1qa strains. The loss of synapses may be a response to, or consequence of, reduced mitochondrial capacity in stressed RGCs. Dendritic mitochondria are known to be more vulnerable than those in the soma due to

their increase exposure to local Ca^{2+} changes, in particular at synapses (Brown *et al.* 2006), increased oxidative stress (Martinez *et al.* 1996) and distance from the soma where DNA damage can be corrected (Stauch *et al.* 2014). These culminate in reduced energy output (Battino *et al.* 1995) and lead to synaptic and dendritic loss as demonstrated in other neurodegenerative diseases (Williams *et al.* 2010; Reddy *et al.* 2012; Williams *et al.* 2012). C1q inhibition may protect these stressed dendrites for a longer period or prevent clearance of functionless dendrites which would be indistinguishable from healthy dendrites when labelled DiOlistically since the dye propagates through passive Brownian motion (Honig and Hume 1986) and is therefore not dependant on functioning physiology. The discrepancy between these results in the mouse and rat for PSD95 IHC may reflect the age difference of the animals since mitochondrial capacity has been shown to decrease with age (Battino *et al.* 1995). It may also be necessary to increase the sample size in the rat as well as introducing an older group in order to preclude IHC variability and age as the causes of the discrepancy.

The long term consequences of disrupting C1q have not been explored here and could prove detrimental. The removal of cellular debris following apoptosis is thought to be an important part of CNS pathological resolution, preventing excitotoxicity and a pro-inflammatory environment (Fu *et al.* 2014); in Parkinson's disease microglia were found performing this role through phagocytosing C1q opsinised debris (Depboylu *et al.* 2011). C1q deficiency may therefore only provide short term protection. Preventing phagocytosis of stressed RGCs via C1q may therefore expand the therapeutic window in which additional interventions can be used to ensure RGCs survival or recovery.

Chapter 5: The role of PNNs in RGC degeneration and remodelling

5.1 Introduction

PNNs stabilise the favourable synaptic connections made during the critical period and prevent further growth and synaptogenesis. CSPGs (Perris and Johansson 1987; Oohira *et al.* 1991; Snow and Letourneau 1992) and other GAGs (Carri *et al.* 1988; Dou and Levine 1995) have been shown to be inhibitory to neurite outgrowth of cultured neurons when used as a plating substrate and these effects have been replicated *in vivo* in areas of glial scarring (Gates *et al.* 1996; Davies *et al.* 1997; Jones *et al.* 2003; Imagama *et al.* 2011). Digestion of PNNs with the bacterial enzyme CSase ABC removes the inhibitory effects of CSPGs *in vitro* (McKeon *et al.* 1991; Canning *et al.* 1996; Perris *et al.* 1996) and *ex vivo* in spinal cord (Dow *et al.* 1994) and brain slices (McKeon *et al.* 1995) allowing neuronal outgrowth. When given *in vivo*, CSase ABC has demonstrated an ability to recover function in conjunction with supporting neuron regrowth. CSase ABC treatment has supported the re-innervation of the striatum following nigrostriatal axotomy (Moon *et al.* 2001), provided sufficient plasticity to shift optical dominance in mature rats (Pizzorusso *et al.* 2002) and restore locomotion following spinal cord injury in mice (Bradbury *et al.* 2002) and partially in cats (Tester and Howland 2008). This physical barrier and associated negative growth cues may be prohibitive to the regrowth of the RGC dendritic tree following glaucomatous insult. Digestion of PNNs by CSase ABC may therefore allow for a regrowth of RGC dendrites following glaucoma. PNNs may also create a physical barrier to synaptogenesis on the neurite surface, preventing the translocation and trafficking of receptors (Frischknecht *et al.* 2009). Disruption of PNNs has shown to enhance synaptic plasticity in cortical neurons (Bukalo *et al.* 2001; Saghatelyan *et al.* 2001; Brakebusch *et al.* 2002), although these synapses are onto dendrite spines which RGCs lack. In epilepsy, seizures result in a reduction of PNN (Dityatev and Fellin 2008; McRae *et al.* 2012) which increases synaptogenesis (McRae *et al.* 2012) while in

stroke, downregulation of PNN components is associated with increased outgrowth and synaptogenesis outside of the infarct (Katsman et al. 2003; Hobohm et al. 2005; Karetko-Sysa et al. 2011). Numerous studies have demonstrated the plastic abilities of RGCs to recover their dendritic tree following the application of exogenous neurotrophins (Peinado-Ramon et al. 1996; Weber and Harman 2008). GAG chains contain binding regions for a number of growth factors and are thought to sequester growth factors in the neurons local environment. CSase ABC digestion may allow RGCs to access the endogenous retinal neurotrophic pool (Cui et al. 2002) by preventing sequestration and may contribute to dendritic recovery. The experimental paradigm (summarised in figure 5.1) was therefore to induce experimental glaucoma using the magnetic bead model, and administer CSase ABC intravitreally following the return and stabilisation of IOP to normal levels. After 2 weeks, the effects of CSase ABC on RGCs were assessed. The effect of CSase ABC administration on healthy retina was also assessed; the nuclear layers of the retina were imaged and cell density quantified.

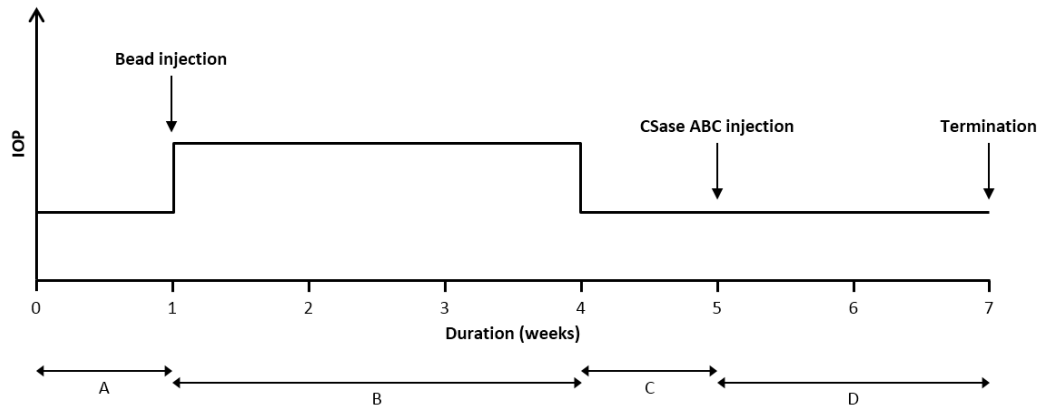


Figure 5.1 Experimental plan for the role of PNNs in RGC degeneration and remodelling. Baseline IOP was established in both eyes (**A**) before inducing glaucoma through the injection of microspheres into the anterior chamber of the left eye (**B**). The resultant IOP increase typically lasted 2-3 weeks. After the return of IOP to the level of the contralateral control eye a week was left (**C**) before injecting CSase ABC or PBS only (vehicle) intravitreally. The animal was then killed following a two week period for any remodelling effects to occur (**D**). For NT CSase ABC control animals no beads were injected so that pressure in the left eye did not increase, however the animals were maintained for the same duration as period **B** and **C** before injecting CSase ABC.

5.1.1 Hypothesis

Digestion of RGC PNNs and extracellular matrix in the inner retinal layers will allow for an expansion of surviving RGC dendrites.

5.1.2 Aims

- To determine the effects of ECM remodelling on retinal neurons following CSase ABC administration, in particular whether it produces a toxic effect.
- To determine whether CSase ABC digestion is protective against RGC dendritic atrophy induced by experimental glaucoma

5.2 Methods

5.2.1 Assessment of CSase ABC toxicity

CSase ABC retinal toxicity was assessed in 8 Wistar rats (3 months). The animal's left eye was subject to an injection of 3 μ l CSase ABC (10U/ml, from *Proteus vulgaris*, AMSBIO) as described in section 2.2.3. Similar concentrations have achieved GAG digestion in the CNS in other studies (Bruckner *et al.* 1998; Pizzorusso *et al.* 2002; Massey *et al.* 2006). Following a single injection the GAG remodelling takes >4 weeks to return to normal (Bruckner *et al.* 1998). The right eye remained as an un-operated control. The animals were killed 2 weeks (n=4) and 6 weeks (n=4) after injection. The retinas were dissected before labelling DiOlistically (section 2.3). TOPRO-3 Iodide was applied (1:1000) in order to visualise all nuclear layers. Retina were flat mounted and RGCs imaged by confocal microscopy (section 2.5.3). RGC dendritic morphology was measured using Sholl and dendrite analysis (section 2.5.3) in order to determine the effect of CSase ABC on RGC dendritic architecture. Cell counts were performed as described in section 2.5.2.2 with the exception that images were also taken of the INL and ONL in the same locations as the GCL so that toxicity to all neuronal cells could be assessed. INL and ONL integrity were assessed using fractal analysis which measures space filling capacity. Images of the INL and OPL were firstly processed in FIJI by converting to binary images and applying noise reduction (despeckle) before running the fractal box count tool (Smith *et al.* 1996). A fractal dimension score was produced on a scale where 1 represents no space filling, and 2 complete space filling capacity. In 1 animal from each time point, whole eyes were instead fixed in 4% PFA before sectioning (2.4.2). These eyes were subject to IHC using stub-antibodies 1B5, 2B6 and 3B3 as detailed below in section 5.2.1.1 in order to confirm activity of CSase ABC *in vivo*.

5.2.1.1 GAG IHC

Primary antibodies 1B5 and 2B6 that recognise CS-stub epitopes C-0-S and C-4-S respectively were used. The primary antibodies were applied at a 1:5 dilution (PBS) following blocking with 5% goat serum (Sigma). For secondary antibody only controls, a number of sections were incubated with only PBS. Goat anti-mouse alexafluor-488 secondary antibody (Life Technologies; IgG, 1:200) was then applied before nuclear staining, mounting and imaging (2.5.1).

5.2.2 Induction of Glaucoma and treatment with CSase ABC

In 27 BN rats, glaucoma (OHT) was induced in the left eyes of 20 animals (as described in section 2.2.2) with the right eye serving as a normotensive control (NT). IOP was measured by rebound tonometry for 3 days preceding glaucoma induction and every 3 days following (see section 2.2.1). In 10 animals (OHT.ABC) from the OHT cohort and the 7 un-injected animals (NT.ABC), an intravitreal injection of 3 μ l CSase ABC (10U/ml) was performed in the left eye 1 week after IOP returning to baseline (or at the equivalent time point for the second cohort). In the remaining 10 animals (OHT.PBS) from the first cohort a vehicle only injection of PBS was performed.

5.2.3 Effect of Glaucoma and CSase ABC treatment on RGC morphology

Seventeen animals were killed 2-3 weeks following intravitreal injection (OHT.PBS n=7, OHT.ABC n=5, NT.ABC n=4). For the assessment of RGC morphology retinas were dissected and subject to DiOlistic labelling before they were fixed, nuclear stained and flat mounted (see section 2.3). Images of the GCL were collected and cell counts performed (2.5.2.2). RGCs were imaged in the flat mounted retina (2.5.2.1) and morphology assessed (2.5.3). The RGC class composition of

each experimental group was determined using the classification model derived in Chapter 3. Briefly, the 10 variables that contributed to the model were measured for each RGC as described in section 3.2.2 and a discriminant analysis performed (see 3.2.5) where the training sample was that used in the model (n=101) and where the hold-out sample was comprised of the experimental group that was to be classified.

5.3 Results

5.3.1 Chondroitinase ABC is not toxic to RGCs and other retinal neurons.

CSase ABC activity in the retina was confirmed (Figure 5.2) by labelling with 'stub' antibody 2B6 which recognises C-4-S on CS/DS sidechains. Digestion of GAGs appeared to be limited to the inner retinal layers in particular around RGCs. This digestion did not appear to induce any retinal cell death. As shown in Figure 5.3 the nuclear layers all appeared to be intact with no visible disruption to integrity. Cell counts in the GCL showed similar numbers of nuclei between control ($699 \pm 48 / 393 \mu\text{m}^2$) and CSase ABC ($698 \pm 69 / 393 \mu\text{m}^2$) injected eyes ($P=0.977$; T-test). Fractal analysis of the INL and OPL showed no significant difference in space filling between groups ($P=0.61$, $P=0.21$ respectively; T-test).

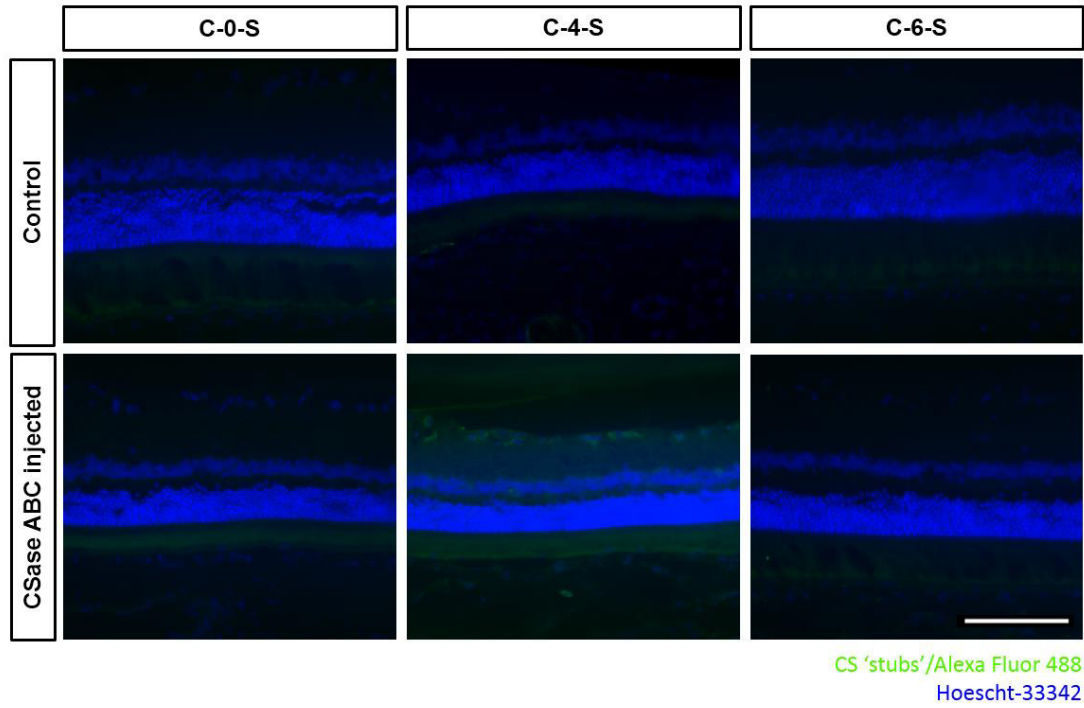


Figure 5.2 CSase ABC action *in vivo* following intravitreal injection. The digestion of GAGs in the retina from intravitreally injected CSase ABC was confirmed by the increase of C-4-S in the inner retina in injected eyes compared to control. This was detected by antibody 2B6 through anti-mouse Alexaflour 488 labelling (green). Nuclear layers were stained with Hoescht-33342 (blue). Scale bar=100 μ m.

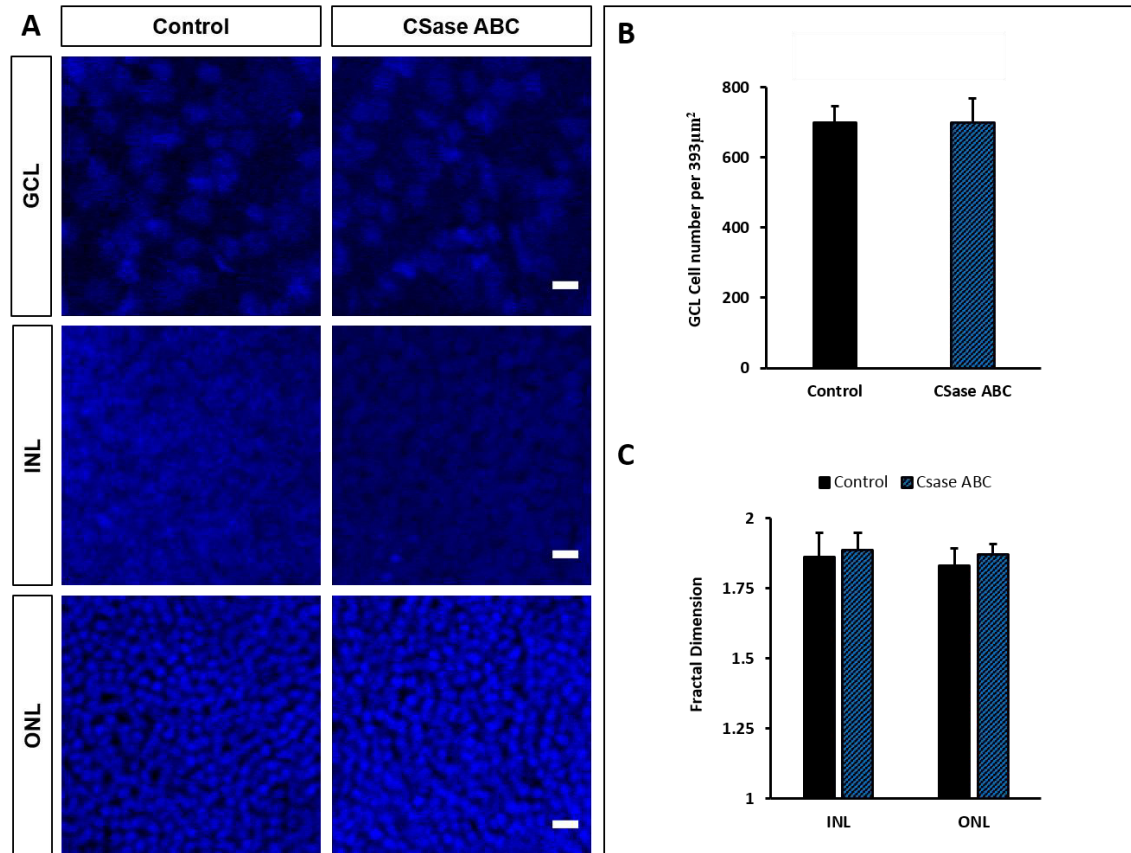


Figure 5.3 CSase ABC non-toxic to retinal neurons. Intravitreal injection of CSase ABC did not affect nuclear layer integrity (A) in the GCL, INL or ONL. Cell nuclei were stained with TOPRO-3 (blue). Cell counts of the GCL (B) showed no significant difference in cell number. Fractal analysis of the INL and ONL (C) showed no significant difference in space filling. Scale bar = 10µm. Error bars show SD.

The dendritic tree was also unaffected by CSase ABC action. RGC morphology in CSase ABC injected (n=16 RGCs 2 weeks, 3 animals; n=24 RGCs 6 weeks, 3 animals) eyes was also unchanged from control (n=28 RGCs) as shown in Figure 5.4. In CSase ABC injected eyes the number of dendrites, total dendritic length and dendritic field area were not significantly different from control at 2 weeks (P=0.667, P=1.0, P=1.0 respectively; One-way ANOVA with post-hoc Bonferroni correction on Log10 transformed data) or 6 weeks (P=1.0, P=1.0, P=1.0; statistical analysis as before;) or from each other (P=0.238, P=0.782, P=1.0; as before). Sholl analysis revealed similar branching density with Sholl AUC showing no significant difference from control at 2 weeks (P=0.732; One-way ANOVA with post-hoc Bonferroni correction following Log10 transform) and 6 weeks (P=1.0; as before) while no difference was observed between 2 and 6 week (P=0.623; as before). At 2 weeks following injection CSaseABC injected eyes exhibited fewer branches than control at distances of 30-70 μ m from the soma (P=0.006, P=0.033, P=0.045, P=0.039, P=0.04 for respective distance; all adjusted significance, Kruskal-Wallis test) and from 6 week eyes at distances of 60-100 μ m from the soma (P=0.001, P=0.005, P=0.005, P=0.001, P=0.005 for respective distance; statistical test as before). This is likely due to the small sample number as the cells appeared unchanged in all other morphological analyses, but could indicate subtle changes to the dendritic structure. CSase ABC therefore does not appear to be toxic to retinal neurons nor alter the morphology of RGCs in normotensive eye

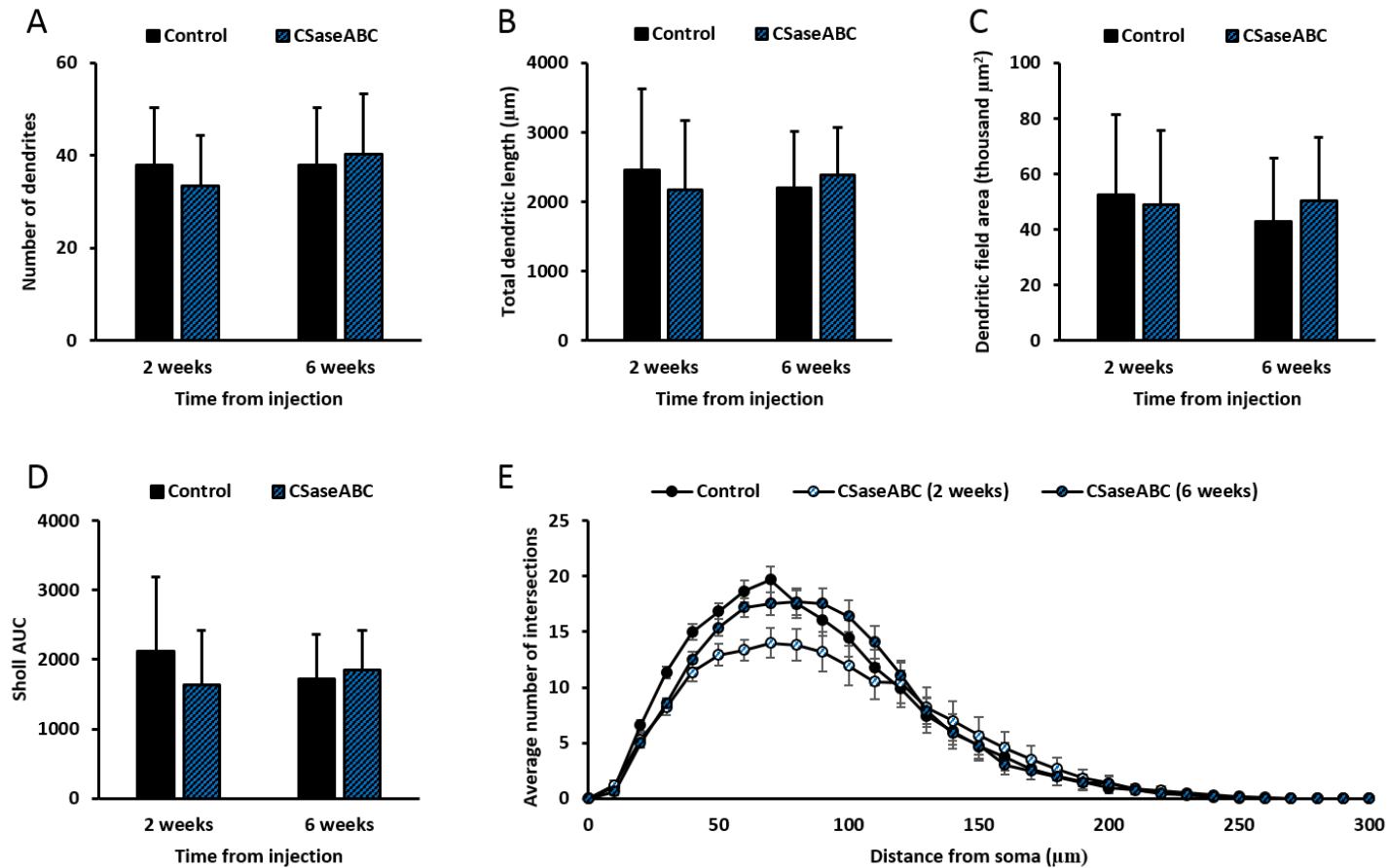


Figure 5.4 CSase ABC effects on RGC morphological analysis in normal eyes. Intravitreal injection of CSase ABC in Wistar eyes resulted in no significant changes to RGC morphology. The mean number of dendrites (A), total dendritic length (B), dendritic field area (C) and Sholl AUC (D) showed that RGC size and branching are unaffected by CSase ABC at both 2 weeks (n=16 RGCs, 3 animals) and 6 weeks (n=24 RGCs, 3 animals) following injection when compared to control (n=14 RGCs 3 animals, n=14 RGCs 3 animals at equivalent time points). Sholl analysis (E) shows a small decrease in branching density of RGCs at 2 weeks following CSase ABC injection compared to control and 6 week RGCs. Control groups were pooled. Error bars show SD for A, B, C, D and SEM for E.

5.3.3 IOP changes in experimental glaucoma

A sufficing pressure increase was not achieved in one animal despite re-injection and so it was not included in the analysis. Analysis of IOP showed no significant difference between baseline, mean and peak IOP nor IOP AUC in right (NT) eyes of all experimental groups and so these were pooled for further analysis (n=26). No significant difference was found between the IOP of right and left eyes prior to microbead injection ($P=0.658$; T-test); this trend remained between NT control eyes and normotensive left eyes injected with CSase ABC (NT.ABC; n=7) throughout the duration of the experiment. Here mean IOP, peak IOP and IOP AUC did not vary significantly from the NT eyes ($P=1.0$, $P=1.0$, $P=1.0$ respectively; One-way ANOVA with post-hoc Bonferroni). This indicated that the injection procedure alone did not significantly alter IOP. A second microbead injection was required in 32% of animals to obtain a sustained IOP increase over the contralateral NT eye. Compared to NT eyes, microbead injected eyes exhibited a significant increase in IOP as demonstrated by a higher mean IOP, peak IOP and IOP AUC in both OHT.PBS (22% increase $P=0.001$, 74% increase $P=0.001$, 48% increase $P=0.001$ respectively; One-way ANOVA with post-hoc Bonferroni) and OHT.ABC eyes (18% increase $P=0.003$, 59% increase $P=0.001$, 48% increase $P=0.001$; as before). IOP in these eyes was also significantly higher than in NT.ABC eyes (For OHT.PBS, Mean IOP $P=0.012$, Peak IOP $P=0.001$, IOP AUC $P=0.008$; For OHT.ABC, Mean IOP $P=0.041$, Peak IOP $P=0.001$, IOP AUC $P=0.009$; One-way ANOVA with post-hoc Bonferroni). The average duration of IOP increase was similar in OHT.PBS (n=10) and OHT.ABC (n=9) at 20 ± 5 days and 18 ± 4 days respectively ($P=0.099$; T-test). The IOP increase in injected eyes was comparable between both OHT.PBS and OHT.ABC groups (Mean IOP $P=1.0$, Peak IOP $P=0.592$, IOP AUC $P=1.0$; One-way ANOVA with post-hoc Bonferroni) indicating that any differences to RGC morphology between these two groups would likely occur independent of IOP.

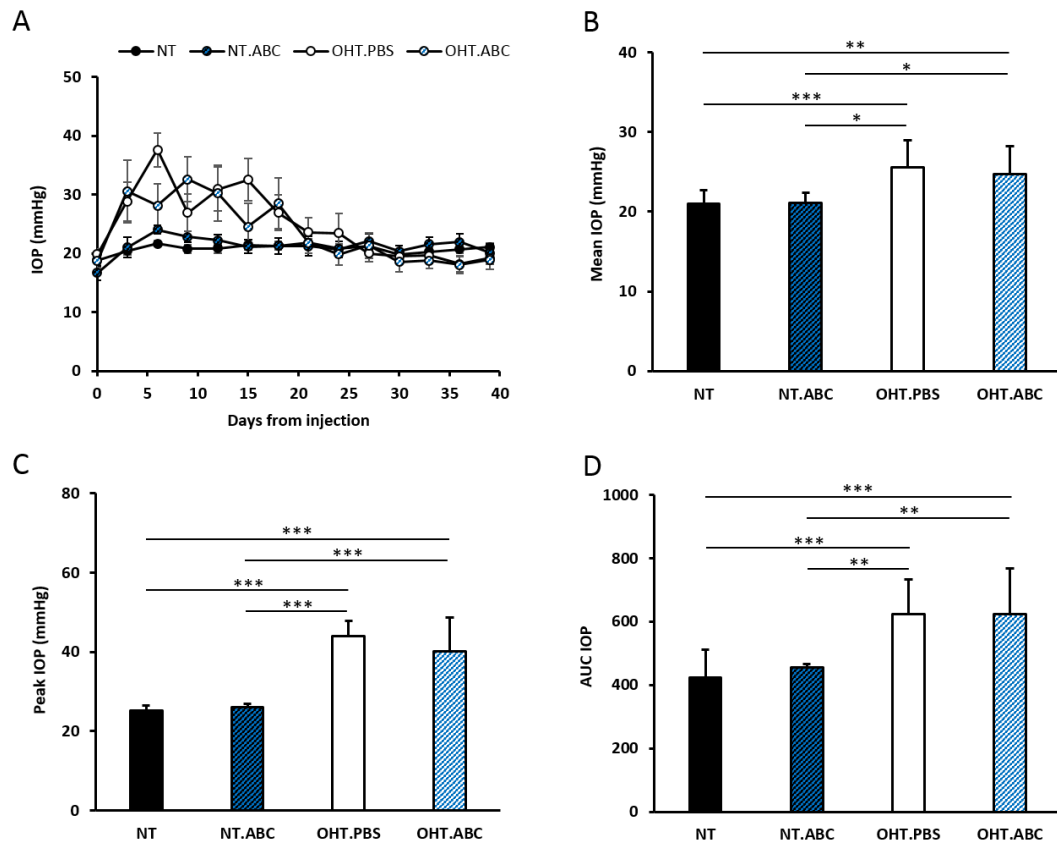


Figure 5.5 IOP changes induced by microbead injection. Intracameral injection of paramagnetic beads into the left eye of 18 animals resulted in an increased IOP (**A**) sustained for an average of 20 ± 5 days (OHT.PBS) and 19 ± 4 days (OHT.ABC) before returning to baseline. IOP then remained stable for 3 weeks before animals were killed. The mean IOP (**B**), peak IOP (**C**) and IOP AUC (**D**) were comparable in OHT.PBS ($n=10$) and OHT.ABC ($n=9$) eyes while significantly increased compared to NT ($n=26$) and NT.ABC ($n=7$) eyes. Injection of CSase ABC alone did not significantly alter IOP from NT levels. Error bars show SEM in **A** and SD in **B**, **C**, and **D**. * $P < 0.05$, ** $P < 0.01$, *** $P < 0.001$.

5.3.4 RGC atrophy and apoptosis following experimental glaucoma

Diolistic labelling gave 87 NT RGCs (17 animals), 43 OHT.PBS RGCs (7 animals), 38 OHT.ABC RGCs (6 animals) and 27 NT.ABC RGCs (4 animals) for analysis. Representative cells are shown in Figure 5.6. Cell counts (summarised in Figure 5.7) of the RGC layer revealed only moderate loss of cells through experimental glaucoma where OHT.PBS (7 animals) eyes showed a 13% reduction from contralateral control eyes (7 animals) ($631 \pm 85 / 393 \mu\text{m}^2$ and $744 \pm 64 / 393 \mu\text{m}^2$ respectively, $P=0.002$, T-test). Early dendritic loss was evident with total dendritic length and Sholl AUC significantly reduced in OHT.PBS from NT control ($P=0.007$ and $P=0.016$ respectively; One-way ANOVA with post-hoc Bonferroni on log₁₀-transformed data). Analysis of the Sholl profile revealed a significant reduction in dendrite intersections at distances of 100 to 160 μm from the soma centre ($P=0.009$, $P=0.001$, $P=0.001$, $P=0.002$, $P=0.011$, $P=0.037$ for respective distance; all adjusted significance, Kruskal-Wallis test). Dendritic field area was not significantly reduced ($P=0.101$; One-way ANOVA with post-hoc Bonferroni on log₁₀-transformed data); taken together these data suggest a loss of branching density and complexity. To further investigate this dendrites were categorised according to the centrifugal method and the total dendritic length measured. This ordinal analysis (Fig 5.8, panel E) of dendrites revealed that primary, secondary and tertiary dendritic length was not altered in OHT.PBS RGCs compared to NT ($P=1.0$, $P=1.0$, $P=1.0$ respectively; One-way ANOVA with post-hoc Bonferroni on log₁₀-transformed data). Subtracting the total length of these from the total length of the dendritic tree gave the total length of the higher order dendrites. The total length of the higher order dendrites was significantly reduced in OHT.PBS RGCs compared to NT ($P=0.001$, adjusted significance; Kruskal-Wallis test). These data again suggest a pruning of dendrites in glaucoma.

On average the distance of NT RGCs from the ONH was $2912 \pm 1115 \mu\text{m}$ compared to $2322 \pm 1017 \mu\text{m}$ in OHT.PBS retinas, this was statistically significant ($P=0.002$; Kruskal-Wallis test). However, no significant correlation between distance from the ONH and dendritic field area, total dendritic length, higher order dendritic length and Sholl AUC was found ($r_s -0.018$, $r_s -0.141$, $r_s 0.141$, $r_s -0.079$ respectively; Spearman's rank order correlation). The difference in morphology was therefore likely the result of glaucomatous atrophy on the OHT.PBS RGCs rather than larger dendritic fields of the more peripheral NT cells.

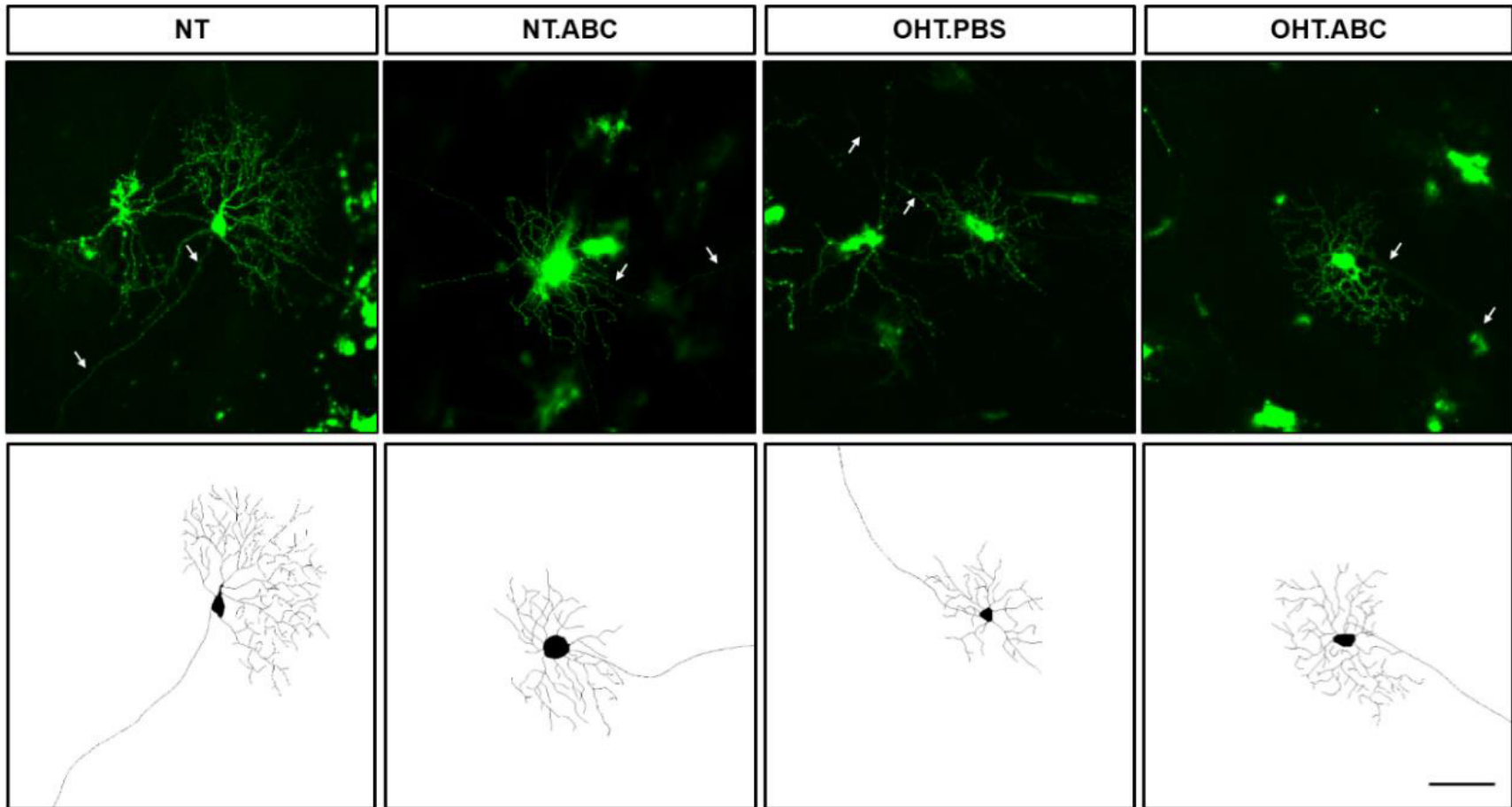


Figure 5.6 Representative RGC morphology. Representative images of DiIolistically labelled RGCs (and skeletonised images) showing reduced branching density in glaucomatous RGCs (OHT.PBS) which is recovered or protected against following CSase ABC treatment (OHT.ABC). Arrows denote axon. Scale bar= 100 μ m.

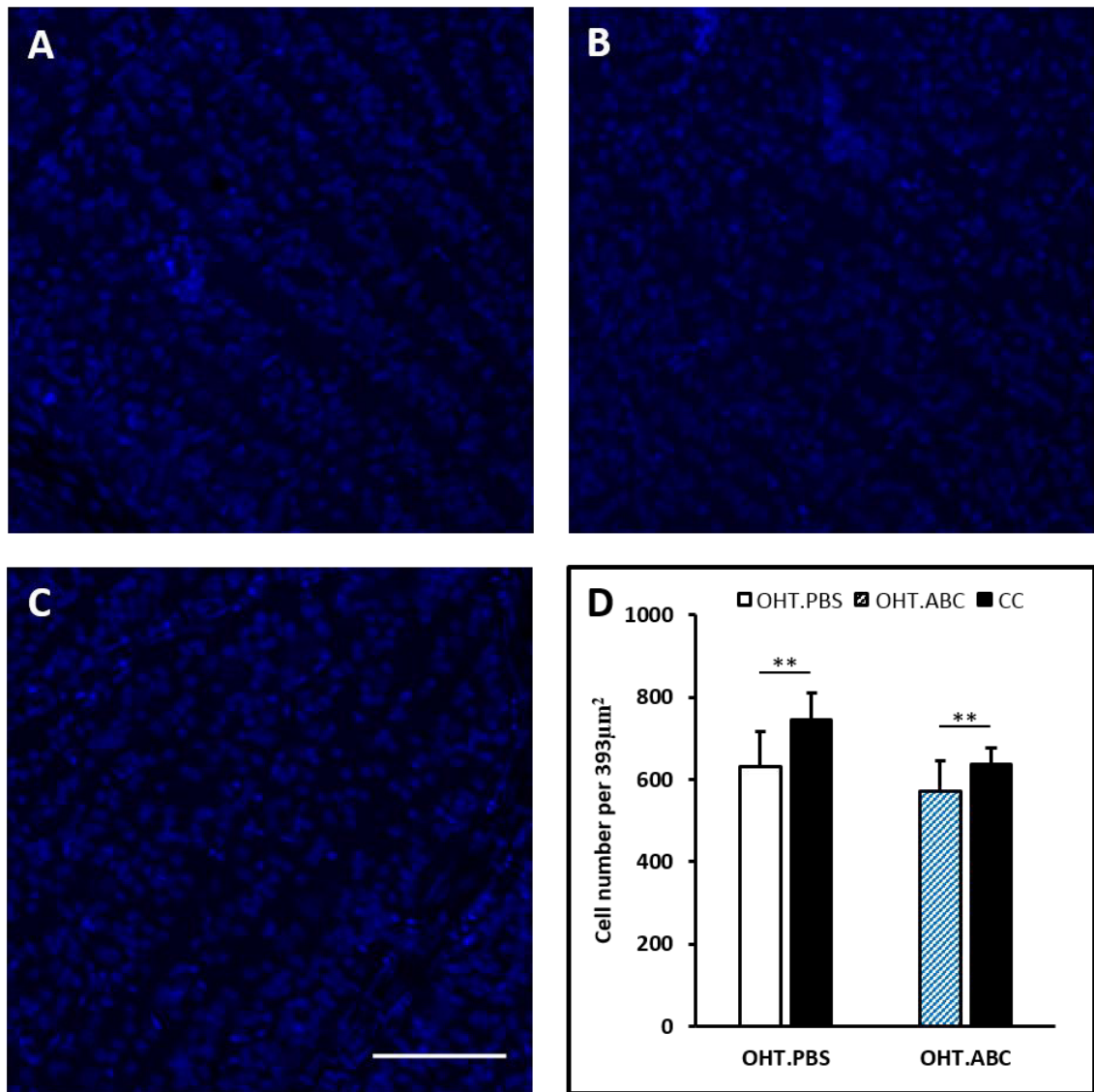


Figure 5.7 Cell counts reveal RGC loss. Representative images of TOPRO-3 (blue) stained nuclei in the GCL from NT (A), OHT.PBS (B) and OHT.ABC (C) retina show mild RGC loss. Both glaucoma groups showed a similar level of cell loss (D) with a significant reduction in cell number compared to contralateral control (CC). Scale bar =100µm. Error bars show SD. **P<0.01.

5.3.5 CSase ABC treatment protects RGC dendrites from glaucomatous damage

The NT.ABC group (n=27 RGCs, 4 animals) confirmed the initial findings of the toxicity study. Dendritic analysis revealed no significant difference in morphology to NT control RGCs (n=87 RGCs, 17 animals) in terms of total dendritic length, dendritic field area and Sholl AUC (P=1.0 P=1.0, P=1.0 respectively; One-way ANOVA with post-hoc Bonferroni on log₁₀-transformed data). The Sholl profile was largely similar, with no significant reduction in dendritic intersections at any distance from the soma. Ordinal dendritic analysis showed no significant difference in primary, secondary, tertiary (P=1.0 P=1.0, P=1.0 respectively; statistical analysis as before) and higher order dendritic length (P=0.168, adjusted significance; Kruskal-Wallis test).

In contrast to the PBS treated eyes, treatment of glaucoma with CSase ABC injection was protective against RGC dendritic atrophy. No significant difference between OHT.ABC (n=38 RGCs, 6 animals) and NT RGCs was detected in total dendritic length, dendritic field area and Sholl AUC (P=0.63 P=0.699, P=1.0 respectively; One-way ANOVA with post-hoc Bonferroni on log₁₀-transformed data). Again the leftward shift in the Sholl profile observed in OHT.PBS eyes was not present in OHT.ABC eyes, with no significant difference in dendritic intersections at any distance from the soma when compared to NT RGCs. Further, ordinal dendritic analysis showed no significant difference in higher order dendritic length (P=0.235, adjusted significance; Kruskal-Wallis test) suggesting that dendritic pruning was reduced. The dendritic protection was in effect despite the presence of cell death, with cell counts revealing on average an 11% loss of RGCs in OHT.ABC eyes (n=6 6 animals) compared to contralateral control ($570 \pm 76 / 393 \mu\text{m}^2$ and $636 \pm 41 / 393 \mu\text{m}^2$ respectively P=0.001, T-test). Comparison of cell counts between OHT.ABC and OHT.PBS showed 10% fewer cells present in the former (P=0.013, T-test), however the losses compared to contralateral eyes were similar at 11% and 13% respectively. OHT.ABC RGCs were

not found at significantly greater distances from the ONH than in NT, NT.ABC nor OHT.PBS retinas ($P=0.126$, $P=0.892$, $P=1.0$; Kruskal-Wallis test) again suggesting that eccentricity had no effect on morphological characteristics.

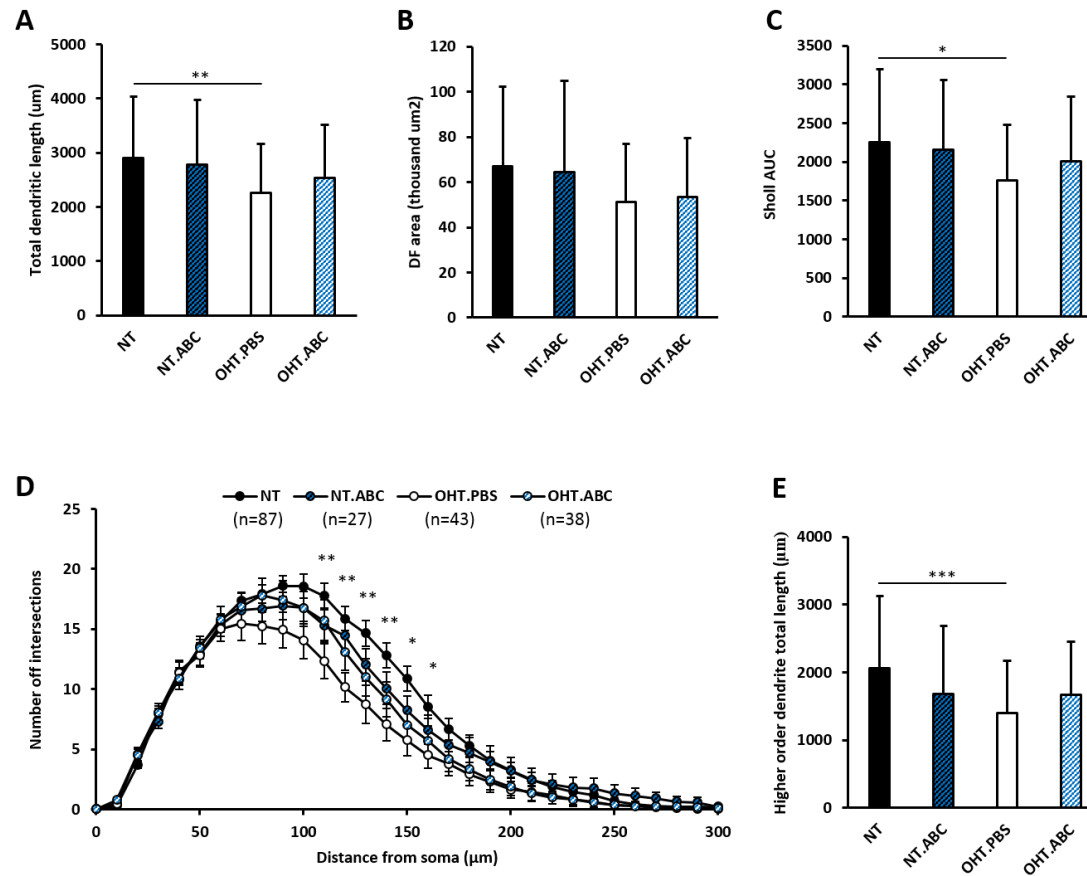


Figure 5.8 CSase ABC protects from RGC dendritic atrophy. Following induction of glaucoma in OHT.PBS eyes dendritic atrophy occurs as shown by reduced total dendritic length (**A**) when compared to NT control; however dendritic field area is not altered significantly (**B**). This represents a loss in branching density as shown by the reduced Sholl AUC (**C**) and leftward shift in the Sholl profile (**D**). Sholl analysis shows fewer branches at distances of 110-160µm from the soma centre (denoted with appropriate P values). Ordinal dendrite analysis revealed that the branches lost were higher order dendrites (**E**). In OHT eyes treated with CSase ABC this atrophy was not present indicating either a protective effect or recovery of dendrites. For NT n=87 RGCs (17 animals), NT.ABC n=27 RGCs (4 animals), OHT.PBS n=43 RGCs (7 animals) and OHT.ABC n=38 RGCs (6 animals). Error bars show SD in **A**, **B**, **C** and SEM in **D**. *P<0.05, **P<0.01, ***P<0.001

5.3.6 No class bias detected in analysis

The classification model derived in Chapter 3 allowed for the estimation of the class composition of the experimental groups. All groups displayed a similar class composition as shown in Table 5.1. RGC_C was the most abundant cell type in all experimental groups, however all cell types were present in a similar ratio to the population collected in Chapter 3. The differences in dendritic morphology are therefore unlikely to have arisen from a disparity of cell types between the experimental groups.

Table 5.1 RGC class distribution among experimental groups

	RGC type (% of total number of RGCs)			
	RGC _A	RGC _B	RGC _C	RGC _D
NT	24	27	39	10
NT.ABC	22	26	37	15
OHT.PBS	23	28	41	9
OHT.ABC	19	30	40	11
<i>Training data (Chapter 3)</i>	24	29	32	15

5.4 Discussion

The findings of this chapter have confirmed the dendritic atrophy associated with glaucoma that have been demonstrated in other experimental models (Weber et al. 1998; Shou et al. 2003; Leung et al. 2011; Li *et al.* 2011; Williams et al. 2013). The overall cell death (~10%) was lower than is usually achieved by similar microbead models (~30%) (Morgan and Tribble 2015), however this allowed for the interesting observation that dendritic complexity was reduced without a loss of overall dendritic field size. It is reasonable to conclude that one of the earliest events in dendritic atrophy is therefore the loss of small higher order dendrites (as evidenced by ordinal analysis), which precedes cell shrinkage (of both the soma and dendritic tree) observed in other models (Weber et al. 1998; Shou et al. 2003). The use of CSase ABC as a treatment for the recovery of dendrites proved successful, with RGC dendritic atrophy seen in vehicle only (OHT.PBS) treated eyes not present in OHT.ABC eyes. The similar overall loss of cells and the magnitude and duration of IOP increase suggest that the CSase ABC treated eyes suffered comparable glaucomatous damage, however it is unclear whether the CSase ABC provided a protective or regenerative effect. This is the first instance, to our knowledge, of treatment with CSase ABC proving effective on dendrites rather than axons.

Digestion of PNNs may have removed the inhibitory effects on neuronal growth. The core protein which is exposed following CSase ABC digestion of the sidechains demonstrate some inhibitory affect independent of those from those of the overall GAG (Inatani *et al.* 2001). PNNs are known to sequester growth molecules (Milev *et al.* 1998a; Milev et al. 1998c) and so their digestion could have freed a larger proportion of the endogenous neurotrophic pool to promote dendritic re-growth. CSPG binding to Protein-tyrosine phosphatase σ has been shown to dephosphorylate TrkB and inhibit BDNF signalling (Kurihara and Yamashita 2012). BDNF has proved efficacious in recovering dendritic trees from glaucoma induced damage (Mansourrobaey et al. 1992; Mey and Thanos 1993; Peinado-Ramon et al. 1996;

Chen and Weber 2001) and could have contributed to the protection observed here. PNNs have also been shown to bind proteins such as semaphorin 3A which are known to restrict plasticity in the adult CNS (Kantor *et al.* 2004). The proteins act as guidance cues during development but also form components of glial scars following injury. Expression of the protein and its receptor continues into adulthood in the retina (de Winter *et al.* 2004). Semaphorin 3A has demonstrated chemoattractant properties for cortical dendrites (Polleux *et al.* 2000). Interestingly, Schulz *et al.* (1990) demonstrated that cultured RGCs could be maintained by the addition of CSPGs derived from the neonatal superior colliculus. It is possible that the CSPG side-chains, once freed from the PNN core proteins could have produced a similar protective effect.

The application of the RGC classification model derived in Chapter 3 showed that a similar class composition was captured in each of the experimental groups here. This gave a degree of confidence that the differences in RGC morphology observed between groups were not the result of sample bias. The groups displayed a higher proportion of RGC_c than expected from the initial population collected in Chapter 3 and those found by others Sun *et al.* (2002a). This likely reflects the propensity of the model to overestimate the number of RGC_c. However, the ratios of misclassification to RGC_c are similar among types and so it is unlikely that the misclassified RGC_c represent distinct types in the different experimental groups.

The findings of this chapter demonstrate that CSase ABC could form a viable treatment for the protection or re-generation of RGC dendritic trees. The assessment of toxicity demonstrated minimal disruption to the nuclear layers suggesting that the injection would be well tolerated and would not affect visual function. Normal RGCs were not altered morphologically apart from reductions in the number of intersections in Sholl analysis at 30-70µm and 60-100µm from the soma, 2 and 6 weeks after CSase ABC injection in Wistar rats.

These were the only morphological changes detected and were likely due to the small sample size of RGCs in these groups given that the CSase ABC injected BN rats showed no changes to RGC morphology.

Chapter 6: GAG pattern changes in glaucoma

6.1 Introduction

Clark *et al.* (2011) demonstrated that within the human retina GAGs are differentially distributed and that sulphation patterns change amongst the retinal layers. Evidence from other neurodegenerative diseases and CNS pathologies suggests that GAG composition in the ECM changes as a result of the pathology. In Alzheimer's disease and other dementia like diseases, DS and HS accumulate in plaques (Snow *et al.* 1988; van Horsen *et al.* 2002) while sulphation patterns change to include a greater proportion of C-4-S (Dewitt *et al.* 1993). The glial scars formed in traumatic brain injury, spinal cord injury and following stroke also contain high proportions of CSPGs (Fawcett and Asher 1999; Asher *et al.* 2002; Katsman *et al.* 2003; Soleman *et al.* 2013) which are likely to be formed as a response of reactive glial cells (Silver and Miller 2004; Properzi *et al.* 2005) to contain the spread of inflammation and neurodegeneration (Faulkner *et al.* 2004). Glial activation results in the upregulation and secretion of CSPGs *in vitro* (Johnsongreen *et al.* 1992; Koops *et al.* 1996; McKeon and Nophachi 1998) and *in vivo* (McKeon *et al.* 1991; Jones *et al.* 2002). In glaucoma, where the presence of reactive glial cells has been well documented, it is possible that the composition of GAGs may be altered. In development GSPGs repulse axons from non-target areas (Bandtlow and Zimmermann 2000). If areas of RGC loss are populated by activated glia then one may also expect increased CSPG secretion and deposition. This may cause a barrier to re-growth and expansion of RGCs into damaged areas, limiting the potential for RGC recovery. Glial scars in CNS injury represent a major barrier to re-innervation (Bradbury and Carter 2010). Over-sulphation of GAGs in these retinal areas could also prove a boundary to the re-growth of RGC dendrites as sulphated GAGs are known to be more inhibitory to neurite outgrowth than non-sulphated GAGs (Snow *et al.* 1990; Properzi *et al.* 2005).

In this chapter, GAG composition and sulphation patterns were explored in glaucomatous rat and human eyes and compared to control. CSase ABC cleaves CS/DS GAG chains leaving specific residues, known as 'stub epitopes', which reflect the sulphation pattern of the chain. These can be detected by antibodies 1B5, 2B6 and 3B3 which recognise C-0-S, C-4-S and C-6-S respectively (Caterson 2012). The donor glaucoma eyes used were complete with visual field tests performed <24 months before death which will allow for investigation of areas with known visual deficits. This allowed for the exploration of the relationship between visual deficits (and by extension disease severity) and the GAG profile of the retina, with particular attention on CSPGs of the GCL and IPL.

6.1.1 Hypothesis

In glaucomatous eyes the distribution and composition of GAGs is altered from the normal state.

6.1.2 Aims

- To determine whether experimental glaucoma induces changes in the GAG pattern in the rat retina.
- To determine whether glaucomatous human donor eyes exhibit changes in the retinal GAG pattern.
- To determine to what extent any changes relate to disease severity as assessed by visual function.

6.2 Methods

6.2.1 Glaucoma induction and intravitreal injection of CSase ABC in BN rats

Of the 27 BN rats described in Chapter 5 (5.2.2), 6 animals with experimental glaucoma (n=3 for OHT.PBS and n=3 for OHT.ABC) and 3 without (NT.ABC) were designated for IHC analysis presented in this chapter. Animals were killed 2 weeks following intravitreal injection (as per the experimental paradigm described in Figure 5.1) via perfusion fixation (see section 2.4.1). Following fixation the eyes were cryo-protected in 30% sucrose and 10 μ m thick sections cut on a cryostat as described in section 2.4.2. Sections were subject to Alcian blue staining and IHC as described below.

6.2.2 Human tissue preparation

Human donor eyes were obtained from the Mayo Clinic (MN, USA) and all work was carried out in accordance with the Human Tissue Act (2004) and US HIPAA regulations. Details of the donor eyes are displayed in Table 6.1 showing glaucoma and age matched controls. Eyes were age matched as closely as possible; glaucoma donors were 74.5 \pm 3.5 years compared to 75.5 \pm 15.5 years for control. Eyes were fixed (4% PFA) within 24 hrs of death. In all instances the cause of death was not deemed to have a direct pathological effect on the retina (e.g. from trauma), nor did the control eyes have any history of retinal pathology. Donor glaucoma eyes (n=4) were accompanied with visual field test information from 1 to 2 years before death taken at the Mayo Clinic. The retina was dissected free from the sclera and cut to leave a 2mm region surrounding the ONH. Four areas of retina corresponding to the anatomical position of 4 visual field test locations (Humphrey 24-2, Threshold test SITA standard strategy, Goldman III target) were chosen from regions of high (n=9) and low visual deficit (n=7). The level of deficit was determined according to the visual field threshold and total deviation. Retinotopically matching

areas were dissected in control retina. Locations were measured relative to the fovea using the conversion of visual degrees to mm distance (Drasdo and Fowler 1974) as conducted by Lei *et al.* (2009). The areas were cryo-protected in 30% sucrose before freezing in OCT (see section 2.4.2). Sections were cut at a thickness of 10µm before conducting Alcian blue staining and IHC analysis.

Table 6.1 Donor eye details

Donor ID	Group	Sex	Age (years)	Time to fixation following death (hrs)	Length of fixation before IHC (years)	Time between visual field test and death (months)
GL239	Glaucoma	M	77	3.8	3.5	23
GL277	Glaucoma	F	72	<24	1.16	18
14-0865R	Control	M	66	10.5	1.16	NA
14-0899L	Control	M	85	6.5	1.16	NA

6.2.3 Alcian blue staining

CS, DS, HS and hyaluronic acid are ionised at pH2.5 and attract the cationic dye Alcian blue through electrostatic linkage (Bancroft *et al.* 1996). The major components of the ECM/PNN can therefore be examined as a whole. 1g of Alcian blue 8GX (Sigma-Aldrich) was dissolved in 0.5M Acetic acid (pH2.5) and cryo-sections were stained in series. Sections were separated using a hydrophobic barrier pen and the stain applied for 8 hours. The sections were then briefly washed with 0.5M Acetic acid (pH2.5) only, before being rinsed with ddH₂O. The nuclei were counter-stained with Celestine blue (Celestine Blue 0.5g, ammonium iron(III) sulphate 5g, glycerol 14ml,

100ml ddH₂O; all Sigma-Aldrich) for 5 minutes before washing with ddH₂O (Maynard *et al.* 2014). The slides were dried, and a coverslip applied over hydromount (National diagnostics). Images were captured using a Leica DMRA2 with a Leica MC170HD camera attached.

6.2.4 GAG IHC

IHC followed the protocol described in section 2.4.3. Primary antibodies 1B5, 2B6 and 3B3 that recognise CS-stub epitopes (C-0-S, C-4-S and C-6-S stubs respectively) were used. The primary antibodies were applied at a 1:5 dilution (PBS) following blocking with 5% Goat serum (Sigma). For secondary antibody only controls, a number of sections were incubated with only PBS. After rehydrating section and before the application of the block sections were incubated with 0.5U/ml CSase ABC (Sigma) in 1M Tris acetate (pH 8 at 37°C). The samples were placed in a humidity chamber and incubated for 8 hours in an orbital incubator at 37°C. Following incubation the samples were washed with PBS for 5 minutes (3 repeats). Primary antibodies were then applied as normal. As a control to this pre-IHC digestion step a number of sections underwent the same protocol but with only Tris acetate applied. Goat anti-mouse alexafluor-488 secondary antibody (Life Technologies; either IgG for 1B5, 2B6 or IgM for 3B3) was applied (1:200). Sections were imaged using a Leica DM6000B as described in section 2.5.1 and fluorescent intensity was quantified.

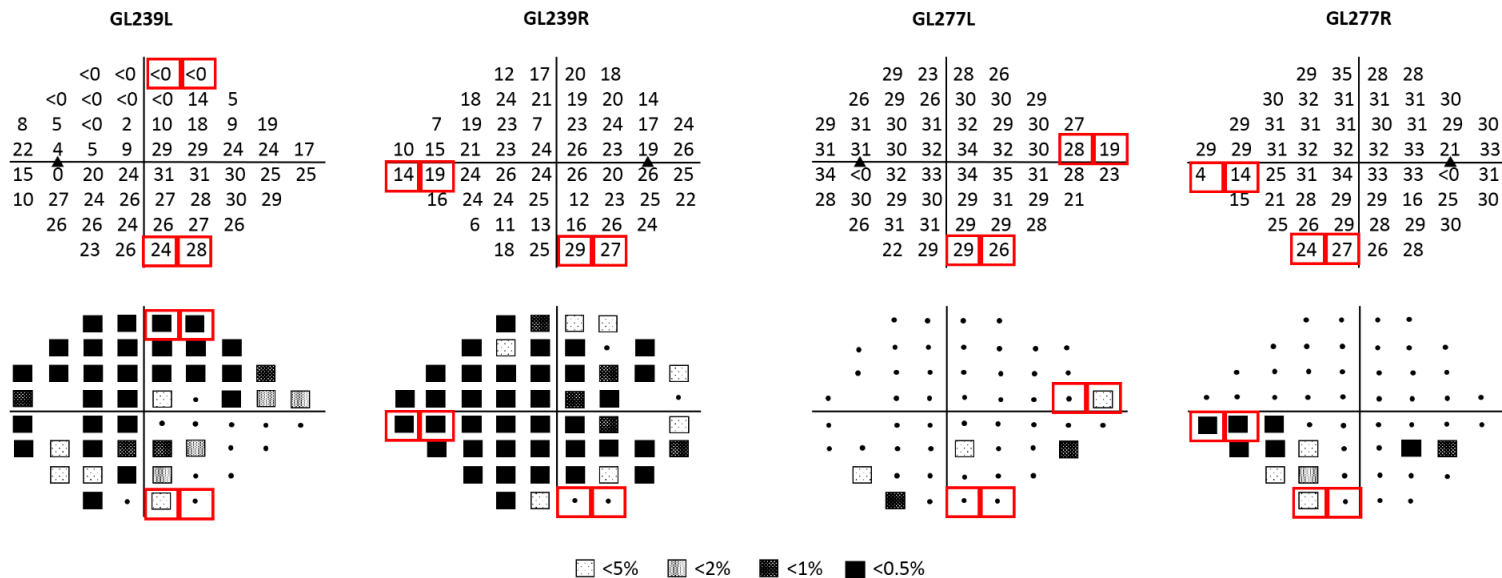


Figure 6.1 Visual field tests corresponding to donor eyes. Visual field thresholds (dB) and corresponding total deviation % grouping for donor eyes GL239 and GL277 conducted 1 to 2 years before death. The field tests were Humphrey 24-2, Threshold test- SITA standard strategy, Goldman III target. Areas of the retina corresponding to the test locations (9 areas of visual deficit and 7 areas of no detectable visual deficit) highlighted in red were dissected and analysed using GAG IHC. The black triangle denotes the position of the ONH.

6.3 Results

6.3.1 The GAG profile in the rat retina is unaltered in experimental glaucoma

Alcian Blue staining in the rat retina showed that GAGs are distributed throughout the retinal layers, but are mostly concentrated within the GCL, ONL and inner segments (IS) of the photoreceptors. This pattern was consistent for experimental glaucoma animals and those treated with CSase ABC. A more detailed and quantifiable assessment of the GAG pattern was investigated using stub antibodies 1B5, 2B6 and 3B3 that recognise C-0-S, C-4-S and C-6-S respectively. Application of CSase ABC directly onto sections revealed the GAG sulphation pattern of the retina. There was no 1B5 labelling present in the rat retina in all experimental groups, with fluorescent intensity not significantly different with respect to secondary only controls. C-4-S was found in all retinal layers in a similar proportion. Experimental glaucoma did not alter the sulphation pattern of the retina as there was no significant difference in the average pixel intensity corresponding to 2B6 labelling between NT and OHT.PBS ($P=1.0$ for all retinal layers; One-way ANOVA with post-hoc Bonferroni). Treatment with CSase ABC also had no effect on C-4-S distribution or intensity compared to NT ($P=1.0$ for all retinal layers; statistical test as before) or OHT.PBS ($P=1.0$; as before). Administration of CSase ABC alone also had no effect with no significant difference between NT.ABC and NT, OHT.PBS and OHT.ABC ($P=1.0$, $P=1.0$, $P=1.0$ respectively; values for all retinal layers; statistical test as before). Weak 3B3 labelling corresponding to C-6-S sulphation was found diffusely throughout the retina, but was concentrated at the photoreceptor inner and outer segments (IS, OS respectively). Again, no significant difference in C-6-S was found between any experimental groups for any of the retinal layers indicating that glaucoma and CSase ABC treatment had no effect on the overall sulphation pattern of the retina.

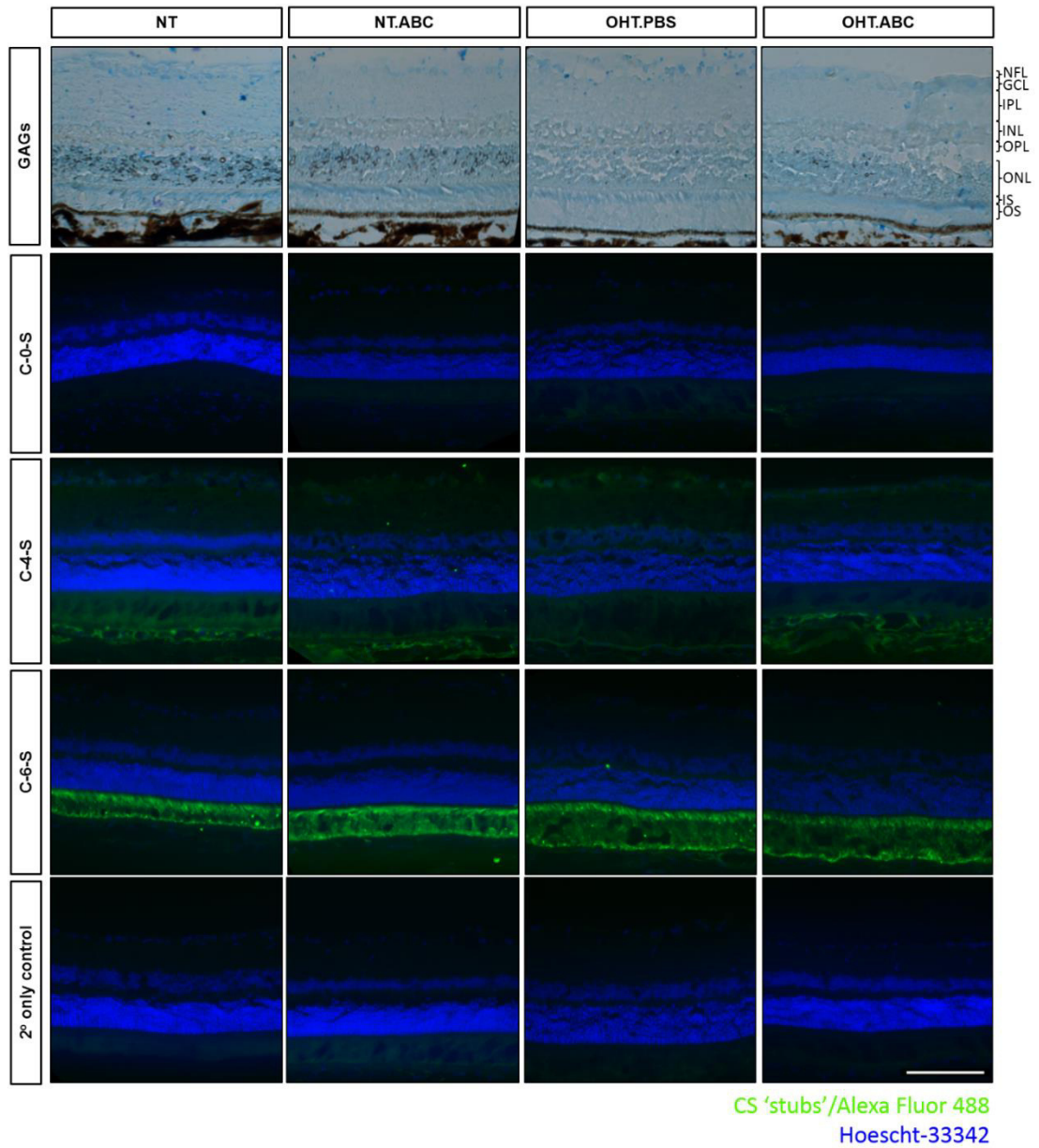


Figure 6.2 GAG labelling in the rat retina. GAG distribution was similar amongst experimental groups. Alcian blue staining revealed that GAGs are located within all retinal layers but are most highly concentrated in the GCL/NFL complex, ONL and photoreceptor IS. Labelling with stub antibodies 1B5, 2B6 and 3B3 (that recognise C-0-S, C-4-S and C-6-S respectively) after CSase ABC digestion of sections showed that the sulphation pattern of GAGs differed in the retinal layers. Only C-4-S sulphation occurred in the inner retinal layers in high levels. C-6-S was mostly localised within the IS and OS. C-0-S was not found in any retinal layers. Pixel intensity analysis revealed that there was no difference in sulphation pattern between any of the experimental groups. Scale bar = 100µm.

6.3.3 The retinal GAG sulphation pattern changes in human glaucoma

The overall distribution of GAGs within the human retina was similar to that seen in the rat. Again, GAGs were stained in all retinal layers and were more highly concentrated in the NFL/GCL, ONL and IS. There did not appear to be any difference in this pattern in glaucomatous eyes in regions of visual deficit (glaucoma) or regions of no visual deficit (Normal Glaucoma, NG). Labelling with stub antibodies following CSase ABC digestion of the sections revealed the sulphation pattern of GAGs in the human retina. In the controls, strong labelling of C-4-S (with antibody 2B6) was present throughout the retina, and was particularly intense in the NFL, nuclear layers and photoreceptor segments. C-6-S labelling (with antibody 3B3) was detected very weakly throughout the retina, but was concentrated at the photoreceptor segments. C-0-S (labelled with antibody 1B5) was not detected in the retina, the fluorescent intensity was not significantly different to secondary only controls in any of the retinal layers. In glaucoma, the average pixel intensity for C-4-S labelling was significantly increased over normal control retina in the NFL/GCL complex (70 ± 22 against 44 ± 16 ; $P=0.004$, One-way ANOVA with post-hoc Bonferroni) and IPL (55.6 ± 16 against 38 ± 13 ; $P=0.013$, statistical test as before). For all other retinal layers there was no significant difference. C-6-S labelling was also altered with the average pixel intensity significantly higher in glaucoma than control in the NFL/GCL complex (11 ± 7 against 4 ± 3 ; $P=0.042$, statistical test as before), but was not significantly changed in all other retinal layers. The GAG sulphation pattern therefore appears to change in glaucomatous eyes in the inner retina with the outer retina unaffected.

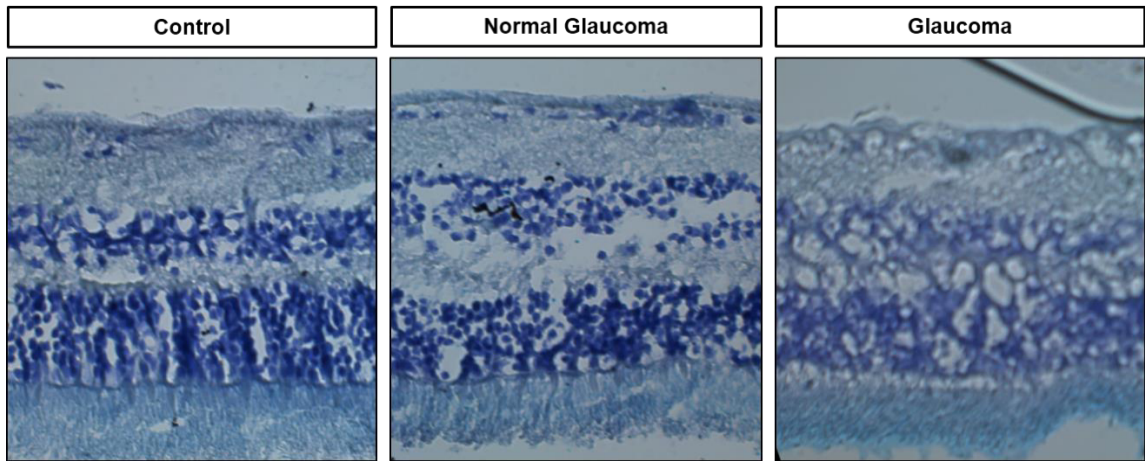


Figure 6.3 Alcian Blue staining of human retina. GAG were again distributed amongst all retinal layers, and were highly concentrated in the IS. There was no clear difference in Alcian blue (blue) staining between control, and glaucomatous retinas. Regions of no visual deficit in glaucomatous eyes (Normal Glaucoma) were similar in their GAG distribution to both control and Glaucoma eyes. Nuclear layers are stained with Celestine blue (purple).

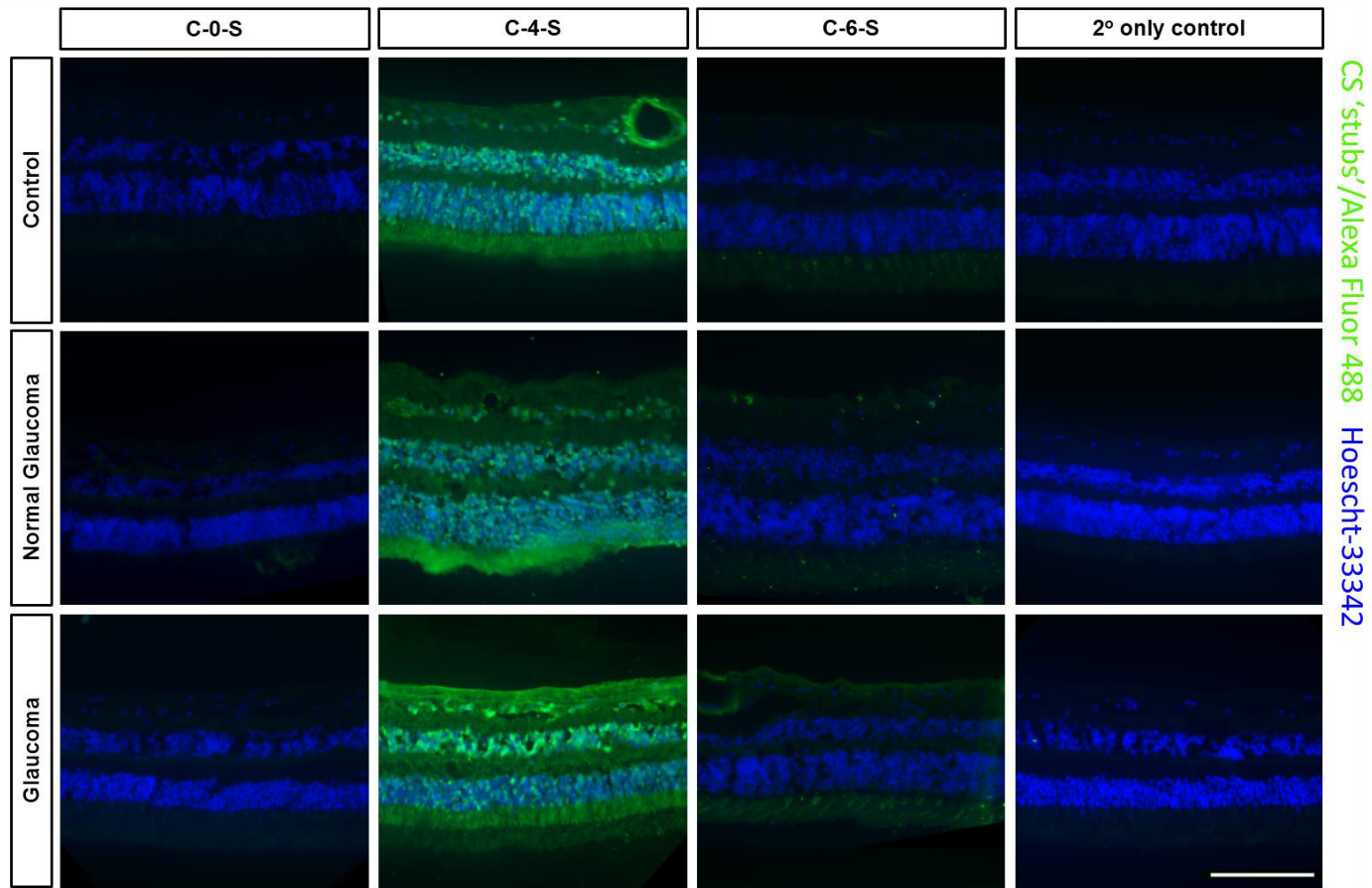


Figure 6.4 Sulphation pattern changes in the human retina in glaucoma. In the human retina, the sulphation pattern was similar to that in the rat with C-4-S sulphation the most abundant and distributed through all retinal layers. C-6-S was found weakly in all layers but was particularly strong in the photoreceptor IS and OS. Again, there was no detectable 1B5 labelling suggesting that there is no C-0-S sulphation in the human retina. Areas of visual deficit in glaucomatous eyes exhibited increased 2B6 labelling in the NFL/GCL and IPL, indicating an increase in C-4-S in these areas. This increase was not seen in areas of no visual deficit (Normal Glaucoma) suggesting that the increase in C-4-S is localised to regions of damage. Scale bar=100µm.

6.3.5 The GAG pattern differs in areas of high visual deficit

In order to relate the changes in GAG patterns to visual deficit the areas were grouped according to visual field total deviation. The total deviation describes how the threshold achieved at each test area differs from a normal control population. Areas that showed significant deviation were grouped as glaucoma, areas that showed no significant deviation were grouped as normal glaucoma (NG) and areas from control retina were grouped as control. C-4-S was unchanged in NG areas compared to control, showing no significant difference in average pixel intensity in the NFL/GCL complex (29 ± 2 against 44 ± 16 ; $P=0.564$, One-way ANOVA with post-hoc Bonferroni) or IPL (22 ± 3 against 38 ± 13 ; $P=0.157$, statistical test as before). Glaucoma areas showed significantly greater C-4-S labelling than NG area in both the NFL/GCL complex (70 ± 22 against 29 ± 2 ; $P=0.001$, as before) and IPL (56 ± 16 against 22 ± 3 ; $P=0.001$, as before). Labelling of C-6-S in NG areas showed no significant difference to control in the NFL/GCL complex (12 ± 7 against 4 ± 3 ; $P=0.070$, as before) but was similar to that in glaucoma areas (11 ± 7 against 12 ± 7 ; $P=1.0$, as before). These data show that the GAG sulphation pattern changes significantly only in the areas of visual deficit.

6.3.6 The magnitude of GAG pattern change in the IPL shows relationship to visual deficit

The magnitude of total deviation (dB) was found to correlate inversely with the intensity of C-4-S labelling in the NFL/GCL complex ($r=-0.566$; $P=0.008$, Spearman's rank order correlation) and IPL ($r=-0.737$; $P=0.001$; statistical test as before) suggesting an increase of C-4-S sulphated GAGs with disease severity (deviation is a negative value). The intensity of C-6-S labelling in the NFL/GCL complex did not correlate significantly with the total deviation, showing no relationship ($r=0.314$; $P=0.204$; statistical test as before). The statistical chance that the total deviation recorded at each test location is not significantly different from a normal control population is also given in the field analysis. These chances are given as <5%, <2%, <1% and <0.5%. For 3 of the chosen deficit areas this was a <5% chance and was a <0.5% chance for the other 6. When the areas were grouped according to this chance, the average total deviation was -22.1 ± 6 dB for the <0.5% chance group, -7.6 ± 5 dB for the <5% chance group, and -2.2 ± 2.2 dB for those areas that are not significantly different from a normal control population. The total deviation was significantly greater in the 0.5% group than normal group ($P=0.001$; Kruskal-Wallis test) and the 5% group ($P=0.021$; statistical test as before) but the 0.5% group was not significantly different from control normal group ($P=0.303$; as before). Grouping according to the % chance therefore reflects the severity of visual deficit. In the GCL/NFL average pixel intensity of C-4-S labelling did not significantly differ when comparing the 0.5% and 5% group (75 ± 22 and 73 ± 21 , $P=1.0$; One-way ANOVA with post-hoc Bonferroni) but was more highly significant in the 0.5% than 5% group when compared to control ($P=0.003$ compared to $P=0.013$; statistical test as before). However in the IPL, average pixel intensity corresponding to C-4-S labelling was significantly greater than control in the 0.5% (57 ± 17 against 31 ± 13 , $P=0.006$; statistical test as before) but not in the 5% group (52 ± 17 and 31 ± 13 , $P=0.160$; as before). The magnitude of GAG pattern change therefore appears to relate to the degree of visual deficit in the IPL but not the GCL. Again, labelling of C-

6-S showed no significant difference to control in the NFL/GCL complex in either the 0.5% or 5% group nor between the two latter groups ($P=0.263$, $P=1.0$, $P=1.0$ respectively; statistical test as before).

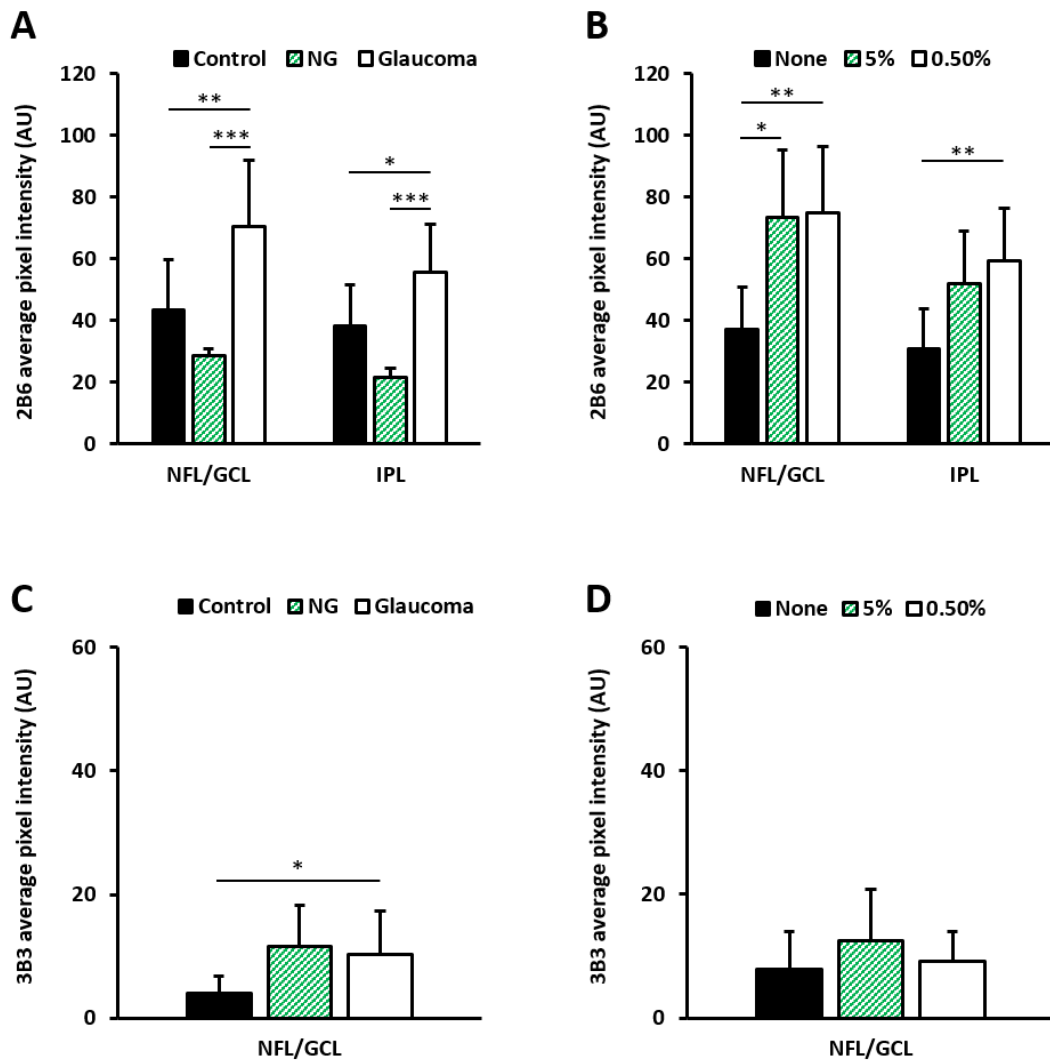


Figure 6.5 The degree of sulphation pattern change varies according to visual deficit. In NFL/GCL complex and IPL C-4-S (labelled through 2B6) was significantly increased in glaucomatous eyes in areas of visual deficit (Glaucoma) compared to areas of no visual deficit (NG) and control eyes (**A**). C-6-S sulphation (labelled through 3B3) was also increase in the NFL/GCL complex in glaucoma compared to control, but not in NG areas (**C**). Grouping the glaucoma areas according to the total deviation (into groups 5% and 0.5%, which reflect the severity of the visual deficit) showed that increases in C-4-S sulphation in the NFL/GCL occurs in areas of both moderate and severe visual deficit (**B**). In the IPL, C-4-S sulphation only increases in areas of severe visual deficit (**B**), while the increase of C-6-S became non-significant (**C**). Increased C-4-S sulphation therefore correlates with visual deficit and may reflect pathological changes to the retina. Error bars show SEM. * $P < 0.05$, ** $P < 0.01$, *** $P < 0.001$.

6.4 Discussion

The findings of this chapter show a differential distribution of GAGs within the retinal layers in both rats and humans. C-4-S, and to a lesser extent C-6-S, were found throughout the retinal layers, with the former particularly strong in the NFL and GCL. These results are in agreement with Clark *et al.* (2011) who also showed C-4-S and C-6-S labelling in the human retina. However, they showed that C-0-S was present throughout the retina whereas no labelling of C-0-S was identified here in rat or human retina, as the average pixel intensity was not significantly different to secondary antibody only controls. Strong C-6-S labelling, and weaker C-4-S labelling, in both the Brown Norway rat and human inner segments has been previously shown Hollyfield *et al.* (1999), consistent with the results presented here. C-4-S demonstrated a localisation around the RGC somas in the GCL in both rats and humans. CSPGs have previously been shown to form a dense surround to RGCs (Aquino *et al.* 1984) as is seen in other PNN bearing neurons.

Human retinas showed an increase in both C-4-S and C-6-S in the NFL/GCL in glaucoma eyes (in regions of visual deficit) with the former also increased in the IPL. Increased CSPG expression, in particular altered sulphation patterns which are a feature of CNS neurodegenerative diseases (Dewitt *et al.* 1993), have been shown in lesions of the optic nerve following crush (Selles-Navarro *et al.* 2001) and in the ONH in glaucoma at the site of the lamina cribrosa in primate eyes (Fukuchi *et al.* 1994) and the optic nerve in Brown Norway rats (Johnson *et al.* 1996). Increased expression of the core proteins to which the CS/DS GAGs attach have also been shown as a response to a number of CNS insults (Jones *et al.* 2002; Matsui *et al.* 2002). Neurocan, which has very few CS/DS GAG sidechains increases after retinal ischemic injury (Inatani *et al.* 2000). Further investigation with antibodies specific to other components of the CNS ECM may therefore uncover even greater changes in the GAG profile of the retina following glaucoma.

The increase in sulphated CS/DS GAGs in glaucoma may be the result of increased synthesis and secretion from reactive glial cells. Glial cells secrete CSPGs in response to CNS (McKeon *et al.* 1991; Haas *et al.* 1999; McKeon *et al.* 1999) and retinal injury (Inatani *et al.* 2000) and CSPG labelling is often associated with that of GFAP (McKeon *et al.* 1991; Dewitt *et al.* 1993). It would be interesting to explore whether in regions of glaucomatous retinas the increased sulphated CS/DS GAGs were co-localised with GFAP labelling. Given that CS/DS sulphation increased in human glaucoma, and that experimental glaucoma models have shown a similar pattern in the ONH (Fukuchi *et al.* 1994; Johnson *et al.* 1996), the lack of change in the rat retina is unexpected. It is possible that a) this reflects the differing nature of experimental and human glaucoma, b) that the experimental glaucoma was too moderate to induce any GAG changes as cell death was only ~10%, c) that the relatively young age of these rats was not conducive to GAG changes or d) that the 6 week period was not long enough for sufficient changes if any to occur.

In the cases of glaucoma described previously (Fukuchi *et al.* 1994; Johnson *et al.* 1996), C-4-S and C-6-S increases were related to the severity of glaucoma. Using the total deviation of visual deficit from the visual field test as a measure of disease severity, the increase of C-4-S seen here in human retina was correlated to the disease severity. Although some prominent studies predict a linear relationship between visual field sensitivity and RGC loss (Quigley *et al.* 1982; Harwerth *et al.* 1999), the relationship is curvilinear and shows a two stage linear relationship when plotted on a logarithmic scale (Garway-Heath *et al.* 2002; Swanson *et al.* 2004). The relation of sensitivity to disease severity is therefore justified, however caution is necessary in interpreting these GAG pattern changes in relation to actual RGC loss. The largest confounder to the validity of these results is the high test-retest variability of visual field analysis (Artes *et*

al. 2002) and the time between the field analysis and death and therefore more retinal areas should be analysed in order to mitigate the effects of any erroneous sensitivity measurements.

Chapter 7: General Discussion

This chapter provides an overview of the results obtained in the experimental chapters, with particular focus on the consequences and potential mechanisms behind the observations of RGC dendritic atrophy, dendritic protection and GAG changes.

7.1 RGC dendritic and synaptic atrophy

This thesis presents further evidence for the loss of dendrites as an early event in experimental glaucoma and concurs with the findings of reduced dendritic branching and field size in other models (Weber et al. 1998; Shou et al. 2003; Morgan et al. 2006; Li et al. 2011; Feng et al. 2013; Williams et al. 2013). In both chapters 4 and 5, OHT eyes suffered significant RGC dendritic atrophy. Interestingly, this loss was milder in the injected eyes in chapter 5 than chapter 4 and likely reflects the impact of differing IOP profiles. The increase over control was, roughly, 50% greater in mean and peak IOP and 25% greater in IOP AUC for the OHT eyes in chapter 4 compared to chapter 5. The extent of dendritic loss mirrored this difference in IOP, with the more acute pressure increase producing greater dendritic atrophy including dendritic field shrinkage. The latter was not observed with the more moderate pressure increase achieved in chapter 5. Further investigation revealed that dendritic loss here was confined to the higher order dendrites. The acute nature of IOP increase has been shown to correlate to the degree of RGC apoptosis (Guo *et al.* 2005) and dendritic atrophy (Li et al. 2011) and so reflects the severity of glaucoma. These results therefore allow for potential insight into the process of dendritic atrophy and are suggestive of an initial loss of higher order dendrites with a maintenance of overall shape in the early disease process. Investigation of the RGC morphology in the human retinas used in chapter 6 would be of particular interest, especially in the areas where no visual deficit was detected as these may be in the stages of early dendritic loss.

To understand why dendritic loss should occur as a consequence of glaucoma it is important to consider the unique nature of RGCs among other neurons. The axons of the RGC must traverse the retinal surface and exit the eye to innervate CNS targets. As such the axons cannot be myelinated without disrupting vision and so must carry action potentials without saltatory conduction for the distance of a few millimetres to centimetres (Crish and Calkins 2011). Mitochondria are therefore concentrated at the axon hillock of the RGC to provide the necessary energy (Barron et al. 2004). Given that one study has estimated the total ATP consumption of a resting cortical neuron at 4.7 billion molecules per second (Zhu *et al.* 2012), it is clear that the highly active RGCs demand considerable energy. The mitochondria of a neuron must also cater for the local demand in dendrites as well as axons - restoring ion gradients through ion channels and maintaining Ca^{2+} buffering (Brown et al. 2006; Schwarz 2013). Live imaging of mitochondria has shown their movement and distribution to be highly dynamic (Jakobs 2006). These organelles are continually turned over, removing those that are old and damaged, with some 10-40% moving at any given time (Ligon and Steward 2000; Wang and Schwarz 2009). Given the evidence of hypoperfusion, oxidative stress and homeostatic disruption in glaucoma (Minckler et al. 1977; Tezel et al. 2010), RGCs would be placed under considerable strain to meet the energy requirements of the cell. Mitochondria in dendrites have shown to be more susceptible to damage than those in the soma due to their relative isolation. These mitochondria have a longer lifespan, exhibit slower movement, and greater exposure and vulnerability to Ca^{2+} flux (Brown et al. 2006) and oxidative stress (Martinez et al. 1996). It is reasonable therefore to suggest that the dendrites bear the brunt of the pressures on energy demand in stressed RGCs, with the most distal tips effected first. Dendritic mitochondria have shown greater age related changes in their energy output (Battino et al. 1995), increased DNA deletion and impaired fission compared to those in the soma (Stauch et al. 2014). Associations between defects in

mitochondrial fission genes and glaucoma have also been found (Abu-Amero *et al.* 2006; Wolf *et al.* 2009; Sundaresan *et al.* 2015), while RGC dendritic atrophy is also a feature in diseases of mitochondrial dysfunction (Williams *et al.* 2010; Williams *et al.* 2012). These findings suggest that failure to maintain a sufficient dendritic pool of mitochondria could contribute to dendritic loss in glaucoma. OHT eyes showed decreased PSD95 labelling in chapter 4, indicting a loss of RGC synapses which may have been associated with stressed dendritic mitochondria. Synaptic loss in Alzheimer's is associated with abnormal mitochondrial function induced by the disease pathology (Reddy *et al.* 2012).

7.2 The influence of the RGC external environment on dendritic atrophy

7.2.1 The immune system

Activation of the immune system is thought to be an early response in glaucoma, with the upregulation of various ligands and cytokines (Ahmed et al. 2004; Agudo et al. 2008; Howell et al. 2011; Johnson et al. 2011) encouraging immune cell infiltration and recruitment to the ONH and retina (Son et al. 2010). Work in this thesis has built upon a growing body of evidence for the involvement of the complement system in glaucoma (Stasi *et al.* 2006; Stevens et al. 2007; Tezel et al. 2010; Howell et al. 2013) showing that RGCs can be partially protected from dendritic atrophy through inhibition of C1q in both rats and mice. C1q binding to cell surface markers of stress has been implicated in the initiation of phagocytosis by immune cells (Gardai et al. 2005; Shi et al. 2006; Fricker et al. 2012). In the data presented in chapter 4 both rats and mice showed a reduction of synapses in the IPL with glaucoma in agreement with others (Della Santina et al. 2013), but this was prevented in rats through C1q inhibition. Given the role of C1q in synapse elimination during development (Bialas and Stevens 2013) it is plausible that similar mechanisms contribute to the dendritic, and by extension, synaptic loss in RGCs (Stevens et al. 2007). Further investigation aimed at identifying co-localisation of C1q, PSD95 and markers of phagocytosis such as IBA1 would provide evidence of direct tagging of synapses for clearance. The upregulation of complement is also a feature of other neurodegenerative diseases where the antigenic profile of glial cells has been noted to resemble that of immature cells (Dangond *et al.* 2004; Fonseca *et al.* 2004) and so could aberrantly function in a manner similar to that during the period of synaptic refinement. During this period synapses are eliminated in an activity dependant manner, where stronger synapses impose both protective and punishment signals, with the latter contributing to the elimination of weaker, neighbouring synapses (Jennings 1994). C1q and C3 have been suggested as one method of punishment signalling (Stevens et al.

2007). Perhaps the weaker synapses in stressed RGCs are preferentially cleared in this manner in neurodegenerative diseases such as glaucoma.

7.2.2 The retinal ECM

During the period of synaptic refinement, and in the preceding stage of retinal synaptogenesis, the GAG ECM environment is heavily involved (Inatani and Tanihara 2002). Dynamic changes in GAG expression act as guidance cues for dendrites and axons but then stabilise to maintain favourable connections (Blue and Parnavelas 1983; Dityatev et al. 2007). The GAG profile then remains unchanged (Inatani and Tanihara 2002). In glaucomatous rats, those treated with CSase ABC did not show significant signs of dendritic atrophy, however the experiment performed cannot distinguish whether this was a protective or regenerative effect. In the case of the latter, application of CSase ABC has allowed for regeneration of axons through GAG rich glial scars (Bradbury et al. 2002) or removed the constrictive PNN allowing a shift in optical dominance (Pizzorusso et al. 2002). Discerning the mechanisms by which these effects would culminate in RGC dendritic survival is complicated by the vast and often conflicting nature of GAG functions. For instance, GAGs have been shown to inhibit neurite outgrowth (McKeon et al. 1991; Inatani et al. 2001) but also promote it through neurotrophic effect (Schulz et al. 1990; Nichol *et al.* 1994). GAGs have also been shown to bind numerous growth factors (Milev et al. 1998a; Milev et al. 1998c) although this is likely for sequestration rather than presentation to the cell; CSPGs for instance have been shown to inhibit BDNF binding to its receptor (Kurihara and Yamashita 2012). If, as hypothesised, digestion of GAGs in the retina removed the inhibition to RGCs from PNNs then the cells could have been free to receive neurotrophic stimuli found endogenously in the retina (Cui et al. 2002). However, the core proteins left following GAG sidechain digestion have themselves shown inhibitory effects on neuronal growth (McKeon et al. 1999). The ECM

environment is clearly multifaceted with respect to neuronal interaction. What impact would the digestion of the ECM have on the neurons that it is tasked with supporting? Investigation of the toxicity of CSase ABC when injected into the vitreous showed no significant neuronal loss in the retina nor changes to RGC morphology in normal eyes. These data suggest that GAG digestion is safe, but digestion could change the hydrodynamic properties, charge density and diffusion parameters of the extracellular space (Bruckner et al. 1998). In Schizophrenia, where impaired synaptic connectivity and pruning are features of the disease pathology (McGlashan and Hoffman 2000), association with polymorphisms in genes encoding PNN components have been found (Muhleisen *et al.* 2012) while post-mortem human tissue has shown a decrease in PNNs (Mauney *et al.* 2013; Pantazopoulos *et al.* 2013). In particular, fast-spiking parvalbumin-positive GABAergic interneurons, which are PNN positive, are known to be functionally impaired in the disease leading to cognitive and perceptual defects (Bitanirwe *et al.* 2009). Disruption to PNNs in schizophrenia may not only effect synapse stability but also alter ion balances and thus disrupt the firing properties of these neurons (Bitanirwe and Woo 2014). These suggest that GAG digestion by CSase ABC could have consequences for the electrophysiological properties of the RGCs that would need to be investigated further before CSase ABC treatment could be considered efficacious in treating glaucoma.

7.2.2 Association of the Immune system with the ECM

In human glaucomatous retina, regions of high visual deficit corresponded with increased levels of sulphated GAGs. This was in agreement with other areas of the eye in glaucoma (Fukuchi et al. 1994; Johnson et al. 1996) and in other neurodegenerative disorders (Haas et al. 1999; McKeon et al. 1999). It appears that GAG deposition is a response of activated glial cells. The increase in GAGs observed could therefore be an indication of increased glial infiltration and

activation in the glaucomatous retina. The sheer diversity of GAGs results in more and more functions and interactions of the ECM being uncovered (Caterson 2012). In particular, it seems that GAGs and the immune system are closely associated. CS/DS sidechains not only bind numerous growth factors but also chemokines and L- and P- selectins (Kawashima *et al.* 2002) which are upregulated in numerous inflammatory diseases including glaucoma (Johnson *et al.* 2011; Howell *et al.* 2012). Certain chemokines in particular are bound with higher affinity in oversulphated GAGs (Kawashima *et al.* 2002), and the authors suggest that this may be an attempt at sequestration. Increased GAG sulphation has also been shown to improve the binding and activity of certain growth factors (Taylor *et al.* 2005). HS and DS have also demonstrated an ability to bind complement factor H (a regulator of the complement system) and deactivate C3b depositions on the cells surface in the retina (Clark *et al.* 2010). The increased sulphation seen in human eyes could therefore be both a consequence of, and attempt to mitigate, glial activation. Further investigation of the effects of GAG digestion by CSase ABC should therefore focus on the impact on immune recruitment and activation in these damaged areas.

7.3 Functional consequences of RGC structure change

The relationship of RGC morphology to the receptive field suggests that even subtle dendritic loss may impact the function at the single cell level. Webber *et al.* (1998) showed reduced spatial and temporal resolution in glaucomatous RGC receptive fields, accompanied by a reduced branching density and dendritic field size. Dendritic atrophy results in the reduced density of bipolar cell synapses and thus would cause a loss of resolution. The loss of dendrites and accompanying synapses would also affect the ability of the RGC to reach firing threshold as fewer inputs would be summated. This would manifest as a reduced spike rate; as observed by Della Santina *et al.* (2013). RGC to RGC gap junctions, which facilitate synchronised firing (Dacey and Brace 1992), are located on the peripheral dendrite tips (Hidaka *et al.* 2004), and may be lost as a result of decreased dendritic branching and field size. A reduction or loss of these gap junctions would impede the RGC in reaching threshold and thus also reduce its spike rate.

The preferential loss of higher order dendrites, as observed in chapter 5, would be favourable for the maintenance of visual function. As bipolar cell synapses are distributed evenly along RGC dendrites (Jakobs *et al.* 2008) this pattern of dendrite loss would preserve the receptive field in the same general shape through minimising the disruption of the loss of bipolar cell synapses. A random or asymmetric loss would drastically alter the shape of the receptive field by eliminating areas of the underlying uniform bipolar cell mosaic (MacNeil *et al.* 2004), rather than reducing the density of connections. Dendritic loss that allows the closest approximation to complete bipolar cell tiling would allow for the greatest retention of function. The receptive fields recorded by Della Santina *et al.* (2013) are suggestive of this as the receptive field size was maintained despite a reduction in synapses, with only the spike rate of the cell altered. The distribution of mitochondria within dendrites may result in this pattern of dendritic loss.

The functional deficits induced by dendritic loss at the level of the receptive field may be masked perceptually in the early disease stages. RGC tiling of the retina and the extensive overlap of dendritic fields (DeVries and Baylor 1997) may allow for the maintenance of overall visual resolution. Visual redundancy is high when viewing natural scenes as opposed to traditional stimuli, with one study suggesting it reaches ~10-fold (Puchalla *et al.* 2005). The summation of RGC inputs may therefore compensate for the reduced spatial resolution and smooth out the effects at the perceptual level. In early glaucoma in humans, standard automated perimetry has revealed that both spatial (Redmond *et al.* 2010) and temporal (Mulholland *et al.* 2015) summation are increased in order to preserve detection thresholds.

7.4 Conclusions and future direction

This thesis presents data supporting the loss of dendrites as an early feature in experimental glaucoma. Given the varying morphology of the RGC types, classification of RGCs is important in avoiding type-specific bias when quantifying dendrite morphological change in disease. The successful derivation of a classification method based on proximal dendrite features (which are spared in early disease), as presented in chapter 3, could therefore prove a useful tool for dendrite analyses. Given a larger sample size this method could be expanded to include RGC subtypes which could reduce misclassification. A feasible short term goal would be to package the morphological analysis of the primary dendrite features as a software application, ideally an image analysis plugin distributable through a GNU general public license for applications such as FIJI. It would allow an easily accessible classification bias check for researchers. Although only applicable to researchers using BN rats, this statistical approach could also be applied to RGCs of other commonly used species and strains.

The impact of the RGCs extracellular environment on dendrite loss and recovery in glaucoma was investigated in chapters 4 and 5, focusing on the complement system and PNNs respectively. Inhibition of the complement system was effective in two experimental glaucoma models in reducing dendritic atrophy and accompanies a growing body of work suggesting the complement system (Howell et al. 2011; Howell et al. 2013) and wider immune system contributes to RGC loss (Gramlich et al. 2015). The administration of CSaseABC to digest the restrictive PNNs surrounding RGCs was also effective in reducing dendritic atrophy in experimental glaucoma. These manipulations require further research to investigate whether dendritic recovery is accompanied by a functional benefit. Analysis of synapses with PSD95 was inconclusive and a more sensitive method would be a necessary step. Biolistic labelling of RGCs with a PSD95-XFP plasmid could reveal whether these treatments gave synaptic protection. A

CMV or equivalent driver would be necessary as ganglion cell specific promoters such as Thy.1 are known to be downregulated in glaucoma (Schlamp et al. 2001; Huang et al. 2006). Functional assessment of vision would also be key. Comparison of pattern ERG recordings before and after treatment could give an indication of gross RGC recovery (Ben-Shlomo *et al.* 2005) while single cell receptive field recordings would offer greater insight into the relationship of dendrite loss and recovery and the resultant single cell function (Della Santina et al. 2013).

If a visual benefit were detected, C1inh and CSase ABC could become potential therapies for glaucoma. However, C1 inhibition would likely be an unfavourable option. The C1inh Cinryza® (as used in chapter 4) is FDA approved for use in hereditary angioedema (U.S. Food and Drug Administration 2008) although only via intravenous administration. Therefore a large dose is needed (1000U), which causes frequent adverse reactions (headaches 1:2, nausea 1:3, rash 1:3) and carries a risk of hypersensitivity reactions and thromboembolic events (New York: Lev Pharmaceuticals Inc. 2009); the latter would not represent a good cost/benefit ratio given the elderly demographic of glaucoma patients. Intravitreal administration would allow a dose 2 magnitudes of order lower (as used in chapter 4) and so would mitigate these adverse reactions. However, as is also the case with CSase ABC injection, that route would not be favourable for patients. A Study of patient adherence to anti-VEGF therapy showed that fear of intravitreal injections is common (~50%) and adherence was largely based on the patient's belief of an ascribed benefit to vision (Droege *et al.* 2013). Without sizable improvement to vision, these would not represent viable therapies in their current form. However, they do offer insights into mechanisms influencing RGC dendritic loss and are therefore worth further study. Increased sulphation of GAGs was detected in post-mortem glaucomatous tissue from donors in chapter 6. Over-sulphation is known to be inhibitory to neuron regrowth and so CSaseABC injections could act to digest the sulphated GAG content of the retina in these patients and would

represent a viable strategy to prime the retina prior to the use of more robust and tractable neuro-regenerative therapies of the future. CSase ABC has been used to enhance stem cell integration into the retina in animal models of disease (Suzuki *et al.* 2007; Ma *et al.* 2011). This thesis shows that a single CSase ABC injection has no detected adverse effects on retinal neurons and so could be used in either of these ways as part of a viable glaucoma therapy in the future.

References

Abbott, C. J., Choe, T. E., Burgoyne, C. F., Cull, G., Wang, L. and Fortune, B. (2014). Comparison of Retinal Nerve Fiber Layer Thickness In Vivo and Axonal Transport after Chronic Intraocular Pressure Elevation in Young versus Older Rats. *Plos One* **9**.

Abu-Amero, K. K., Morales, J. and Bosley, T. M. (2006). Mitochondrial abnormalities in patients with primary open-angle glaucoma. *Investigative Ophthalmology & Visual Science* **47**:2533-2541.

Agis, I. (2000). The Advanced Glaucoma Intervention Study (AGIS): 7. The relationship between control of intraocular pressure and visual field deterioration. *American Journal of Ophthalmology* **130**:429-440.

Agudo, M., Perez-Marin, M. C., Loengren, U., Sobrado, P., Conesa, A., Canovas, I., Salinas-Navarro, M. *et al.* (2008). Time course profiling of the retinal transcriptome after optic nerve transection and optic nerve crush. *Molecular Vision* **14**:1050-1063.

Ahmed, F., Brown, K. M., Stephan, D. A., Morrison, J. C., Johnson, E. C. and Tomarev, S. I. (2004). Microarray analysis of changes in mRNA levels in the rat retina after experimental elevation of intraocular pressure. *Investigative Ophthalmology & Visual Science* **45**:1247-1258.

Ahmed, F., Chaudhary, P. and Sharma, S. C. (2001). Effects of increased intraocular pressure on rat retinal ganglion cells. *International Journal of Developmental Neuroscience* **19**.

Ahnelt, P. and Kolb, H. (1994). Horizontal cells and cone photoreceptors in human retina - a golgi-electron microscopic study of spectral connectivity. *Journal of Comparative Neurology* **343**:406-427.

Ahnelt, P. K. (1998). The photoreceptor mosaic. *Eye* **12**:531-540.

Alasil, T., Wang, K., Yu, F., Field, M. G., Lee, H., Baniyadi, N., de Boer, J. F. *et al.* (2014). Correlation of Retinal Nerve Fiber Layer Thickness and Visual Fields in Glaucoma: A Broken Stick Model. *American Journal of Ophthalmology* **157**:953-959.

Amthor, F. R., Takahashi, E. S. and Oyster, C. W. (1989a). Morphologies of rabbit retinal ganglion-cells with complex receptive-fields. *Journal of Comparative Neurology* **280**:97-121.

Amthor, F. R., Takahashi, E. S. and Oyster, C. W. (1989b). Morphologies of rabbit retinal ganglion-cells with concentric receptive-fields. *Journal of Comparative Neurology* **280**:72-96.

Anderson, D. R. (2011). Normal-tension glaucoma (Low-tension glaucoma). *Indian Journal of Ophthalmology* **59**:S97-S101.

Anderson, D. R. and Hendrick, A. (1974). Effect of intraocular-pressure on rapid axoplasmic-transport in monkey optic-nerve. *Investigative Ophthalmology* **13**:771-783.

Anderson, M. G., Libby, R. T., Gould, D. B., Smith, R. S. and John, S. W. M. (2005). High-dose radiation with bone marrow transfer prevents neurodegeneration in an inherited glaucoma. *Proceedings of the National Academy of Sciences of the United States of America* **102**:4566-4571.

Anderson, M. G., Smith, R. S., Hawes, N. L., Zabaleta, A., Chang, B., Wiggs, J. L. and John, S. W. M. (2002). Mutations in genes encoding melanosomal proteins cause pigmentary glaucoma in DBA/2J mice. *Nature Genetics* **30**:81-85.

Aquino, D. A., Margolis, R. U. and Margolis, R. K. (1984). Immunocytochemical localization of a chondroitin sulfate proteoglycan in nervous-tissue .1. Adult brain, retina, and peripheral-nerve. *Journal of Cell Biology* **99**:1117-1129.

Artes, P. H., Iwase, A., Ohno, Y., Kitazawa, Y. and Chauban, B. C. (2002). Properties of perimetric threshold estimates from full threshold, SITA standard, and SITA fast strategies. *Investigative Ophthalmology & Visual Science* **43**:2654-2659.

Asher, R. A., Morgenstern, D. A., Shearer, M. C., Adcock, K. H., Pesheva, P. and Fawcett, J. W. (2002). Versican is upregulated in CNS injury and is a product of oligodendrocyte lineage cells. *Journal of Neuroscience* **22**:2225-2236.

Bally, I., Rossi, V., Lunardi, T., Thielens, N. M., Gaboriaud, C. and Arlaud, G. J. (2009). Identification of the C1q-binding Sites of Human C1r and C1s a refined three-dimensional model of the c1 complex of complement. *Journal of Biological Chemistry* **284**:19340-19348.

Bancroft, J. D., Stevens, A., Bancroft, J. D. and Stevens, A. (1996). Theory and practice of histological techniques, Fourth edition. pp. xiii+766p-xiii+766p.

Bandtlow, C. E. and Zimmermann, D. R. (2000). Proteoglycans in the developing brain: New conceptual insights for old proteins. *Physiological Reviews* **80**:1267-1290.

Barlow, H. B. and Hill, R. M. (1963). Selective sensitivity to direction of movement in ganglion cells of rabbit retina. *Science* **139**:412-&.

Barnstable, C. J. and Drager, U. C. (1984). THY-1 ANTIGEN - A GANGLION-CELL SPECIFIC MARKER IN RODENT RETINA. *Neuroscience* **11**:847-&.

Barron, M. J., Griffiths, P., Turnbull, D. M., Bates, D. and Nichols, P. (2004). The distributions of mitochondria and sodium channels reflect the specific energy requirements and conduction properties of the human optic nerve head. *British Journal of Ophthalmology* **88**:286-290.

Battino, M., Gorini, A., Villa, R. F., Genova, M. L., Bovina, C., Sassi, S., Littarru, G. P. *et al.* (1995). Coenzyme-Q content in synaptic and nonsynaptic mitochondria from different brain-regions in the aging rat. *Mechanisms of Ageing and Development* **78**:173-187.

Baxter, G. T., Radeke, M. J., Kuo, R. C., Makrides, V., Hinkle, B., Hoang, R., MedinaSelby, A. *et al.* (1997). Signal transduction mediated by the truncated trkB receptor isoforms, trkB.T1 and trkB.T2. *Journal of Neuroscience* **17**:2683-2690.

Beirowski, B., Babetto, E., Coleman, M. P. and Martin, K. R. (2008). The WldS gene delays axonal but not somatic degeneration in a rat glaucoma model. *Eur J Neurosci* **28**:1166-1179.

Bell, K., Gramlich, O. W., Hohenstein-Blaul, N. V. T. U., Beck, S., Funke, S., Wilding, C., Pfeiffer, N. *et al.* (2013). Does autoimmunity play a part in the pathogenesis of glaucoma? *Progress in Retinal and Eye Research* **36**:199-216.

Ben-Shlomo, G., Bakalash, S., Lambrou, G. N., Latour, E., Dawson, W. W., Schwartz, M. and Ofri, R. (2005). Pattern electroretinography in a rat model of ocular hypertension: functional evidence for early detection of inner retinal damage. *Experimental Eye Research* **81**:340-349.

Bengtsson, B., Patella, V. M. and Heijl, A. (2009). Prediction of Glaucomatous Visual Field Loss by Extrapolation of Linear Trends. *Archives of Ophthalmology* **127**:1610-1615.

Berretta, S., Pantazopoulos, H., Markota, M., Brown, C. and Batzianouli, E. T. (2015). Losing the sugar coating: Potential impact of perineuronal net abnormalities on interneurons in schizophrenia. *Schizophrenia Research* **167**:18-27.

Berson, D. M. (2003). Strange vision: ganglion cells as circadian photoreceptors. *Trends in Neurosciences* **26**:314-320.

Berson, D. M., Isayama, T., O'Brien, B. J. and Pu, M. (1999a). The kappa ganglion cell type of cat and ferret retina. *Investigative Ophthalmology & Visual Science* **40**:S813-S813.

Berson, D. M., Isayama, T. and Pu, M. (1999b). The eta ganglion cell type of cat retina. *Journal of Comparative Neurology* **408**:204-219.

Bialas, A. R. and Stevens, B. (2013). TGF-beta signaling regulates neuronal Clq expression and developmental synaptic refinement. *Nature Neuroscience* **16**:1773-1782.

Bitanhirwe, B. K. Y., Lim, M. P., Kelley, J. F., Kaneko, T. and Woo, T. U. W. (2009). Glutamatergic deficits and parvalbumin-containing inhibitory neurons in the prefrontal cortex in schizophrenia. *Bmc Psychiatry* **9**.

Bitanhirwe, B. K. Y. and Woo, T. U. W. (2014). Perineuronal nets and schizophrenia: The importance of neuronal coatings. *Neuroscience and Biobehavioral Reviews* **45**:85-99.

Blue, M. E. and Parnavelas, J. G. (1983). The formation and maturation of synapses in the visual-cortex of the rat .1. Qualitative-analysis. *Journal of Neurocytology* **12**:599-616.

Bosco, A., Steele, M. R. and Vetter, M. L. (2011). Early Microglia Activation in a Mouse Model of Chronic Glaucoma. *Journal of Comparative Neurology* **519**:599-620.

Bowd, C., Weinreb, R. N., Williams, J. M. and Zangwill, L. M. (2000). The retinal nerve fiber layer thickness in ocular hypertensive, normal, and glaucomatous eyes with optical coherence tomography. *Archives of Ophthalmology* **118**:22-26.

Boycott, B. B., Dowling, J. E. and Kolb, H. (1969). Organization of primate retina - light microscopy - a second type of midget bipolar cell in primate retina. *Philosophical Transactions of the Royal Society of London Series B-Biological Sciences* **255**:109-&.

Bradbury, E. J. and Carter, L. M. (2011). Manipulating the glial scar: Chondroitinase ABC as a therapy for spinal cord injury. *Brain Research Bulletin* **84**:306-316.

Bradbury, E. J., Moon, L. D. F., Popat, R. J., King, V. R., Bennett, G. S., Patel, P. N., Fawcett, J. W. *et al.* (2002). Chondroitinase ABC promotes functional recovery after spinal cord injury. *Nature* **416**:636-640.

Brakebusch, C., Seidenbecher, C. I., Asztely, F., Rauch, U., Matthies, H., Meyer, H., Krug, M. *et al.* (2002). Brevican-deficient mice display impaired hippocampal CA1 long-term potentiation but show no obvious deficits in learning and memory. *Molecular and Cellular Biology* **22**:7417-7427.

Brauer, K., Hartig, W., Gartner, U., Bruckner, G. and Arendt, T. (2000). Different myelination of rat septohippocampal fibres as revealed by immunofluorescence double-labelling. *Brain Research* **878**:188-193.

Brittis, P. A., Canning, D. R. and Silver, J. (1992). Chondroitin sulfate as a regulator of neuronal patterning in the retina. *Science* **255**:733-736.

Brooks, D. E., Strubbe, D. T., Kubilis, P. S., Mackay, E. O., Samuelson, D. A. and Gelatt, K. N. (1995). Histomorphometry of the optic nerves of normal dogs and dogs with hereditary glaucoma. *Experimental Eye Research* **60**:71-89.

Brown, G. C. and Neher, J. J. (2012). Eaten alive! Cell death by primary phagocytosis: 'phagoptosis'. *Trends in Biochemical Sciences* **37**:325-332.

Brown, G. C. and Neher, J. J. (2014). Microglial phagocytosis of live neurons. *Nature Reviews Neuroscience* **15**:209-216.

Brown, J. E. and Major, D. (1966). Cat retinal ganglion cell dendritic fields. *Experimental Neurology* **15**:70-&.

Brown, M. R., Sullivan, P. G. and Geddes, J. W. (2006). Synaptic mitochondria are more susceptible to Ca²⁺ overload than nonsynaptic mitochondria. *Journal of Biological Chemistry* **281**:11658-11668.

Brown, S. P., He, S. G. and Masland, R. H. (2000). Receptive field microstructure and dendritic geometry of retinal ganglion cells. *Neuron* **27**:371-383.

Bruckner, G., Bringmann, A., Hartig, W., Koppe, G., Delpech, B. and Brauer, K. (1998). Acute and long-lasting changes in extracellular-matrix chondroitin-sulphate proteoglycans induced by injection of chondroitinase ABC in the adult rat brain. *Experimental Brain Research* **121**:300-310.

Buckingham, B. P., Inman, D. M., Lambert, W., Oglesby, E., Calkins, D. J., Steele, M. R., Vetter, M. L. *et al.* (2008). Progressive ganglion cell degeneration precedes neuronal loss in a mouse model of glaucoma. *Journal of Neuroscience* **28**:2735-2744.

Buhl, E. H. and Dann, J. F. (1988). Morphological diversity of displaced retinal ganglion-cells in the rat - a lucifer yellow study. *Journal of Comparative Neurology* **269**:210-218.

Bukalo, O., Schachner, M. and Dityatev, A. (2001). Modification of extracellular matrix by enzymatic removal of chondroitin sulfate and by lack of Tenascin-R differentially affects several forms of synaptic plasticity in the hippocampus. *Neuroscience* **104**:359-369.

Bunt-Milam, A. H., Dennis, M. B. and Bensinger, R. E. (1987). Optic-nerve head axonal-transport in rabbits with hereditary glaucoma. *Experimental Eye Research* **44**:537-551.

Burgoyne, C. F., Downs, J. C., Bellezza, A. J., Suh, J. K. F. and Hart, R. T. (2005). The optic nerve head as a biomechanical structure: a new paradigm for understanding the role of IOP-related stress and strain in the pathophysiology of glaucomatous optic nerve head damage. *Progress in Retinal and Eye Research* **24**:39-73.

Calandrella, N., Scarsella, G., Pescosolido, N. and Risuleo, G. (2007). Degenerative and apoptotic events at retinal and optic nerve level after experimental induction of ocular hypertension. *Molecular and Cellular Biochemistry* **301**:155-163.

Canning, D. R., Hoke, A., Malemud, C. J. and Silver, J. (1996). A potent inhibitor of neurite outgrowth that predominates in the extracellular matrix of reactive astrocytes. *International Journal of Developmental Neuroscience* **14**:153-175.

Carmichael, S. T., Archibeque, I., Luke, L., Nolan, T., Momiy, J. and Li, S. L. (2005). Growth-associated gene expression after stroke: Evidence for a growth-promoting region in peri-infarct cortex. *Experimental Neurology* **193**:291-311.

Carri, N. G., Perris, R., Johansson, S. and Ebendal, T. (1988). Differential outgrowth of retinal neurites on purified extracellular-matrix molecules. *Journal of Neuroscience Research* **19**:428-439.

Carulli, D., Pizzorusso, T., Kwok, J. C. F., Putignano, E., Poli, A., Forostyak, S., Andrews, M. R. *et al.* (2010). Animals lacking link protein have attenuated perineuronal nets and persistent plasticity. *Brain* **133**:2331-2347.

Caterson, B. (2012). Fell-Muir Lecture: Chondroitin sulphate glycosaminoglycans: fun for some and confusion for others. *International Journal of Experimental Pathology* **93**:1-10.

Chang, B., Smith, R. S., Hawes, N. L., Anderson, M. G., Zabaleta, A., Savinova, O., Roderick, T. H. *et al.* (1999). Interacting loci cause severe iris atrophy and glaucoma in DBA/2J mice. *Nature Genetics* **21**:405-409.

Chaudhary, P., Ahmed, F., Quebada, P. and Sharma, S. C. (1999). Caspase inhibitors block the retinal ganglion cell death following optic nerve transection. *Molecular Brain Research* **67**:36-45.

Chauhan, B. C., Pan, J. Y., Archibald, M. L., LeVatte, T. L., Kelly, M. E. M. and Tremblay, F. (2002). Effect of intraocular pressure on optic disc topography, electroretinography, and axonal loss in a chronic pressure-induced rat model of optic nerve damage. *Investigative Ophthalmology & Visual Science* **43**:2969-2976.

Chen, H. and Weber, A. J. (2001). BDNF enhances retinal ganglion cell survival in cats with optic nerve damage. *Investigative Ophthalmology & Visual Science* **42**:966-974.

Chen, H. and Weber, A. J. (2004). Brain-derived neurotrophic factor reduces TrkB protein and mRNA in the normal retina and following optic nerve crush in adult rats. *Brain Research* **1011**:99-106.

Chen, S.-J., Lu, P., Zhang, W.-F. and Lu, J.-H. (2012). High myopia as a risk factor in primary open angle glaucoma. *International Journal of Ophthalmology* **5**:750-753.

Chen, X. Y. and Wolpaw, J. R. (1994). Triceps surae motoneuron morphology in the rat - a quantitative light-microscopic study. *Journal of Comparative Neurology* **343**:143-157.

Chidlow, G., Ebner, A., Wood, J. P. M. and Casson, R. J. (2011). The optic nerve head is the site of axonal transport disruption, axonal cytoskeleton damage and putative axonal regeneration failure in a rat model of glaucoma. *Acta Neuropathologica* **121**:737-751.

Clark, S. J., Bishop, P. N. and Day, A. J. (2010). Complement factor H and age-related macular degeneration: the role of glycosaminoglycan recognition in disease pathology. *Biochemical Society Transactions* **38**:1342-1348.

Clark, S. J., Keenan, T. D. L., Fielder, H. L., Collinson, L. J., Holley, R. J., Merry, C. L. R., van Kuppevelt, T. H. *et al.* (2011). Mapping the Differential Distribution of Glycosaminoglycans in the Adult Human Retina, Choroid, and Sclera. *Investigative Ophthalmology & Visual Science* **52**:6511-6521.

Cole, G. J. and McCabe, C. F. (1991). Identification of a developmentally regulated keratan sulfate proteoglycan that inhibits cell-adhesion and neurite outgrowth. *Neuron* **7**:1007-1018.

Coleman, M. P. and Perry, V. H. (2002). Axon pathology in neurological disease: a neglected therapeutic target. *Trends in Neurosciences* **25**:532-537.

Colton, C. A. and Gilbert, D. L. (1987). Production of superoxide anions by a cns macrophage, the microglia. *Febs Letters* **223**:284-288.

Cone, F. E., Steinhart, M. R., Oglesby, E. N., Kalesnykas, G., Pease, M. E. and Quigley, H. A. (2012). The effects of anesthesia, mouse strain and age on intraocular pressure and an improved murine model of experimental glaucoma. *Experimental Eye Research* **99**:27-35.

Coombs, J., van der List, D., Wang, G. Y. and Chalupa, L. M. (2006). Morphological properties of mouse retinal ganglion cells. *Neuroscience* **140**:123-136.

Cordeiro, M. F., Migdal, C., Bloom, P., Fitzke, F. W. and Moss, S. E. (2011). Imaging apoptosis in the eye. *Eye* **25**:545-553.

Crish, S. D. and Calkins, D. J. (2011). Neurodegeneration in glaucoma: progression and calcium-dependent intracellular mechanisms. *Neuroscience* **176**:1-11.

Cross, S. (2012). The Role of Complement in Retinal Ganglion Cell Loss in Glaucoma. Thesis PhD, Cardiff University.

Cui, Q., Tang, L. S., Hu, B., So, K. F. and Yip, H. K. (2002). Expression of trkA, trkB, and trkC in injured and regenerating retinal ganglion cells of adult rats. *Investigative Ophthalmology & Visual Science* **43**:1954-1964.

Cull, G. A., Reynaud, J., Wang, L., Cioffi, G. A., Burgoyne, C. F. and Fortune, B. (2012). Relationship between Orbital Optic Nerve Axon Counts and Retinal Nerve Fiber Layer Thickness Measured by Spectral Domain Optical Coherence Tomography. *Investigative Ophthalmology & Visual Science* **53**:7766-7773.

Cummings, R. D. (2009). The repertoire of glycan determinants in the human glycome. *Molecular Biosystems* **5**:1087-1104.

Curcio, C. A., Sloan, K. R., Packer, O., Hendrickson, A. E. and Kalina, R. E. (1987). Distribution of cones in human and monkey retina - individual variability and radial asymmetry. *Science* **236**:579-582.

Daborg, J., Andreasson, U., Pekna, M., Lautner, R., Hanse, E., Minthon, L., Blennow, K. *et al.* (2012). Cerebrospinal fluid levels of complement proteins C3, C4 and CR1 in Alzheimer's disease. *Journal of Neural Transmission* **119**:789-797.

Dacey, D. M. (1993). Morphology of a small-field bistratified ganglion-cell type in the macaque and human retina. *Visual Neuroscience* **10**:1081-1098.

Dacey, D. M. and Brace, S. (1992). A coupled network for parasol but not midget ganglion-cells in the primate retina. *Visual Neuroscience* **9**:279-290.

Dai, C., Khaw, P. T., Yin, Z. Q., Li, D., Raisman, G. and Li, Y. (2012a). Olfactory Ensheathing Cells Rescue Optic Nerve Fibers in a Rat Glaucoma Model. *Translational Vision Science & Technology* **1**:3.

Dai, C., Khaw, P. T., Yin, Z. Q., Li, D., Raisman, G. and Li, Y. (2012b). Structural basis of glaucoma: The fortified astrocytes of the optic nerve head are the target of raised intraocular pressure. *Glia* **60**:13-28.

Dangond, F., Hwang, D., Camelo, S., Pasinelli, P., Frosch, M. P., Stephanopoulos, G., Brown, R. H. *et al.* (2004). Molecular signature of late-stage human ALS revealed by expression profiling of postmortem spinal cord gray matter. *Physiological Genomics* **16**:229-239.

Davies, S. J. A., Fitch, M. T., Memberg, S. P., Hall, A. K., Raisman, G. and Silver, J. (1997). Regeneration of adult axons in white matter tracts of the central nervous system. *Nature* **390**:680-683.

de Winter, F., Cui, Q., Symons, N., Verhaagen, J. and Harvey, A. R. (2004). Expression of class-3 semaphorins and their receptors in the neonatal and adult rat retina. *Investigative Ophthalmology & Visual Science* **45**:4554-4562.

Della Santina, L., Inman, D. M., Lupien, C. B., Horner, P. J. and Wong, R. O. L. (2013). Differential Progression of Structural and Functional Alterations in Distinct Retinal Ganglion Cell Types in a Mouse Model of Glaucoma. *Journal of Neuroscience* **33**:17444-17457.

Demonasterio, F. M. (1978). Properties of concentrically organized X and Y ganglion-cells of macaque retina. *Journal of Neurophysiology* **41**:1394-1417.

Depboylu, C., Schaefer, M. K. H., Arias-Carrion, O., Oertel, W. H., Weihe, E. and Hoeglinger, G. U. (2011). Possible Involvement of Complement Factor C1q in the Clearance of Extracellular Neuromelanin From the Substantia Nigra in Parkinson Disease. *Journal of Neuropathology and Experimental Neurology* **70**:125-132.

DeVries, S. H. (2000). Bipolar cells use kainate and AMPA receptors to filter visual information into separate channels. *Neuron* **28**:847-856.

DeVries, S. H. and Baylor, D. A. (1997). Mosaic arrangement of ganglion cell receptive fields in rabbit retina. *Journal of Neurophysiology* **78**:2048-2060.

Dewitt, D. A., Silver, J., Canning, D. R. and Perry, G. (1993). Chondroitin sulfate proteoglycans are associated with the lesions of alzheimers-disease. *Experimental Neurology* **121**:149-152.

Dhande, O. S., Estevez, M. E., Quattrochi, L. E., El-Danaf, R. N., Nguyen, P. L., Berson, D. M. and Huberman, A. D. (2013). Genetic Dissection of Retinal Inputs to Brainstem Nuclei Controlling Image Stabilization. *Journal of Neuroscience* **33**:17797-17813.

Dielemans, I., Vingerling, J. R., Wolfs, R. C. W., Hofman, A., Grobbee, D. E. and Dejong, P. (1994). The prevalence of primary open-angle glaucoma in a population-based study in the Netherlands - The Rotterdam study. *Ophthalmology* **101**:1851-1855.

DiScipio, R. G. and Schraufstatter, L. U. (2007). The role of the complement anaphylatoxins in the recruitment of eosinophils. *International Immunopharmacology* **7**:1909-1923.

Dityatev, A. (2010). Remodeling of extracellular matrix and epileptogenesis. *Epilepsia* **51**:61-65.

Dityatev, A., Brueckner, G., Dityateva, G., Grosche, J., Kleene, R. and Schachner, M. (2007). Activity-dependent formation and functions of chondroitin sulfate-rich extracellular matrix of perineuronal nets. *Developmental Neurobiology* **67**:570-588.

Dityatev, A. and Fellin, T. (2008). Extracellular matrix in plasticity and epileptogenesis. *Neuron Glia Biology* **4**:235-247.

Dou, C. L. and Levine, J. M. (1995). Differential effects of glycosaminoglycans on neurite growth on laminin and L1 substrates. *Journal of Neuroscience* **15**:8053-8066.

Dow, K. E., Ethell, D. W., Steeves, J. D. and Riopelle, R. J. (1994). Molecular correlates of spinal-cord repair in the embryonic chick - heparan-sulfate and chondroitin sulfate proteoglycans. *Experimental Neurology* **128**:233-238.

Dowling, J. (2012). The retina: an approachable part of the brain. Revised edition. Belknap Press.

Dowling, J. E. and Boycott, B. B. (1966). Organization of primate retina - electron microscopy. *Proceedings of the Royal Society Series B-Biological Sciences* **166**:80-&.

Downs, J. C., Roberts, M. D. and Sigal, I. A. (2011). Glaucomatous cupping of the lamina cribrosa: A review of the evidence for active progressive remodeling as a mechanism. *Experimental Eye Research* **93**:133-140.

Drasdo, N. and Fowler, C. W. (1974). Nonlinear projection of retinal image in a wide-angle schematic eye. *British Journal of Ophthalmology* **58**:709-714.

Droege, K. M., Muether, P. S., Hermann, M. M., Caramoy, A., Viebahn, U., Kirchhof, B. and Fauser, S. (2013). Adherence to ranibizumab treatment for neovascular age-related macular degeneration in real life. *Graefes Archive for Clinical and Experimental Ophthalmology* **251**:1281-1284.

Duan, X., Qiao, M., Bei, F., Kim, I.-J., He, Z. and Sanes, J. R. (2015). Subtype-Specific Regeneration of Retinal Ganglion Cells following Axotomy: Effects of Osteopontin and mTOR Signaling. *Neuron* **85**:1244-1256.

Dunkelberger, J. R. and Song, W.-C. (2010). Complement and its role in innate and adaptive immune responses. *Cell Research* **20**:34-50.

Eide, F. F., Vining, E. R., Eide, B. L., Zang, K. L., Wang, X. Y. and Reichardt, L. F. (1996). Naturally occurring truncated trkB receptors have dominant inhibitory effects on brain-derived neurotrophic factor signaling. *Journal of Neuroscience* **16**:3123-3129.

El-Danaf, R. N. and Huberman, A. D. (2015). Characteristic Patterns of Dendritic Remodeling in Early-Stage Glaucoma: Evidence from Genetically Identified Retinal Ganglion Cell Types. *Journal of Neuroscience* **35**:2329-2343.

Evers, M. R., Salmen, B., Bukalo, O., Rollenhagen, A., Bosl, M. R., Morellini, F., Bartsch, U. *et al.* (2002). Impairment of L-type Ca²⁺ channel-dependent forms of hippocampal synaptic plasticity in mice deficient in the extracellular matrix glycoprotein tenascin-C. *Journal of Neuroscience* **22**:7177-7194.

Faissner, A., Kruse, J., Chiquete-Herrmann, R. and Mackie, E. (1988). The high-molecular-weight J1 glycoproteins are immunochemically related to tenascin. *Differentiation* **37**:104-114.

Famiglietti, E. V. and Kolb, H. (1976). Structural basis for on-center and off-center responses in retinal ganglion-cells. *Science* **194**:193-195.

- Faulkner, J. R., Herrmann, J. E., Woo, M. J., Tansey, K. E., Doan, N. B. and Sofroniew, M. V. (2004). Reactive astrocytes protect tissue and preserve function after spinal cord injury. *Journal of Neuroscience* **24**:2143-2155.
- Fawcett, J. W. and Asher, R. A. (1999). The glial scar and central nervous system repair. *Brain Research Bulletin* **49**:377-391.
- Feng, L., Zhao, Y., Yoshida, M., Chen, H., Yang, J. F., Kim, T. S., Cang, J. H. *et al.* (2013). Sustained Ocular Hypertension Induces Dendritic Degeneration of Mouse Retinal Ganglion Cells That Depends on Cell Type and Location. *Investigative Ophthalmology & Visual Science* **54**:1106-1117.
- Fine, I. H. (1991). Architecture and construction of a self-sealing incision for cataract-surgery. *Journal of Cataract and Refractive Surgery* **17**:672-676.
- Fischer, A. J., Schmidt, M., Omar, G. and Reh, T. A. (2004). BMP4 and CNTF are neuroprotective and suppress damage-induced proliferation of Muller glia in the retina. *Molecular and Cellular Neuroscience* **27**:531-542.
- Flores-Herr, N., Protti, D. A. and Wassle, H. (2001). Synaptic currents generating the inhibitory surround of ganglion cells in the mammalian retina. *Journal of Neuroscience* **21**:4852-4863.
- Fonseca, M. I., Kawas, C. H., Troncoso, J. C. and Tenner, A. J. (2004). Neuronal localization of C1q in preclinical Alzheimer's disease. *Neurobiology of Disease* **15**:40-46.
- Foxton, R. H., Finkelstein, A., Vijay, S., Dahlmann-Noor, A., Khaw, P. T., Morgan, J. E., Shima, D. T. *et al.* (2013). VEGF-A Is Necessary and Sufficient for Retinal Neuroprotection in Models of Experimental Glaucoma. *The American journal of pathology* **182**:1379-1390.
- Frankfort, B. J., Khan, A. K., Tse, D. Y., Chung, I., Pang, J.-J., Yang, Z., Gross, R. L. *et al.* (2013). Elevated Intraocular Pressure Causes Inner Retinal Dysfunction Before Cell Loss in a Mouse Model of Experimental Glaucoma. *Investigative Ophthalmology & Visual Science* **54**:762-770.
- Fraser, D. A., Bohlsion, S. S., Jasinskiene, N., Rawal, N., Palmarini, G., Ruiz, S., Rochford, R. *et al.* (2006). C1q and MBL, components of the innate immune system, influence monocyte cytokine expression. *Journal of Leukocyte Biology* **80**:107-116.
- Freed, M. A., Smith, R. G. and Sterling, P. (1992). Computational model of the on-alpha ganglion-cell receptive-field based on bipolar cell circuitry. *Proceedings of the National Academy of Sciences of the United States of America* **89**:236-240.

Fricker, M., Oliva-Martin, M. J. and Brown, G. C. (2012). Primary phagocytosis of viable neurons by microglia activated with LPS or A beta is dependent on calreticulin/LRP phagocytic signalling. *Journal of Neuroinflammation* **9**.

Frischknecht, R., Heine, M., Perrais, D., Seidenbecher, C. I., Choquet, D. and Gundelfinger, E. D. (2009). Brain extracellular matrix affects AMPA receptor lateral mobility and short-term synaptic plasticity. *Nature Neuroscience* **12**:897-U115.

Fu, Q.-I., Li, X., Shi, J., Xu, G., Wen, W., Lee, D. H. S. and So, K.-F. (2009). Synaptic Degeneration of Retinal Ganglion Cells in a Rat Ocular Hypertension Glaucoma Model. *Cellular and Molecular Neurobiology* **29**:575-581.

Fu, R., Shen, Q., Xu, P., Luo, J. J. and Tang, Y. (2014). Phagocytosis of Microglia in the Central Nervous System Diseases. *Molecular Neurobiology* **49**:1422-1434.

Fukuchi, T., Sawaguchi, S., Hara, H., Shirakashi, M. and Iwata, K. (1992). Extracellular-matrix changes of the optic-nerve lamina-cribrosa in monkey eyes with experimentally chronic glaucoma. *Graefes Archive for Clinical and Experimental Ophthalmology* **230**:421-427.

Fukuchi, T., Sawaguchi, S., Yue, B., Iwata, K., Hara, H. and Kaiya, T. (1994). Sulfated proteoglycans in the lamina-cribrosa of normal monkey eyes and monkey eyes with laser-induced glaucoma. *Experimental Eye Research* **58**:231-243.

Gaasterl.D and Kupfer, C. (1974). Experimental glaucoma in rhesus-monkey. *Investigative Ophthalmology* **13**:455-457.

Gal, P., Barna, L., Kocsis, A. and Zavodszky, P. (2007). Serine proteases of the classical and lectin pathways: Similarities and differences. *Immunobiology* **212**:267-277.

Gallego, B. I., Salazar, J. J., de Hoz, R., Rojas, B., Ramirez, A. I., Salinas-Navarro, M., Ortin-Martinez, A. *et al.* (2012). IOP induces upregulation of GFAP and MHC-II and microglia reactivity in mice retina contralateral to experimental glaucoma. *Journal of Neuroinflammation* **9**.

Galtrey, C. M. and Fawcett, J. W. (2007). The role of chondroitin sulfate proteoglycans in regeneration and plasticity in the central nervous system. *Brain Research Reviews* **54**:1-18.

Gan, W. B., Grutzendler, J., Wong, W. T., Wong, R. O. L. and Lichtman, J. W. (2000). Multicolor "DiOlistic" labeling of the nervous system using lipophilic dye combinations. *Neuron* **27**:219-225.

Gardai, S. J., McPhillips, K. A., Frasch, S. C., Janssen, W. J., Starefeldt, A., Murphy-Ullrich, J. E., Bratton, D. L. *et al.* (2005). Cell-surface calreticulin initiates clearance of viable or apoptotic cells through trans-activation of LRP on the phagocyte. *Cell* **123**:321-334.

Garway-Heath, D. F., Holder, G. E., Fitzke, F. W. and Hitchings, R. A. (2002). Relationship between electrophysiological, psychophysical, and anatomical measurements in glaucoma. *Investigative Ophthalmology & Visual Science* **43**:2213-2220.

Gates, M. A., Fillmore, H. and Steindler, D. A. (1996). Chondroitin sulfate proteoglycan and tenascin in the wounded adult mouse neostriatum in vitro: Dopamine neuron attachment and process outgrowth. *Journal of Neuroscience* **16**:8005-8018.

Gelatt, K. N., Peiffer, R. L., Gwin, R. M., Gum, G. G. and Williams, L. W. (1977). Clinical manifestations of inherited glaucoma in beagle. *Investigative Ophthalmology & Visual Science* **16**:1135-1142.

Gogolla, N., Caroni, P., Luthi, A. and Herry, C. (2009). Perineuronal Nets Protect Fear Memories from Erasure. *Science* **325**:1258-1261.

Golgi, C. (1898). Intorno alla struttura delle cellule nervose. *Bollettino della Societa medico-chirurgica di Pavia* **1**:1-14.

Golgi, C. (1989). On the structure of nerve-cells. *Journal of Microscopy-Oxford* **155**:3-7.

Gordon, M. O., Beiser, J. A., Brandt, J. D., Heuer, D. K., Higginbotham, E. J., Johnson, C. A., Keltner, J. L. *et al.* (2002). The Ocular Hypertension Treatment Study - Baseline factors that predict the onset of primary open-angle glaucoma. *Archives of Ophthalmology* **120**:714-720.

Gramlich, O. W., Ding, Q. J., Zhu, W., Cook, A., Anderson, M. G. and Kuehn, M. H. (2015). Adoptive transfer of immune cells from glaucomatous mice provokes retinal ganglion cell loss in recipients. *Acta Neuropathologica Communications* **3**.

Grumet, M., Flaccus, A. and Margolis, R. U. (1993). Functional-characterization of chondroitin sulfate proteoglycans of brain - interactions with neurons and neural cell-adhesion molecules. *Journal of Cell Biology* **120**:815-824.

Guo, L., Moss, S. E., Alexander, R. A., Ali, R. R., Fitzke, F. W. and Cordeiro, M. F. (2005). Retinal ganglion cell apoptosis in glaucoma is related to intraocular pressure and IOP-induced effects on extracellular matrix. *Investigative Ophthalmology & Visual Science* **46**:175-182.

Gutierrez, H. and Davies, A. M. (2007). A fast and accurate procedure for deriving the Sholl profile in quantitative studies of neuronal morphology. *Journal of Neuroscience Methods* **163**:24-30.

Haapasalo, A., Sipola, L., Larsson, K., Akerman, K. E. O., Stoilov, P., Stamm, S., Wong, G. *et al.* (2002). Regulation of TRKB surface expression by brain-derived neurotrophic factor and truncated TRIM Isoforms. *Journal of Biological Chemistry* **277**:43160-43167.

Haas, C. A., Rauch, U., Thon, N., Merten, T. and Deller, T. (1999). Entorhinal cortex lesion in adult rats induces the expression of the neuronal chondroitin sulfate proteoglycan neurocan in reactive astrocytes. *Journal of Neuroscience* **19**:9953-9963.

Harada, C., Guo, X., Namekata, K., Kimura, A., Nakamura, K., Tanaka, K., Parada, L. F. *et al.* (2011). Glia- and neuron-specific functions of TrkB signalling during retinal degeneration and regeneration. *Nature Communications* **2**.

Hartline, H. K. (1938). The response of single optic nerve fibers of the vertebrate eye to illumination of the retina. *American Journal of Physiology* **121**:400-415.

Harwerth, R. S., Carter-Dawson, L., Shen, F., Smith, E. L. and Crawford, M. L. J. (1999). Ganglion cell losses underlying visual field defects from experimental glaucoma. *Investigative Ophthalmology & Visual Science* **40**:2242-2250.

He, S. G. and Masland, R. H. (1997). Retinal direction selectivity after targeted laser ablation of starburst amacrine cells. *Nature* **389**.

Heine, W. F. and Passaglia, C. L. (2011). Spatial receptive field properties of rat retinal ganglion cells. *Visual Neuroscience* **28**:403-417.

Hernandez, M. R., Andrzejewska, W. M. and Neufeld, A. H. (1990). Changes in the extracellular-matrix of the human optic-nerve head in primary open-angle glaucoma. *American Journal of Ophthalmology* **109**:180-188.

Hernandez, M. R., Hanninen, L. A., Hubbard, W. C., Kaufman, P. L. and Weber, A. J. (1995). Astrocytes responses in the lamina-cribrosa in pressure-dependent glaucoma in monkeys. *Investigative Ophthalmology & Visual Science* **36**:S606-S606.

Herzog, K. H. and von Bartheld, C. S. (1998). Contributions of the optic tectum and the retina as sources of brain-derived neurotrophic factor for retinal ganglion cells in the chick embryo. *Journal of Neuroscience* **18**:2891-2906.

Hidaka, S., Akahori, Y. and Kurosawa, Y. (2004). Dendrodendritic electrical synapses between mammalian retinal ganglion cells. *Journal of Neuroscience* **24**:10553-10567.

Higginbotham, E. J., Gordon, M. O., Beiser, J. A., Drake, M. V., Bennett, G. R., Wilson, M. R., Kass, M. A. *et al.* (2004). The Ocular Hypertension Treatment Study - Topical medication delays or prevents primary open-angle glaucoma in African American individuals. *Archives of Ophthalmology* **122**:813-820.

Hobohm, C., Gunther, A., Grosche, J., Rossner, S., Schneider, D. and Bruckner, G. (2005). Decomposition and long-lasting downregulation of extracellular matrix in Perineuronal nets induced by focal cerebral ischemia in rats. *Journal of Neuroscience Research* **80**:539-548.

Hollyfield, J. G., Rayborn, M. E., Midura, R. J., Shadrach, K. G. and Acharya, S. (1999). Chondroitin sulfate proteoglycan core proteins in the interphotoreceptor matrix: A comparative study using biochemical and immunohistochemical analysis. *Experimental Eye Research* **69**:311-322.

Honig, M. G. and Hume, R. I. (1986). Fluorescent carbocyanine dyes allow living neurons of identified origin to be studied in long-term cultures. *Journal of Cell Biology* **103**:171-187.

Howell, G. R., Libby, R. T., Jakobs, T. C., Smith, R. S., Phalan, F. C., Barter, J. W., Barbay, J. M. *et al.* (2007a). Axons of retinal ganglion cells are insulated in the optic nerve early in DBA/2J glaucoma. *Journal of Cell Biology* **179**:1523-1537.

Howell, G. R., Libby, R. T., Marchant, J. K., Wilson, L. A., Cosma, I. M., Smith, R. S., Anderson, M. G. *et al.* (2007b). Absence of glaucoma in DBA/2J mice homozygous for wild-type versions of Gpnmb and Tyrp1. *Bmc Genetics* **8**.

Howell, G. R., Macalinao, D. G., Sousa, G. L., Walden, M., Soto, I., Kneeland, S. C., Barbay, J. M. *et al.* (2011). Molecular clustering identifies complement and endothelin induction as early events in a mouse model of glaucoma. *Journal of Clinical Investigation* **121**:1429-1444.

Howell, G. R., Soto, I., Ryan, M., Graham, L. C., Smith, R. S. and John, S. W. M. (2013). Deficiency of complement component 5 ameliorates glaucoma in DBA/2J mice. *Journal of Neuroinflammation* **10**.

Howell, G. R., Soto, I., Zhu, X., Ryan, M., Macalinao, D. G., Sousa, G. L., Caddle, L. B. *et al.* (2012). Radiation treatment inhibits monocyte entry into the optic nerve head and prevents neuronal damage in a mouse model of glaucoma. *Journal of Clinical Investigation* **122**:1246-1261.

Hu, P. and Kalb, R. G. (2003). BDNF heightens the sensitivity of motor neurons to excitotoxic insults through activation of TrkB. *Journal of Neurochemistry* **84**:1421-1430.

Huang, W., Dobberfuhr, A., Filippopoulos, T., Ingelsson, M., Fileta, J. B., Poulin, N. R. and Grosskreutz, C. L. (2005). Transcriptional up-regulation and activation of initiating caspases in experimental glaucoma. *American Journal of Pathology* **167**:673-681.

Huang, W., Fileta, J., Guo, Y. and Grosskreutz, C. L. (2006). Downregulation of Thy1 in retinal ganglion cells in experimental glaucoma. *Current Eye Research* **31**:265-271.

Hughes, A. and Vaney, D. I. (1980). Coronate cells - displaced amacrine cells of the rabbit retina. *Journal of Comparative Neurology* **189**:169-189.

Huxlin, K. R. and Goodchild, A. K. (1997). Retinal ganglion cells in the albino rat: Revised morphological classification. *Journal of Comparative Neurology* **385**:309-323.

Imagama, S., Sakamoto, K., Tauchi, R., Shinjo, R., Ohgomori, T., Ito, Z., Zhang, H. *et al.* (2011). Keratan Sulfate Restricts Neural Plasticity after Spinal Cord Injury. *Journal of Neuroscience* **31**:17091-17102.

Inatani, M., Honjo, M., Otori, Y., Oohira, A., Kido, N., Tano, Y., Honda, Y. *et al.* (2001). Inhibitory effects of neurocan and phosphacan on neurite outgrowth from retinal ganglion cells in culture. *Investigative Ophthalmology & Visual Science* **42**:1930-1938.

Inatani, M. and Tanihara, H. (2002). Proteoglycans in retina. *Progress in Retinal and Eye Research* **21**:429-447.

Inatani, M., Tanihara, H., Oohira, A., Honjo, M. and Honda, Y. (1999). Identification of a nervous tissue-specific chondroitin sulfate proteoglycan, neurocan, in developing rat retina. *Investigative Ophthalmology & Visual Science* **40**:2350-2359.

Inatani, M., Tanihara, H., Oohira, A., Honjo, M., Kido, N. and Honda, Y. (2000). Upregulated expression of neurocan, a nervous tissue specific proteoglycan, in transient retinal ischemia. *Investigative Ophthalmology & Visual Science* **41**:2748-2754.

- Inman, D. M. and Horner, P. J. (2007). Reactive nonproliferative gliosis predominates in a chronic mouse model of glaucoma. *Glia* **55**:942-953.
- Isayama, T., Berson, D. M., O'Brien, B. J. and Pu, M. (1999). The lambda ganglion cell type of cat and ferret retina. *Investigative Ophthalmology & Visual Science* **40**:S813-S813.
- Ishiguro, H., Sato, S., Fujita, N., Inuzuka, T., Nakano, R. and Miyatake, T. (1991). Immunohistochemical localization of myelin-associated glycoprotein isoforms during the development in the mouse-brain. *Brain Research* **563**:288-292.
- Jackman, S. L., Choi, S.-Y., Thoreson, W. B., Rabl, K., Bartoletti, T. M. and Kramer, R. H. (2009). Role of the synaptic ribbon in transmitting the cone light response. *Nature Neuroscience* **12**:303-310.
- Jakobs, S. (2006). High resolution imaging of live mitochondria. *Biochimica Et Biophysica Acta-Molecular Cell Research* **1763**:561-575.
- Jakobs, T. C., Koizumi, A. and Masland, R. H. (2008). The spatial distribution of glutamatergic inputs to dendrites of retinal ganglion cells. *Journal of Comparative Neurology* **510**:221-236.
- Jakobs, T. C., Libby, R. T., Ben, Y. X., John, S. W. M. and Masland, R. H. (2005). Retinal ganglion cell degeneration is topological but not cell type specific in DBA/2J mice. *Journal of Cell Biology* **171**:313-325.
- Janeway, C., Travers, P., Walport, M. and Shlomchik, M. (2001). Immunobiology. 5th ed. Garland Science.
- Jelinek, H. F. and Fernandez, E. (1998). Neurons and fractals: how reliable and useful are calculations of fractal dimensions? *Journal of Neuroscience Methods* **81**:9-18.
- Jelsma, T. N., Friedman, H. H., Berkelaar, M., Bray, G. M. and Aguayo, A. J. (1993). Different forms of the neurotrophin receptor TrkB messenger-RNA predominate in rat retina and optic-nerve. *Journal of Neurobiology* **24**:1207-1214.
- Jennings, C. (1994). Developmental neurobiology - death of a synapse. *Nature* **372**:498-499.
- Jeon, C. J., Strettoi, E. and Masland, R. H. (1998). The major cell populations of the mouse retina. *Journal of Neuroscience* **18**:8936-8946.

Jia, L. J., Cepurna, W. O., Johnson, E. C. and Morrison, J. C. (2000). Effect of general anesthetics on IOP in rats with experimental aqueous outflow obstruction. *Investigative Ophthalmology & Visual Science* **41**:3415-3419.

Joachim, S. C., Gramlich, O. W., Laspas, P., Schmid, H., Beck, S., von Pein, H. D., Dick, H. B. *et al.* (2012). Retinal Ganglion Cell Loss Is Accompanied by Antibody Depositions and Increased Levels of Microglia after Immunization with Retinal Antigens. *Plos One* **7**.

John, S. W. M., Smith, R. S., Savinova, O. V., Hawes, N. L., Chang, B., Turnbull, D., Davisson, M. *et al.* (1998). Essential iris atrophy, pigment dispersion, and glaucoma in DBA/2J mice. *Investigative Ophthalmology & Visual Science* **39**:951-962.

Johnson, E. C., Cepurna, W. O., Choi, D., Choe, T. E. and Morrison, J. C. (2015). Radiation Pretreatment Does Not Protect the Rat Optic Nerve From Elevated Intraocular Pressure-Induced Injury. *Investigative Ophthalmology & Visual Science* **56**:412-419.

Johnson, E. C., Deppmeier, L. M. H., Wentzien, S. K. F., Hsu, I. and Morrison, J. C. (2000). Chronology of optic nerve head and retinal responses to elevated intraocular pressure. *Investigative Ophthalmology & Visual Science* **41**:431-442.

Johnson, E. C., Doser, T. A., Cepurna, W. O., Dyck, J. A., Jia, L., Guo, Y., Lambert, W. S. *et al.* (2011). Cell Proliferation and Interleukin-6-Type Cytokine Signaling Are Implicated by Gene Expression Responses in Early Optic Nerve Head Injury in Rat Glaucoma. *Investigative Ophthalmology & Visual Science* **52**:504-518.

Johnson, E. C., Jia, L., Cepurna, W. O., Doser, T. A. and Morrison, J. C. (2007). Global changes in optic nerve head gene expression after exposure to elevated intraocular pressure in a rat glaucoma model. *Investigative Ophthalmology & Visual Science* **48**:3161-3177.

Johnson, E. C., Morrison, J. C., Farrell, S., Deppmeier, L., Moore, C. G. and McGinty, M. R. (1996). The effect of chronically elevated intraocular pressure on the rat optic nerve head extracellular matrix. *Experimental Eye Research* **62**:663-673.

Johnson, J. E., Barde, Y. A., Schwab, M. and Thoenen, H. (1986). BRAIN-DERIVED Neurotrophic factor supports the survival of cultured rat retinal ganglion-cells. *Journal of Neuroscience* **6**:3031-3038.

Johnsongreen, P. C., Dow, K. E. and Riopelle, R. J. (1992). Neurite growth modulation associated with astrocyte proteoglycans - influence of activators of inflammation. *Glia* **5**:33-42.

Jones, L. L., Margolis, R. U. and Tuszynski, M. H. (2003). The chondroitin sulfate proteoglycans neurocan, brevican, phosphacan, and versican are differentially regulated following spinal cord injury. *Experimental Neurology* **182**:399-411.

Jones, L. L., Yamaguchi, Y., Stallcup, W. B. and Tuszynski, M. H. (2002). NG2 is a major chondroitin sulfate proteoglycan produced after spinal cord injury and is expressed by macrophages and oligodendrocyte progenitors. *Journal of Neuroscience* **22**:2792-2803.

Kalesnykas, G., Oglesby, E. N., Zack, D. J., Cone, F. E., Steinhart, M. R., Tian, J., Pease, M. E. *et al.* (2012). Retinal ganglion cell morphology after optic nerve crush and experimental glaucoma. *Investigative ophthalmology & visual science* **53**:3847-3857.

Kanamori, A., Nakamura, M., Nakanishi, Y., Yamada, Y. and Negi, A. (2005). Long-term glial reactivity in rat retinas ipsilateral and contralateral to experimental glaucoma. *Experimental Eye Research* **81**:48-56.

Kantor, D. B., Chivatakarn, O., Peer, K. L., Oster, S. F., Inatani, M., Hansen, M. J., Flanagan, J. G. *et al.* (2004). Semaphorin 5A is a bifunctional axon guidance cue regulated by heparan and chondroitin sulfate proteoglycans. *Neuron* **44**:961-975.

Karetko, M. and Skangiel-Kramska, J. (2009). Diverse functions of perineuronal nets. *Acta Neurobiologiae Experimentalis* **69**:564-577.

Karetko-Sysa, M., Skangiel-Kramska, J. and Nowicka, D. (2011). Disturbance of perineuronal nets in the perilesional area after photothrombosis is not associated with neuronal death. *Experimental Neurology* **231**:113-126.

Kass, M. A., Gordon, M. O., Gao, F., Heuer, D. K., Higginbotham, E. J., Johnson, C. A., Keltner, J. K. *et al.* (2010). Delaying Treatment of Ocular Hypertension The Ocular Hypertension Treatment Study. *Archives of Ophthalmology* **128**:276-287.

Katsman, D., Zheng, J., Spinelli, K. and Carmichael, S. T. (2003). Tissue microenvironments within functional cortical subdivisions adjacent to focal stroke. *Journal of Cerebral Blood Flow and Metabolism* **23**:997-1009.

Kawashima, H., Atarashi, K., Hirose, M., Hirose, J., Yamada, S., Sugahara, K. and Miyasaka, M. (2002). Oversulfated chondroitin/dermatan sulfates containing GlcA beta 1/IdoA alpha 1-3GalNAc(4,6-O-disulfate) interact with L- and P-selectin and chemokines. *Journal of Biological Chemistry* **277**:12921-12930.

Kay, J. N., De la Huerta, I., Kim, I.-J., Zhang, Y., Yamagata, M., Chu, M. W., Meister, M. *et al.* (2011). Retinal Ganglion Cells with Distinct Directional Preferences Differ in Molecular Identity, Structure, and Central Projections. *Journal of Neuroscience* **31**:7753-7762.

Kermer, P., Ankerhold, R., Klocker, N., Krajewski, S., Reed, J. C. and Bahr, M. (2000). Caspase-9: Involvement in secondary death of axotomized rat retinal ganglion cells in vivo. *Molecular Brain Research* **85**:144-150.

Kerrigan, L. A., Zack, D. J., Quigley, H. A., Smith, S. D. and Pease, M. E. (1997). TUNEL-positive ganglion cells in human primary open-angle glaucoma. *Archives of Ophthalmology* **115**:1031-1035.

Kim, C. Y., Kuehn, M. H., Grozdanic, S. D., Ostojic, J., Bellin, M. and Kwon, Y. H. (2005). Comparative analysis of optic nerve head gene expression changes in human glaucoma and in rodent models of ocular hypertension. *Investigative Ophthalmology & Visual Science* **46**.

King, A., Azuara-Blanco, A. and Tuulonen, A. (2013). Glaucoma. *Bmj-British Medical Journal* **346**.

King, W. M., Sarup, V., Sauve, Y., Moreland, C. M., Carpenter, D. O. and Sharma, S. C. (2006). Expansion of visual receptive fields in experimental glaucoma. *Visual Neuroscience* **23**:137-142.

Kitaoka, Y., Kwong, J. M. K., Ross-Cisneros, F. N., Wang, J. T., Tsai, R. K., Sadun, A. A. and Lam, T. T. (2006). TNF-alpha-induced optic nerve degeneration and nuclear factor-kappa B p65. *Investigative Ophthalmology & Visual Science* **47**:1448-1457.

Kitaoka, Y., Munemasa, Y., Kojima, K., Hirano, A., Ueno, S. and Takagi, H. (2013). Axonal protection by Nmnat3 overexpression with involvement of autophagy in optic nerve degeneration. *Cell Death & Disease* **4**.

Klein, B. E. K., Klein, R., Sponsel, W. E., Franke, T., Cantor, L. B., Martone, J. and Menage, M. J. (1992). Prevalence of glaucoma - The Beaver-Dam eye study. *Ophthalmology* **99**:1499-1504.

Kolb, H. (1970). Organization of outer plexiform layer of primate retina - electron microscopy of golgi-impregnated cells. *Philosophical Transactions of the Royal Society of London Series B-Biological Sciences* **258**:261-&.

Kolb, H., Linberg, K. A. and Fisher, S. K. (1992). Neurons of the human retina - a golgi-study. *Journal of Comparative Neurology* **318**:147-187.

Kolb, H. and Nelson, R. (1993). Off-alpha and off-beta ganglion-cells in cat retina .2. Neural circuitry as revealed by electron-microscopy of HRP stains. *Journal of Comparative Neurology* **329**:85-110.

Kolb, H., Nelson, R., Ahnelt, P. and Cuenca, N. (2001). Cellular organization of the vertebrate retina. *Progress in brain research* **131**:3-26.

Kolb, H., Nelson, R. and Mariani, A. (1981). Amacrine cells, bipolar cells and ganglion-cells of the cat retina - a golgi-study. *Vision Research* **21**:1081-1114.

Kolb, H. and West, R. W. (1977). Synaptic connections of inter-plexiform cell in retina of cat. *Journal of Neurocytology* **6**:155-170.

Kolker, A. E., Moses, R. A., Constant, M. A. and Becker, B. (1963). The development of glaucoma in rabbits. *Investigative Ophthalmology* **2**:316-321.

Koops, A., Kappler, J., Junghans, U., Kuhn, G., Kresse, H. and Muller, H. W. (1996). Cultured astrocytes express biglycan, a chondroitin/dermatan sulfate proteoglycan supporting the survival of neocortical neurons. *Molecular Brain Research* **41**:65-73.

Kuehn, M. H., Kim, C. Y., Ostojic, J., Bellin, M., Alward, W. L. M., Stone, E. M., Sakaguchi, D. S. *et al.* (2006). Retinal synthesis and deposition of complement components induced by ocular hypertension. *Experimental Eye Research* **83**:620-628.

Kurihara, D. and Yamashita, T. (2012). Chondroitin Sulfate Proteoglycans Down-regulate Spine Formation in Cortical Neurons by Targeting Tropomyosin-related Kinase B (TrkB) Protein. *Journal of Biological Chemistry* **287**:13822-13828.

Lam, T. T., Kwong, J. M. K. and Tso, M. O. M. (2003). Early glial responses after acute elevated intraocular pressure in rats. *Investigative Ophthalmology & Visual Science* **44**:638-645.

Lander, A. D., Fujii, D. K. and Reichardt, L. F. (1985). Purification of a factor that promotes neurite outgrowth - isolation of laminin and associated molecules. *Journal of Cell Biology* **101**:898-913.

Laughlin, S. B. (2001). Energy as a constraint on the coding and processing of sensory information. *Current Opinion in Neurobiology* **11**:475-480.

- Le, A., Mukesh, B. N., McCarty, C. A. and Taylor, H. R. (2003). Risk factors associated with the incidence of open-angle glaucoma: The Visual Impairment Project. *Investigative Ophthalmology & Visual Science* **44**:3783-3789.
- Lee, H., Leamey, C. A. and Sawatari, A. (2012). Perineuronal Nets Play a Role in Regulating Striatal Function in the Mouse. *Plos One* **7**.
- Lee, R., Kermani, P., Teng, K. K. and Hempstead, B. L. (2001). Regulation of cell survival by secreted proneurotrophins. *Science* **294**:1945-1948.
- Lee, S., Van Bergen, N. J., Kong, G. Y., Chrysostomou, V., Waugh, H. S., O'Neill, E. C., Crowston, J. G. *et al.* (2011). Mitochondrial dysfunction in glaucoma and emerging bioenergetic therapies. *Experimental Eye Research* **93**:204-212.
- Lei, Y., Garrahan, N., Hermann, B., Fautsch, M. P., Johnson, D. H., Hernandez, M. R., Boulton, M. *et al.* (2009). Topography of neuron loss in the retinal ganglion cell layer in human glaucoma. *British Journal of Ophthalmology* **93**:1676-1679.
- Leske, M. C., Connell, A. M. S., Wu, S. Y., Hyman, L. G., Schachat, A. P., Grimson, R., McManmon, E. P. *et al.* (1995). Risk-factors for open-angle glaucoma - the Barbados eye study. *Archives of Ophthalmology* **113**:918-924.
- Leung, C. K.-s., Weinreb, R. N., Li, Z. W., Liu, S., Lindsey, J. D., Choi, N., Liu, L. *et al.* (2011). Long-Term In Vivo Imaging and Measurement of Dendritic Shrinkage of Retinal Ganglion Cells. *Investigative Ophthalmology & Visual Science* **52**:1539-1547.
- Li, K., Sacks, S. H. and Zhou, W. (2007). The relative importance of local and systemic complement production in ischaemia, transplantation and other pathologies. *Molecular Immunology* **44**:3866-3874.
- Li, Z.-w., Liu, S., Weinreb, R. N., Lindsey, J. D., Yu, M., Liu, L., Ye, C. *et al.* (2011). Tracking Dendritic Shrinkage of Retinal Ganglion Cells after Acute Elevation of Intraocular Pressure. *Investigative Ophthalmology & Visual Science* **52**.
- Libby, R. T., Anderson, M. G., Pang, I. H., Robinson, Z. H., Savinova, O. V., Cosma, I. M., Snow, A. *et al.* (2005a). Inherited glaucoma in DBA/2J mice: Pertinent disease features for studying the neurodegeneration. *Visual Neuroscience* **22**:637-648.

Libby, R. T., Li, Y., Savinova, O. V., Barter, J., Smith, R. S., Nickells, R. W. and John, S. W. M. (2005b). Susceptibility to neurodegeneration in a glaucoma is modified by Bax gene dosage. *Plos Genetics* **1**:17-26.

Ligon, L. A. and Steward, O. (2000). Movement of mitochondria in the axons and dendrites of cultured hippocampal neurons. *Journal of Comparative Neurology* **427**:340-350.

Lillis, A. P., Mikhailenko, I. and Strickland, D. K. (2005). Beyond endocytosis: LRP function in cell migration, proliferation and vascular permeability. *Journal of Thrombosis and Haemostasis* **3**:1884-1893.

Lin, B., Martin, P. R., Solomon, S. G. and Grunert, U. (2000). Distribution of glycine receptor subunits on primate retinal ganglion cells: a quantitative analysis. *European Journal of Neuroscience* **12**:4155-4170.

Linnartz, B., Kopatz, J., Tenner, A. J. and Neumann, H. (2012). Sialic Acid on the Neuronal Glycocalyx Prevents Complement C1 Binding and Complement Receptor-3-Mediated Removal by Microglia. *Journal of Neuroscience* **32**:946-952.

Liu, Y., McDowell, C. M., Zhang, Z., Tebow, H. E., Wordinger, R. J. and Clark, A. F. (2014). Monitoring Retinal Morphologic and Functional Changes in Mice Following Optic Nerve Crush. *Investigative Ophthalmology & Visual Science* **55**:3766-3774.

Liu, Y. X., Qin, L. Y., Wilson, B. C., An, L. J., Hong, J. S. and Liu, B. (2002). Inhibition by naloxone stereoisomers of beta-amyloid peptide (1-42)-induced superoxide production in microglia and degeneration of cortical and mesencephalic neurons. *Journal of Pharmacology and Experimental Therapeutics* **302**:1212-1219.

Longair, M. H., Baker, D. A. and Armstrong, J. D. (2011). Simple Neurite Tracer: open source software for reconstruction, visualization and analysis of neuronal processes. *Bioinformatics* **27**:2453-2454.

Loopuijt, L. D., da Silva Filho, M., Hirt, B., Vonthein, R. and Kremers, J. (2007). Dendritic thickness: a morphometric parameter to classify mouse retinal ganglion cells. *Brazilian Journal of Medical and Biological Research* **40**:1367-1382.

Ma, J., Kabi, M., Tucker, B. A., Ge, J. and Young, M. J. (2011). Combining chondroitinase ABC and growth factors promotes the integration of murine retinal progenitor cells transplanted into Rho(-/-) mice. *Molecular Vision* **17**:1759-1770.

MacNeil, M. A., Heussy, J. K., Dacheux, R. F., Raviola, E. and Masland, R. H. (2004). The population of bipolar cells in the rabbit retina. *Journal of Comparative Neurology* **472**:73-86.

Maier, M., Peng, Y., Jiang, L., Seabrook, T. J., Carroll, M. C. and Lemere, C. A. (2008). Complement C3 deficiency leads to accelerated amyloid beta plaque deposition and neurodegeneration and modulation of the microglia/macrophage phenotype in amyloid precursor protein transgenic mice. *Journal of Neuroscience* **28**:6333-6341.

Malik, R., Swanson, W. H. and Garway-Heath, D. F. (2012). 'Structure-function relationship' in glaucoma: past thinking and current concepts. *Clinical and Experimental Ophthalmology* **40**:369-380.

Mansourrobaey, S., Bray, G. M. and Aguayo, A. J. (1992). In vivo effects of brain-derived neurotrophic factor (BDNF) and injury on the survival of axotomized retinal ganglion-cells (RGCS) in adult-rats. *Molecular Biology of the Cell* **3**:A333-A333.

Martin, K. R. G., Quigley, H. A., Valenta, D., Kielczewski, J. and Pease, M. E. (2006). Optic nerve dynein motor protein distribution changes with intraocular pressure elevation in a rat model of glaucoma. *Experimental Eye Research* **83**:255-262.

Martinez, M., Hernandez, A. I., Martinez, N. and Ferrandiz, M. L. (1996). Age-related increase in oxidized proteins in mouse synaptic mitochondria. *Brain Research* **731**:246-248.

Massey, J. M., Hubscher, C. H., Wagoner, M. R., Decker, J. A., Ams, J., Silver, J. and Onifer, S. M. (2006). Chondroitinase ABC digestion of the perineuronal net promotes functional collateral sprouting in the cuneate nucleus after cervical spinal cord injury. *Journal of Neuroscience* **26**:4406-4414.

Matsui, F., Kawashima, S., Shuo, T., Yamauchi, S., Tokita, Y., Aono, S., Keino, H. *et al.* (2002). Transient expression of juvenile-type neurocan by reactive astrocytes in adult rat brains injured by kainate-induced seizures as well as surgical incision. *Neuroscience* **112**:773-781.

Mattson, M. P. and Duan, W. Z. (1999). "Apoptotic" biochemical cascades in synaptic compartments: Roles in adaptive plasticity and neurodegenerative disorders. *Journal of Neuroscience Research* **58**:152-166.

Mauney, S. A., Athanas, K. M., Pantazopoulos, H., Shaskan, N., Passeri, E., Berretta, S. and Woo, T. U. W. (2013). Developmental Pattern of Perineuronal Nets in the Human Prefrontal Cortex and Their Deficit in Schizophrenia. *Biological Psychiatry* **74**:427-435.

Maynard, R., Downes, N. and Finney, B. (2014). *Histological Techniques: An Introduction for Beginners in Toxicology*. Royal Society of Chemistry.

McGillem, G. S., Rotolo, T. C. and Dacheux, R. F. (2000). GABA responses of rod bipolar cells in rabbit retinal slices. *Visual Neuroscience* **17**:381-389.

McGlashan, T. H. and Hoffman, R. E. (2000). Schizophrenia as a disorder of developmentally reduced synaptic connectivity. *Archives of General Psychiatry* **57**:637-648.

McKeon, R. J., Hoke, A. and Silver, J. (1995). Injury-induced proteoglycans inhibit the potential for laminin-mediated axon growth on astrocytic scars. *Experimental Neurology* **136**:32-43.

McKeon, R. J., Jurynek, M. J. and Buck, C. R. (1999). The chondroitin sulfate proteoglycans neurocan and phosphacan are expressed by reactive astrocytes in the chronic CNS glial scar. *Journal of Neuroscience* **19**:10778-10788.

McKeon, R. J. and Nophachi, S. V. (1998). Transforming growth factor-beta stimulates the expression of a neurite growth inhibitory chondroitin sulfate proteoglycan by astrocytes. *Society for Neuroscience Abstracts* **24**:555-555.

McKeon, R. J., Schreiber, R. C., Rudge, J. S. and Silver, J. (1991). Reduction of neurite outgrowth in a model of glial scarring following CNS injury is correlated with the expression of inhibitory molecules on reactive astrocytes. *Journal of Neuroscience* **11**:3398-3411.

McRae, P. A., Baranov, E., Rogers, S. L. and Porter, B. E. (2012). Persistent decrease in multiple components of the perineuronal net following status epilepticus. *European Journal of Neuroscience* **36**:3471-3482.

McRae, P. A., Rocco, M. M., Kelly, G., Brumberg, J. C. and Matthews, R. T. (2007). Sensory deprivation alters aggrecan and perineuronal net expression in the mouse barrel cortex. *Journal of Neuroscience* **27**:5405-5413.

Mey, J. and Thanos, S. (1993). Intravitreal injections of neurotrophic factors support the survival of axotomized retinal ganglion-cells in adult-rats *in vivo*. *Brain Research* **602**:304-317.

Meyer-Luehmann, M., Spires-Jones, T. L., Prada, C., Garcia-Alloza, M., de Calignon, A., Rozkalne, A., Koenigsknecht-Talboo, J. *et al.* (2008). Rapid appearance and local toxicity of amyloid-beta plaques in a mouse model of Alzheimer's disease. *Nature* **451**:720-U725.

Milev, P., Chiba, A., Haring, M., Rauvala, H., Schachner, M., Ranscht, B., Margolis, R. K. *et al.* (1998a). High affinity binding and overlapping localization of neurocan and phosphacan protein-tyrosine phosphatase-zeta/beta with tenascin-R, amphoterin, and the heparin-binding growth-associated molecule. *Journal of Biological Chemistry* **273**:6998-7005.

Milev, P., Maurel, P., Chiba, A., Mevissen, M., Popp, S., Yamaguchi, Y., Margolis, R. K. *et al.* (1998b). Differential regulation of expression of hyaluronan-binding proteoglycans in developing brain: Aggrecan, versican, neurocan, and brevican. *Biochemical and Biophysical Research Communications* **247**:207-212.

Milev, P., Monnerie, H., Popp, S., Margolis, R. K. and Margolis, R. U. (1998c). The core protein of the chondroitin sulfate proteoglycan phosphacan is a high-affinity ligand of fibroblast growth factor-2 and potentiates its mitogenic activity. *Journal of Biological Chemistry* **273**:21439-21442.

Miller, R. F. and Dacheux, R. F. (1976). Synaptic organization and ionic basis of on and off channels in mudpuppy retina .3. Model of ganglion-cell receptive-field organization based on chloride-free experiments. *Journal of General Physiology* **67**:679-690.

Minckler, D. S., Bunt, A. H. and Johanson, G. W. (1977). Orthograde and retrograde axoplasmic-transport during acute ocular hypertension in monkey. *Investigative Ophthalmology & Visual Science* **16**:426-441.

Misra, U. K. and Pizzo, S. V. (1998). Binding of receptor-recognized forms of alpha(2)-macroglobulin to the alpha(2)-macroglobulin signaling receptor activates phosphatidylinositol 3-kinase. *Journal of Biological Chemistry* **273**:13399-13402.

Moon, L. D. F., Asher, R. A., Rhodes, K. E. and Fawcett, J. W. (2001). Regeneration of CNS axons back to their target following treatment of adult rat brain with chondroitinase ABC. *Nature Neuroscience* **4**:465-466.

Moore, C. G., Johnson, E. C. and Morrison, J. C. (1996). Circadian rhythm of intraocular pressure in the rat. *Current Eye Research* **15**:185-191.

Morcos, Y. and Chan-Ling, T. L. (2000). Concentration of astrocytic filaments at the retinal optic nerve junction is coincident with the absence of intra-retinal myelination: comparative and developmental evidence. *Journal of Neurocytology* **29**:665-678.

Morgan, J. E. (2002). Retinal ganglion cell shrinkage in glaucoma. *Journal of Glaucoma* **11**:365-370.

Morgan, J. E., Datta, A. V., Erichsen, J. T., Albon, J. and Boulton, M. E. (2006). Retinal ganglion cell remodelling in experimental glaucoma. In: Hollyfield, J.G.A.R.E.L.M.M. (ed.) *Retinal Degenerative Diseases*. Vol. 572. pp. 397-402.

Morgan, J. E. and Tribble, J. R. (2015). Microbead models in glaucoma. *Experimental Eye Research* **141**:9-14.

Morgan, J. E., Uchida, H. and Caprioli, J. (2000). Retinal ganglion cell death in experimental glaucoma. *British Journal of Ophthalmology* **84**:303-310.

Morganti, M. C., Taylor, J., Pesheva, P. and Schachner, M. (1990). Oligodendrocyte-derived J1-160/180 extracellular-matrix glycoproteins are adhesive or repulsive depending on the partner cell type and time of interaction. *Experimental Neurology* **109**:98-110.

Morrison, J., Farrell, S., Johnson, E., Deppmeier, L., Moore, C. G. and Grossmann, E. (1995). Structure and composition of the rodent lamina-cribrosa. *Experimental Eye Research* **60**:127-135.

Morrison, J. C., Moore, C. G., Deppmeier, L. M. H., Gold, B. G., Meshul, C. K. and Johnson, E. C. (1997). A rat model of chronic pressure-induced optic nerve damage. *Experimental Eye Research* **64**:85-96.

Mueller, L. P. D. S., Shelley, J. and Weiler, R. (2007). Displaced amacrine cells of the mouse retina. *Journal of Comparative Neurology* **505**:177-189.

Muhleisen, T. W., Mattheisen, M., Strohmaier, J., Degenhardt, F., Priebe, L., Schultz, C. C., Breuer, R. *et al.* (2012). Association between schizophrenia and common variation in neurocan (NCAN), a genetic risk factor for bipolar disorder. *Schizophrenia Research* **138**:69-73.

Mulholland, P. J., Redmond, T., Garway-Heath, D. F., Zlatkova, M. B. and Anderson, R. S. (2015). Spatiotemporal Summation of Perimetric Stimuli in Early Glaucoma. *Investigative ophthalmology & visual science* **56**:6473-6482.

Nabavi, S., Fox, R., Proulx, C. D., Lin, J. Y., Tsien, R. Y. and Malinow, R. (2014). Engineering a memory with LTD and LTP. *Nature* **511**:348-+.

Nadal-Nicolas, F. M., Jimenez-Lopez, M., Sobrado-Calvo, P., Nieto-Lopez, L., Canovas-Martinez, I., Salinas-Navarro, M., Vidal-Sanz, M. *et al.* (2009). Brn3a as a Marker of Retinal Ganglion Cells:

Qualitative and Quantitative Time Course Studies in Naive and Optic Nerve-Injured Retinas. *Investigative Ophthalmology & Visual Science* **50**:3860-3868.

Nakamura, M., Nakano, K., Morita, S., Nakashima, T., Oohira, A. and Miyata, S. (2009). Expression of chondroitin sulfate proteoglycans in barrel field of mouse and rat somatosensory cortex. *Brain Research* **1252**:117-129.

Naskar, R., Wissing, M. and Thanos, S. (2002). Detection of early neuron degeneration and accompanying microglial responses in the retina of a rat model of glaucoma. *Investigative Ophthalmology & Visual Science* **43**.

Neher, J. J., Neniskyte, U., Zhao, J.-W., Bal-Price, A., Tolkovsky, A. M. and Brown, G. C. (2011). Inhibition of Microglial Phagocytosis Is Sufficient To Prevent Inflammatory Neuronal Death. *Journal of Immunology* **186**:4973-4983.

Neufeld, A. H. (1999a). Microglia in the optic nerve head and the region of parapapillary chorioretinal atrophy in glaucoma. *Archives of Ophthalmology* **117**:1050-1056.

Neufeld, A. H. (1999b). Nitric oxide: A potential mediator of retinal ganglion cell damage in glaucoma. *Survey of Ophthalmology* **43**:S129-S135.

Neufeld, A. H., Kawai, S. I., Das, S., Vora, S., Gachie, E., Connor, J. R. and Manning, P. T. (2002). Loss of retinal ganglion cells following retinal ischemia: The role of inducible nitric oxide synthase. *Experimental Eye Research* **75**:521-528.

Nichol, K. A., Everett, A. W., Schulz, M. and Bennett, M. R. (1994). Retinal ganglion-cell survival in-vitro maintained by a chondroitin sulfate proteoglycan from the superior colliculus carrying the HNK-1 epitope. *Journal of Neuroscience Research* **37**:623-632.

Nickells, R. W. (2012). The Cell and Molecular Biology of Glaucoma: Mechanisms of Retinal Ganglion Cell Death. *Investigative Ophthalmology & Visual Science* **53**:2476-2481.

Nimmerjahn, A., Kirchhoff, F. and Helmchen, F. (2005). Resting microglial cells are highly dynamic surveillants of brain parenchyma in vivo. *Science* **308**:1314-1318.

Norton, W. T., Aquino, D. A., Hozumi, I., Chiu, F. C. and Brosnan, C. F. (1992). Quantitative aspects of reactive gliosis - a review. *Neurochemical Research* **17**:877-885.

O'Brien, B. J., Isayama, T. and Berson, D. M. (1999). Light responses of morphologically identified cat ganglion cells. *Investigative Ophthalmology & Visual Science* **40**:S815-S815.

Oohira, A., Matsui, F. and Katohsema, R. (1991). Inhibitory effects of brain chondroitin sulfate proteoglycans on neurite outgrowth from PC12D Cells. *Journal of Neuroscience* **11**:822-827.

Orsini, F., De Blasio, D., Zangari, R., Zanier, E. R. and De Simoni, M.-G. (2014). Versatility of the complement system in neuroinflammation, neurodegeneration and brain homeostasis. *Frontiers in Cellular Neuroscience* **8**.

Oshitari, T., Dezawa, M., Okada, S., Takano, M., Negishi, H., Horie, H., Sawada, H. *et al.* (2002). The role of c-fos in cell death and regeneration of retinal ganglion cells. *Investigative Ophthalmology & Visual Science* **43**:2442-2449.

Paidassi, H., Tacnet-Delorme, P., Verneret, M., Gaboriaud, C., Houen, G., Duus, K., Ling, W. L. *et al.* (2011). Investigations on the C1q-Calreticulin-Phosphatidylserine Interactions Yield New Insights into Apoptotic Cell Recognition. *Journal of Molecular Biology* **408**:277-290.

Pantazopoulos, H., Boyer-Boiteau, A., Holbrook, E. H., Jang, W., Hahn, C. G., Arnold, S. E. and Berretta, S. (2013). Proteoglycan abnormalities in olfactory epithelium tissue from subjects diagnosed with schizophrenia. *Schizophrenia Research* **150**:366-372.

Park, H.-Y. L., Kim, J. H. and Park, C. K. (2014). Alterations of the synapse of the inner retinal layers after chronic intraocular pressure elevation in glaucoma animal model. *Molecular Brain* **7**.

Pasterkamp, R. J. and Kolodkin, A. L. (2003). Semaphorin junction: making tracks toward neural connectivity. *Current Opinion in Neurobiology* **13**:79-89.

Pastrana, E., Moreno-Flores, M. T., Gurzov, E. N., Avila, J., Wandosell, F. and Diaz-Nido, J. (2006). Genes associated with adult axon regeneration promoted by olfactory ensheathing cells: A new role for matrix metalloproteinase 2. *Journal of Neuroscience* **26**:5347-5359.

Pavlidis, M., Stupp, T., Naskar, R., Cengiz, C. and Thanos, S. (2003). Retinal ganglion cells resistant to advanced glaucoma: A postmortem study of human retinas with the carbocyanine dye Dil. *Investigative Ophthalmology & Visual Science* **44**:5196-5205.

Pease, M. E., McKinnon, S. J., Quigley, H. A., Kerrigan-Baumrind, L. A. and Zack, D. J. (2000). Obstructed axonal transport of BDNF and its receptor TrkB in experimental glaucoma. *Investigative Ophthalmology & Visual Science* **41**:764-774.

- Pederson, J. E. and Anderson, D. R. (1980). Mode of progressive disk cupping in ocular hypertension and glaucoma. *Archives of Ophthalmology* **98**:490-498.
- Peinado-Ramon, P., Salvador, M., Villegas-Perez, M. P. and VidalSanz, M. (1996). Effects of axotomy and intraocular administration of NT-4, NT-3, and brain-derived neurotrophic factor on the survival of adult rat retinal ganglion cells - A quantitative in vivo study. *Investigative Ophthalmology & Visual Science* **37**:489-500.
- Pereira Carneiro Muniz, J. A., de Athaide, L. M., Gomes, B. D., Finlay, B. L. and de Lima Silveira, L. C. (2014). Ganglion Cell and Displaced Amacrine Cell Density Distribution in the Retina of the Howler Monkey (*Alouatta caraya*). *Plos One* **9**.
- Perris, R. and Johansson, S. (1987). Amphibian neural crest cell-migration on purified extracellular-matrix components - a chondroitin sulfate proteoglycan inhibits locomotion on fibronectin substrates. *Journal of Cell Biology* **105**:2511-2521.
- Perris, R., Perissinotto, D., Pettway, Z., BronnerFraser, M., Morgelin, M. and Kimata, K. (1996). Inhibitory effects of PG-H/aggrecan and PG-M/versican on avian neural crest cell migration. *Faseb Journal* **10**:293-301.
- Perry, V. H. (1981). Evidence for an amacrine cell system in the ganglion-cell layer of the rat retina. *Neuroscience* **6**:931-944.
- Perry, V. H., Oehler, R. and Cowey, A. (1984). Retinal ganglion-cells that project to the dorsal lateral geniculate-nucleus in the macaque monkey. *Neuroscience* **12**:1101-1123.
- Perry, V. H. and Walker, M. (1980). Amacrine cells, displaced amacrine cells and interplexiform cells in in the retina of the rat. *Proceedings of the Royal Society Series B-Biological Sciences* **208**:415-431.
- Peters, D., Bengtsson, B. and Heijl, A. (2014). Factors associated with lifetime risk of open-angle glaucoma blindness. *Acta Ophthalmologica* **92**:421-425.
- Petrusca, D., Grivich, M. I., Sher, A., Field, G. D., Gauthier, J. L., Greschner, M., Shlens, J. *et al.* (2007). Identification and characterization of a Y-like primate retinal ganglion cell type. *Journal of Neuroscience* **27**:11019-11027.
- Pettigrew, J. and Sanderson, W. (1986). Comparative visual physiology. *Visual Neuroscience*. Cambridge University press.

Pettigrew, J. D., Dreher, B., Hopkins, C. S., McCall, M. J. and Brown, M. (1988). Peak density and distribution of ganglion-cells in the retinae of microchiropteran bats - implications for visual-acuity. *Brain Behavior and Evolution* **32**:39-56.

Pizzorusso, T., Medini, P., Berardi, N., Chierzi, S., Fawcett, J. W. and Maffei, L. (2002). Reactivation of ocular dominance plasticity in the adult visual cortex. *Science* **298**:1248-1251.

Podack, E. R., Tschoop, J. and Mullereberhard, H. J. (1982). Molecular-organization of C9 within the membrane attack complex of complement - induction of circular C9 polymerization by the C5b-8 assembly. *Journal of Experimental Medicine* **156**:268-282.

Polleux, F., Morrow, T. and Ghosh, A. (2000). Semaphorin 3A is a chemoattractant for cortical apical dendrites. *Nature* **404**:567-573.

Polyak, S. L. (1941). The retina The anatomy and the histology of the retina in man, ape, and monkey, including the consideration of visual functions, the history of physiological optics, and the histological laboratory technique. *The retina The anatomy and the histology of the retina in man, ape, and monkey, including the consideration of visual functions, the history of physiological optics, and the histological laboratory technique* x + 607p. 602 maps, 697 pl. (601 col.)-x + 607p. 602 maps, 697 pl. (601 col.).

Prashar, A., Guggenheim, J. A., Erichsen, J. T., Hocking, P. and Morgan, J. E. (2007). Measurement of intraocular pressure (IOP) in chickens using a rebound tonometer: Quantitative evaluation of variance due to position inaccuracies. *Experimental Eye Research* **85**:563-571.

Properzi, F., Carulli, D., Asher, R. A., Muir, E., Camargo, L. M., van Kuppevelt, T. H., ten Dam, G. B. *et al.* (2005). Chondroitin 6-sulphate synthesis is up-regulated in injured CNS, induced by injury-related cytokines and enhanced in axon-growth inhibitory glia. *European Journal of Neuroscience* **21**:378-390.

Puchalla, J. L., Schneidman, E., Harris, R. A. and Berry, M. J. (2005). Redundancy in the population code of the retina. *Neuron* **46**:493-504.

Quigley, H. A. and Addicks, E. M. (1980). Chronic experimental glaucoma in primates .1. production of elevated intraocular-pressure by anterior-chamber injection of autologous ghost red-blood-cells. *Investigative Ophthalmology & Visual Science* **19**:126-136.

Quigley, H. A., Addicks, E. M. and Green, W. R. (1982). Optic-nerve damage in human glaucoma .3. Quantitative correlation of nerve-fiber loss and visual-field defect in glaucoma, ischemic neuropathy, papilledema, and toxic neuropathy. *Archives of Ophthalmology* **100**:135-146.

Quigley, H. A. and Anderson, D. R. (1976). Dynamics and location of axonal-transport blockade by acute intraocular-pressure elevation in primate optic-nerve. *Investigative Ophthalmology* **15**:606-616.

Quigley, H. A. and Broman, A. T. (2006). The number of people with glaucoma worldwide in 2010 and 2020. *British Journal of Ophthalmology* **90**:262-267.

Quigley, H. A., Dunkelberger, G. R. and Green, W. R. (1989). Retinal ganglion-cell atrophy correlated with automated perimetry in human eyes with glaucoma. *American Journal of Ophthalmology* **107**:453-464.

Quigley, H. A., Hohman, R. M., Addicks, E. M., Massof, R. W. and Green, W. R. (1983). MORPHOLOGIC CHANGES IN THE LAMINA CRIBROSA CORRELATED WITH NEURAL LOSS IN OPEN-ANGLE GLAUCOMA. *American Journal of Ophthalmology* **95**:673-691.

Quigley, H. A., McKinnon, S. J., Zack, D. J., Pease, M. E., Kerrigan-Baumrind, L. A., Kerrigan, D. F. and Mitchell, R. S. (2000). Retrograde axonal transport of BDNF in retinal ganglion cells is blocked by acute IOP elevation in rats. *Investigative Ophthalmology & Visual Science* **41**:3460-3466.

Ramirez, A. I., Salazar, J. J., de Hoz, R., Rojas, B., Gallego, B. I., Salinas-Navarro, M., Alarcon-Martinez, L. *et al.* (2010). Quantification of the Effect of Different Levels of IOP in the Astroglia of the Rat Retina Ipsilateral and Contralateral to Experimental Glaucoma. *Investigative Ophthalmology & Visual Science* **51**:5690-5696.

Reddy, P. H., Tripathi, R., Quang, T., Tirumala, K., Reddy, T. P., Anekonda, V., Shirendeb, U. P. *et al.* (2012). Abnormal mitochondrial dynamics and synaptic degeneration as early events in Alzheimer's disease: Implications to mitochondria-targeted antioxidant therapeutics. *Biochimica Et Biophysica Acta-Molecular Basis of Disease* **1822**:639-649.

Redmond, T., Garway-Heath, D. F., Zlatkova, M. B. and Anderson, R. S. (2010). Sensitivity Loss in Early Glaucoma Can Be Mapped to an Enlargement of the Area of Complete Spatial Summation. *Investigative Ophthalmology & Visual Science* **51**.

Reichenbach, A. and Bringmann, A. (2013). New functions of Muller cells. *Glia* **61**:651-678.

Resnikoff, S., Pascolini, D., Etya'ale, D., Kocur, I., Pararajasegaram, R., Pokharel, G. P. and Mariotti, S. P. (2004). Global data on visual impairment in the year 2002. *Bulletin of the World Health Organization* **82**:844-851.

Ricklin, D. and Lambris, J. D. (2007). Complement-targeted therapeutics. *Nature Biotechnology* **25**:1265-1275.

Roberts, M. D., Grau, V., Grimm, J., Reynaud, J., Bellezza, A. J., Burgoyne, C. F. and Downs, J. C. (2009). Remodeling of the Connective Tissue Microarchitecture of the Lamina Cribrosa in Early Experimental Glaucoma. *Investigative Ophthalmology & Visual Science* **50**:681-690.

Rockhill, R. L., Daly, F. J., MacNeil, M. A., Brown, S. P. and Masland, R. H. (2002). The diversity of ganglion cells in a mammalian retina. *Journal of Neuroscience* **22**:3831-3843.

Rojas, B., Gallego, B. I., Ramirez, A. I., Salazar, J. J., de Hoz, R., Valiente-Soriano, F. J., Aviles-Trigueros, M. *et al.* (2014). Microglia in mouse retina contralateral to experimental glaucoma exhibit multiple signs of activation in all retinal layers. *Journal of Neuroinflammation* **11**.

Romberg, C., Yang, S. J., Melani, R., Andrews, M. R., Horner, A. E., Spillantini, M. G., Bussey, T. J. *et al.* (2013). Depletion of Perineuronal Nets Enhances Recognition Memory and Long-Term Depression in the Perirhinal Cortex. *Journal of Neuroscience* **33**:7057-7065.

Saghatelian, A. K., Dityatev, A., Schmidt, S., Schuster, T., Bartsch, U. and Schachner, M. (2001). Reduced perisomatic inhibition, increased excitatory transmission, and impaired long-term potentiation in mice deficient for the extracellular matrix glycoprotein tenascin-R. *Molecular and Cellular Neuroscience* **17**:226-240.

Salinas-Navarro, M., Alarcon-Martinez, L., Valiente-Soriano, F. J., Jimenez-Lopez, M., Mayor-Torroglosa, S., Aviles-Trigueros, M., Paz Villegas-Perez, M. *et al.* (2010). Ocular hypertension impairs optic nerve axonal transport leading to progressive retinal ganglion cell degeneration. *Experimental Eye Research* **90**:168-183.

Samsel, P. A., Kisiswa, L., Erichsen, J. T., Cross, S. D. and Morgan, J. E. (2011). A Novel Method for the Induction of Experimental Glaucoma Using Magnetic Microspheres. *Investigative Ophthalmology & Visual Science* **52**:1671-1675.

Sanes, J. R. and Masland, R. H. (2015). The Types of Retinal Ganglion Cells: Current Status and Implications for Neuronal Classification. *Annual Review of Neuroscience, Vol 38* **38**:221-246.

Sappington, R. M., Carlson, B. J., Crish, S. D. and Calkins, D. J. (2010). The Microbead Occlusion Model: A Paradigm for Induced Ocular Hypertension in Rats and Mice. *Investigative Ophthalmology & Visual Science* **51**:207-216.

Schindelin, J., Arganda-Carreras, I., Frise, E., Kaynig, V., Longair, M., Pietzsch, T., Preibisch, S. *et al.* (2012). Fiji: an open-source platform for biological-image analysis. *Nat Methods* **9**:676-682.

Schlamp, C. L., Johnson, E. C., Li, Y., Morrison, J. C. and Nickells, R. W. (2001). Changes in Thy1 gene expression associated with damaged retinal ganglion cells. *Molecular Vision* **7**:192-201.

Schlamp, C. L., Li, Y., Dietz, J. A., Janssen, K. T. and Nickells, R. W. (2006). Progressive ganglion cell loss and optic nerve degeneration in DBA/2J mice is variable and asymmetric. *Bmc Neuroscience* **7**.

Schulz, M., Raju, T., Ralston, G. and Bennett, M. R. (1990). A retinal ganglion-cell neurotrophic factor purified from the superior colliculus. *Journal of Neurochemistry* **55**:832-841.

Schwarz, T. L. (2013). Mitochondrial Trafficking in Neurons. *Cold Spring Harbor Perspectives in Biology* **5**.

Selles-Navarro, I., Ellezam, B., Fajardo, R., Latour, M. and McKerracher, L. (2001). Retinal ganglion cell and nonneuronal cell responses to a microcrush lesion of adult rat optic nerve. *Experimental Neurology* **167**:282-289.

Shi, Y. H., Tohyama, Y., Kadono, T., He, J. S., Miah, S. M. S., Hazama, R., Tanaka, C. *et al.* (2006). Protein-tyrosine kinase Syk is required for pathogen engulfment in complement-mediated phagocytosis. *Blood* **107**:4554-4562.

Shou, T. D., Liu, J., Wang, W., Zhou, Y. F. and Zhao, K. X. (2003). Differential dendritic shrinkage of alpha and beta retinal ganglion cells in cats with chronic glaucoma. *Investigative Ophthalmology & Visual Science* **44**:3005-3010.

Sihota, R., Gupta, V., Tuli, D., Sharma, A., Sony, P. and Srinivasan, G. (2007). Classifying patterns of localized glaucomatous visual field defects on automated perimetry. *Journal of Glaucoma* **16**:146-152.

Silver, J. and Miller, J. H. (2004). Regeneration beyond the glial scar. *Nature Reviews Neuroscience* **5**:146-156.

Sjostrand, F. S. (1958). Ultrastructure of retinal rod synapses of the guinea pig eye as revealed by 3-dimensional reconstructions from serial sections. *Journal of Ultrastructure Research* **2**:122-170.

Smedowski, A., Pietrucha-Dutczak, M., Kaamiranta, K. and Lewin-Kowalik, J. (2014). A rat experimental model of glaucoma incorporating rapid-onset elevation of intraocular pressure. *Scientific Reports* **4**.

Smith, R. S., John, S. W. M., Nishina, P. M. and Sundberg, J. P. (2001). Systemic Evaluation of the Mouse Eye: Anatomy, Pathology and Biometrics. CRC Press.

Smith, T. G., Lange, G. D. and Marks, W. B. (1996). Fractal methods and results in cellular morphology - Dimensions, lacunarity and multifractals. *Journal of Neuroscience Methods* **69**:123-136.

Snow, A. D., Mar, H., Nochlin, D., Kimata, K., Kato, M., Suzuki, S., Hassell, J. *et al.* (1988). The presence of heparan-sulfate proteoglycans in the neuritic plaques and congophilic angiopathy in alzheimer's-disease. *American Journal of Pathology* **133**:456-463.

Snow, D. M., Lemmon, V., Carrino, D. A., Caplan, A. I. and Silver, J. (1990). Sulfated proteoglycans in astroglial barriers inhibit neurite outgrowth invitro. *Experimental Neurology* **109**:111-130.

Snow, D. M. and Letourneau, P. C. (1992). Neurite outgrowth on a step gradient of chondroitin sulfate proteoglycan (CS-PG). *Journal of Neurobiology* **23**:322-336.

Soleman, S., Filippov, M. A., Dityatev, A. and Fawcett, J. W. (2013). Targeting the neural extracellular matrix in neurological disorders. *Neuroscience* **253**:194-213.

Son, J. L., Soto, I., Oglesby, E., Lopez-Roca, T., Pease, M. E., Quigley, H. A. and Marsh-Armstrong, N. (2010). Glaucomatous Optic Nerve Injury Involves Early Astrocyte Reactivity and Late Oligodendrocyte Loss. *Glia* **58**:780-789.

Soto, I., Pease, M. E., Son, J. L., Shi, X., Quigley, H. A. and Marsh-Armstrong, N. (2011). Retinal Ganglion Cell Loss in a Rat Ocular Hypertension Model Is Sectorial and Involves Early Optic Nerve Axon Loss. *Investigative Ophthalmology & Visual Science* **52**:434-441.

Spalding, K. L., Rush, R. A. and Harvey, A. R. (2004). Target-derived and locally derived neurotrophins support retinal ganglion cell survival in the neonatal rat retina. *Journal of Neurobiology* **60**:319-327.

Stacey, M., Chang, G. W., Davies, J. Q., Kwakkenbos, M. J., Sanderson, R. D., Hamann, J., Gordon, S. *et al.* (2003). The epidermal growth factor-like domains of the human EMR2

receptor mediate cell attachment through chondroitin sulfate glycosaminoglycans. *Blood* **102**:2916-2924.

Stasi, K., Nagel, D., Yang, X. Y., Wang, R. F., Ren, L. Z., Podos, S. M., Mittag, T. *et al.* (2006). Complement component 1Q (C1Q) upregulation in retina of murine, primate, and human glaucomatous eyes. *Investigative Ophthalmology & Visual Science* **47**:1024-1029.

Stauch, K. L., Purnell, P. R. and Fox, H. S. (2014). Quantitative Proteomics of Synaptic and Nonsynaptic Mitochondria: Insights for Synaptic Mitochondrial Vulnerability. *Journal of Proteome Research* **13**:2620-2636.

Stell, W. K. (1967). Structure and relationships of horizontal cells and photoreceptor-bipolar synaptic complexes in goldfish retina. *American Journal of Anatomy* **121**:401-&.

Stevens, B., Allen, N. J., Vazquez, L. E., Howell, G. R., Christopherson, K. S., Nouri, N., Micheva, K. D. *et al.* (2007). The classical complement cascade mediates CNS synapse elimination. *Cell* **131**:1164-1178.

Stevens, J. K., McGuire, B. A. and Sterling, P. (1980). Toward a functional architecture of the retina - serial reconstruction of adjacent ganglion-cells. *Science* **207**:317-319.

Stewart, W. C., Kolker, A. E., Sharpe, E. D., Day, D. G., Holmes, K. T., Leech, J. N., Johnson, M. *et al.* (2000). Factors associated with long-term progression or stability in primary open-angle glaucoma. *American Journal of Ophthalmology* **130**:274-279.

Stoll, G., Jander, S. and Myers, R. R. (2002). Degeneration and regeneration of the peripheral nervous system: From Augustus Waller's observations to neuroinflammation. *Journal of the Peripheral Nervous System* **7**:13-27.

Stone, J., Makarov, F. and Hollander, H. (1995). The glial ensheathment of the soma and axon hillock of retinal ganglion-cells. *Visual Neuroscience* **12**:273-279.

Streit, W. J. (2000). Microglial response to brain injury: A brief synopsis. *Toxicologic Pathology* **28**:28-30.

Sun, W., Deng, Q., Levick, W. R. and He, S. (2006). ON direction-selective ganglion cells in the mouse retina. *Journal of Physiology-London* **576**:197-202.

Sun, W. Z., Li, N. and He, S. G. (2002a). Large-scale morphological survey of rat retinal ganglion cells. *Visual Neuroscience* **19**.

Sun, W. Z., Li, N. and He, S. G. (2002b). Large-scale morphological survey of mouse retinal ganglion cells. *Journal of Comparative Neurology* **451**:115-126.

Sundaresan, P., Simpson, D. A., Sambare, C., Duffy, S., Lechner, J., Dastane, A., Dervan, E. W. *et al.* (2015). Whole-mitochondrial genome sequencing in primary open-angle glaucoma using massively parallel sequencing identifies novel and known pathogenic variants. *Genetics in Medicine* **17**:279-284.

Suzuki, T., Akimoto, M., Imai, H., Ueda, Y., Mandai, M., Yoshimura, N., Swaroop, A. *et al.* (2007). Chondroitinase ABC treatment enhances synaptogenesis between transplant and host neurons in model of retinal degeneration. *Cell Transplantation* **16**:493-503.

Suzuki, Y., Iwase, A., Araie, M., Yamamoto, T., Abe, H., Shirato, S., Kuwayama, Y. *et al.* (2006). Risk factors for open-angle glaucoma in a Japanese population - The Tajimi Study. *Ophthalmology* **113**:1613-1617.

Swanson, W. H., Feliuss, J. and Pan, F. (2004). Perimetric defects and ganglion cell damage: Interpreting linear relations using a two-stage neural model. *Investigative Ophthalmology & Visual Science* **45**:466-472.

Tamura, N., Hazeki, K., Okazaki, N., Kametani, Y., Murakami, H., Takaba, Y., Ishikawa, Y. *et al.* (2009). Specific role of phosphoinositide 3-kinase p110 alpha in the regulation of phagocytosis and pinocytosis in macrophages. *Biochemical Journal* **423**:99-108.

Tanihara, H., Hangai, M., Sawaguchi, S., Abe, H., Kageyama, M., Nakazawa, F., Shirasawa, E. *et al.* (1997). Up-regulation of glial fibrillary acidic protein in the retina of primate eyes with experimental glaucoma. *Archives of Ophthalmology* **115**:752-756.

Taylor, K. R., Rudisill, J. A. and Gallo, R. L. (2005). Structural and sequence motifs in dermatan sulfate for promoting fibroblast growth factor-2 (FGF-2) and FGF-7 activity. *Journal of Biological Chemistry* **280**:5300-5306.

Taylor, W. R. (1999). TTX attenuates surround inhibition in rabbit retinal ganglion cells. *Visual Neuroscience* **16**:285-290.

Teismann, P., Tieu, K., Cohen, O., Choi, D. K., Wu, D. C., Marks, D., Vila, M. *et al.* (2003). Pathogenic role of glial cells in Parkinson's disease. *Movement Disorders* **18**:121-129.

Teng, H. K., Teng, K. K., Lee, R., Wright, S., Tevar, S., Almeida, R. D., Kermani, P. *et al.* (2005). ProBDNF induces neuronal apoptosis via activation of a receptor complex of p75(NTR) and sortilin. *Journal of Neuroscience* **25**:5455-5463.

Tester, N. J. and Howland, D. R. (2008). Chondroitinase ABC improves basic and skilled locomotion in spinal cord injured cats. *Experimental Neurology* **209**:483-496.

Tezel, G. and Wax, M. B. (2000). Increased production of tumor necrosis factor-alpha by glial cells exposed to simulated ischemia or elevated hydrostatic pressure induces apoptosis in cocultured retinal ganglion cells. *Journal of Neuroscience* **20**:8693-8700.

Tezel, G. and Wax, M. B. (2007). Glaucoma. *Chem Immunol Allergy*. Vol. 92. Switzerland, pp. 221-227.

Tezel, G., Yang, X., Luo, C., Kain, A. D., Powell, D. W., Kuehn, M. H. and Kaplan, H. J. (2010). Oxidative Stress and the Regulation of Complement Activation in Human Glaucoma. *Investigative Ophthalmology & Visual Science* **51**:5071-5082.

Thanos, S. (1988). Alterations in the morphology of ganglion-cell dendrites in the adult-rat retina after optic-nerve transection and grafting of peripheral-nerve segments. *Cell and Tissue Research* **254**.

Thanos, S., Bahr, M., Barde, Y. A. and Vanselow, J. (1989). Survival and axonal elongation of adult-rat retinal ganglion-cells - invitro effects of lesioned sciatic-nerve and brain derived neurotrophic factor. *European Journal of Neuroscience* **1**:19-26.

Tielsch, J. M., Katz, J., Sommer, A., Quigley, H. A. and Javitt, J. C. (1994). Family history and risk of primary open-angle glaucoma - the Baltimore eye survey. *Archives of Ophthalmology* **112**:69-73.

Troy, J. B. and Shou, T. (2002). The receptive fields of cat retinal ganglion cells in physiological and pathological states: where we are after half a century of research. *Progress in Retinal and Eye Research* **21**:263-302.

Ugolini, G., Cremisi, F. and Maffei, L. (1995). TrkA, TrkB and p75 mRNA expression is developmentally regulated in the rat retina. *Brain Research* **704**:121-124.

Ulfhake, B. and Cullheim, S. (1981). A quantitative light microscopic study of the dendrites of cat spinal gamma-motoneurons after intracellular staining with horseradish-peroxidase. *Journal of Comparative Neurology* **202**:585-596.

Ulfhake, B. and Kellerth, J. O. (1981). A quantitative light microscopic study of the dendrites of cat spinal alpha-motoneurons after intracellular staining with horseradish-peroxidase. *Journal of Comparative Neurology* **202**:571-583.

Urcola, J. H., Hernandez, M. and Vecino, E. (2006). Three experimental glaucoma models in rats: Comparison of the effects of intraocular pressure elevation on retinal ganglion cell size and death. *Experimental Eye Research* **83**:429-437.

van Horssen, J., Kleinnijenhuis, J., Maass, C. N., Rensink, A. A. M., Otte-Holler, I., David, G., van den Heuvel, L. *et al.* (2002). Accumulation of heparan sulfate proteoglycans in cerebellar senile plaques. *Neurobiology of Aging* **23**:537-545.

van Wyk, M., Taylor, W. R. and Vaney, D. I. (2006). Local edge detectors: A substrate for fine spatial vision at low temporal frequencies in rabbit retina. *Journal of Neuroscience* **26**:13250-13263.

Varela, H. J. and Hernandez, M. R. (1997). Astrocyte responses in human optic nerve head with primary open-angle glaucoma. *Journal of Glaucoma* **6**:303-313.

Vecino, E., Caminos, E., Ugarte, M., Martin-Zanca, D. and Osborne, N. N. (1998). Immunohistochemical distribution of neurotrophins and their receptors in the rat retina and the effects of ischemia and reperfusion. *General Pharmacology-the Vascular System* **30**:305-314.

Vecino, E., Garcia-Grespo, D., Garcia, M., Martinez-Millan, L., Sharma, S. C. and Carrascal, E. (2002). Rat retinal ganglion cells co-express brain derived neurotrophic factor (BDNF) and its receptor TrkB. *Vision Research* **42**:151-157.

Voelgyi, B., Chheda, S. and Bloomfield, S. A. (2009). Tracer Coupling Patterns of the Ganglion Cell Subtypes in the Mouse Retina. *Journal of Comparative Neurology* **512**:664-687.

Wang, D. and Fawcett, J. (2012). The perineuronal net and the control of CNS plasticity. *Cell and Tissue Research* **349**:147-160.

Wang, H., Katagiri, Y., McCann, T. E., Unsworth, E., Goldsmith, P., Yu, Z.-X., Tan, F. *et al.* (2008). Chondroitin-4-sulfation negatively regulates axonal guidance and growth. *Journal of Cell Science* **121**:3083-3091.

Wang, J. T., Kunzevitzky, N. J., Dugas, J. C., Cameron, M., Barres, B. A. and Goldberg, J. L. (2007). Disease gene candidates revealed by expression profiling of retinal ganglion cell development. *Journal of Neuroscience* **27**:8593-8603.

Wang, L., Cioffi, G. A., Cull, G., Dong, J. and Fortune, B. (2002). Immunohistologic evidence for retinal glial cell changes in human glaucoma. *Investigative Ophthalmology & Visual Science* **43**:1088-1094.

Wang, X. and Schwarz, T. L. (2009). The Mechanism of Ca²⁺-Dependent Regulation of Kinesin-Mediated Mitochondrial Motility. *Cell* **136**:163-174.

Wang, X., Tay, S. S. W. and Ng, Y. K. (2000). An immunohistochemical study of neuronal and glial cell reactions in retinae of rats with experimental glaucoma. *Experimental Brain Research* **132**:476-484.

Wang, Y., Hancock, A. M., Bradner, J., Chung, K. A., Quinn, J. F., Peskind, E. R., Galasko, D. *et al.* (2011). Complement 3 and Factor H in Human Cerebrospinal Fluid in Parkinson's Disease, Alzheimer's Disease, and Multiple-System Atrophy. *American Journal of Pathology* **178**:1509-1516.

Wassle, H., Chun, M. H. and Muller, F. (1987). Amacrine cells in the ganglion-cell layer of the cat retina. *Journal of Comparative Neurology* **265**:391-408.

Wax, M. B., Tezel, G., Yang, J., Peng, G., Patil, R. V., Agarwal, N., Sappington, R. M. *et al.* (2008). Induced Autoimmunity to Heat Shock Proteins Elicits Glaucomatous Loss of Retinal Ganglion Cell Neurons via Activated T-Cell-Derived Fas-Ligand. *Journal of Neuroscience* **28**:12085-12096.

Weber, A. J. and Harman, C. D. (2005). Structure-function relations of parasol cells in the normal and glaucomatous primate retina. *Investigative Ophthalmology & Visual Science* **46**:3197-3207.

Weber, A. J. and Harman, C. D. (2008). BDNF preserves the dendritic morphology of alpha and beta ganglion cells in the cat retina after optic nerve injury. *Investigative Ophthalmology & Visual Science* **49**:2456-2463.

Weber, A. J., Kaufman, P. L. and Hubbard, W. C. (1998). Morphology of single ganglion cells in the glaucomatous primate retina. *Investigative Ophthalmology & Visual Science* **39**:2304-2320.

Weber, A. J. and Zelenak, D. (2001). Experimental glaucoma in the primate induced by latex microspheres. *Journal of Neuroscience Methods* **111**:39-48.

Werblin, F. S. (2010). Six different roles for crossover inhibition in the retina: Correcting the nonlinearities of synaptic transmission. *Visual Neuroscience* **27**:1-8.

Whitmore, A. V., Libby, R. T. and John, S. W. M. (2005). Glaucoma: Thinking in new ways - a role for autonomous axonal self-destruction and other compartmentalised processes? *Progress in Retinal and Eye Research* **24**:639-662.

Wilks, T., Harvey, A. and Rodger, J. (2013). Functional brain mapping and the endeavor to understand the working brain. In: Signorelli, F. and Chirchiglia, D. (eds.) Intech Open access.

Williams, D. W., Kondo, S., Krzyzanowska, A., Hiromi, Y. and Truman, J. W. (2006). Local caspase activity directs engulfment of dendrites during pruning. *Nature Neuroscience* **9**:1234-1236.

Williams, P. A., Howell, G. R., Barbay, J. M., Braine, C. E., Sousa, G. L., John, S. W. M. and Morgan, J. E. (2013). Retinal Ganglion Cell Dendritic Atrophy in DBA/2J Glaucoma. *Plos One* **8**.

Williams, P. A., Morgan, J. E. and Votruba, M. (2010). Opa1 deficiency in a mouse model of dominant optic atrophy leads to retinal ganglion cell dendropathy. *Brain* **133**:2942-2951.

Williams, P. A., Piechota, M., von Ruhland, C., Taylor, E., Morgan, J. E. and Votruba, M. (2012). Opa1 is essential for retinal ganglion cell synaptic architecture and connectivity. *Brain* **135**:493-505.

Wolf, C., Gramer, E., Mueller-Myhsok, B., Pasutto, F., Reinthal, E., Wissinger, B. and Weisschuh, N. (2009). Evaluation of nine candidate genes in patients with normal tension glaucoma: a case control study. *Bmc Medical Genetics* **10**.

Woodruff, T. M., Ager, R. R., Tenner, A. J., Noakes, P. G. and Taylor, S. M. (2010). The Role of the Complement System and the Activation Fragment C5a in the Central Nervous System. *Neuromolecular Medicine* **12**:179-192.

Yamada, E. S., Bordt, A. S. and Marshak, D. W. (2005). Wide-field ganglion cells in macaque retinas. *Visual Neuroscience* **22**:383-393.

Yamaguchi, Y. (2000). Lecticans: organizers of the brain extracellular matrix. *Cellular and Molecular Life Sciences* **57**:276-289.

Yang, G. and Masland, R. H. (1992). Direct visualization of the dendritic and receptive-fields of directionally selective retinal ganglion-cells. *Science* **258**:1949-1952.

Yang, H., Downs, J. C., Bellezza, A., Thompson, H. and Burgoyne, C. F. (2007a). 3-D histomorphometry of the normal and early glaucomatous monkey optic nerve head: Prelaminar neural tissues and cupping. *Investigative Ophthalmology & Visual Science* **48**:5068-5084.

Yang, H., Downs, J. C., Girkin, C., Sakata, L., Bellezza, A., Thompson, H. and Burgoyne, C. F. (2007b). 3-d histomorphometry of the normal and early glaucomatous monkey optic nerve head: Lamina cribrosa and peripapillary scleral position and thickness. *Investigative Ophthalmology & Visual Science* **48**:4597-4607.

Yonehara, K., Ishikane, H., Sakuta, H., Shintani, T., Nakamura-Yonehara, K., Kamiji, N. L., Usui, S. *et al.* (2009). Identification of Retinal Ganglion Cells and Their Projections Involved in Central Transmission of Information about Upward and Downward Image Motion. *Plos One* **4**.

Zador, A. (1998). Impact of synaptic unreliability on the information transmitted by spiking neurons. *Journal of Neurophysiology* **79**:1219-1229.

Zhu, X.-H., Qiao, H., Du, F., Xiong, Q., Liu, X., Zhang, X., Ugurbil, K. *et al.* (2012). Quantitative imaging of energy expenditure in human brain. *Neuroimage* **60**:2107-2117.

Appendix

Appendix A

Table A RGC morphology measurements

Measurement	RGC _A	RGC _B	RGC _C	RGC _D
Soma Diameter (μm)	22.7 \pm 3.5	15.6 \pm 2.3	18.8 \pm 3.0	18.7 \pm 2.5
PDL (μm)	25.8 \pm 13.6	22.5 \pm 14.8	22.2 \pm 9.0	20.1 \pm 8.2
PDN	4.3 \pm 1.1	3.2 \pm 0.8	3.9 \pm 0.8	3.1 \pm 0.7
PBPF area (μm^2)	1664 \pm 1081	758 \pm 791	1716 \pm 1052	724 \pm 486
SBPF area (μm^2)	12352 \pm 8383	3391 \pm 3291	7830 \pm 5893	3981 \pm 2184
COG PBPF (%)	22.9 \pm 12.3	56.8 \pm 55.3	23.4 \pm 28.3	68.3 \pm 43.0
COG SBPF (%)	17.6 \pm 7.1	37.6 \pm 35.7	19.4 \pm 9.7	32.2 \pm 18.8
PD asymmetry ($^\circ$)	78.8 \pm 38.6	166.0 \pm 74.8	111.4 \pm 62.4	182.5 \pm 55.5
Proximal branching Density	8.4 \pm 5.4	8.3 \pm 11.0	7.3 \pm 13.2	6.9 \pm 4.4
PD cross-sectional area (μm^2)	27.6 \pm 10.3	11.7 \pm 5.9	18.4 \pm 6.2	20.0 \pm 7.9
PD max Feret diameter (μm)	7.0 \pm 1.2	4.7 \pm 1.2	5.8 \pm 1.1	6.0 \pm 1.2
PD min Feret diameter (μm)	5.1 \pm 1.0	3.2 \pm 1.0	4.2 \pm 0.8	4.5 \pm 1.0
Vector distance from ONH (μm)	3150 \pm 1241	3076 \pm 1042	3067 \pm 946	3148 \pm 803

Values are mean \pm SD.

Appendix B

Papers arising from this thesis:

Tribble, J.R., Cross, S.D., Samsel, P.A., Sengpiel, F. and Morgan, J.E. (2014) A novel system for the classification of diseased retinal ganglion cells. *Visual Neuroscience* 31(6), pp. 373-380.

Williams, P.A., Tribble, J.R., Pepper, K.W., Cross, S.D., Morgan, B.P., Morgan, J.E., John, S.W., Howell, G.R. (2016) Inhibition of the classical pathway of the complement cascade prevents early dendritic and synaptic degeneration in glaucoma. *Molecular Neurodegeneration* 6;11:26